International Journal of Antennas and Propagation

Reflectarray Antennas: Analysis and Synthesis Techniques

Guest Editors: Sandra Costanzo, Raphaël Gillard, and Manuel Arrebola

Reflectarray Antennas: Analysis and Synthesis Techniques

International Journal of Antennas and Propagation

Reflectarray Antennas: Analysis and Synthesis Techniques

Guest Editors: Sandra Costanzo, Raphaël Gillard, and Manuel Arrebola

Editorial Board

Contents

Hindawi Publishing Corporation
International Journal of Antennas and Propagation
Volume 2012, Article ID 945682, 3 pages
doi:10.1155/2012/945682

Editorial

Reflectarray Antennas: Analysis and Synthesis Techniques

Sandra Costanzo

Dipartimento di Elettronica, Informatica e Sistemistica, Università della Calabria, 87036 Rende, Italy

Correspondence should be addressed to Sandra Costanzo, costanzo@deis.unical.it

Received 2 September 2012; Accepted 2 September 2012

The Reflectarray consists of a surface or aperture that is characterized by a surface impedance, and a primary radiator that illuminates this surface The surface impedance can be chosen to produce reflected fields that form a pencil beam in any direction, or shaped beams
(Berry et al. (1963))

The reflectarray concept was firstly introduced in 1963 [1] to define a new class of antennas combining the performance versatility of arrays with the simplicity of reflectors. A waveguide array type was presented in [1] to validate the reflectarray principle, but the real interest in this new kind of antenna came in the late 1980s [2–4], when low-profile reflectarrays were introduced.

Printed reflectarrays consist of an array of microstrip elements illuminated by a primary radiator, typically represented by a horn antenna. The printed elements, giving a flat reflecting surface, are designed to reradiate the incident field with a planar phase front in a prescribed direction. The use of microstrip technology gives significant improvements, in terms of low-cost, less-weight, and easy installation, with respect to standard parabolic reflectors. On the other hand, the feeding mechanism inherited from reflector antennas avoids the disadvantages, in terms of complexity and losses, due to the feeding networks usually adopted in phased arrays.

Various configurations of passive printed reflectarrays, adopting different tuning mechanisms, have been introduced in literature [5–8]. Dynamic phase control techniques have been also investigated for the design of active reflectarrays [9–13], and significant achievements have been obtained in the improvement of bandwidth performances [14–16]. Analysis methods based on different approaches, such as that assuming an infinite array model [17] or that considering each radiator as an isolated element on a grounded dielectric substrate [18], have been considered in literature, and various numerical methods have been implemented for both single-layer and multilayer reflectarrays. A very efficient synthesis technique, based on the intersection approach [19] and properly taking into account both the amplitude and the phase of the field reflected by the reflectarray unit cell, has been developed and applied in [20–22]. Experimental methods alternative to the standard waveguide simulator approach [23] have been developed, with the adoption of open resonator [24, 25] and near field [26–28] techniques for the characterization of both passive and active reflectarray unit cell.

Today, the use of microstrip reflectarrays is largely diffused in many application fields, such as remote sensing and satellite communications. With the new emerging technologies, advanced features are required in terms of broadband, dual-polarization, and beam-scanning operations.

The aim of this special issue is to provide an overview of innovative design methodologies and simulation techniques to face the increasing complexity of new microstrip reflectarray configurations.

This special issue collects 13 papers from 36 authors belonging to several countries and institutions. New emerging ideas and results are presented, with particular focus on the following issues:

(i) synthesis of dual-polarized and conformal reflectarrays;

(ii) reflectarray elements with enhanced bandwidth features;

(iii) beam-scanning and reconfigurable reflectarrays at microwave and millimeter frequencies;

(iv) innovative reflectarrays analysis techniques;

(v) new methods for the numerical and the experimental characterization of reflectarray elements.

The first paper by Venneri et al. proposes a new active reflectarray configuration able to guarantee a full phase tuning range with a single varactor diode and presents interesting results coming from the synthesis of a reconfigurable reflectarray prototype.

The second paper by Venneri et al. presents innovative results concerning the bandwidth evaluation and improvement of slot-coupled reflectarrays.

The paper by Di Massa et al. proposes a new technique for the experimental evaluation of the phase response relative to reflectarray elements, which is based on the adoption of an open cavity system.

The paper by Marnat et al. presents and compares four optimization strategies for the synthesis of dual-polarized microstrip reflectarrays.

The paper by Nayeri et al. introduces a generalized analysis approach to characterize the radiation performance of conformal reflectarrays.

The paper by Tienda et al. presents a general analysis technique for both dual-reflector antennas with a reflectarray subreflector and dual-reflectarray antennas with flat or parabolic main reflectarray.

The paper by Tayebi et al. proposes a new method to automatically design reflectarray antennas.

The paper by Alvarez et al. presents a phase-only optimization method as a systematic framework able to deal with a general reflectarray synthesis problem.

The paper by Van Ha et al. proposes a concentric double square ring configuration as innovative radiating element for large bandwidth reflectarrays.

The paper by Freni et al. presents a modelling technique, based on the use of an artificial neural network, and able to characterize the behaviour of arbitrary reflectarray element structure.

The paper by Delgado et al. proposes a new domain decomposition method for a fast analysis of complex reflectarray structures.

The paper by Carrasco et al. discusses the use of an aperture-coupled reflectarray element for reconfigurable-beam antennas using surface-mounted MEMS.

The paper by Ismail and Inam presents an accurate analysis of different radiating elements structures to be used for the design of both passive and active reflectarrays.

Acknowledgments

The Lead Editor wishes to thank all authors, who have submitted to this special issue some relevant results coming from their research activities, and the reviewers, whose precious suggestions have strongly contributed to improve the quality of the papers. Finally, a very special acknowledgement is due to the Guest Editors and colleagues, Raphaël Gillard and Manuel Arrebola, for their precious cooperation, and to the Editorial Board of the International Journal of Antennas and Propagation, who has made possible the publication of this special issue.

Sandra Costanzo

References

[1] D. G. Berry, R. G. Malech, and W. A. Kennedy, "The reflectarray antenna," in *IEEE Transactions on Antennas and Propagation*, vol. 11, pp. 645–651, 1963.

[2] C. S. Malagisi, "Microstrip disc element reflect array," in *Proceedings of the Electronics and Aerospace Systems Convention (EASCON '78)*, pp. 186–192, 1978.

[3] J. P. Montgomery, "A microstrip reflectarray antenna element," in *Proceedings of the Antenna Applications Symposium*, Urbana, Ohio, USA, 1978.

[4] J. Huang, "Microstrip reflectarray," in *Proceedings of the Antennas and Propagation Society International Symposium Digest*, vol. 2, pp. 612–615, Ontario, Canada, 1991.

[5] D. M. Pozar and T. A. Metzler, "Analysis of a reflectarray antenna using microstrip patches of variable size," *Electronics Letters*, vol. 29, no. 8, pp. 657–658, 1993.

[6] R. E. Munson and H. Haddad, "Microstrip reflectarray for satellite communication and RCS enhancement or reduction," U. S. Patent 4, 684, 952, 1987.

[7] J. Huang and R. J. Pogorzelski, "A ka-band microstrip reflectarray with elements having variable rotation angles," *IEEE Transactions on Antennas and Propagation*, vol. 46, no. 5, pp. 650–656, 1998.

[8] M. R. Chaharmir, J. Shaker, M. Cuhaci, and A. Sebak, "Reflectarray with variable slots on ground plane," *IEE Proceedings*, vol. 150, no. 6, pp. 436–439, 2003.

[9] S. V. Hum, M. Okoniewski, and R. J. Davies, "Realizing an electronically tunable reflectarray using varactor diode-tuned elements," *IEEE Microwave and Wireless Components Letters*, vol. 15, no. 6, pp. 422–424, 2005.

[10] R. Sorrentino, R. Vincenti Gatti, L. Marcaccioli, and B. Mencagli, "Beam steering reflectarrays," in *Proceedings of the 4th ESA Workshop on Millimetre Wave Technology and Applications*, Espoo, Finland, 2006.

[11] H. Legay, G. Caille, E. Girard et al., "MEMS controlled linearly polarized reflect array elements," in *Proceedings of the 15th International Symposium of ANtenna Technology and applied ElectroMagnetics (ANTEM '06)*, Montreal, Canada, 2006.

[12] F. Venneri, S. Costanzo, G. Di Massa, A. Borgia, P. Corsonello, and M. Salzano, "Design of a reconfigurable reflectarray based on a varactor tuned element," in *Proceedings of the 6th European Conference on Antennas and Propagation (EuCAP '12)*, pp. 2628–2631, 2012.

[13] F. Venneri, S. Costanzo, and G. Di Massa, "Reconfigurable aperture-coupled reflectarray element tuned by single varactor diode," *Electronics Letters*, vol. 48, no. 2, pp. 68–69, 2012.

[14] J. A. Encinar, "Design of two-layer printed reflectarrays using patches of variable size," *IEEE Transactions on Antennas and Propagation*, vol. 49, no. 10, pp. 1403–1410, 2001.

[15] S. Costanzo, F. Venneri, and G. Di Massa, "Bandwidth enhancement of aperture-coupled reflectarrays," *Electronics Letters*, vol. 42, no. 23, pp. 1320–1322, 2006.

[16] F. Venneri, S. Costanzo, G. Di Massa, and G. Amendola, "Aperture-coupled reflectarrays with enhanced bandwidth features," *Journal of Electromagnetic Waves and Applications*, vol. 22, no. 11-12, pp. 1527–1537, 2008.
[17] D. M. Pozar, "Microstrip reflectarrays: myths and realities," in *Proceedings of the International Symposium on Antennas (JINA '04)*, pp. 175–179, Nice, France, 2004.
[18] F. Venneri, G. Angiulli, and G. Di Massa, "Design of microstrip reflect array using data from isolated patch analysis," *Microwave and Optical Technology Letters*, vol. 34, no. 6, pp. 411–414, 2002.
[19] O. M. Bucci, G. Franceschetti, G. Mazzarella, and G. Panariello, "Intersection approach to array pattern synthesis," *IEE Proceedings H*, vol. 137, no. 6, pp. 349–357, 1990.
[20] S. Costanzo, F. Venneri, G. Di Massa, and G. Angiulli, "Synthesis of microstrip reflectarrays as planar scatterers for SAR interferometry," *Electronics Letters*, vol. 39, no. 3, pp. 266–267, 2003.
[21] F. Venneri, S. Costanzo, G. Di Massa, and G. Angiulli, "An improved synthesis algorithm for reflectarrays design," *IEEE Antennas and Wireless Propagation Letters*, vol. 4, no. 1, pp. 258–261, 2005.
[22] S. Costanzo, F. Venneri, A. Borgia, I. Venneri, and G. Di Massa, "60 GHz microstrip reflectarray on a benzocyclobutene dielectric substrate," *IET Science, Measurement and Technology*, vol. 5, no. 4, pp. 134–139, 2011.
[23] F. C. E. Tsai and M. E. Bialkowski, "An equivalent waveguide approach to designing of reflect arrays with the use of variable-size microstrip patches," *Microwave and Optical Technology Letters*, vol. 34, no. 3, pp. 172–175, 2002.
[24] S. Costanzo, G. Di Massa, and O. H. Moreno, "Improved open resonator technique for dielectric characterization," in *Proceedings of the 6th European Conference on Antennas and Propagation (EuCAP '12)*, pp. 2127–2129, 2012.
[25] G. Di Massa, S. Costanzo, and O. H. Moreno, "Accurate circuit model of open resonator system for dielectric material characterization," *Journal of Electromagnetic Waves and Applications*, vol. 26, no. 5-6, pp. 783–794, 2012.
[26] S. Costanzo and G. Di Massa, "Far-field reconstruction from phaseless near-field data on a cylindrical helix," *Journal of Electromagnetic Waves and Applications*, vol. 18, no. 8, pp. 1057–1071, 2004.
[27] S. Costanzo and G. Di Massa, "Direct far-field computation from bi-polar near-field samples," *Journal of Electromagnetic Waves and Applications*, vol. 20, no. 9, pp. 1137–1148, 2006.
[28] S. Costanzo and G. Di Massa, "Near-field to far-field transformation with planar spiral scanning," *Progress in Electromagnetics Research*, vol. 73, pp. 49–59, 2007.

Hindawi Publishing Corporation
International Journal of Antennas and Propagation
Volume 2012, Article ID 386429, 12 pages
doi:10.1155/2012/386429

Review Article

Recent Developments of Reflectarray Antennas for Reconfigurable Beams Using Surface-Mounted RF-MEMS

Eduardo Carrasco,[1] Mariano Barba,[1] Manuel Arrebola,[2] and Jose A. Encinar[1]

[1] *Departamento de Electromagnetismo y Teoria de Circuitos, Universidad Politécnica de Madrid, Ciudad Universitaria s/n, 28040 Madrid, Spain*
[2] *Area de Teoria de la Señal y Comunicaciones, Universidad de Oviedo, Edificio Polivalente de Viesques, Modulo 8, Planta 1, 33203 Gijón, Spain*

Correspondence should be addressed to Eduardo Carrasco, e.carrasco@ieee.org

Received 3 March 2012; Revised 18 June 2012; Accepted 23 June 2012

Academic Editor: Sandra Costanzo

Some of the most recent developments in reconfigurable reflectarrays using surface-mounted RF-MEMS, which have been developed at the Universidad Politécnica de Madrid, are summarized in this paper. The results include reconfigurable elements based on patches aperture-coupled to delay lines in two configurations: single elements and gathered elements which form subarrays with common phase control. The former include traditional aperture-coupled elements and a novel wideband reflectarray element which has been designed using two stacked patches. The latter are proposed as a low cost solution for reducing the number of electronic control devices as well as the manufacturing complexity of large reflectarrays. The main advantages and drawbacks of the grouping are evaluated in both pencil and shaped-beam antennas. In all the cases, the effects of the MEMS switches and their assembly circuitry are evaluated when they are used in a 2-bit phase shifter which can be extended to more bits, demonstrating that the proposed elements can be used efficiently in reconfigurable-beam reflectarrays.

1. Introduction

One of the main advantages of reflectarray antennas is the possibility of producing switching, scanning, or reconfiguration of the radiated beam if electronically controllable devices are included. The introduction of these elements allows the phase of the reflected field to be changed at each reflectarray cell. Several concepts have been developed to implement this kind of pattern flexibility, some of them provide a discrete phase control by using switches, such as pin diodes [1–3] or Micro-Electro-Mechanical Systems (MEMS) [4–8], and other realizations provide a continuous phase control by using varactor diodes [1, 9–11], ferroelectric materials [12], or liquid crystal [13, 14]. Depending on the phase-control technique, the first step in the design of a reflectarray element to be used in steering or reconfigurable beam antennas is the suitable choice of the element configuration.

Reflectarray elements based on aperture-coupled patches using a microstrip delay line to control the phase of the reflected field [15], like that shown in Figure 1 have demonstrated a significant improvement in the bandwidth of large fixed-beam reflectarrays [16], through the introduction of true-time delay (TTD) which compensates the effects of the differential spatial phase delay [17]. These elements have also been used to produce shaped-beams, like those required by Local Multipoint Distribution System (LMDS) base stations [18]. The element consists of a square patch which is coupled to a variable length microstrip line using a rectangular slot. If the metallization dimensions are well adjusted, a phase response proportional to twice the length of the delay line can be achieved with very linear phase-delay within a range greater than 360°. This range is only limited by the room available on the cell to increase the microstrip line.

The aperture-coupled elements offer several advantages besides those related to the aforementioned TTD, such as

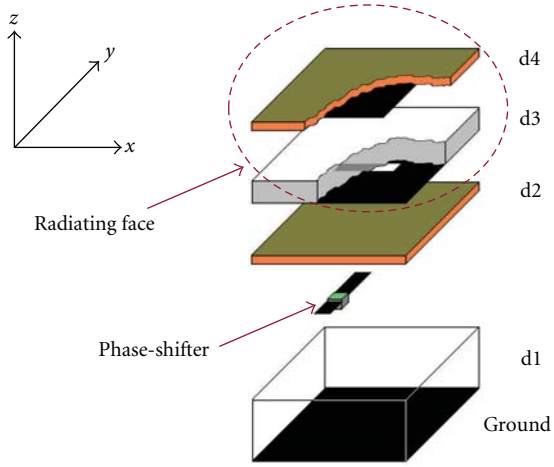

Figure 1: Expanded view of a single reconfigurable periodic element based on patches aperture-coupled to delay lines.

low losses, low cross polarization levels, and the possibility of implementing electronic devices which allow the phase to be controlled in reconfigurable antennas [1, 7, 8, 10, 11]. Two major benefits are the isolation of the radiating elements from the phase control network and phase-shifters because they are on opposite sides of the ground plane, as well as the possibility of gathering two adjacent elements to form a subarray with the aim of reducing both the number of control elements and manufacturing complexity [19], especially in large reflectarrays.

The proposed reflectarray element allows the phase of the reflected field to be controlled by modifying the electrical length of the phase delay. This can be done by dividing the microstrip into different segments which can be connected in series using electronic devices. MEMS switches offer attractive advantages because of their practically null power consumption, very high isolation, low insertion loss, total independence between DC and RF signals, and high level of integration because they can be monolithically implemented in the delay-line wafer [4, 7]. However, this monolithically integration is not economically affordable in X-band antennas requiring the use of other alternatives for the manufacturing. One possibility is the use of surface-mounted MEMS which can be connected to the microstrip lines by means of a standard wire bonding process [8].

In the following sections the aperture-coupled reflectarray element is shown as a well-situated solution to implementing reconfigurable-beam antennas using surface-mounted MEMS. Three practical cases are presented at 10.40 GHz: single elements, gathered elements, and a wideband single element obtained by stacking two patches.

2. Reconfigurable Element Based on Surface-Mounted Devices

2.1. Reconfigurable Single Element Based on Patches, Aperture-Coupled to Delay Lines. For the present work, MEMS series switches designed and manufactured by CEA-LETI Minatec [20] have been used. These MEMS switches are implemented in a 50 Ω coplanar waveguide (CPW) with a gap in the signal conductor and a silicon nitride fixed-fixed membrane with a patterned metallic contact in the centre [21, 22]. This contact gives continuity to the signal line of the CPW when a DC voltage is applied between two symmetric electrodes and the ground plane. The devices have been supplied as individual dice after the wafer cutting, with side dimensions of around 800 μm and 80 μm for the pad width. These dimensions combined with the fact that the dielectric substrate which will contain the MEMS is very thin make the use of long gold wires necessary for the bonding which introduces inductive effects and an inherent phase-shift which must be taken into account.

The proposed electronically controllable element can be analysed using a cascading technique, as shown in Figure 2. With a full wave approach using CST Microwave Studio [23], the two-port scattering matrix of the fixed phase reflectarray element is obtained under local periodicity conditions. In this case, the first port refers to the top surface of the upper dielectric, while the second port refers to the end of a microstrip line. The reflection coefficient in the free space of the reconfigurable element is obtained by loading the first port with the intrinsic impedance of air and the second port with the impedance which represents the MEMS assembly plus a microstrip segment which can be open ended or connected to another MEMS assembly. The MEMS assembly which includes the MEMS device and the wire bonding lines is obtained through an equivalent circuit, which has been deduced and demonstrated in [8]. Depending on the voltage applied to the switch, the MEMS contact can be modelled as a series resistance or a capacitance. For the particular case of the MEMS used in this work, these values are, respectively, $R_s = 2.15\,\Omega$ and $C_{\text{up}} = 1\,fF$.

Prior to the reconfigurable element analysis, the design of the passive element must be carried out. The proposed single element has been designed using a local periodicity approach with a period of 18.5 mm × 18.5 mm, which means 0.64 λ at 10.40 GHz. The period has been chosen as a tradeoff in order to allow more room for long delay lines, for the control devices and their associated DC lines, on one side, and to avoid the appearance of grating lobes, on the other side. For a whole reflectarray, the grating lobes will appear for incidence angles greater than 34°. The square patches are 9.1 × 9.1 mm^2, the slot 7.0 × 1.4 mm^2, and the delay line width 0.388 mm (70 Ω). This impedance has been chosen with the aim of improving the matching between the microstrip line and the MEMS assembly, taking into account that the 25 μm of the gold wires present high impedance, in the order of 200 Ω. With the aim of obtaining a very linear phase curve of the reflection coefficient as a function of the length of the line, the matching stub of the element has been fixed to 1.90 mm, measured from the centre of the slot. The main features of the dielectric substrates are shown in Table 1.

Figure 3 shows the reflection coefficient in free space for the passive element as a function of the line length. The losses of the element are around 0.25 dB at the central frequency. A practically linear phase delay is obtained in a bandwidth of more than 10%, with a phase range of at least 2 cycles of 360°.

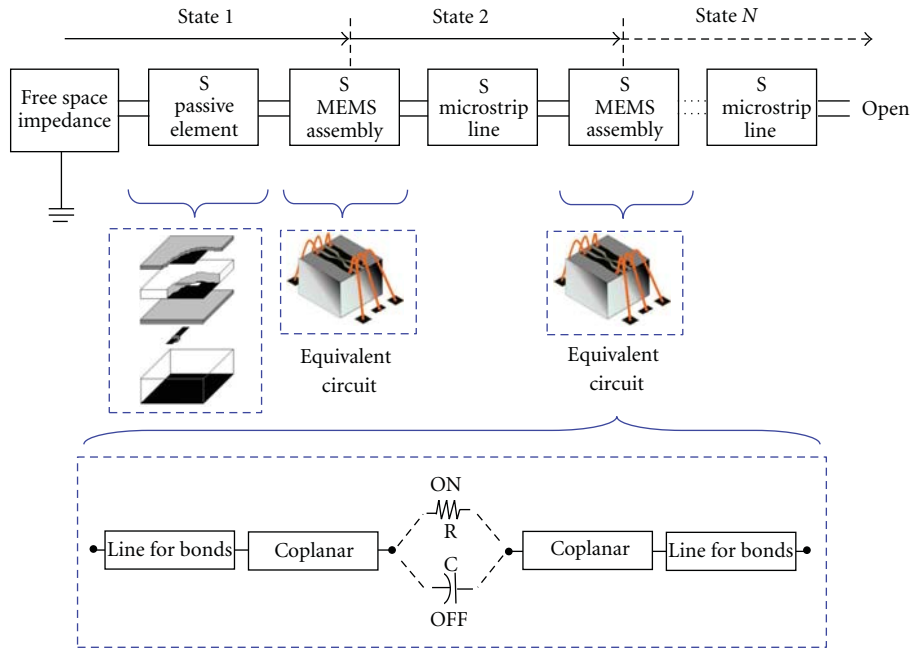

Figure 2: Modelling of the reflectarray element with phase control.

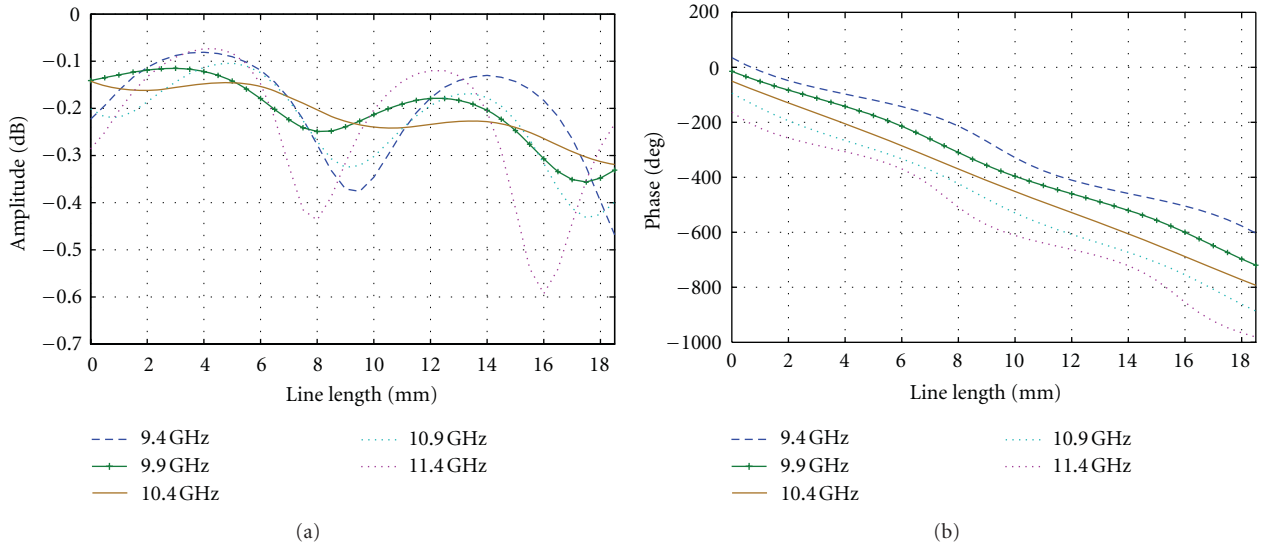

Figure 3: Reflection coefficient in free space for the passive single element as a function of the delay line length. (a) Amplitude. (b) Phase.

Table 1: Dielectric substrates.

Layer	ε_r	$\tan\delta$	Thickness (mm)
d4	3.380	0.0035	0.508
d3	1.067	0.0002	2.000
d2	3.380	0.0035	0.305
d1	1.000	0.0002	7.200

This phase range is only limited by the cell room and can be easily incremented by bending the delay line to form an L or a U shape as in [15]. Once the passive element has been designed, the effects of connecting the MEMS devices can be evaluated. Here, it is important to note that, depending on the application, the proposed element can be tuned to any phase value (switching beam) or to certain discrete values (reconfigurable beam). Here, the element has been evaluated as a 2-bit phase shifter which allows 4 states to be produced equally separated by 90°, but can be extended to more states by increasing the number of switches which are connected to the delay line. The amplitude of the reflection coefficient for the 4 states as well as for the passive element is shown

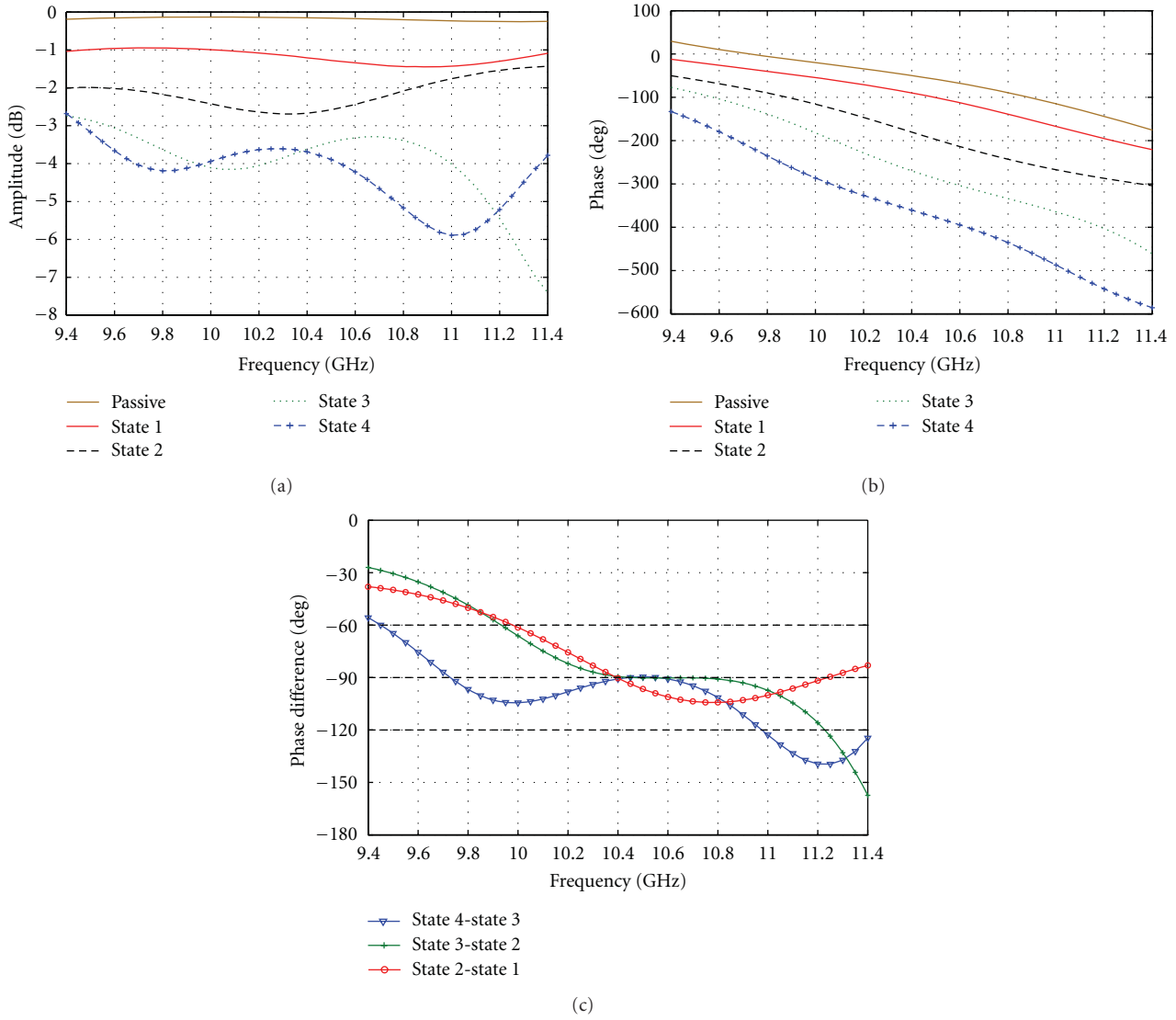

Figure 4: Reflection coefficient versus frequency for a 2-bit reflectarray element in a periodic environment. (a) Amplitude. (b) Phase. (c) Phase difference between the adjacent states.

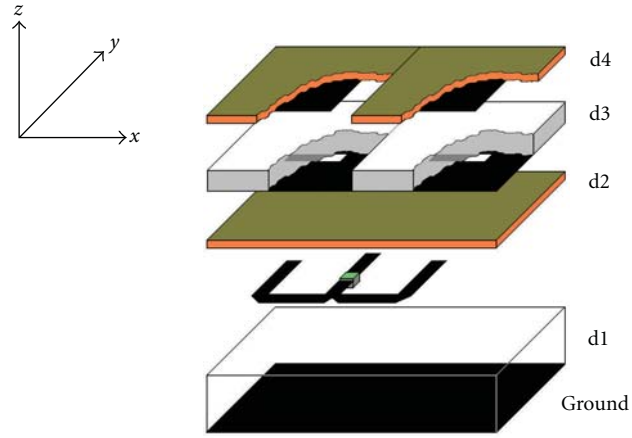

Figure 5: Expanded view of a gathered reconfigurable element based on patches, aperture-coupled to delay lines.

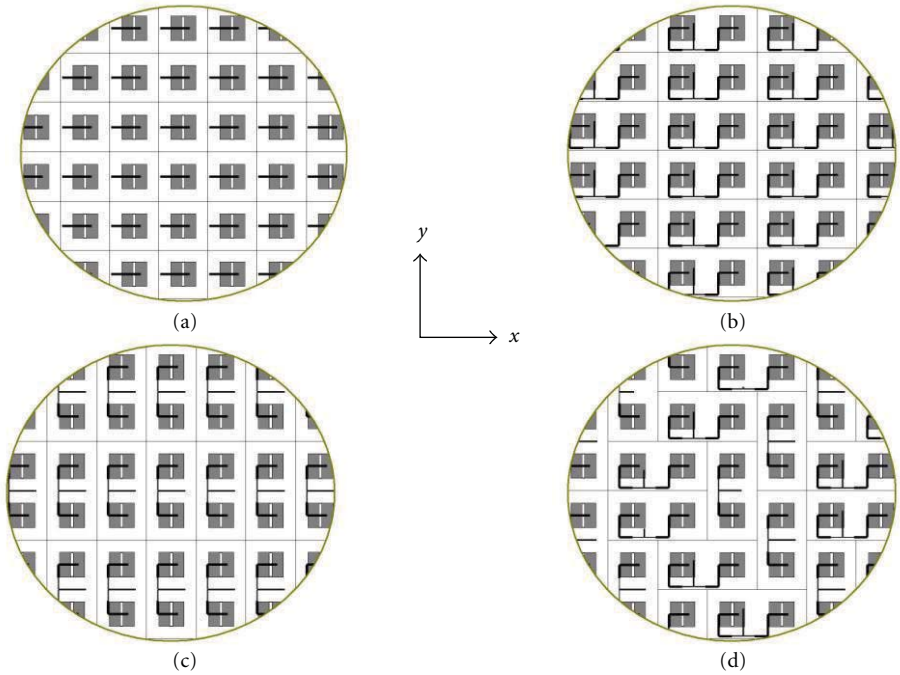

Figure 6: Detailed view of different lattices for a reflectarray based on aperture-coupled elements. (a) Single elements. (b) Gathered elements along the x-axis. (c) Gathered elements along the y-axis. (d) Irregular gathering.

in Figure 4(a), in the frequency band from 9.4 GHz to 11.40 GHz which is the band in which the MEMS assembly has been previously characterized and validated [8]. The losses of the element are mainly produced by the Z_s which is presented between the contact in the membrane and the CPW when the switch is in the ON position and by the mismatch produced between the microstrip and the wire bonding which has more impact as the bonding wires are longer. These large wires are also responsible for the inherent phase-delay introduced by the MEMS assembly, which is around 60° when the MEMS is in the OFF position and 120° when the MEMS is ON. Phase values lower than these can be achieved by introducing an extra 360° cycle. The phase response of the element is shown in Figure 4(b). If the phase variation between adjacent states is limited to $\pm 30°$, which is a very acceptable value for a 2-bit phase-shifter, the proposed reflectarray element provides a 10% bandwidth, as can be seen in Figure 4(c).

2.2. Reconfigurable Gathered Elements Based on Patches, Aperture-Coupled to Delay Lines. Large reflectarrays with reconfigurable beams can require hundreds or thousands of electronic devices with their associated DC lines to control the phase of the reflected field at each element. This means a significant increase in the cost of the antenna as well as the manufacturing complexity. The number of control devices can be drastically reduced if sparse elements are used [24]. However the reflection produced by the ground plane in the zones between the elements makes the design of the reflectarray antenna difficult. Another alternative is the grouping together of two or more neighbouring elements to form a subarray [19, 25]. Because of the independence between the radiating face and the phase-shifting device, the proposed aperture-coupled element allows two or more elements to be controlled with the same delay line without a significant degradation in the reflectarray performance. Figure 5 shows the expanded view of a gathered reflectarray element where two aperture-coupled patches are controlled by the same delay line. It should be noted that, for the design of the gathered element, first a single-element must be designed in order to obtain a reflection coefficient with low losses and a very linear phase response, proportional to twice the length of the delay line, as in Section 2.1. The second step is to design a microstrip circuit (T-junction, quarter of wavelength transformers, bends and delay line) in order to joint two adjacent elements. The two elements are gathered using the previously designed microstrip circuit and a small readjustment of the individual elements must be performed in order to compensate the effects introduced by the grouping and therefore to keep the linear phase response.

As expected, the gathering of the elements in pairs will change the response of the reflected field by two factors. Firstly, the phase required to produce the desired beam, which depends on the radiation pattern, the feed and elements position, is limited in resolution. This means that the phase delay that must be provided by the two adjacent elements, controlled by the same delay line, must be adjusted to the value that introduces the lower phase error (quantization error) with respect to the original phase which was synthesized for the two single elements. An increase in the grating lobes level will also be produced because the period of the sub-array is greater than the wavelength. This second factor can have more impact on the antenna performance.

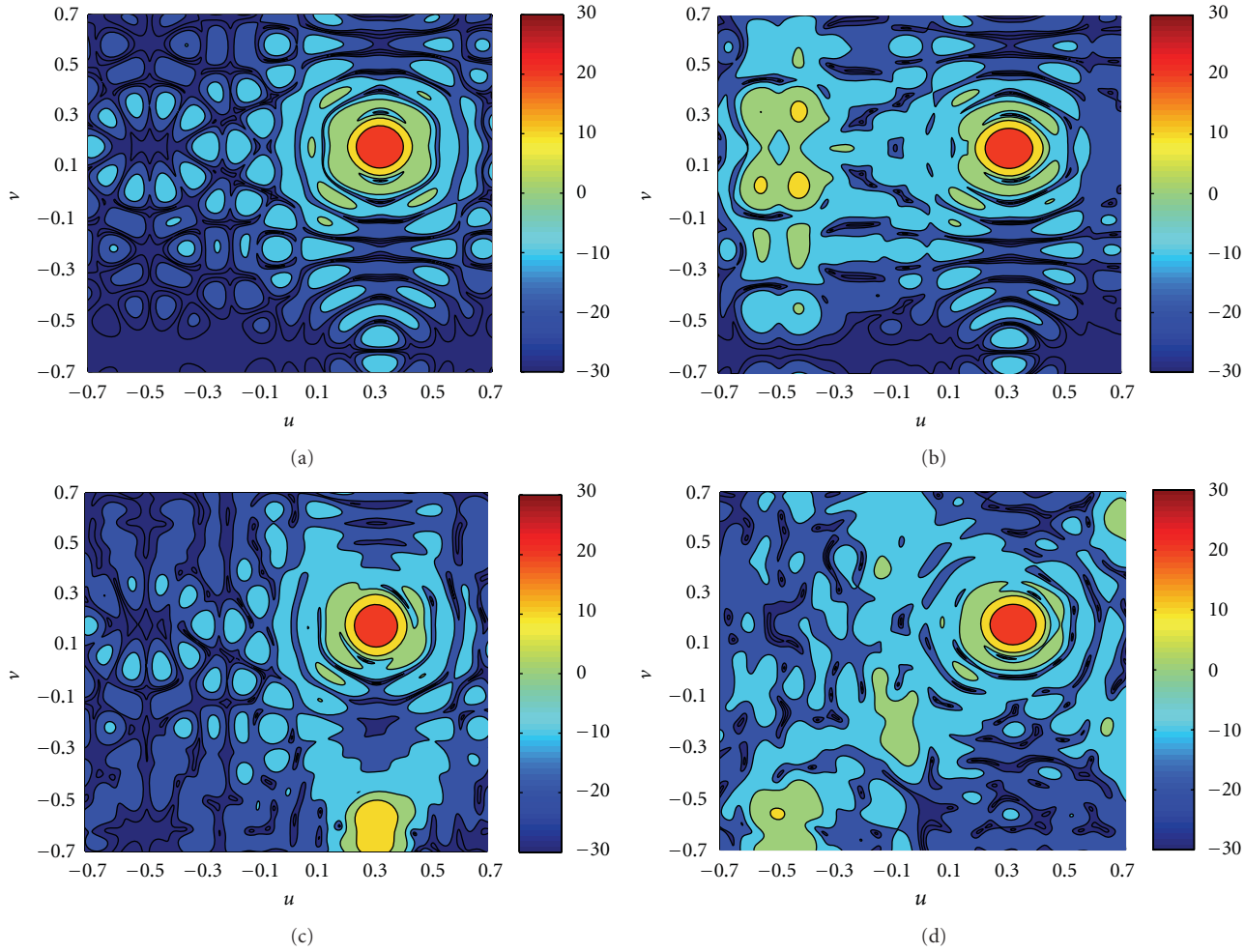

Figure 7: Radiation patterns produced with the pencil-beam reflectarray antenna using different lattices. (a) Without any grouping. (b) Grouping along the x-axis. (c) Grouping along the y-axis. (d) Grouping in an irregular lattice.

The undesired grating lobes can be drastically reduced or even eliminated if the gathering is carried out using irregular lattices [26, 27]. The effects of the grouping have been evaluated for both cases: pencil- and shaped-beam reflectarrays with the features shown in Table 2, using ideal elements. In the two cases different lattices for the gathering have been analysed as can be seen in Figure 6. The first lattice corresponds to the original antenna, where the elements have not been grouped together conserving all the required phase values and the original cell period. The second lattice corresponds to a grouping along the x-axis, while in the third lattice the grouping has been carried out along the y-axis. Finally, the fourth lattice called an irregular lattice corresponds to a nonregular combination of elements grouped together along both the x-axis and the y-axis breaking the period of the lattice along the main planes.

For the case of a pencil-beam reflectarray radiating in certain direction defined by the angles (θ, φ) in spherical coordinates, the impact of the grating lobes will be greater as θ increases. As an example, the case of a circular reflectarray antenna radiates a beam towards 11° in a switching plane which is tilted at 18.3° in respect the horizon. The radiation patterns associated to the corresponding phase distributions obtained with the aforementioned lattices have been computed in directivity, by dividing by the total power radiated by the feed, and including the spillover losses, that is without taking into account the losses of the elements since the objective here is to evaluate the impact of the gathering for each lattice. The feed horn has been modelled as a $\cos^q$ function, being $q = 10$, at the central frequency of 10.40 GHz.

Table 2: Reflectarray antennas features.

	Pencil beam	Shaped beam
Diameter (mm)	324	396
Number of elements	244 (122 subarrays)	362 (181 subarrays)
Feed position (mm)		
x	−100	−140
y	0	0
z	330	450

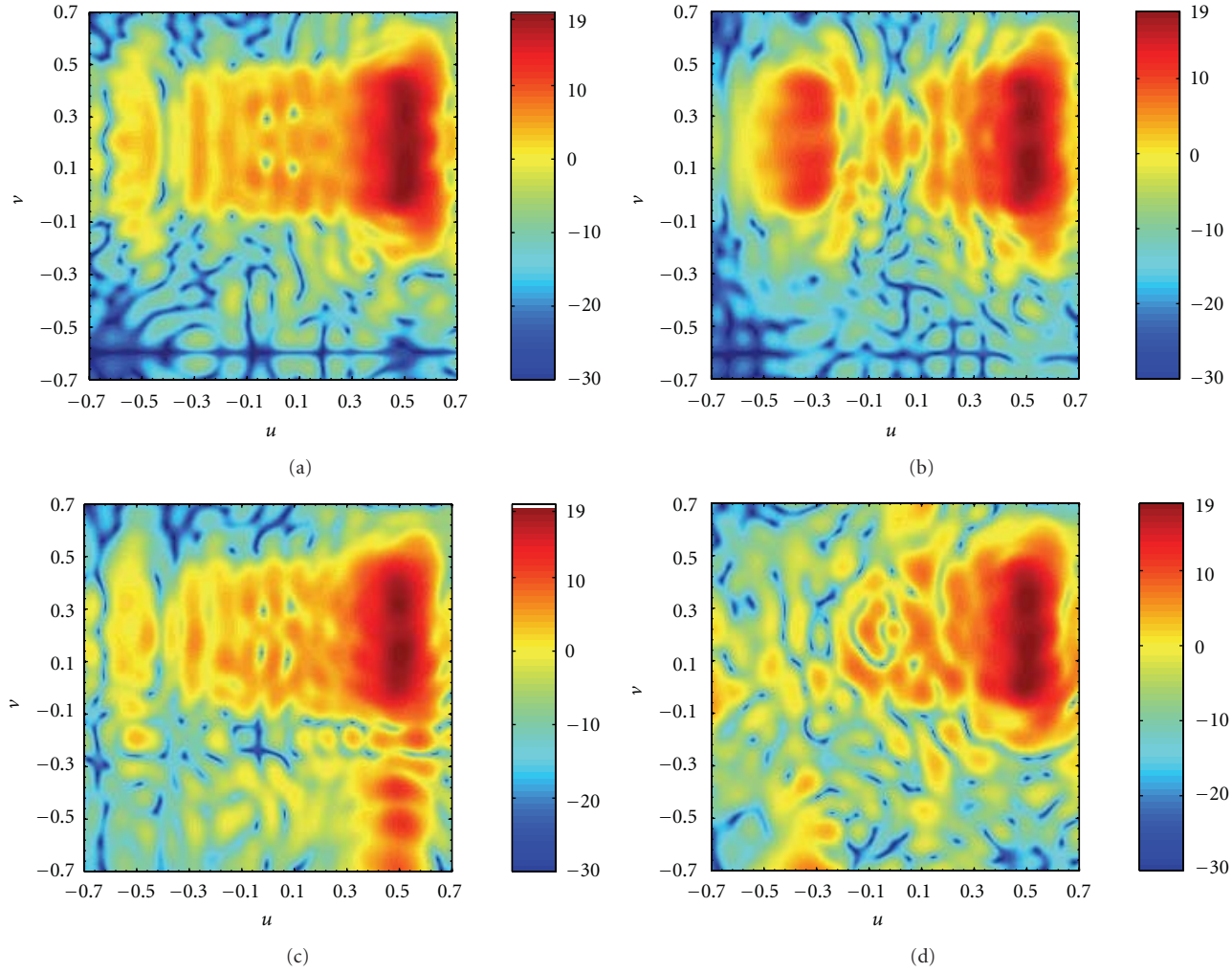

Figure 8: Radiation patterns produced with the shaped-beam reflectarray antenna using different lattices. (a) Without any grouping. (b) Grouping along the x-axis. (c) Grouping along the y-axis. (d) Grouping in an irregular lattice.

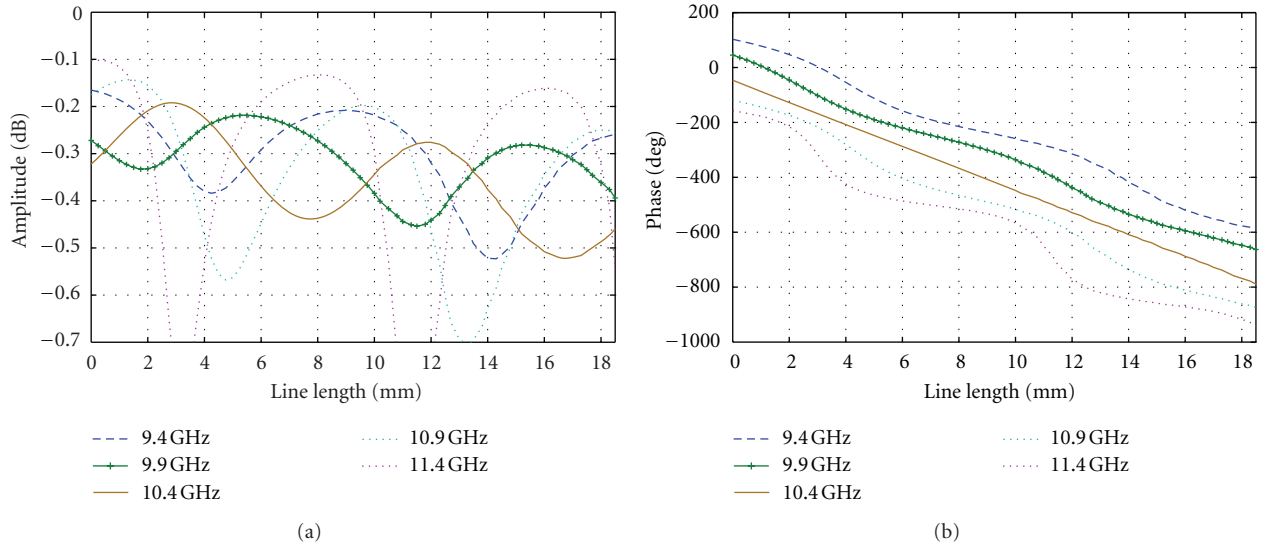

Figure 9: Reflection coefficient in free space for the two-element subarray. (a) Amplitude. (b) Phase.

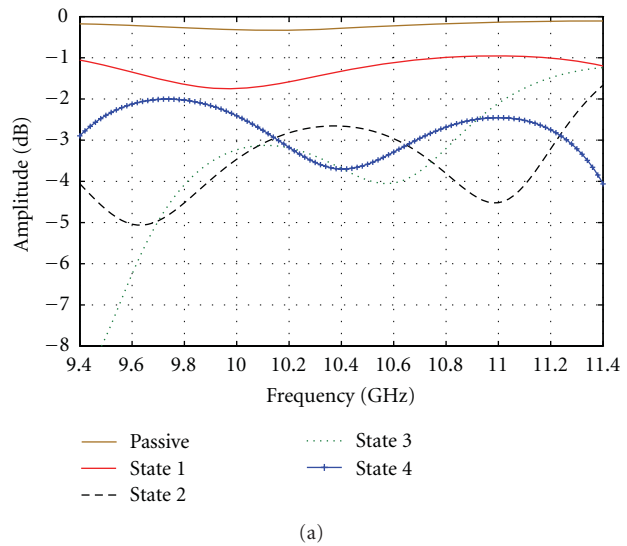

(a)

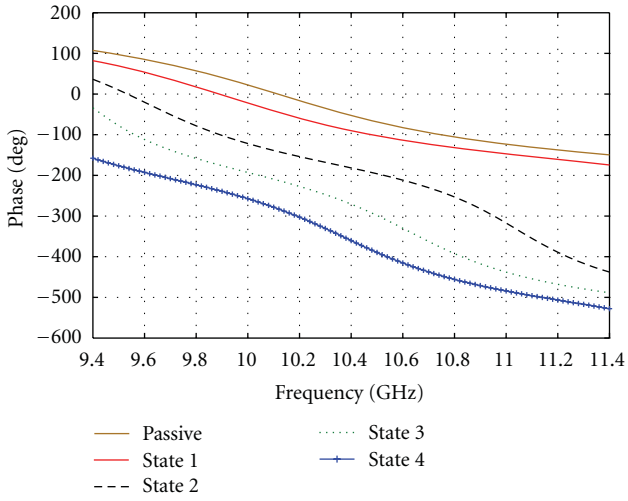

(b)

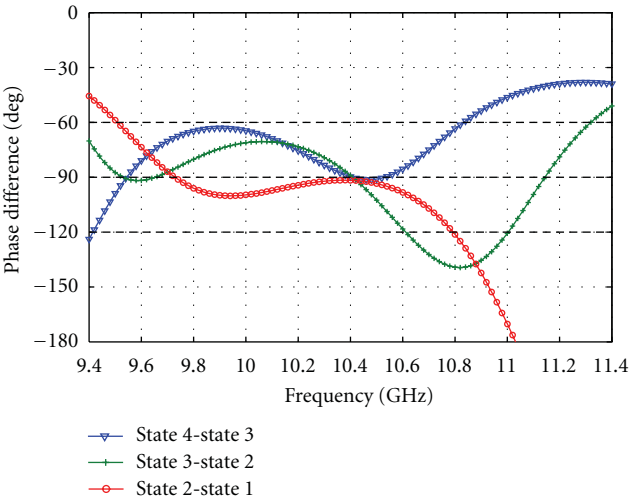

(c)

Figure 10: Reflection coefficient for the 2-bit gathered element in a periodic environment. (a) Amplitude. (b) Phase. (c) Phase difference between the adjacent states.

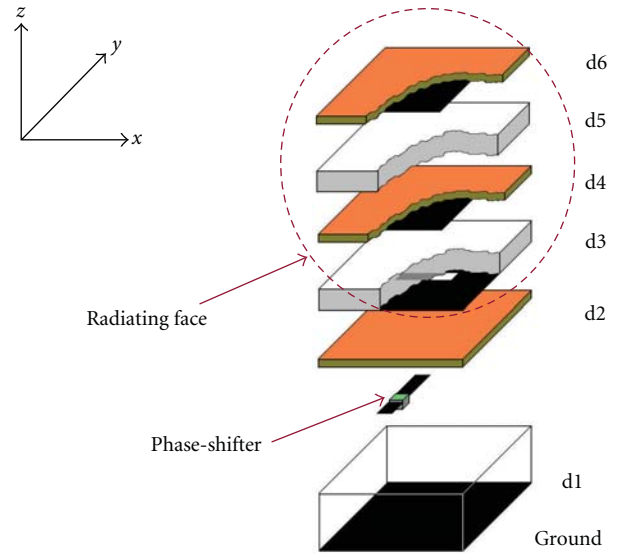

Figure 11: Expanded view of a single reconfigurable element based on patches, aperture-coupled to delay lines with two stacked patches.

Figure 7 shows the three-dimensional radiation patterns for the respective cases in the u-v coordinates, where $u = \sin\theta\cos\varphi$ and $v = \sin\theta\sin\varphi$. For the reference pattern, which is the pattern without any grouping and therefore compensating the phase at each individual element, there are no grating lobes and the directivity is 28.4 dB. For the reflectarray with gathered elements in the x-direction, the grating lobes appear in the elevation plane, while in the case of gathered elements in the y-direction the grating lobes appear in the azimuth plane and can eventually cause interference. For these cases the directivity values are 27.71 and 27.18, respectively. Finally, in the non-regular lattice the grating lobes are produced in a region furthest from the main lobe with a very small width.

In the second example, a shaped-beam reflectarray has been designed to produce a square cosecant beam in the elevation plane tilted by 30° and a 30° sector beam deviated 15° with respect to the antenna boresight. The radiation patterns for this antenna have also been obtained in directivity, using the different lattices for the grouping together of the elements. Figure 8 shows the 3-D radiation patterns also in the u-v coordinates. As expected, there are no grating lobes for the case without grouping. In the antenna with gathered elements along the x-axis, the grating lobes appear in the elevation plane with levels of only 5 dB below the main beam, which is an inadmissible value for the majority of the applications. For the antenna with gathered elements along the y-axis, a grating lobe appears in the azimuth plane with a level of 7 dB below the main lobe. As in the previous case, this lobe must be eliminated or drastically reduced. Finally, by using an irregular lattice which breaks the periodicity of the grouping, the grating lobe is practically eliminated. In all of the cases, the directivity values are greater than 16.25 dB,

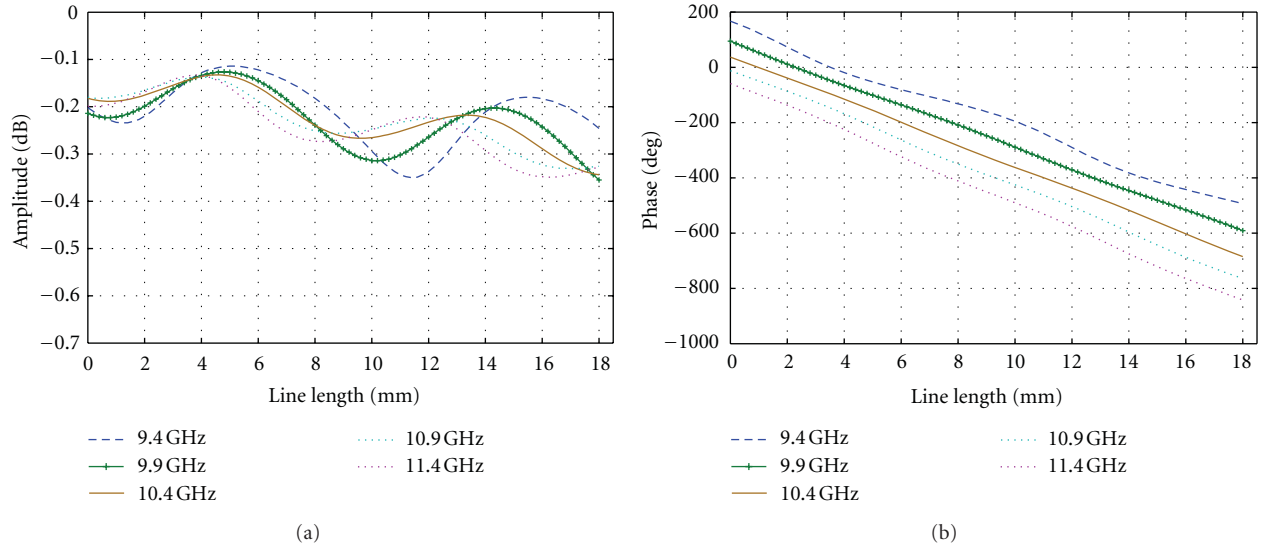

Figure 12: Reflection coefficient in free space versus the line length for the reflectarray element with two stacked patches. (a) Amplitude. (b) Phase.

fulfilling with the required specifications for this particular case.

Once the impact of grouping two adjacent elements together with a common control has been evaluated, a reconfigurable gathered element is presented. As in the case of a reconfigurable simple element, the first step is to design a passive element which will be connected to the phase control network. The modelling approach of Figure 2 is also valid if the scattering matrix of the gathered element is used in the place of the single element scattering matrix. The dielectric materials are the same as in the case of a single element, but the dimensions of the element have been updated as follows in order to keep the linearity of the phase response. The size of the sub-array is 36 mm × 18 mm, which means $1.24\,\lambda \times 0.62\,\lambda$, at the designing frequency of 10.40 GHz. As can be observed, the period of the single element (18.5 mm) has been slightly reduced (18.0 mm). The side of the square patches is 9.1 mm and the rectangular slots are 8.9 mm × 1 mm. In this case the width of the microstrip line is also 0.39 to obtain a 70 Ω characteristic impedance. The matching stub length is 1.87 mm, measured from the centre of the slot. Figure 9 shows the reflection coefficient in free space of the proposed sub-array as a function of the line length in the band from 9.40 GHz to 11.40 GHz. The average losses at the central frequency of 10.40 GHz are 0.35 dB which is slightly greater than that of a single element. At extreme frequencies the losses increase as a result of the gathering. The frequency curves remain very linear from 9.4 GHz to 10.40 GHz, with an increase in the slope at the higher frequencies which was expected as a result of the effects introduced by the T-junction and the impedance transformers required in the element grouping.

Note that the reflection coefficient for each sub-array formed by two gathered elements has been computed using a local-periodicity approach (Floquet's conditions). This approach gives very accurate results in this kind of element because independently on the lattice (along x, along y or irregular), all the elements are exactly equal in the patches and slots layers. The only difference between neighbouring elements is found in the microstrip lines layer. The mutual coupling between elements is more important in the slots and patches layer, while in the delay line layer (which is the layer which changes for each kind of lattice) the coupling is negligible.

As in the case of a single element, the results for a 2-bit reflectarray element are shown, but now with gathering elements. This means that one half of the required MEMS and their associated DC network can be saved, with a significant reduction in the cost and the manufacturing complexity of large reflectarrays, and without any significant change in the performance of the element. Figure 10 shows the amplitude and phase of the reflection coefficient for the 2-bit element as a function of the frequency. The average losses of the four states for the phase-controllable gathered elements are 2.84 dB, at the central frequency. As can be seen, the losses are not proportional to the number of switches because they also depend on the standing wave produced by the open-ended delay line and by the mismatch between the microstrip and the MEMS assembly. An almost linear phase response with the frequency can be observed at certain frequencies from the phase curves, giving rise to a True-Time Delay behaviour. Considering a phase error of ±30°, which is a very restrictive value for a 2-bit phase-shifter, the bandwidth of the elements is 10% (from 9.50 GHz to 10.60 GHz).

2.3. Wideband Reconfigurable Single Element Based on Two Stacked Patches, Aperture-Coupled to Delay Lines. A passive reflectarray element with more than 30% of bandwidth to be used in reconfigurable-beam antennas has been designed using the same configuration of aperture-coupled elements, but by adding an additional patch to enlarge the bandwidth

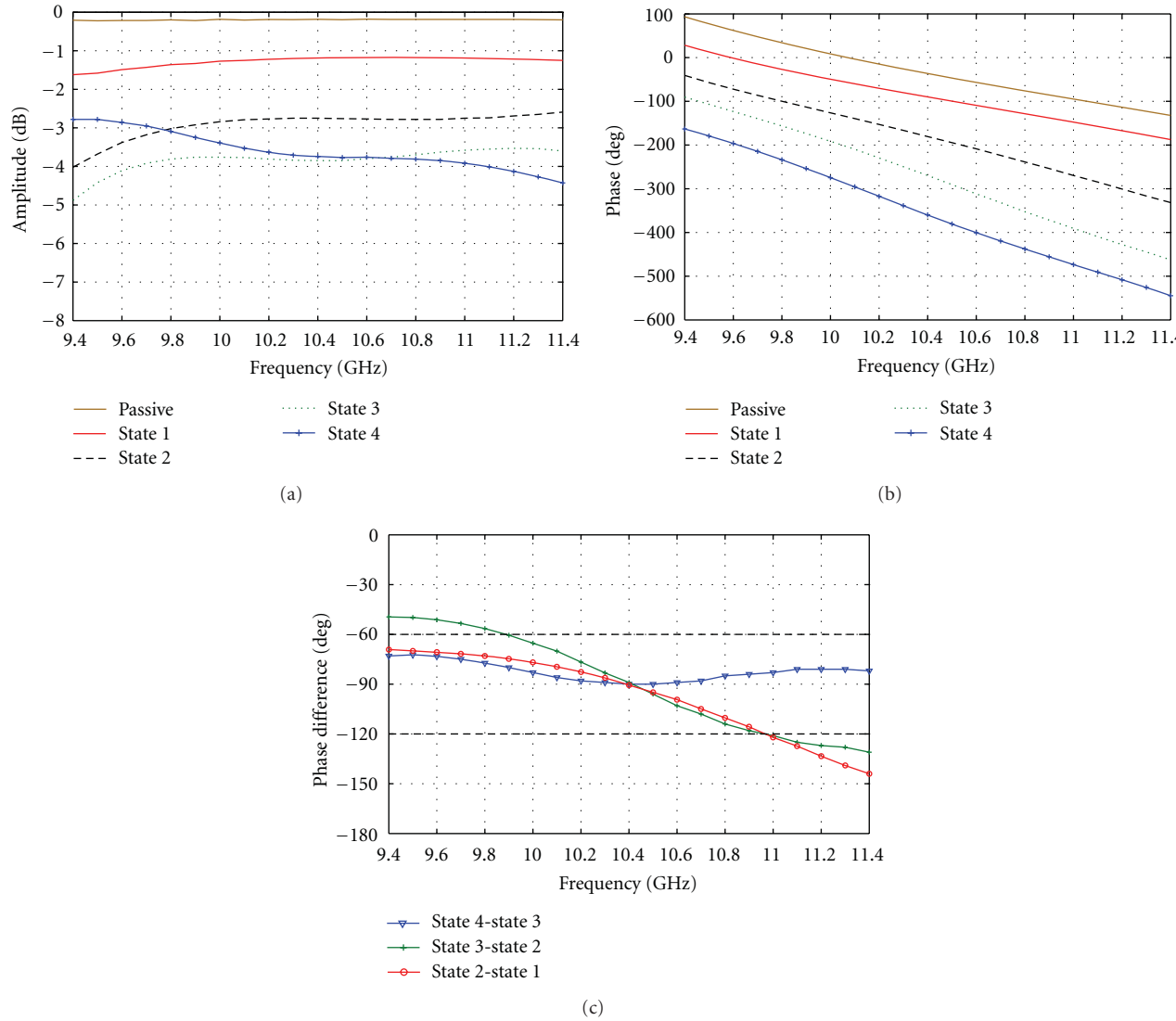

FIGURE 13: Reflection coefficient for the 2-bit wideband element with two stacked patches in a periodic environment. (a) Amplitude. (b) Phase. (c) Phase difference between the adjacent states.

as typically done in the case of elements printed arrays with stacked patches [28]. The proposed element is shown in Figure 11. As in previous cases, the element has been designed using a local periodicity approach with a period of 18.5 mm × 18.5, ($0.64\lambda \times 0.64\lambda$), at 10.40 GHz. The square patches are 8.9 × 8.9 mm^2 and 6.23 × 6.23 mm^2 (upper patch = 0.7 × lower patch), the slot 7.35 × 1.5 mm^2 and the delay line width 0.388 mm (70 Ω). In this case, the matching stub has been fixed at 1.55 mm, measured from the centre of the slot. The dielectric materials are the same as in Table 1. The additional materials have been defined as d5 = d3 and d6 = d4.

Figure 12 shows the reflection coefficient in free-space for the wideband element as a function of the delay line length for different frequencies. As can be seen, this element provides a practically linear phase delay in all of the analysed frequencies within a 30% bandwidth. If three MEMS are assembled along the delay line to forming a 2-bit phase shifter, the losses are much more stable in practically the entire band, compared with the original single-patch reflectarray element. The phase variations between adjacent states are also smaller than in the case of the single element with only one patch. In fact, the ±30° variation is fulfilled in practically the whole band. The amplitude, phase and phase variation between adjacent states can be seen in Figure 13. A tradeoff between the manufacturing difficulties generated by the need for the second stacked patch and the bandwidth requirements of each specific application must be made before deciding to use a single element with one patch or a single element with two stacked patches. It is clear that for the gathered element it is also possible to include an additional patch in order to increase the bandwidth. However it

is also necessary to take into account the band limitations introduced by the T-junction and the impedance transformers which are needed in the case of a sub-array.

3. Conclusions

The feasibility of implementing surface-mounted MEMS switches in aperture-coupled reflectarray elements has been demonstrated in three cases: single elements, gathered elements, and a wideband single element with stacked patches. In all the cases, the effect of the MEMS assembly which includes wire bonding has been considered in the analysis.

The number of MEMS as well as their control network can be reduced through the grouping of adjacent reflectarray elements in pairs with a significant reduction in the cost and manufacturing complexity. The main drawback of the proposed gathering is the generation of grating lobes in the grouping direction, but its impact can be easily reduced by using irregular lattices.

Finally, the average losses of the elements can be drastically improved by reducing the series resistance of the MEMS switches to values of around 0.15 Ω as well as reducing the mismatch between the microstrip lines and the bonding wires by manufacturing thinner MEMS devices. These are two technological issues on which the MEMS' manufacturer is working.

Acknowledgments

The work presented in this contribution has been supported in part by the Spanish Ministry of Economy and Competitiveness, under the Project Contracts TEC2010-17567, and by the Seventh Framework of the European Union, under the ARASCOM project FP7-ICT-2007-3.6 : 222620. The authors acknowledge CEA-LETI Minatec from France for providing the MEMS devices which were characterized and used in the simulations.

References

[1] M. Barba, E. Carrasco, J. E. Page, and J. A. Encinar, "Electronic controllable reflectarray elements in X band," *Frequenz*, vol. 61, no. 9-10, pp. 203–206, 2007.

[2] H. Kamoda, T. Iwasaki, J. Tsumochi, T. Kuki, and O. Hashimoto, "60-GHz electronically reconfigurable large reflectarray using single-bit phase shifters," *IEEE Transactions on Antennas and Propagation*, vol. 59, no. 7, pp. 2524–2531, 2011.

[3] E. Carrasco, M. Barba, and J. A. Encinar, "Demonstration of a switchable-beam reflectarray antenna with PIN diodes in X-band," in *Proceedings of the 33rd ESA Antenna Workshop on Challenges for Space Antenna Systems (ESA/ESTEC '11)*, Noordwijk, The Netherlands, October 2011.

[4] B. Mencagli, R. V. Gatti, L. Marcaccioli, and R. Sorrentino, "Design of large mm-wave beam-scanning reflectarrays," in *Proceedings of the 35th European Microwave Conference (EuMC '05)*, pp. 1875–1878, France, Paris, October 2005.

[5] H. Rajagopalan, Y. Rahmat-Samii, and W. A. Imbriale, "RF MEMS actuated reconfigurable reflectarray patch-slot element," *IEEE Transactions on Antennas and Propagation*, vol. 56, no. 12, pp. 3689–3699, 2008.

[6] J. Perruisseau-Carrier, F. Bongard, R. Golubovic-Niciforovic, R. Torres-Sanchez, and J. R. Mosig, "Contributions to the modeling and design of reconfigurable reflecting cells embedding discrete control elements," *IEEE Transactions on Microwave Theory and Techniques*, vol. 58, no. 6, pp. 1621–1628, 2010.

[7] O. Bayraktar, O. A. Civi, and T. Akin, "Beam switching reflectarray with MEMS controls," in *Proceedings of the 4th European Conference on Antennas and Propagation (EuCAP '10)*, Barcelona, Spain, April 2010.

[8] E. Carrasco, M. Barba, B. Reig, C. Dieppedale, and J. A. Encinar, "Characterization of a reflectarray gathered element with electronic control using ohmic RF MEMS and patches aperture-coupled to a delay line," *IEEE Transactions on Antennas and Propagation*, vol. 60, no. 9, 2012.

[9] S. V. Hum, M. Okoniewski, and R. J. Davies, "Realizing an electronically tunable reflectarray using varactor diode-tuned elements," *IEEE Microwave and Wireless Components Letters*, vol. 15, no. 6, pp. 422–424, 2005.

[10] M. Riel and J. J. Laurin, "Design of an electronically beam scanning reflectarray using aperture-coupled elements," *IEEE Transactions on Antennas and Propagation*, vol. 55, no. 5, pp. 1260–1266, 2007.

[11] F. Venneri, S. Costanzo, and G. Di Massa, "Reconfigurable aperture-coupled reflectarray element tuned by single varactor diode," *Electronics Letters*, vol. 48, no. 2, pp. 68–69, 2012.

[12] R. R. Romanofsky, "Advances in scanning reflectarray antennas based on ferroelectric thin-film phase shifters for deep-space communications," *Proceedings of the IEEE*, vol. 95, no. 10, pp. 1968–1975, 2007.

[13] W. Hu, R. Cahill, J. A. Encinar et al., "Design and measurement of reconfigurable millimeter wave reflectarray cells with nematic liquid crystal," *IEEE Transactions on Antennas and Propagation*, vol. 56, no. 10, pp. 3112–3117, 2008.

[14] G. Pérez-Palomino, J. A. Encinar, M. Barba, and E. Carrasco, "Design and evaluation of multi-resonant unit-cells based on liquid crystals for reconfigurable reflectarrays," *IET Microwaves, Antennas and Propagation*, vol. 6, no. 3, pp. 348–354, 2012.

[15] E. Carrasco, M. Barba, and J. A. Encinar, "Reflectarray element based on aperture-coupled patches with slots and lines of variable length," *IEEE Transactions on Antennas and Propagation*, vol. 55, no. 3, pp. 820–825, 2007.

[16] E. Carrasco, J. A. Encinar, and M. Barba, "Bandwidth improvement in large reflectarrays by using true-time delay," *IEEE Transactions on Antennas and Propagation*, vol. 56, no. 8, pp. 2496–2503, 2008.

[17] J. Huang, "Bandwidth study of microstrip reflectarray and a novel phased reflectarray concept," in *Proceedings of the IEEE Antennas and Propagation Society International Symposium*, pp. 582–585, Newport Beach, Calif, USA, June 1995.

[18] E. Carrasco, M. Arrebola, J. A. Encinar, and M. Barba, "Demonstration of a shaped beam reflectarray using aperture-coupled delay lines for LMDS central station antenna," *IEEE Transactions on Antennas and Propagation*, vol. 56, no. 10, pp. 3103–3111, 2008.

[19] E. Carrasco, M. Barba, and J. A. Encinar, "Design and validation of gathered elements for steerable-beam reflectarrays based on patches aperture-coupled to delay lines," *IEEE Transactions on Antennas and Propagation*, vol. 59, no. 5, pp. 1756–1761, 2011.

[20] CEA LETI, http://www.leti.fr/.

[21] F. Souchon, P. L. Charvet, C. Maeder-Pachurka, and M. Audoin, "Dielectric charging sensitivity on MEMS switches,"

in *Proceedings of the14th International Conference on Solid-State Sensors, Actuators and Microsystems*, pp. 363–366, Lyon, France, June 2007.

[22] N. Torres Matabosch, F. Coccetti, R. Plana, B. Reig, and J. L. Cazaux, "A High Isolation T-switch for reconfigurable switching matrix," in *Proceedings of the 11th International Symposium on RF MEMS and RF Microsystems (MEMSWAVE '10)*, Otranto, ITALY, June 2010.

[23] CST Microwave Studio®, http://www.cst.com/.

[24] D. Caratelli, M. C. Vigano, G. Toso, and P. Angeletti, "Analytical technique for constrained sparse array synthesis problems," in *Proceedings of the 32nd ESA Antenna Workshop on Antennas for Space Applications*, Noordwijk, The Netherlands, October 2010.

[25] H. Legay and B. Salome, "Low-loss reconfigurable reflector array antenna," U. S. Patent 7, 142, 164 B2, 2006.

[26] E. Carrasco, M. Barba, and J. A. Encinar, "Switchable-beam reflectarray antenna with gathered elements using different lattices," in *Proceedings of the 6th Loughborough Antennas and Propagation Conference (LAPC '10)*, pp. 197–200, Loughborough, UK, November 2010.

[27] E. Carrasco, M. Arrebola, M. Barba, and J. A. Encinar, "Shaped-beam reconfigurable reflectarray with gathered elements in an irregular lattice for LMDS base station," in *Proceedings of the 5th European Conference on Antennas and Propagation (EUCAP '11)*, pp. 975–978, Rome, Italy, April 2011.

[28] P. Gay-Balmaz, J. A. Encinar, and J. R. Mosig, "Analysis of multilayer printed arrays by a modular approach based on the generalized scattering matrix," *IEEE Transactions on Antennas and Propagation*, vol. 48, no. 1, pp. 26–34, 2000.

Hindawi Publishing Corporation
International Journal of Antennas and Propagation
Volume 2012, Article ID 535673, 6 pages
doi:10.1155/2012/535673

Research Article

Direct Synthesis of Dual-Parameter Concentric Ring RA with Enhanced Bandwidth

Bui Van Ha,[1] Paola Pirinoli,[2] Riccardo E. Zich,[1] and Marco Mussetta[1]

[1] *Dipartimento di Energia, Politecnico di Milano, 20156 Milan, Italy*
[2] *Dipartimento di Elettronica e Telecomunicazioni, Politecnico di Torino, 10129 Turin, Italy*

Correspondence should be addressed to Paola Pirinoli, paola.pirinoli@polito.it

Received 3 March 2012; Accepted 25 June 2012

Academic Editor: Sandra Costanzo

Reflectarray antennas (RAs) are nowadays a quite popular technology, used in several applications, due to a significant number of attractive properties, such as low cost, low weight, conformal deployment, and the possibility of introducing suitable reconfigurable capabilities. Unfortunately, they present also some intrinsic limitations and drawbacks compared with other solutions and, in particular, a relatively narrow bandwidth; that of course could be enlarged, but generally with a drastic increase of the structure complexity. The objective of this work is the design of a single-layer passive reflectarray, in which the reradiated elements have no conventional shape and enough degrees of freedom to compensate both the spatial and frequency phase variation of the reradiated field. In particular, here we focus on a reradiating element consisting in two concentric square rings in which two different and quite independent geometric parameters are varied.

1. Background and Aim of the Work

As it is well known, reflectarray (RA) antennas consist of one or more feed antennas illuminating a usually flat reflecting surface, whose electromagnetic reflecting performances have to be suitably designed in order to obtain the required performances of the whole radiating system. Reflectarray antennas have been first proposed in 1963 by Berry et al. [1], where the reflecting surface consisted of a planar array of variable length shorted waveguide components. So, the original reflectarray antenna was definitively not a low cost, easy to manage, light antenna, allowing foldability or any other of the interesting features that nowadays are typical properties of reflectarray solutions.

Probably this is the reason why for more than a decade this strange solution, without apparent advantages but with evident drawbacks compared, for example, with parabolic reflectors, has not been considered again, till 1975, when the feasibility of a reflectarray with scanning possibilities has been claimed in a US patent [2]. In this case a reflecting surface consisting of spiral antenna elements has been proposed, where each reradiating element uses a suitable set of diodes to manage properly the phase of the reflected wave allowing even some beam scanning of the whole system. So it is possible to say that, from the very beginning, the usual way of enhancing reflectarray antenna electromagnetic performances in order to introduce them in real life application is to exploit complexity at most.

The real breakthrough in reflectarray technology came when the evolution of printed circuit technology and high-frequency laminates synthesis allowed low-profile, light-weight implementations. In fact, even if the first reflectarray patent introducing a microstrip patch antenna-based reflecting surface has been published in 1977 [3], it is only from the late eighties that this kind of solution spread out.

Furthermore, in order to achieve good antenna performances, a very large array of patches has to be suitably designed exploiting in the proper way all the possible geometrical free parameters, requiring the adoption of numerical electromagnetic solvers, sophisticated numerical optimization tools, and in any case a significant numerical effort.

These, that is, the technology enablement and the numerical modeling tool availability, are the reasons why only nowadays printed reflectarrays technology became well assessed, and in the last years it substituted other technologies in many fields of applications, in particular where it is

of paramount importance to fulfill constraints such as high gain, narrow beam with low side lobes, light weight and smaller volume, easiness of deployment, and foldability.

The main limitation now to a complete diffusion of this kind of solutions is due to the fact that the most recent antenna systems require a very large bandwidth, typically even the multiband operability or the possibility of beam steering, features that are still difficult goals to be achieved with a printed reflectarray.

In fact, for what concerns the bandwidth, it is intrinsically limited for two different orders of reasons: the poor bandwidth of printed radiating elements themselves, usually no larger than the 3–6%, and, most important, the frequency dependence of the phase delay of the incident field. In particular this second aspect is quite critical and becomes dominant in large RAs [4, 5], since it requires that the RA elements should be able to compensate different phase delays at different operating frequencies.

The usual assessed way to enhance the RA bandwidth is that of using radiating elements that consist in two or more stacked printed single radiators (see, for instance, [6–8]). However, this technique results in a heavier, bulkier, and quite complex reradiating structure, requiring a careful and expensive manufacturing and presenting some difficulties for its foldability.

Recently, alternative solutions have been proposed, in which the RA elements are single-layer printed patches of nonconventional shape [9–14], properly chosen in order to present more degrees of freedom with respect to the one usually adopted for multilayer stacked structures, which can be used to compensate the frequency variation of the phase, allowing the bandwidth enhancement. Among all the different types of patches that have been considered for this purpose, particular interest has been devoted to concentric rings of different shape, since this kind of choice looks promising as an effective compromise between a moderate increase of the complexity of the single patch geometry and its phase compensation capabilities. Furthermore, this type of radiating elements intrinsically possess different degrees of freedom, since the size and the width of the single rings could be varied independently; moreover it has a reduced resonance sizes and finally it has been seen that if such kind of elements are used in a multilayer structure, in which the elements of each layer work in a different frequency band, they do not affect each others, allowing the realization of a multilayer, multiband structure. Despite of the large number of degrees of freedom, in most of the RAs in which concentric rings are used, only one geometric parameter is independently varied [11–13], while the others are changed proportionally: in this way it is possible to easily enlarge the bandwidth but not enough to fulfill the requirements in several applications.

These are the reasons why, in the framework of this paper, we consider as radiating element a concentric double-square ring configuration, in which at least two geometrical parameters are varied. In this way, it is possible to compensate with one parameter the spatial phase shift and with the other the frequency variation of the incident field phase, so that the reradiated field remains almost the same in the whole bandwidth, overcoming the previously considered limitations. In other words, it means that each element of the array has to provide a phase contribution to the reradiated field that varies both with the element position and with the frequency. With the aim of validating the effectiveness of the such reradiating element, we considered different RAs with increasing size: the results of their full-wave analysis show that the proposed reradiating element is a good candidate for single-layer, large-bandwidth reflectarrays.

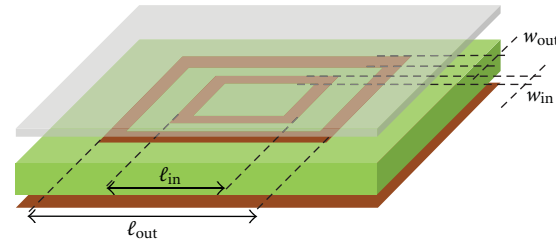

Figure 1: Geometry of the considered reradiating element.

2. RA Unit Cell

The RA reradiating element considered in this work is of the type sketched in Figure 1, and it consists of two square concentric rings, each one characterized by its side length ℓ, and width w. The structure in Figure 1 is therefore characterized by several degrees of freedom, that is, the two lengths, the two widths, and the aspect ratios, which are not completely independent: since the choice of which one of them has to be varied to control that the phase of the reradiated field is not electromagnetically equivalent, the first analysis carried out has been finalized to figure out which set of all the possible different geometrical parameters of a two concentric ring configuration may present the best phase variation.

In order to achieve this result, for all of them the variation of the reradiated field with a suitable set of different couples of geometrical parameters has been computed, considering the element embedded in an infinite periodic lattice and adopting a full-wave MoM approach. An example of the kind of obtained results is reported in Figure 2, where the phase variation provided is reported as a function of the size ℓ_{out} of the outermost ring and the aspect ratio p, which relates the size of the inner ring to that of the outer one; that is, $\ell_{in} = p\ell_{out}$; the two ring widths (w_{out}, w_{in} in Figure 1) have been instead maintained proportional to the size of the relative ring. This couple of geometrical parameters is the one used to design the entire RAs, whose numerical results are shown in the next section.

Figures 3 and 4 report the phase variation due to the variation of the side length ℓ_{out}, for a fixed value of the aspect ratio p and due to the variation of p, fixed ℓ_{out}, respectively. The three curves in the two figures refer to different frequencies. From these figures, it is possible to conclude that all these phase curves present a significant phase range, more remarkable when ℓ_{out} is varied, running from around 300 to more than 600 degrees, and an important

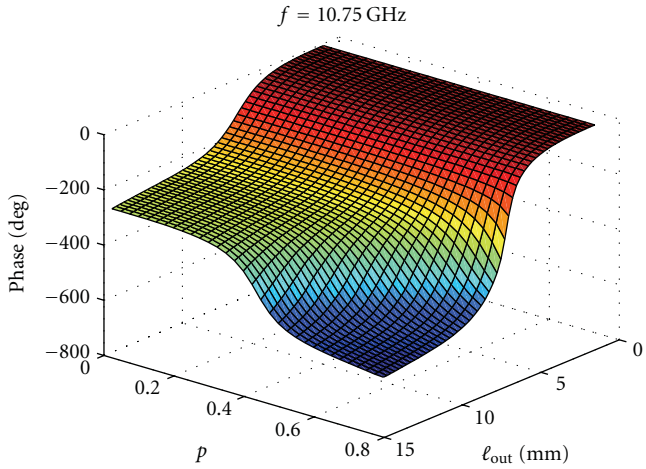

Figure 2: Phase variation provided at 10.75 GHz as a function of two geometrical parameters.

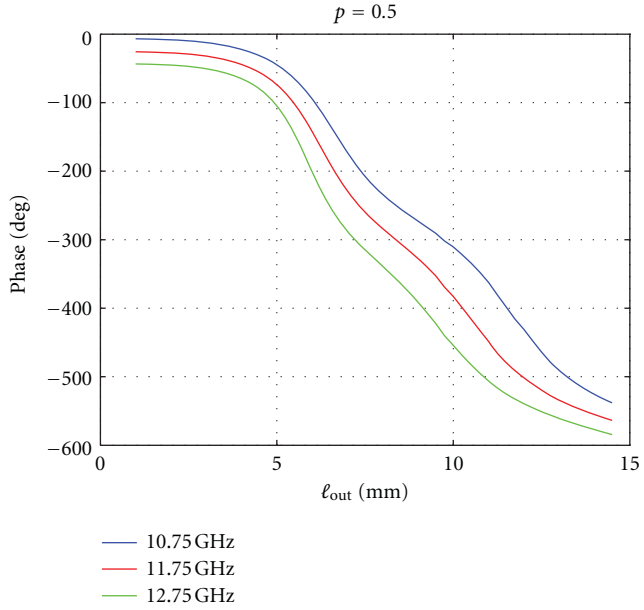

Figure 3: Phase variation provided a as a function of ℓ_{out}.

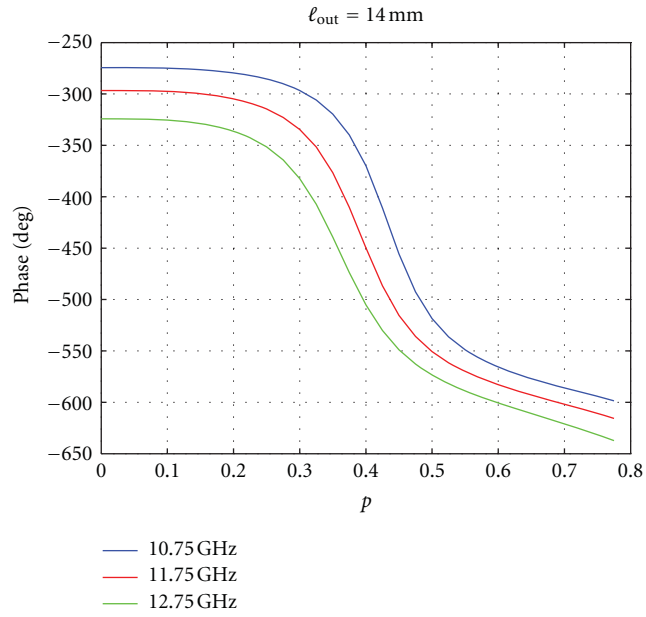

Figure 4: Phase variation provided as a function p.

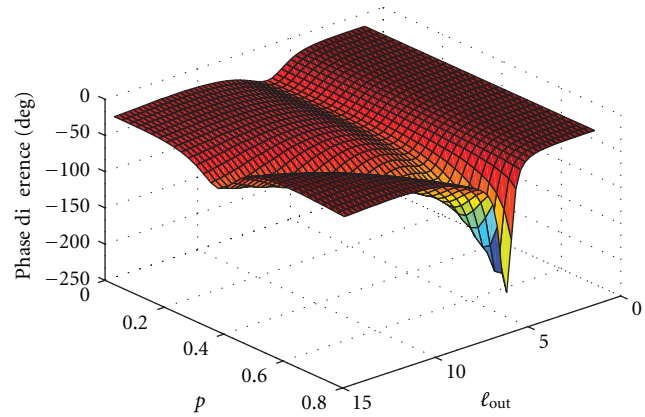

Figure 5: Difference between the phase at the central frequency and at one extreme of the band as a function of ℓ_{out} and p.

quasi-linear behavior: moreover, curves corresponding to different frequencies are almost parallel.

The design of each reradiating element in a RA, which implies the optimal choice of ℓ_{out} and p giving the proper phase value to compensate both the phase delay introduced by the distance between the feed and the element and the variation due to the frequency, requires not only the phase maps like the one shown in Figure 2, but also those like the one in Figure 5, reporting the difference between the curves of the phase variation with the two selected geometrical parameters computed at the central frequency and at an extreme of the band. Adopting the design procedure described in [14], it is therefore possible to find the proper values of ℓ_{out} guaranteeing the compensation of the phase delay introduced by the path between the feed and each element; then it is possible to act on p to assure the proper variation of this phase with frequency.

3. Numerical Results

In order to experimentally validate the synthesis design concepts previously detailed and, in particular, to prove the real possibility to enhance the bandwidth with the use of the introduced double parameters reradiating element, two reflectarray configurations of different size have been considered. Both of them are offset fed, since in that case the distances between the feeder and the lower and upper sides of the reflector are quite different and the frequency compensation of the introduced delays is more complex to achieve. The planar reflectors have been designed in such a way that the direction of maximum radiation is slanted with respect to the broadside: in this way it is possible to

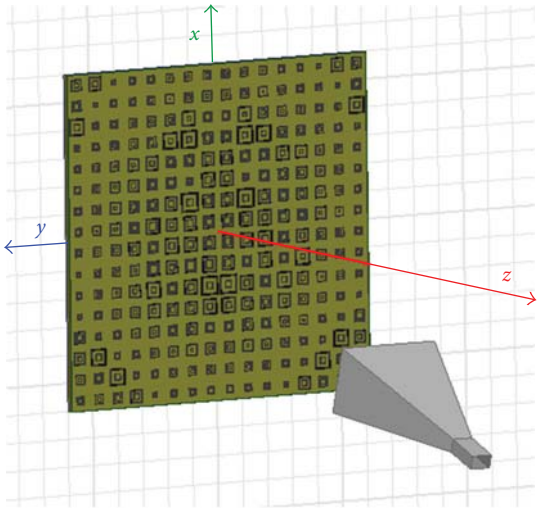

Figure 6: View of the designed 16 × 16 RA geometry.

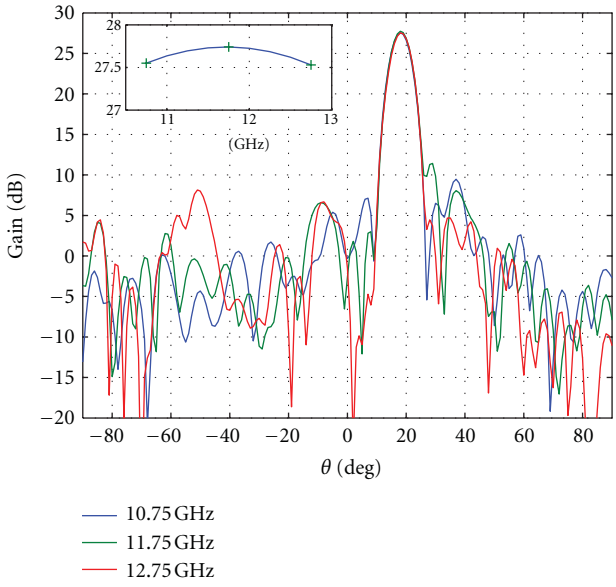

Figure 7: Radiation patterns of the 16 × 16 RA computed at three different frequencies in the plane $\phi = 0°$. Inset: gain frequency variation.

better control if the phase compensation introduced by the reradiating elements is effective at the different frequency, checking if the direction of maximum radiation remains constant. The first RA we considered is the configuration depicted in Figure 6, consisting in a 16 × 16 planar reflector fed by a rectangular horn located at a distance of 390 mm along the z-axis and of 125 mm along the x-axis from the center of the coordinate system, which is coincident with the central point of the reflector. To improve the reradiating elements performances, a two-layered dielectric structure has been used, consisting of a substrate characterized by height $h_1 = 5$ mm and relative dielectric constant $\epsilon_{r1} = 1.1$ and in a cover with $h_2 = 0.85$ mm and $\epsilon_{r2} = 2.5$.

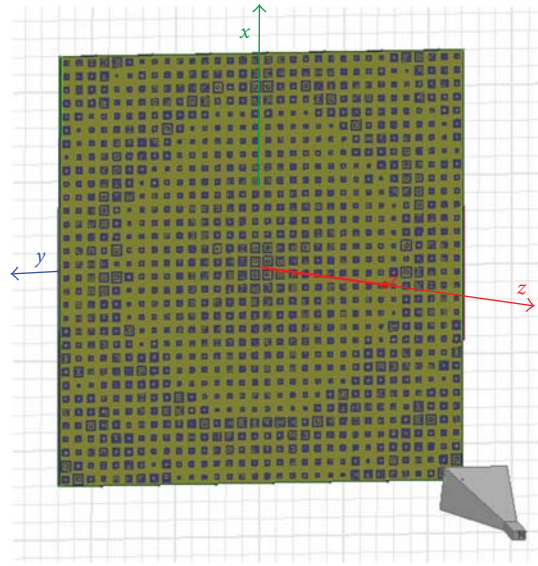

Figure 8: View of the designed 32 × 32 RA geometry.

The structure has been designed using the two degrees of freedom of the double-ring reradiating elements to obtain the maximum reradiation in a direction tilted of 18° with respect to the normal and to minimize the gain variation in the frequency range [10.75–12.75] GHz, as reported in Figure 7.

The entire RA has been analyzed using a commercial full-wave simulator [15], and the radiation patterns for different frequencies have been computed. In Figure 7 the radiation patterns in the plane $\phi = 0°$ computed at the extremes and at the center of the frequency band are shown: in this case, not only the gain variation is really small, lower than 0.5 dB in the entire band, but the side lobe level remains almost constant and below −18 dB with respect to the maximum.

The second considered configuration is the 32 × 32 planar reflector depicted in Figure 8. In this case the rectangular horn is located at a distance of 671 mm along the z-axis and of 217.5 mm along the x-axis from the center of the coordinate system, which is coincident with the central point of the reflector. As in the previous design, in order to improve the reradiating elements performances, the same two-layered dielectric structure has been used, consisting in a substrate characterized by height $h_1 = 5$ mm and relative dielectric constant $\epsilon_{r1} = 1.1$ and in a cover with $h_2 = 0.85$ mm and $\epsilon_{r2} = 2.5$. As in the previous case, the planar reflector has been optimized to work on the frequency band [10.75–12.75] GHz and to have a direction of maximum radiation tilted of 18° with respect to broadside.

In Figure 9 the 3D radiation pattern of the reflectarray, computed at the central frequency, is reported, showing the high directivity of the designed structure and the absence of unwanted high lobes apart from those around the maximum.

Finally, in Figure 10 the cuts in the vertical plain for three different frequency values are shown: the main lobe is almost coincident in the three cases, and no shift of the main beam occurs changing frequency. The side lobes

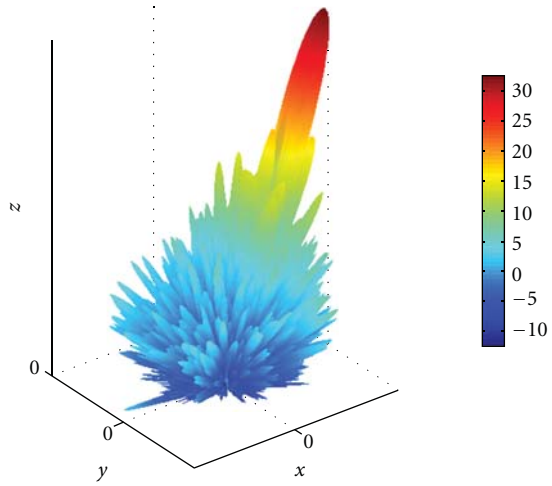

Figure 9: 3D radiation patterns of the 32 × 32 RA computed at the central frequency.

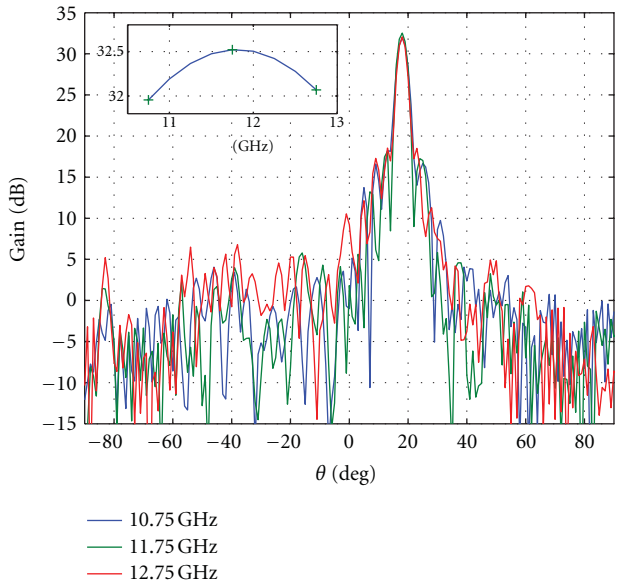

Figure 10: Radiation patterns of the 32 × 32 RA computed at three different frequencies in the plane $\phi = 0°$. Inset: gain frequency variation.

slightly increase with the frequency, but in any case they are well controlled. Finally, in the figure inset it is reported the frequency behavior of the gain, showing that also in this case it remains almost constant on the entire bandwidth.

4. Conclusions

In this paper we present the design of planar reflectarray antennas using concentric square rings as reradiating elements. In opposite to what already published, here two geometric parameters have been varied in order to better control both the spatial and frequency phase variation of the reradiated field and to overcome one of the main drawbacks of the RAs, that is, their narrow bandwidth. The full-wave numerical analyses, carried out on two sample antennas of 256 and 1024 elements, respectively, show a 1 dB gain bandwidth of almost the 17% and confirm the promising characteristics of such radiating elements.

Acknowledgment

This work was partially supported by the Italian Ministry of Education in the frame of the National Interest Research Project "Active reflectarray antenna for mobile terminal" (2008N3B2LP_001).

References

[1] D. Berry, R. Malech, and W. Kennedy, "The reflectarray antenna," *IEEE Transactions on Antennas and Propagation*, vol. 11, no. 6, pp. 645–651, 1963.

[2] H. R. Phelan, US3925784, 1975.

[3] C. S. Malagisi, US4053895, 1977.

[4] J. Huang, "Bandwidth study of microstrip reflectarray and a novel phased reflectarray concept," in *Proceedings of the IEEE International Symposium on Antennas and Propagation*, pp. 582–585, Newport Beach, California, USA, June 1995.

[5] D. M. Pozar, "Bandwidth of reflectarrays," *Electronics Letters*, vol. 39, no. 21, pp. 1490–1491, 2003.

[6] J. A. Encinar, "Design of two-layer printed reflectarrays using patches of variable size," *IEEE Transactions on Antennas and Propagation*, vol. 49, no. 10, pp. 1403–1410, 2001.

[7] J. A. Encinar, M. Arrebola, L. F. de la Fuente, and G. Toso, "A transmit-receive reflectarray antenna for direct broadcast satellite applications," *IEEE Transactions on Antennas and Propagation*, vol. 59, no. 9, pp. 3255–3264, 2011.

[8] L. S. Ren, Y. C. Jiao, F. Li, J. J. Zhao, and G. Zhao, "A dual-layer T-shaped element for broadband circularly polarized reflectarray with linearly polarized feed," *IEEE Antennas and Wireless Propagation Letters*, vol. 10, pp. 407–410, 2011.

[9] L. Moustafa, R. Gillard, F. Peris, R. Loison, H. Legay, and E. Girard, "The phoenix cell: a new reflectarray cell with large bandwidth and rebirth capabilities," *IEEE Antennas and Wireless Propagation Letters*, vol. 10, pp. 71–74, 2011.

[10] S. H. Yusop, N. Misran, M. T. Islam, and M. Y. Ismail, "Analysis on split concept of reflectarray antenna element for bandwidth enhancement," in *Proceedings of the IEEE International Conference on Space Science and Communication*, pp. 273–276, Penang, Malaysia, 2011.

[11] M. E. Bialkowski and K. H. Sayidmarie, "Investigations into phase characteristics of a single-layer reflectarray employing patch or ring elements of variable size," *IEEE Transactions on Antennas and Propagation*, vol. 56, no. 11, pp. 3366–3372, 2008.

[12] D. Zhou, Z. Niu, and R. Li, "Investigation on a single-layer microstrip circular-patch/ring-combination reflectarray element," in *Proceedings of the Cross Strait Quad-Regional Radio Science and Wireless Technology Conference (CSQRWC '11)*, vol. 1, pp. 664–667, Haerbin, China, 2011.

[13] M. Mussetta, P. Pirinoli, P. T. Cong, M. Orefice, and R. E. Zich, "Characterization of microstrip reflectarray square ring elements by means of an Artificial Neural Network," in *Proceedings of the 4th European Conference on Antennas and Propagation (EuCAP '10)*, pp. 1–4, April 2010.

[14] P. de Vita, A. Freni, G. L. Dassano, P. Pirinoli, and R. E. Zich, "Broadband element for high-gain single-layer printed reflectarray antenna," *Electronics Letters*, vol. 43, no. 23, pp. 1247–1249, 2007.

[15] ANSYS HFSS^{TM}, http://www.ansys.com/.

Hindawi Publishing Corporation
International Journal of Antennas and Propagation
Volume 2012, Article ID 846017, 11 pages
doi:10.1155/2012/846017

Research Article

Bandwidth Behavior of Closely Spaced Aperture-Coupled Reflectarrays

F. Venneri, S. Costanzo, and G. Di Massa

Dipartimento di Elettronica, Informatica e Sistemistica, Università della Calabria, 87036 Rende, Italy

Correspondence should be addressed to S. Costanzo, costanzo@deis.unical.it

Received 2 March 2012; Revised 7 June 2012; Accepted 14 June 2012

Academic Editor: Raphaël Gillard

The bandwidth features of reflectarray antennas are analyzed by examining in detail the phase errors due to the compensation mechanism for spatial phase delays. A bandwidth estimation rule is defined, taking into account the combined effects due to the overall antenna geometry and the frequency response of the single reflectarray element. An aperture-coupled reflectarray configuration with reduced interelement spacing is considered as broadband solution for the implementation of small reflectarrays. A 20 GHz aperture-coupled element is synthesized for the design of a 12λ diameter reflectarray, showing a simulated 1 dB gain bandwidth of 23%.

1. Introduction

Reflectarray antennas offer many advantages over traditional reflector antennas. They combine the best features of microstrip technology with those related to parabolic reflectors. As a matter of fact, reflectarrays are low profile antennas, characterized by a cheaper fabrication process, also offering improved efficiencies due to the spatial feeding approach. As counterpart to the above advantages, reflectarrays are usually constrained to operate over a small frequency band, mainly caused by the limited bandwidth of microstrip radiators and the frequency dependence of the spatial phase delay in the paths from feed to array elements. This last effect is dominant for reflectarrays with large aperture diameters D and small focal distances F from the feed, resulting in reduced F/D ratios (typically $F/D \leq 0.6$). Conversely, in the case of reflectarrays with moderate aperture dimension and F/D ratio greater than 0.6, the dominant factor limiting the antenna bandwidth is the frequency band of the single radiator.

Different solutions have been proposed to improve the bandwidth performances of reflectarray antennas.

A first class of solutions, essentially based on the exact compensation of the phase error accumulated in the different feed-element paths, comprises the use of real delay lines [1] and stacked configuration based on the use of a three-layer reflectarray with different size patches [2]. A piecewise planar reflectarray configuration is also proposed in [3], which approximates the parabolic surface thus introducing a geometric compensation of the feed-elements path delay, just as in the case of parabolic reflectors.

A second group of solutions focuses on the design of broadband reflectarray elements. A complete overview of all existing wideband reflectarray configurations is presented in [4], including the use of thicker substrates with low permittivity, two-layer stacked patches having variable size, and aperture-coupled configuration with a phase tuning line. These structures are suitable for the implementation of small reflectarrays ($D < 50\lambda_0$ at the operating frequency f_0) with wideband performances.

A further improvement in the bandwidth of aperture-coupled reflectarrays has been demonstrated by the authors in [5] through the reduction of the array lattice spacing. As a matter of fact, the use of closely spaced elements gives reflection phase curves with a smoother behavior with respect to the fixed tuning parameter as well as the frequency. As demonstrated in [6], this configuration can be effectively adopted for the design of broadband reflectarrays with reduced size.

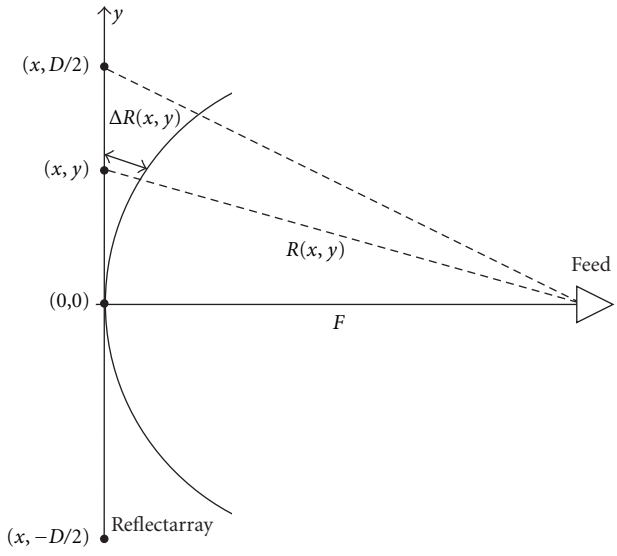

Figure 1: Reflectarray geometry.

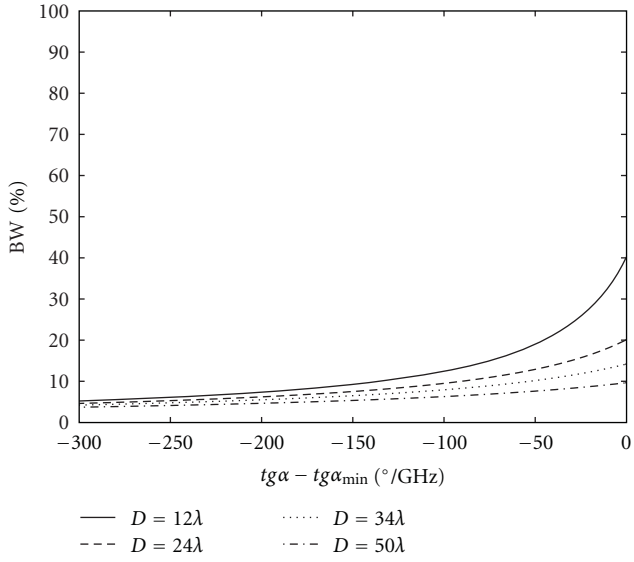

Figure 2: Percent bandwidth versus normalized phase curve slope for different array diameters ($F/D = 0.5$).

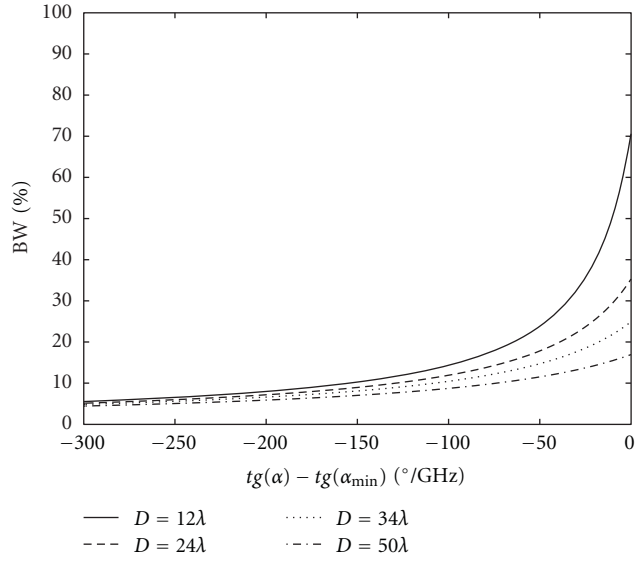

Figure 3: Percent bandwidth versus element phase curve slope for different array diameters ($F/D = 1$).

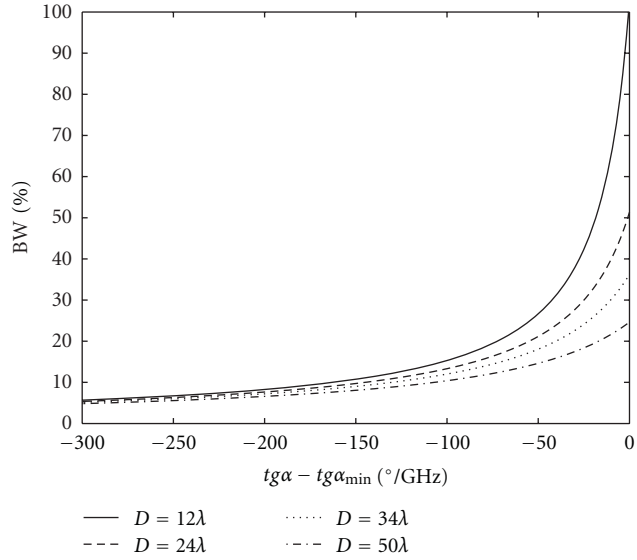

Figure 4: Percent bandwidth versus element phase curve slope for different array diameters ($F/D = 1.5$).

In this work, the bandwidth features of small reflectarrays are analyzed in terms of the phase errors due to the compensation mechanism for the spatial phase delays. A bandwidth estimation formula is derived which takes into account for the combined effects due to the overall antenna geometry and the frequency response of the single reflectarray element. The above formula provides an upper limit to the bandwidth achievable in the case of small reflectarrays with fixed geometry (D and F/D values), giving a way to quantify the enhancement contribution due to elements with smoother phase curves. The adopted bandwidth evaluation approach is applied to the analysis of some reflectarrays prototypes, and it is shown that the relative 1 dB gain bandwidth value follows very well the behavior given by the proposed formula. As a matter of fact, other approaches existing in the literature [7, 8] for the bandwidth evaluation of reflectarrays assumed as validation reference the frequency range limiting the 1 dB gain of the antenna, that is, a zone where small or very negligible gain variations occur. In our case, the slope variations of the phase curves are taken into account to give a better upper bound with respect to the methods proposed in literature [7, 8]. Although it is not demonstrated that an exact correlation exists between the proposed formula and the 1 dB gain bandwidth, the comparisons with this parameter are useful to make a qualitative analysis of the

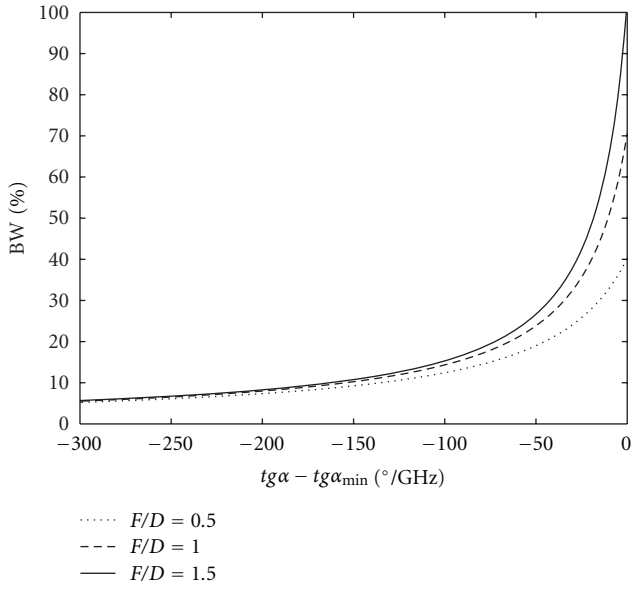

Figure 5: Percent bandwidth versus element phase curve slope for different F/D ratios ($D = 12.4\lambda$).

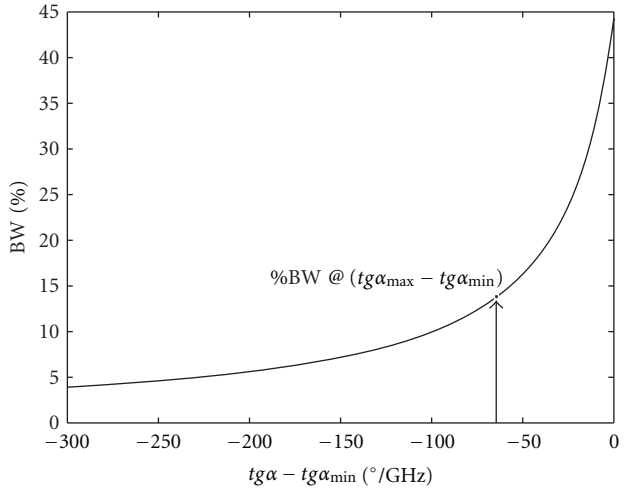

Figure 6: Percent bandwidth estimation for a 28 GHz reflectarray ($D = 14\lambda_0 - F/D = 0.69$) at a fixed phase curve slope.

reflectarray bandwidth improvement due to a proper choice of the single element configuration.

Furthermore, a 20 GHz aperture-coupled element with a unit cell size smaller than $\lambda/2$ is presented as broadband reflectarray radiator. The patch is printed on a 1 mm-thick substrate of foam which also contributes to the element bandwidth enlargement. The synthesized element offers a phase curve with a very smooth behavior, essentially caused by the mutual coupling among the patches.

A significant bandwidth improvement (corresponding to a 1 dB gain bandwidth equal to 23%) is demonstrated for a 12λ diameter reflectarray operating at the frequency $f = 20$ GHz.

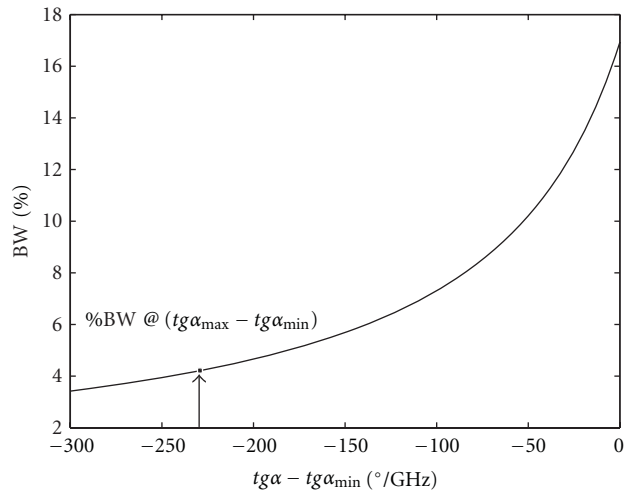

Figure 7: Percent bandwidth estimation for a 28 GHz reflectarray ($D = 21\lambda_0 - F/D = 0.32$) at a fixed phase curve slope.

2. Bandwidth Estimation for Small Reflectarray Antennas

The bandwidth of reflectarray antennas is strongly affected by the compensation mechanism for different phase delays in the paths from the feed to each array element. This effect is dominant in the case of large reflectarrays, so the development of techniques able to exactly compensate the differential phase delay in a large frequency range is required. Some of these techniques have been implemented in [1–4], giving appreciable bandwidth improvements. As demonstrated in [4, 7, 8], the frequency dependence of the differential phase delay has a minor effect on the bandwidth of small reflectarrays. In this case, it is usually sufficient to adopt a wideband element configuration, in order to obtain a reflectarray with a relative large bandwidth. However, also for small aperture reflectarrays, the antenna frequency behavior must be optimized by considering the combined effect due to the bandwidth of the single element as well as the frequency dependence of the phase delay in the signal incident on each array element. Infact, the reflectarray geometry features, namely, the antenna diameter D and the focal distance F, restrict the achievable bandwidth below an upper bound level [7, 8] that cannot be increased by the adoption of an element structure with wider bandwidth behavior. In order to demonstrate the above assertion, we consider the geometry of a center-fed reflectarray depicted in Figure 1. The feed antenna produces a spherical wave impinging on the reflectarray aperture. The path difference between the focal distance F and each ray departing from the feed up to the generic element position (x, y) is equal to the following:

$$\Delta R(x, y) = \sqrt{F^2 + x^2 + y^2} - F. \quad (1)$$

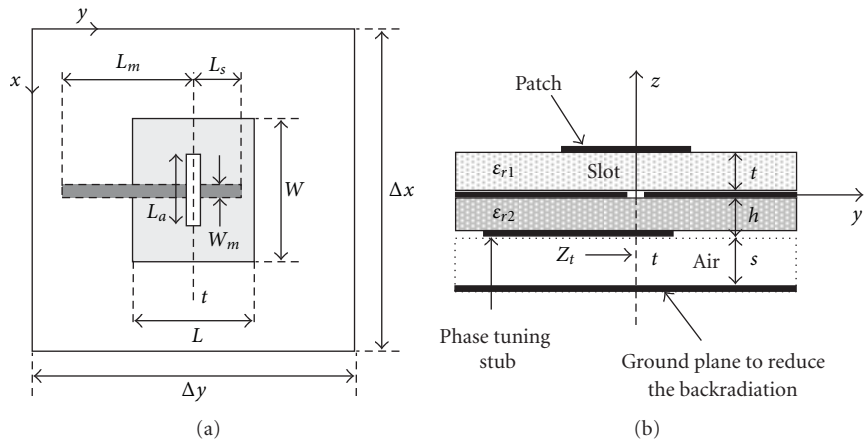

Figure 8: Aperture-coupled reflectarray unit cell—(a) top view and (b) side view.

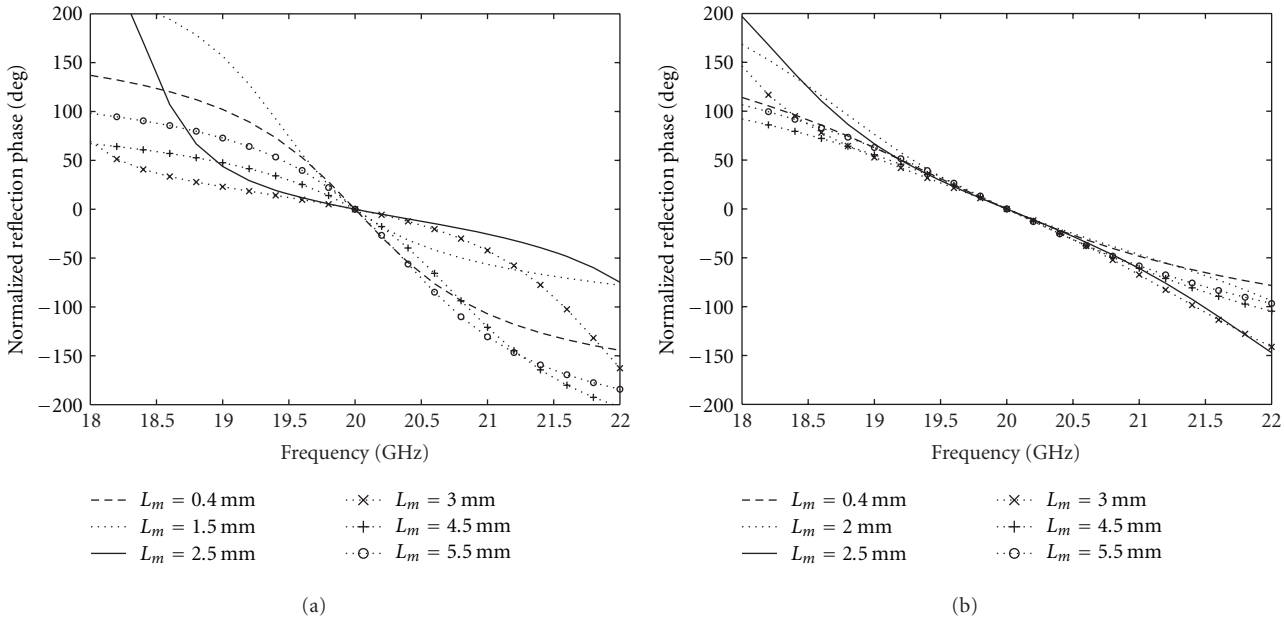

Figure 9: Calculated phase curves against frequency for various tuning line length—(a) $\Delta x = \Delta y = 0.6\lambda$; (b) $\Delta x = \Delta y = 0.4\lambda$.

A differential phase delay proportional to the above distance is imposed on each array position, giving the following incident phase:

$$\phi_{\text{inc}}(x, y, f) = -\frac{2\pi}{c_0} f\left(\sqrt{F^2 + x^2 + y^2} - F\right), \tag{2}$$

where c_0 is the light velocity in vacuum.

Each reflectarray element must be designed in order to compensate for the phase delay (2) and to steer the main beam along a desired direction, at a given frequency f_0 [9].

For simplicity, the case of a broadside reflectarray is considered, for which the compensating phase to be introduced by the array elements is given as

$$\phi_{\text{refl}}(x, y, f_0) = \frac{2\pi}{c_0} f_0\left(\sqrt{F^2 + x^2 + y^2} - F\right) \tag{3}$$

or

$$\phi_{\text{refl}}(x, y, f_0) = -\frac{2\pi}{c_0} f_0\left(\sqrt{F^2 + \frac{D^2}{4}} - \sqrt{F^2 + x^2 + y^2}\right), \tag{4}$$

according to the assumed phase normalization positions in the array grid, which are, respectively, the central element with coordinates $(x, y) = (0, 0)$ and the elements onto the rim of the array, namely, $(x, y) = (\pm D/2, 0)$ or $(x, y) = (0, \pm D/2)$.

This phase compensation approach guarantees the fulfillment of the imposed reflectarray design constraints only at the operating frequency f_0. Expression (2) shows that the phase of the signal incident on each element is a function of the frequency f, thus a wideband operation mode can be obtained only if the adopted reflectarray elements are able

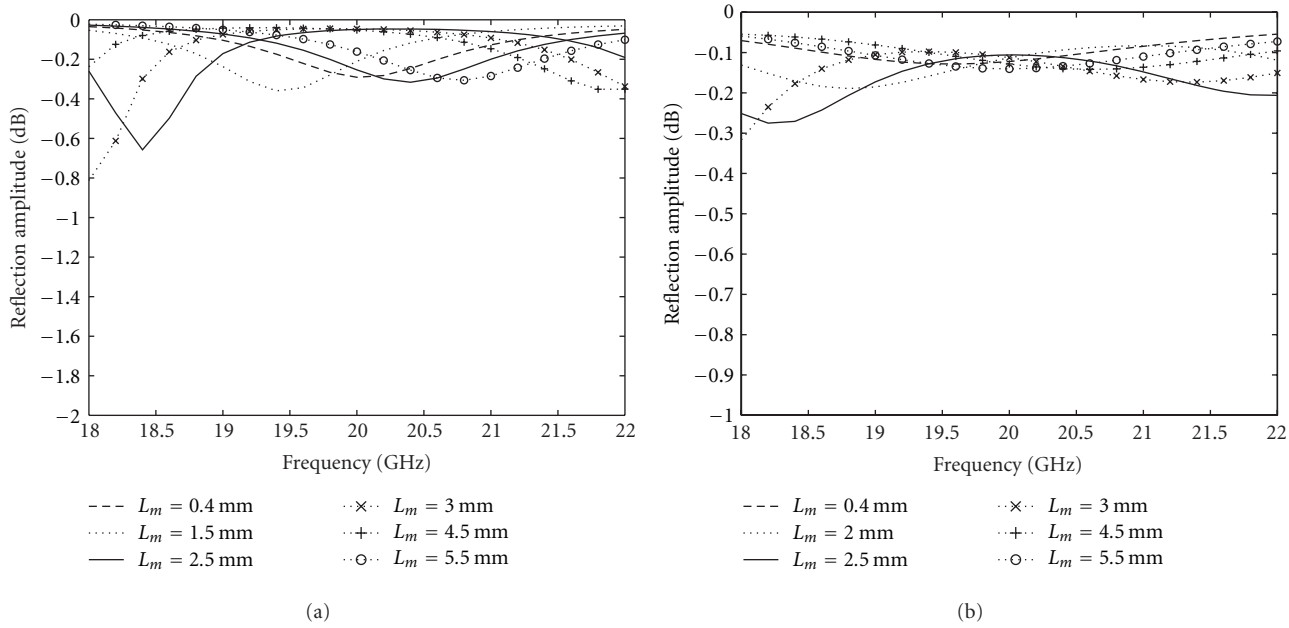

Figure 10: Calculated reflection amplitude against frequency for various tuning line length— (a) $\Delta x = \Delta y = 0.6\lambda$; (b) $\Delta x = \Delta y = 0.4\lambda$.

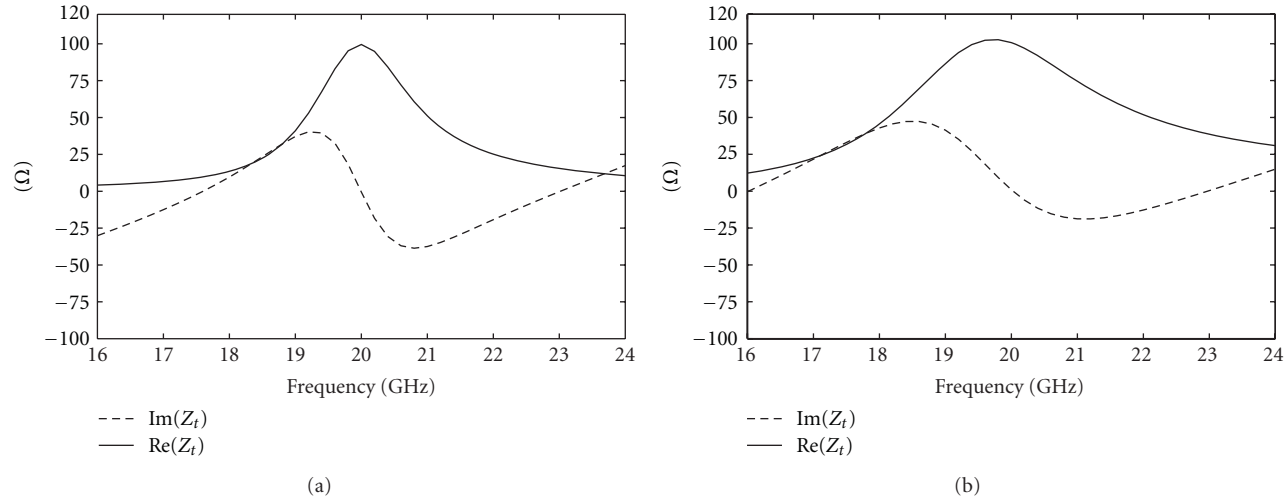

Figure 11: Simulated input impedance Z_t—(a) $\Delta x = \Delta y = 0.6\lambda$; (b) $\Delta x = \Delta y = 0.4\lambda$.

to exactly compensate the phase delay (2) in a rather wide neighborhood of f_0.

A further point to be considered is that the phase reflected by each reflectarray element is itself frequency-dependent, that is, $\phi_{\text{refl}}(x, y, f)$. Its behavior is strictly related to the nature of the considered compensation technique, (e.g., variable size patches, aperture-coupled patches with variable lines, etc.) and, usually, it does not match the condition imposed by the frequency compensation of the incident phase (2). This last condition, infact, would require a linear behavior of $\phi_{\text{refl}}(x, y, f)$ with respect to the frequency, with a slope equal to the opposite value of the frequency derivative of (2). This means that the phase of the field reflected by the elements should have a frequency dependence with slightly different slopes for each position of the array grid [8]. It is very difficult to achieve this goal with the commonly used reflectarray configurations. In fact, they are not able to separately control the compensating phase value at the operating frequency f_0, given by (3), and the rate of phase change with respect to the frequency f, given by the derivative $(\partial/\partial f)\phi_{\text{refl}}(x, y, f)$. Reflectarray configurations, based on the use of a single-phase tuning parameter, have a fixed frequency dependence for each achievable phase delay at the design frequency f_0.

Furthermore, the reflection phase curves of a broadband reflectarray element are almost parallel in a broad frequency range. This means that the slope of the reflection phase curves for a fixed reflectarray configuration can be assumed

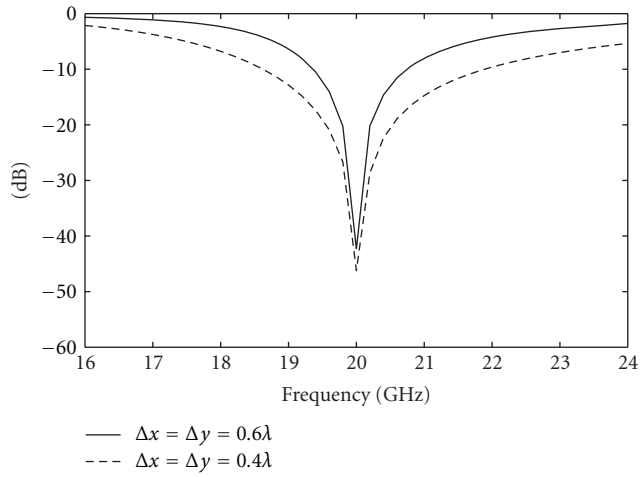

Figure 12: Simulated return loss.

constant with respect to the tuning parameter values. Thus, unless to develop reflectarray configurations offering more than one tuning parameter, in order to control both the required phase delay and the slope of the reflection phase curve, the bandwidth of this type of antenna cannot be optimized by the proper allocation of the elements in the array grid, according to the phase change rate requirements imposed by the derivative of expression (2).

Established that the incident phase (2) cannot be compensated for all frequencies, a phase error will occur, thus limiting the operating bandwidth of reflectarray antennas. In particular, the phase error increases when the operating frequency departs from the design frequency f_0, so introducing a reduction in the reflectarray gain bandwidth as well as a distortion of the synthesized radiation pattern.

The way to enlarge the bandwidth of a small reflectarray basically consists of the choice of an element configuration with a very slow frequency variation. However, the amount of achievable improvements by the adoption of phase curves with small slopes is limited by the antenna geometry. This fact is demonstrated below, by computing a new bandwidth estimation formula, like those presented in [7, 8], including also the dependence from the slope of the considered reflection phase curves. At this purpose, the frequency variation of the total phase obtained on the array surface is considered as follows:

$$\phi_{\text{tot}}(x, y, f) = \phi_{\text{inc}}(x, y, f) + \phi_{\text{refl}}(x, y, f) \tag{5}$$

with

$$\phi_{\text{refl}}(x, y, f) = \phi_{\text{refl}}(x, y, f_0) + tg\alpha(f - f_0), \tag{6}$$

where $tg\alpha$ is the phase variation rate versus frequency of the phase curve relative to the reflectarray elements. In general, $tg\alpha$ varies with the tuning parameter, then it is a function of the location (x, y). Furthermore, expression (6) assumes that the phase curves have a linear frequency dependence, but it is true only within a neighborhood of the frequency f_0, in accordance with the bandwidth performances of the adopted element configuration.

When the frequency varies from f_1 to f_2, with $f_1 < f_0 < f_2$, the maximum phase change at each element position is given as:

$$\Delta\phi_{\text{tot}}(x, y) = (f_1 - f_2)\left[tg\alpha - \frac{2\pi}{c_0}\left(\sqrt{F^2 + x^2 + y^2} - F\right)\right]. \tag{7}$$

In the case of broadband elements, characterized by phase curves with a strong similar slope for the various tuning parameter values, the phase error contribution in (7), due to the frequency dependence of the single radiator, can be considered identical in each location (x, y) of the array, thus it can be omitted. This condition is equivalent to the assumption made in [7, 8], where a bandwidth estimation formula is computed by neglecting the frequency dependence of the phase reflected by the single reflectarray element, that is, $tg\alpha = 0°/\text{GHz}$. Thus, in this case the achievable maximum bandwidth is substantially imposed by the antenna geometry.

In the other cases, namely, those concerning relatively narrowband elements, or broadband elements with phase curves not so parallel, the phase curves slope varies within a certain range, namely $tg\alpha \in (tg\alpha_{\min} \div tg\alpha_{\max})$. In this latter case, the bandwidth could result to be much lower than the upper bound value computed in [7, 8]. In particular, the wider is the slope variation range, the lower is the bandwidth upper bound level imposed in conjunction with the antenna geometry. At this purpose, the formula presented in [7] is changed in order to take into account the effects of the slope variation in the phase design curves associated to the adopted reflectarray elements.

Assuming a 360° phase error at the edge of the aperture due to the considered frequency excursion, just like in [7], the percentage bandwidth $\text{BW} = (f_2 - f_1)/f_0\%$ can be evaluated as follows:

$$\text{BW} = \frac{-2\pi}{f_0\left[\left(tg(\alpha) - tg(\alpha_{\min})\right) - (2\pi/c_0)\left(\sqrt{F^2 + (D^2/4)} - F\right)\right]} \times 100, \tag{8}$$

in which the coordinates (x, y) are fixed to the values corresponding to the edge aperture elements, that is, $(\pm D/2, 0)$ or $(0, \pm D/2)$. Furthermore, the phase error (7) is normalized with respect to the phase error contribution due to the minimum phase curve slope $tg\alpha_{\min}$, which is identical for each location (x, y).

As follows, expression (8) is considered for the estimation of the phase curves slope effect on the reflectarray bandwidth, for different values of the antenna geometrical parameters.

Figure 2 shows the behavior of the percentage bandwidth versus the normalized phase change rate $tg(\alpha) - tg(\alpha_{\min})$, for different values of the reflectarray diameter. The F/D ratio is fixed to a value equal to 0.5. It can be observed that BW decreases rapidly for higher phase change rates. Furthermore, for aperture diameters above the 40λ value, the bandwidth is less dependent from the element phase curve

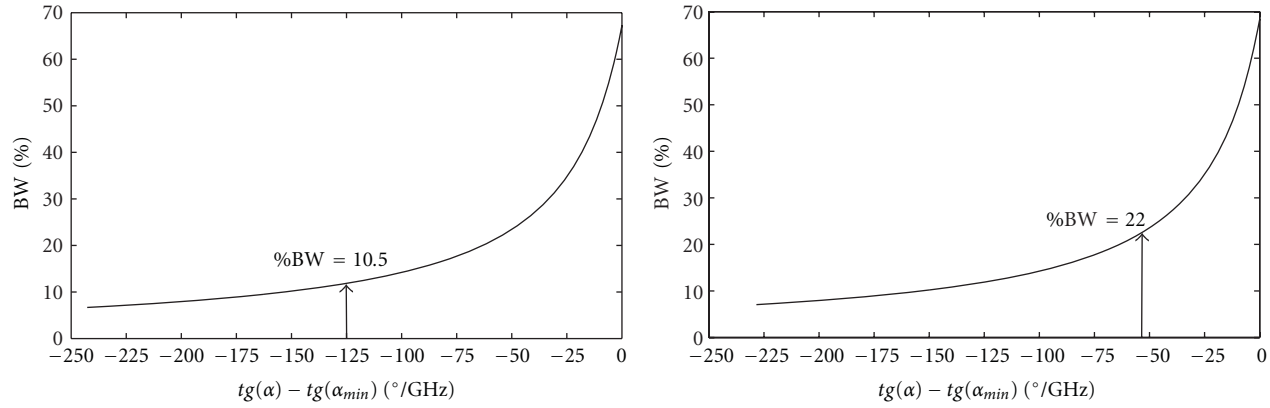

Figure 13: Percent bandwidth estimation ($D = 12.4\lambda_0$ – $F/D = 1$)—(a) $\Delta x = \Delta y = 0.6\lambda$; (b) $\Delta x = \Delta y = 0.4\lambda$.

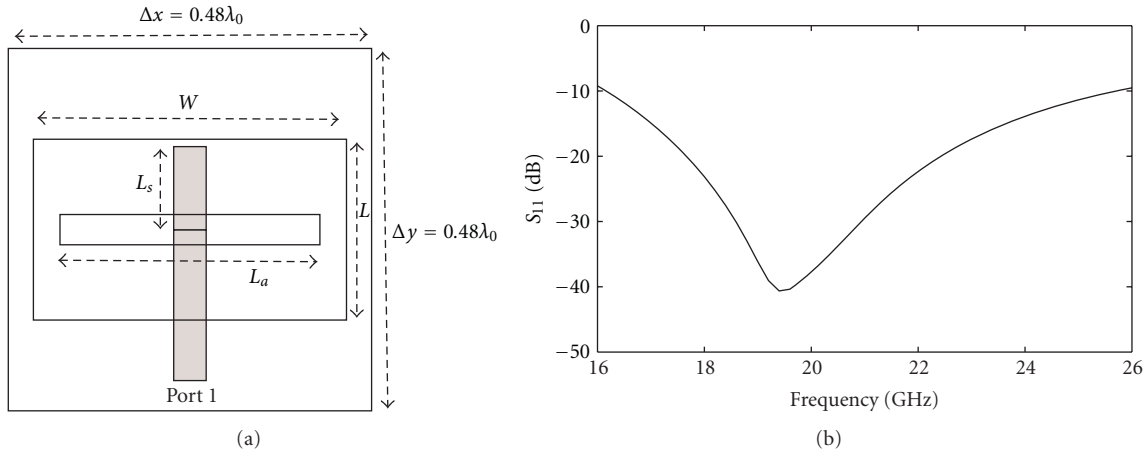

Figure 14: Aperture-coupled reflectarray unit cell—(a) top view and (b) simulated return loss at port 1.

slope. Similar considerations can be made for the graphs reported under Figures 3 and 4, illustrating the percentage bandwidth of a reflectarray with F/D ratios, respectively equal to 1 and 1.5. Also in these cases different values of the array diameter are considered. From the comparison of the three plots (Figures 2–4), it can be observed that the bandwidth increases for higher F/D ratios, but this trend is more pronounced for smaller array diameters. In every cases, it can be noted that a normalized phase change rate below the $-150°$/GHz value, makes the percentage bandwidth independent from the antenna geometry. As a matter of fact, in this case it is dominant the effect of the intrinsic narroband behavior of the single radiator.

A small variation in the normalized phase curve slope within the $[-50 \div 0]°$/GHz range may give a very large change in the estimated bandwidth value. This observation can be better appreciated in Figure 5, where the curves obtained for a 12.4λ aperture diameter are compared for different F/D ratios.

The bandwidth estimation, given by (8), is subject to certain changes due to the simplified assumption that the phase curves computed for different values of the tuning parameter are linear. However, the deviations from this ideal conditions are very small within the operating frequency range of broadband reflectarray element configurations. So, formula (8) gives a quite good trend of the bandwidth behavior for small reflectarray antennas.

In order to prove the effectiveness of the derived formula (8), this is adopted for the bandwidth estimation of two different reflectarrays with variable size elements, which have been presented in [9]. The antennas are characterized by the features reported in Table 1. In particular, the $tg(\alpha_{\max})$—column refers to the slope of the reflection phase curves computed for the element length giving the resonance at the operating frequency f_0, corresponding to the maximum phase curve slope. Since both the considered reflectarray configurations are narrowband, the slope of the phase curves varies very rapidly with both the frequency and the element length within the range $(tg\alpha_{\min} \div tg\alpha_{\max})$ specified in Table 1.

In the same table, a comparison with previuosly published data is also reported, which are, respectively, referred to the measured reflectarray gain bandwidth, reported in

Table 1: Bandwidth estimation values compared to previously published data.

Antenna parameters					Bandwidth values		
f_0 (GHz)	D (m)	F/D	$tg(\alpha_{\max})$ (°/GHz)	$tg(\alpha_{\min})$ (°/GHz)	Percentage BW measured [9]	Percentage BW calculated [8]	Percentage BW calculated (8)
28	0.152 ($\cong 14\lambda_0$)	0.69	−62	−1.5	5	22.1	13
28	0.23 ($\cong 21\lambda_0$)	0.32	−228	−0.8	2	8.5	4

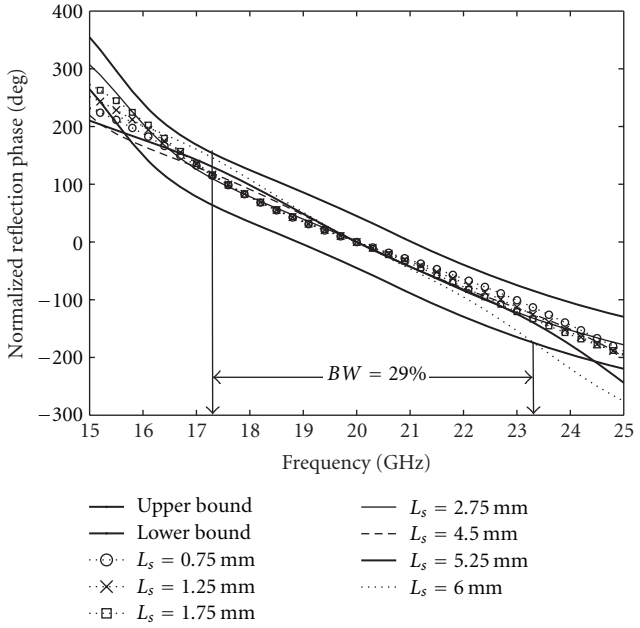

Figure 15: Calculated phase curves against frequency for various tuning line length.

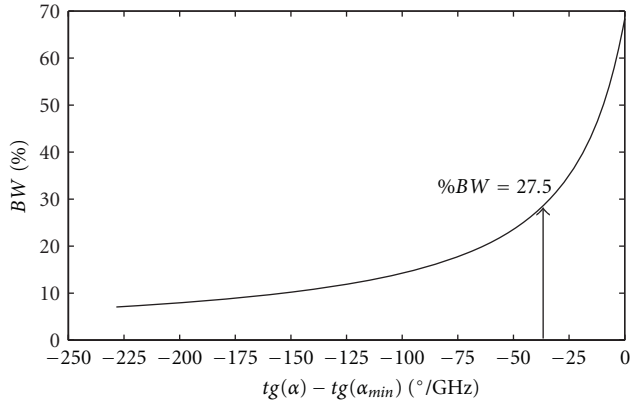

Figure 16: Percent bandwidth estimation ($D = 12\lambda_0$, $F/D = 1$, $\Delta x = \Delta y = 0.48\lambda$).

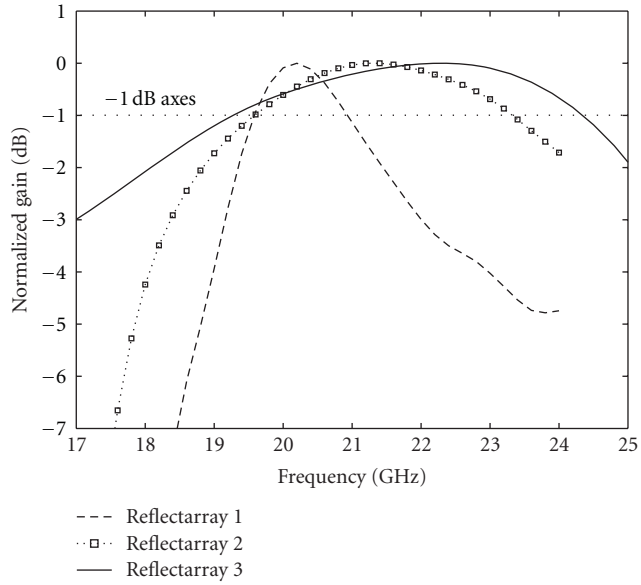

Figure 17: Comparison among the normalized gain patterns (broadside direction).

Table 2: Element stratification (reflectarray prototypes presented in [6, 7]).

Layer	Material	Thickness
Patch	Copper	35 μm
d1	Diclad 870 ($\varepsilon_{r1} = 2.33$)	$t = 0.762$ mm
Ground plane with slot	Copper	35 μm
d2	Diclad 870 ($\varepsilon_{r2} = 2.33$)	$h = 0.762$ mm
Phasing line	Copper	35 μm
d3	Air	$s = 3.7$ mm
Ground plane reducing back radiation	Copper	—

Table 3: Antenna dimensions (reflectarray unitary cell equal to: $\Delta x = \Delta y = 0.6\lambda$ and $\Delta x = \Delta y = 0.4\lambda$.

Layer	$\Delta x = \Delta y = 0.6\lambda$	$\Delta x = \Delta y = 0.4\lambda$
Patch ($W \times L$)	4.9 mm × 3.68 mm	4.9 mm × 3.2 mm
Slot ($W_a \times L_a$)	0.4 mm × 3.25 mm	0.4 mm × 3.8 mm
Stub ($W_m \times L_s$)	0.65 mm × 1.98 mm	0.65 mm × 2.1 mm

[9], and the bandwidth calculated in [8]. The BW values estimated with the formula (8) are derived from the curves illustrated in Figures 6 and 7, by fixing the phase change rate $tg(\alpha)$ to the values reported in Table 1. It can be observed that (8) gives a quite good estimation of the reflectarrays bandwidth which is closer to the measured values reported in [9]. Other parameters affect the measured 1 dB gain bandwidth, which are not considered into (8), such as the field pattern of the feed illuminating the array and the dielectric/conductor losses of the elements. However, the

Table 4: Element stratification.

Layer	Material	Thickness
Covering dielectric	Diclad 870 ($\varepsilon_r = 2.33$)	0.762 mm
Patch	Copper	35 μm
d1	Foam ($\varepsilon_{r1} = 1.07$)	1 mm
Ground plane with slot	Copper	35 μm
d2	Diclad 870 ($\varepsilon_{r2} = 2.33$)	0.762 mm
Phasing line	Copper	35 μm
d3	Air	3.7 mm
Ground plane reducing back radiation	Copper	—

provided estimation formula, as discussed above, gives a closer upper bound to the effective measured bandwidth values, when compared to the existing approaches [7, 8].

3. Broadband Aperture-Coupled Reflectarray Configurations with Reduced Interelement Spacing

The analysis performed in the previous paragraph has confirmed the fact that the bandwidth of small reflectarrays is strongly affected by the slope variation of the single elements phase curves versus frequency. Furthermore, the reflectarray bandwidth depends on the extent of the frequency range within which the slope of overall phase curves can be considered identical. So, the bandwidth behavior of reflectarrays with moderate size is controlled by the combined effect of the single element bandwidth and the slope of the reflection phase curves. As a result, the choice of the single element configuration, satisfying the bandwidth requirements on the overall reflectarray antenna, must be done looking at the value of the reflected phase curve derivative versus the frequency. As demonstrated by the curves illustrated in Figures 3–5, in order to maximize the reflectarray bandwidth, the value of the curves slope should tend to zero or equivalently the curves must be almost parallel. Anyway, it must be fixed by taking into account the geometry of the antenna to be realized, such as the aperture diameter D and the F/D ratio.

In order to obtain a broader-band reflectarray with moderate size, the aperture-coupled configuration depicted in Figure 8, with a phase tuning stub slot-coupled to a rectangular patch, is optimized. The reflection phase is controlled by varying the length of the line section L_m, while all other antenna dimensions are fixed in order to match the aperture coupled patch with the variable length line.

This element is proposed as broadband reflectarray configuration [4, 10], because it offers smoother phase variations when compared to the standard reflectarray configuration with patches of different size. Further bandwidth improvements of the aperture-coupled configuration have been demonstrated in [5, 6], by reducing the spacing between adjacent elements in the array grid. These enhancements are principally due to the mutual coupling among the array elements which has the effects to reduce the slope of the phase curves versus frequency. In [5, 6], the comparison between two reflectarrays characterized by different grid spacing is reported. The two considered configurations are characterized by the same layers stratification reported under Table 2, but they have different cell dimensions that are, respectively, $\Delta x = \Delta y = 0.6\lambda_0$ and $\Delta x = \Delta y = 0.4\lambda_0$ at the operating frequency $f_0 = 20$ GHz. The dimensions of the two synthesized reflectarray elements are reported under Table 3. The characteristic impedance of the tuning line is fixed to a value of 100 Ω. A wider band behavior has been demonstrated in [6] for the configuration with reduced spacing. Both the configurations have been analyzed with a full-wave code based on the infinite array approach and by assuming a normally incident plane wave.

For the sake of clarity, some results obtained in [5, 6] are reported below. In particular, Figures 9 and 10 show, respectively, the phase and the amplitude of the reflection coefficient computed for the two considered cases. The phase curves computed in the case of a $0.4\lambda_0$ spacing show a smoother behavior which extends over a larger frequency range with respect to the case of a $0.6\lambda_0$ cell. All the phase curves are normalized with respect to the central frequency f_0. The maximum slope $tg\alpha_{\max}$ of the computed curves is evaluated to be equal to $-150°$/GHz and $-88°$/GHz for the $0.6\lambda_0$ and the $0.4\lambda_0$ unit cell size, respectively, while the minimum curve slope $tg\alpha_{\min}$ is equal to $-25°$/GHz and $-35°$/GHz, respectively. Similarly, the amplitude of the reflection coefficient (Figure 10) shows slower variations with respect to the frequency in the case of the $0.4\lambda_0$ cell. Anyway, it can be observed that in both cases the total losses due to the dielectric and the conductors are very low. As a matter of fact, the reflection amplitude remains above the -0.8 dB level. This means that the losses associated to the single radiator will cause a negligible reduction of the reflectarray antenna efficiency, which in turn will be principally affected by the spillover and the tapering losses [9].

The strong bandwidth improvement obtained in the case of the reduced cell size is determined by the coupling between the patches. In the case of slot-coupled configuration, such as in multiresonant antennas [11], this allows to increase the impedance bandwidth between the slot-coupled patches and the variable length lines. As it is well known, a reflectarray element well matched to the phasing stub in a given frequency band is able to provide the appropriate phasing in the whole band [4]. Figures 11 and 12 illustrate the input impedance and the reflection coefficient seen at the line section t (see Figure 8). It is evident that a broadband impedance bandwidth is obtained when the patch is embedded into an infinite array with a more dense lattice.

In order to verify the bandwidth enhancement due to the adoption of reflectarray elements with smoother phase curves, the 1 dB gain bandwidth has been computed in [6] for few reflectarrays with different aperture diameters, based on the two differently spaced element configurations.

The normalized gain patterns against frequency is calculated as described in [9], by the superimposition of the spherical waves radiated by each unitary cell composing the

Table 5: Designed reflectarrays features. (operating frequency $f_0 = 20$ GHz; F/D ratio = 1).

Reflectarray configuration	D	Δx	Patch substrate	$\Delta tg(\alpha)$ (°/GHz)	1-dB gain bandwidth
1	$12.6\lambda_0$	$0.6\lambda_0$	$\varepsilon_{r1} = 2.33$ $t = 0.762$ mm	−125	6.7%
2	$12.4\lambda_0$	$0.4\lambda_0$	$\varepsilon_{r1} = 2.33$ $t = 0.762$ mm	−53	17%
3	$12\lambda_0$	$0.48\lambda_0$	$\varepsilon_{r1} = 1.07$ $t = 1$ mm	−37	23%

antenna, which are proportional to the reflection coefficients illustrated in Figures 9 and 10. The field pattern of the feed is also taken into account and modeled by the expression $G_f(\theta, \varphi) = \cos^n(\theta)$, as usually adopted in the literature [9].

A bandwidth improvement is demonstrated for all considered case when Δx is reduced to $0.4\lambda_0$. In particular, when $D \cong 12.4\lambda_0$ and $F/D = 1$, the gain bandwidth increases from the value of 6.7% ($\Delta x = \Delta y = 0.6\lambda_0$) to the value of 17% ($\Delta x = \Delta y = 0.6\lambda_0$). These bandwidth values follow enough the behavior provided by the estimation formula (8), as it can be observed in Figure 13.

In order to obtain a further improvement in the bandwidth of the considered reflectarray configuration, a 1 mm thick foam substrate is adopted as patch dielectric support, while a reduced unit-cell size equal to $0.48\lambda_0$ is considered. The designed element is characterized by the layers stratification reported under Table 4, while its top view is illustrated in Figure 14(a). The dimensions of the synthesized structure are the following: $W = 6.2$ mm, $L = 3.6$ mm, $L_a = 5.15$ mm, $W_a = 0.6$ mm, $L_s = 1.65$ mm, and $W_s = 0.65$ mm.

The element shows a very large bandwidth in terms of −10 dB return loss at the input port 1 (Figure 14(b)), which extends from 16.2 GHz to 25.8 GHz. However, this high bandwidth value, usually, does not exactly match the bandwidth of the reflectarray element evaluated with respect to the reflection curves behavior [4]. The bandwidth of the designed reflectarray element is calculated using the approach described in [6], based on the evaluation of the frequency range within which all the phase curves computed for different values of the tuning stub L_m are almost parallel. Then, normalizing all the curves with respect to the central frequency f_0, the operating band is computed by considering the parallelism condition satisfied, apart from a margin error $\Delta\phi$ equal to ±45°. This bandwidth evaluation approach, applied to the above reflectarray element, gives the results illustrated in Figure 15, where an upper and a lower bound curve are used to delimitate the operating frequency range. The two curves are computed as the summation of a fixed reference curve with the error $\Delta\phi$. As it can be observed, the resulting bandwidth is equal to the value of about 29%, while the maximum curves slope $tg(\alpha_{\max})$ is equal to about −67°/GHz and the minimum slope $tg(\alpha_{\min})$ is about −30°/GHz. Matching this last values with the bandwidth estimating curve in Figure 16, a BW equal to 27.5% is obtained for a reflectarray with $D = 12\lambda_0$ and $F/D = 1$.

The designed aperture-coupled element is adopted for the design of a reflectarray antenna operating at the frequency $f_0 = 20$ GHz. The antenna is characterized by a circular reflecting surface with a diameter D of about $12\lambda_0$. The synthesized reflectarray has a unit cell size equal to $0.48\lambda_0 \times 0.48\lambda_0$, with an overall number of 438 elements. The bandwidth behavior of the antenna is compared with the results obtained in [6] for two reflectarrays operating at the same frequency f_0 and having $D \cong 12.4\lambda_0$. For all considered reflectarrays, the F/D ratio is fixed to 1, while the power radiation pattern of the feed is modeled by the expression $G_f(\theta, \varphi) = \cos^n(\theta)$, with $n = 10$.

A synthesis algorithm based on the iterative projection method [12, 13] is applied to compensate for the path delay on each reflecting element, so concentrating the impinging energy in the broadside direction.

Table 5 summarizes the principal features of all considered reflectarray antennas. The same table reports the 1 dB gain bandwidth value calculated for each antenna prototype. The comparison among the three normalized gain patterns is illustrated in Figure 17. It can be observed a significant enlargement in the bandwidth of the reflectarray based on the aperture-coupled element proposed in this work. As previously discussed, this wider band behavior is due to the smaller slope of the almost parallel reflection phase curves related to the designed reflectarray element.

4. Conclusion

A bandwidth estimation criterion for the reflectarray bandwidth has been derived, taking into account the combined effect due to the antenna geometry and the frequency dependence of the phase reflected by each reflectarray element. The formula has been adopted for the estimation of the maximum achievable bandwidth for some closely spaced aperture-coupled reflectarrays, showing a good agreement with the calculated 1 dB gain bandwidth for each considered case. A significant bandwidth enlargement has been demonstrated by reducing the phase curve slopes through a proper tuning of the coupling between the closely spaced elements [14]. Concerning Future developments, the application of the proposed method to broadband millimeter-wave [15, 16] passive and/or active [17–19] reflectarrays on innovative dielectric materials [20] will be considered, and experimental characterizations will be provided also by the adoption of innovative near-field [21–23] and openresonator [24] techniques.

References

[1] J. Huang, "Analysis of a microstrip reflectarray antenna for microspacecraft applications," TDA Progress Report, 1995.

[2] J. A. Encinar and J. A. Zornoza, "Broadband design of three-layer printed reflectarrays," *IEEE Transactions on Antennas and Propagation*, vol. 51, no. 7, pp. 1662–1664, 2003.

[3] A. Roederer, "Reflector antenna comprising a plurality of panels," US6411255, 2002.

[4] J. Huang and J. A. Encinar, *Reflectarray Antennas*, IEEE Press, Wiley-Interscience, 2008.

[5] S. Costanzo, F. Venneri, and G. Di Massa, "Bandwidth enhancement of aperture-coupled reflectarrays," *Electronics Letters*, vol. 42, no. 23, pp. 1320–1321, 2006.

[6] F. Venneri, S. Costanzo, G. Di Massa, and G. D. Amendola, "Aperture-coupled reflectarrays with enhanced bandwidth features," *Journal of Electromagnetic Waves and Applications*, vol. 22, no. 11-12, pp. 1527–1537, 2008.

[7] D. M. Pozar, "Bandwidth of reflectarrays," *Electronics Letters*, vol. 39, no. 21, pp. 1490–1491, 2003.

[8] M. E. Bialkowski and K. H. Saydmarie, "Bandwidth cinsiderations for a microstrip reflectarray," *Progress In Electromagnetics Research B*, vol. 3, pp. 173–187, 2008.

[9] D. M. Pozar, S. D. Targonski, and H. D. Syrigos, "Design of millimeter wave microstrip reflectarrays," *IEEE Transactions on Antennas and Propagation*, vol. 45, no. 2, pp. 287–296, 1997.

[10] F. Venneri, S. Costanzo, and G. Di Massa, "Transmission line analysis of aperture-coupled reflectarrays," *Progress in Electromagnetics Research C*, vol. 4, pp. 1–12, 2008.

[11] K. L. Wong, *Compact and Broadband Microstrip Antennas*, John Wiley & Sons, 2002.

[12] F. Venneri, S. Costanzo, G. Di Massa, and G. Angiulli, "An improved synthesis algorithm for reflectarrays design," *IEEE Antennas and Wireless Propagation Letters*, vol. 4, no. 1, pp. 258–261, 2005.

[13] S. Costanzo, F. Venneri, G. Di Massa, and G. Angiulli, "Synthesis of microstrip reflectarrays as planar scatterers for SAR interferometry," *Electronics Letters*, vol. 39, no. 3, pp. 266–267, 2003.

[14] F. Caminita, S. Costanzo, G. Di Massa et al., "Reduction of patch antenna coupling by using a compact EBG formed by shorted strips with interlocked branch-stubs," *IEEE Antennas and Wireless Propagation Letters*, vol. 8, pp. 811–814, 2009.

[15] S. Costanzo, I. Venneri, G. Di Massa, and G. Arriendola, "Hybrid array antenna for broadband millimeter-wave applications," *Progress In Electromagnetics Research—PIER*, vol. 83, pp. 173–183, 2008.

[16] S. Costanzo, "Synthesis of multi-step coplanarwaveguidetomicrostrip transition," *Progress In Electromagnetics Research—PIER*, vol. 113, pp. 111–126, 2011.

[17] F. Venneri, S. Costanzo, and G. Di Massa, "Reconfigurable aperturecoupled reflectarray element tuned by single varactor diode," *Electronics Letters*, vol. 48, no. 2, pp. 68–69, 2012.

[18] F. Venneri, S. Costanzo, G. Di Massa et al., "Beam-scanning reflectarray based on a single varactor-tuned element," *International Journal of Antennas and Propagation*, vol. 2012, Article ID 290285, 5 pages, 2012.

[19] F. Venneri, S. Costanzo, G. Di Massa, P. Corsonello, and M. Salzano, "Design of a reconfigurable reflectarray based on a varactor tuned element," in *Proceedings of the 6th European Conference on Antennas and Propagation (EUCAP '12)*, pp. 2628–2631, Prague, Czech Republic, March 2012.

[20] S. Costanzo, I. Venneri, G. Di Massa, and A. Borgia, "Benzocyclobutene as substrate material for planar millimeter-wave structures: dielectric characterization and application," *Journal of Infrared, Millimeter and Terahertz Waves*, vol. 31, no. 1, pp. 66–77, 2010.

[21] S. Costanzo and G. Di Massa, "Far-field reconstruction from phaseless near-field data on a cylindrical helix," *Journal of Electromagnetic Waves and Applications*, vol. 18, no. 8, pp. 1057–1071, 2004.

[22] S. Costanzo and G. Di Massa, "Direct far-field computation from bi-polar near-field samples," *Journal of Electromagnetic Waves and Applications*, vol. 20, no. 9, pp. 1137–1148, 2006.

[23] S. Costanzo and G. Di Massa, "Near-field to far-field transformation with planar spiral scanning," *Progress In Electromagnetics Research—PIER*, vol. 73, pp. 49–59, 2007.

[24] G. Di Massa, S. Costanzo, and O. H. Moreno, "Open resonator system for reflectarray elements characterization," *International Journal of Antennas and Propagation*, vol. 2012, Article ID 912809, 7 pages, 2012.

Hindawi Publishing Corporation
International Journal of Antennas and Propagation
Volume 2012, Article ID 474073, 9 pages
doi:10.1155/2012/474073

Research Article

Systematic Framework for Reflectarray Synthesis Based on Phase Optimization

J. Álvarez, M. Arrebola, R. G. Ayestarán, and F. Las-Heras

Área de Teoría de la Señal y Comunicaciones, Departamento de Ingeniería Eléctrica, Universidad de Oviedo, Edificio Polivalente, Modulo 8, Campus Universitario de Gijón, Asturias, 33203 Gijón, Spain

Correspondence should be addressed to J. Álvarez, jalvarez@tsc.uniovi.es

Received 2 March 2012; Revised 4 June 2012; Accepted 5 June 2012

Academic Editor: Raphaël Gillard

A new systematic synthesis framework for reflectarray antennas is discussed. Optimization based on the Levenberg-Marquardt algorithm is used to obtain the phase distribution of the reflection coefficients required on the reflectarray surface, in order to achieve the pattern specifications. A Local Multipoint Distribution System (LMDS) base station working in the 24.5–26.5 GHz frequency band has been proposed to evaluate the method. The 3D requirements are defined by the combination of the elevation and templates and considering a maximum acceptable ripple in the beam shaping. Some illustrative results are obtained.

1. Introduction

Printed reflectarray antennas are very attractive alternatives to classic reflectors and phased arrays in many applications, such as beam shaping and electronic beam control [1]. They present low profile, mass, and volume and offer an easy manufacturing process. In general, a reflectarray consists of a planar array of printed elements illuminated by a primary feed, typically a horn antenna. Each element of the reflectarray should introduce a phase shift into the impinging wave from the feed, in order to obtain a beam shaped or focused in a given direction. The amplitude of the field reflected by each cell of the reflectarray is imposed by the illumination provided by the primary feed and the ohmic losses of the reflectarray.

The possibilities of contoured and focused beam reflectarrays are interesting in a wide range of applications. Multiple-beam antennas typically based on large-phased arrays are used in radar and communications applications [2, 3] or reflectors with feed-horn clusters and mechanical devices [4]. Moreover, reflectarrays can be a suitable technology for multibeam antennas, considering one feed per beam in order to obtain focused beams [5]. Eventually, single offset reflectarrays have been demonstrated for real DBS (Direct Broadcast Satellite) mission requirements [6, 7].

Two tasks should be carried out in the design of a contoured beam reflectarray. The phase distribution of the reflection coefficient to obtain the required beam shaping should be synthesized. Then, the dimensions of the elements should be adjusted element by element in order to match the phase shift requirements. Some phase-only synthesis methods have been proposed in order to obtain the phase-shift of the reflectarray cells, considering the large numbers of unknowns in the problem and avoiding the local minima [8–10]. However, these approaches do not provide a systematic synthesis framework for reflectarrays, requiring different combinations of techniques in order to adapt the method to the problem to be addressed.

In this paper, a phase-only optimization method is proposed as a systematic framework able to deal with general reflectarray synthesis problems, avoiding the need to control the process while the optimization is being carried out. In order to evaluate its performance, it has been used to obtain shaped-beam reflectarrays for a Local Multipoint Distribution Service (LMDS) base station application [11], squared cosecant in elevation and sectored in azimuth. A reflectarray has been synthesized at the central frequency of the application band (25.5 GHz), considering the illumination of a pyramidal horn antenna as primary feed. The synthesis method is based on the definition of a proper cost function,

where the allowed minimum and maximum levels at each angular direction of the far field are previously established [12, 13]. The function is then minimized according to the required phase values, using an optimization method based on the *Levenberg-Marquardt* (LM) algorithm [14]. Some well-known optimization and random search algorithms exist in the scientific literature able to solve this problem, such as *Newton-Raphson* (NR) [15], *Genetic Algorithms* [16], or *Differential Evolution Algorithm* [17], but LM has been chosen as a reasonable tradeoff between complexity and performance on synthesis tasks, due to its robustness in the resolution of nonlinear least squared problems [18]. Moreover, this method has been found useful in some synthesis problems, dealing with phase-only optimization [19], or magnitude and phase synthesis of the feeding weights [20] when it is applied to linear arrays. In this paper, using and adequate cost function, the method can be applied to a planar reflectarrays, subject to demanding full 2D requirements, such as the specifications of an antenna for an LMDS central station.

The proposed synthesis technique provides the phase of the reflection coefficients which obtains the shaped beam required for this application, sectored in azimuth and squared cosecant in elevation. The accuracy and time efficiency of this technique are demonstrated using some results over a 30×30 element reflectarray illuminated by a feed horn. The radiation patterns of the entire antenna are shown and compared with the required LMDS templates.

This paper is organized as follows. Section 2 explains the scheme and characteristics of reflectarray antennas. In Section 3, the phase synthesis method is described, after being adapted to the reflectarray synthesis problem. Finally, Section 4 exposes the results for an LMDS base station application, and some conclusions are remarked in Section 5.

2. Antenna Definition

A planar reflectarray is used to illustrate the proposed technique. The scheme of the considered antenna configuration is shown in Figure 1. The reflectarray under study is a multilayer flat structure of printed stacked patches over a ground plane, with a horn antenna as primary feed. In order to account for both structures, two coordinate reference systems are established: a reflectarray reference system, whose origin is placed at the centre of the reflectarray surface and defined by $(\hat{x}_R, \hat{y}_R, \hat{z}_R)$, and a feed reference system located at the horn phase-centre and denoted by $(\hat{x}_F, \hat{y}_F, \hat{z}_F)$. The $\hat{z}_F$-axis identifies the pointing direction of the feed horn. Moreover, each reflectarray cell can be identified by the indexes $n = 1 \cdots N$ and $m = 1 \cdots M$, to describe its position in the $\hat{x}_R$-axis and the $\hat{y}_R$-axis, respectively, being N, M the number of elements in each direction.

The feed horn illuminates the reflectarray and produces the incident field $E_{\text{inc}}^{X/Y}(x_R[n], y_R[m])$ on each reflectarray cell (denoted for simplicity by $E_{\text{inc}}^{X/Y}(n,m)$). Although a near-field can be used to accurately model the field radiated by the feed horn, a far-field simple model based on $\cos^q(\theta)$ function of the feed pattern can be used [21]. Since the feed is

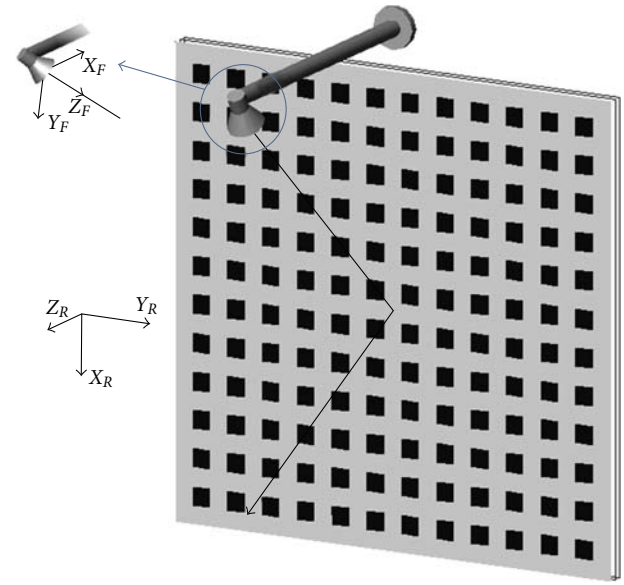

Figure 1: Scheme of the flat reflectarray.

Table 1: Font sizes for papers values of q factor used to model the feed horn.

Frequency (GHz)	24.5	25.5	26.5
q-factor in E-plane	33	35	37
q-factor in H-plane	37	39	41
q in $\cos^q(\theta)$ (averaged)	35	37	39

a pyramidal horn, the beamwidth in E-plane and H-plane is not the same, and therefore different q values are estimated in each plane and an averaged value is used in the model. The q-factor also depends on the frequency and has been calculated at the central and extreme frequencies of the application band [7], see Table 1. A vertical and horizontal polarizations, X_R and Y_R, can be considered, so the superindex X/Y denotes this polarization of the feed, used to produce an electric field mainly in the X_R or Y_R direction. Note in Figure 1 that the vertical polarization corresponds to X_R-polarization, because the electric field in the X_R-direction is vertical, according to the considered reference system. For each polarization, the two components of the tangential electric field on the reflectarray surface are calculated, so the incident field is given by

$$\vec{E}_{\text{inc}}^{X/Y}(n,m) = E_{x,\text{inc}}^{X/Y}\hat{x}_R + E_{y,\text{inc}}^{X/Y}\hat{y}_R. \quad (1)$$

The field reflected on the reflectarray surface is used for the computation of the far-field radiation patterns of the entire antenna. The reflected field can be written as

$$\vec{E}_{\text{ref}}^{X/Y}(n,m) = E_{x,\text{ref}}^{X/Y}\hat{x}_R + E_{y,\text{ref}}^{X/Y}\hat{y}_R. \quad (2)$$

The relation between the incident and the reflected fields in each element (n,m) of the reflectarray can be represented as

$$\left[E_{x,\text{ref}}^{X/Y}\hat{x}_R, E_{y,\text{ref}}^{X/Y}\hat{y}_R\right]^T = \mathbf{R}(n,m) \cdot \left[E_{x,\text{inc}}^{X/Y}\hat{x}_R, E_{y,\text{inc}}^{X/Y}\hat{y}_R\right]^T, \quad (3)$$

where $(\cdot)^T$ indicates the transpose and $\mathbf{R}(n,m)$ is a complex matrix, which refers to the reflection coefficient of each reflectarray element:

$$\mathbf{R}(n,m) = \begin{pmatrix} \rho_{xx}(n,m) & \rho_{xy}(n,m) \\ \rho_{yx}(n,m) & \rho_{yy}(n,m) \end{pmatrix}. \quad (4)$$

The $\mathbf{R}$ matrix characterizes the behavior of each reflectarray element. The components $\rho_{xx}(n,m)$ and $\rho_{yx}(n,m)$ are the direct and cross-reflection coefficients for an incident wave with the tangential component of the electric field in the X_R direction, and $\rho_{yy}(n,m)$ and $\rho_{xy}(n,m)$ are the reflection coefficients for the Y_R component. All of them depend on the angle of incidence of the impinging wave coming from the feed horn, and on the element geometry, adjusted to produce the required phase-shift, so that the matrix is different for each element of the reflectarray.

The calculation of the $\mathbf{R}$ matrix and the incident field given in (1) should be properly obtained. Considering the development in [9], the direct coefficient $\rho_{xx}(n,m)$ in (4) is the only used to calculate the copolar component of the radiation pattern when linear X_R-polarization is considered, since the term of $\rho_{xy}(n,m)$ can be neglected because of its low contribution to the total radiated field. The same criteria would be done over $\rho_{yy}(n,m)$ and $\rho_{yx}(n,m)$ for Y_R-polarization. Given this assumption, the copolar reflected field in each cell can be considered as

$$\vec{E}^{X/Y}_{\text{ref}}(n,m) \cong \rho_{xx}(n,m) \cdot E^{X/Y}_{x,\text{inc}}(n,m)\hat{x}_R. \quad (5)$$

The phase of each reflection coefficient $\rho_{xx}(n,m)$ is achieved by adjusting the dimensions of the printed elements, and it must be obtained using an optimization method, as the technique presented in the next section.

3. Phase Synthesis Method

3.1. Far Field Radiation Pattern of the Reflectarray. Once the reflectarray antenna is described, the aim of this section is to obtain the phase of the reflection coefficient of each reflectarray element in order to fulfill the required pattern for the beam.

Considering the total field reflected by the reflectarray calculated in (5), the radiation pattern of the antenna is computed. Assuming the second principle of equivalence, the radiated far field is given by

$$\vec{E}^{X/Y}(u,v) = \sum_{m=1}^{M}\sum_{n=1}^{N} \vec{E}^{X/Y}_{\text{ref}}(n,m) e^{jn(2\pi/\lambda)d_x u} e^{jm(2\pi/\lambda)d_y v}, \quad (6)$$

where $u = \sin(\theta)\cos(\phi)$, $v = \sin(\theta)\sin(\phi)$ are the elevation and azimuth angles, respectively, $\vec{E}^{X/Y}(u,v)$ is the far field produced by the entire antenna in (u,v) direction, λ is the wavelength in vacuum, and d_x, d_y are the distances between radiating elements in the $\vec{x}_R$ and $\vec{y}_R$ axes of the reflectarray.

Let $\vec{E}^{X/Y}_0(u,v)$ be the radiation pattern of an element cell located at the origin of the coordinate system (the centre of the reflectarray), (6) can be rewritten using the formulation of the array factor as

$$\begin{aligned} \vec{E}^{X/Y}(u,v) &= \vec{E}^{X/Y}_0(u,v) \\ &\quad \times \sum_{m=1}^{M}\sum_{n=1}^{N} \left(|\omega_{nm}| e^{j\varphi(\omega_{nm})}\right) e^{jn(2\pi/\lambda)d_x u} e^{jm(2\pi/\lambda)d_y v} \\ &= \vec{E}^{X/Y}_0(u,v) A_F(u,v), \end{aligned} \quad (7)$$

where $\omega(n,m)$ can be considered as the excitation at element (n,m), which determines how the reflection on each cell modifies the element radiation pattern $\vec{E}^{X/Y}_0(u,v)$, and $\varphi(\omega_{nm})$ specifies its phase. Since the far field produced by the reflectarray is provided by the reflected distribution originated in the fed horn and considering (5), the magnitude $|\omega_{nm}|$ will be determined by the illumination of the primary feed as explained in the previous section. On the other hand, $\varphi(\omega_{nm})$ represents the phase of the reflection coefficient $\rho_{xx}(n,m)$. Thus, in order to obtain the required phase terms $\varphi(\omega_{nm})$ that modify the shape of the final radiation pattern, the synthesis process is only dependent on $A_F(u,v)$.

3.2. Phase Synthesis Using Least Squares Optimization and Levenberg-Marquardt Algorithm. The goal in many practical synthesis problems is obtaining a radiated far-field distribution concentrated between a set of bounds specified using a mask. One of the techniques for achieving this objective is the use of optimization, defining a cost function which penalizes the no-allowed field levels [12, 13]. This function is given by defining the minimum and maximum bounds for the field values at each direction, and if only a set of T possible directions $r_t = (u,v)_t$, $t = 1 \cdots T$, is considered, this cost function can be expressed as

$$\begin{aligned} F = \sum_{t=1}^{T} F_t = \sum_{t=1}^{T} C_t \Bigg[& \left(G^2_M(r_t) - \left|\vec{E}^{X/Y}(r_t)\right|^2 \right) \\ & \times \left(G^2_m(r_t) - \left|\vec{E}^{X/Y}(r_t)\right|^2 \right) \\ & + \left| G^2_M(r_t) - \left|\vec{E}^{X/Y}(r_t)\right|^2 \right| \\ & \times \left| G^2_m(r_t) - \left|\vec{E}^{X/Y}(r_t)\right|^2 \right| \Bigg], \end{aligned} \quad (8)$$

where $G_M(r_t)$, $G_m(r_t)$ are the maximum and minimum values specified for the field radiated at the direction r_t, $\vec{E}^{X/Y}(r_t)$ is defined in (7) and $C_t \in \mathbb{R}^+$ is introduced to emphasize the error in some directions, useful when the field values are very low. $G_M(r_t)$, $G_m(r_t)$, and $\vec{E}^{X/Y}(r_t)$ may be normalized in order to facilitate the optimization. F_t in (8) represents the error at r_t, and it is null in those directions where the radiated field is inbounds, showing a higher value when an error exists:

$$F_t = \begin{cases} 0, & \forall t | G_m^2(r_t) \le \left|\vec{E}^{X/Y}(r_t)\right|^2 \le G_M^2(r_t) \\ 2C_t\left(G_M^2(r_t) - \left|\vec{E}^{X/Y}(r_t)\right|^2\right)\left(G_m^2(r_t) - \left|\vec{E}^{X/Y}(r_t)\right|^2\right), & \text{otherwise.} \end{cases} \tag{9}$$

Operating over (9), the error addends in F can be expressed as a sum of differences, so F_t is written as

$$F_t = \begin{cases} 0, & \forall t | G_m^2(r_t) \le \left|\vec{E}^{X/Y}(r_t)\right|^2 \le G_M^2(r_t), \\ y_t - f_t(\boldsymbol{\alpha}), & \text{otherwise,} \end{cases} \tag{10}$$

where y_t identifies the objective value for the direction t, and $f_t(\boldsymbol{\alpha})$ is the function to fit by calculating the set of parameters $\boldsymbol{\alpha}$, so that F becomes minimal:

$$f_t(\boldsymbol{\alpha}) = 2C_t\left|\vec{E}^{X/Y}(r_t)\right|^2\left(G_M^2(r_t) + G_m^2(r_t) - \left|\vec{E}^{X/Y}(r_t)\right|^2\right)$$
$$y_t = 2C_t(G_M^2(r_t)G_m^2(r_t)). \tag{11}$$

The vector $\boldsymbol{\alpha}$ contains the variables to be synthesized, that is, the phase values $\varphi(\omega_{nm})$, $n = 1 \cdots N, m = 1 \cdots M$, and it is represented as

$$\boldsymbol{\alpha} = \left[\alpha_1 \cdots \alpha_p \cdots \alpha_P\right], \quad p = 1 \cdots P,$$
$$\alpha_p = tg(\varphi(\omega_{nm})) = \frac{\mathrm{Im}(\omega_{nm})}{\mathrm{Re}(\omega_{nm})}, \tag{12}$$

where $P = N \cdot M$ is the dimension of $\boldsymbol{\alpha}$, and $\mathrm{Re}(\omega_{nm}), \mathrm{Im}(\omega_{nm})$ are the real and imaginary parts of ω_{nm}. In spite of the fact that the unknowns of the above problem are the phases $\varphi(\omega_{nm})$, the elements of $\boldsymbol{\alpha}$ in (12) are the tangent of each phase, in order to avoid problems related to the periodicity in the solutions.

This synthesis process requires the use of an optimization algorithm able to minimize F. In this paper, the well-known Levenberg-Marquardt (LM) algorithm [14] has been selected for this purpose, as a tradeoff between accuracy and simplicity. LM is an iterative algorithm able to solve certain nonlinear cost functions. One of the minimization problems where LM achieves good results arises in least squares. In order to apply the LM algorithm to (8), the cost function must be expressed as a least squares quadratic function, so the real cost function to implement needs to be defined as

$$F_{\mathrm{LM}} = \sum_{t=1}^{T} F_t^2, \tag{13}$$

where F_t is defined in (10). Note that the meaning of F and F_{LM} are the same, even though the squared addends.

The LM method requires the calculation of a Jacobian matrix, denoted as $\mathbf{J}$, so that F_{LM} can be minimized. It is a $T \times P$ matrix whose elements are calculated using the partial derivatives over F_t, respect to each element of $\boldsymbol{\alpha}$. Thus, considering (10), each element of $\mathbf{J}$ is either null (for those tth rows where $|\vec{E}^{X/Y}(r_t)|$ is in bounds, i.e., $F_t = 0$) or defined as

$$\mathbf{J}(t,p) = \left.\frac{\partial \mathbf{f}}{\partial \boldsymbol{\alpha}}\right|_{t,p} = \frac{\partial f_t(\boldsymbol{\alpha})}{\partial \alpha_p}$$
$$= 4C_t\left|\vec{E}_0^{X/Y}(r_t)\right|^2\left[\mathrm{Re}(A_F(r_t))\frac{\partial \mathrm{Re}[A_F(r_t)]}{\partial \alpha_p} + \mathrm{Im}(A_F(r_t))\frac{\partial \mathrm{Im}[A_F(r_t)]}{\partial \alpha_p}\right]$$
$$\cdot\left[(G_M^2(r_t) + G_m^2(r_t)) - 2\left|\vec{E}^{X/Y}(r_t)\right|^2\right] \tag{14}$$

in those directions r_t where $|\vec{E}^{X/Y}(r_t)|^2 < G_m^2(r_t)$ or $|\vec{E}^{X/Y}(r_t)|^2 > G_M^2(r_t)$. Note that $|A_F(r_t)|^2 = [\mathrm{Re}(A_F(r_t))]^2 + [\mathrm{Im}(A_F(r_t))]^2$, and each partial derivate is directly demonstrated from (7) as

$$\frac{\partial \mathrm{Re}(A_F(r_t))}{\partial \alpha_p} = \sum_{m=1}^{M}\sum_{n=1}^{N} -\mathrm{Re}(\omega_{nm}) \times\left[\cos\left(n\frac{2\pi}{\lambda}d_x u(r_t)\right)\sin\left(m\frac{2\pi}{\lambda}d_y v(r_t)\right) + \sin\left(n\frac{2\pi}{\lambda}d_x u(r_t)\right)\cos\left(m\frac{2\pi}{\lambda}d_y v(r_t)\right)\right],$$
$$\frac{\partial \mathrm{Im}(A_F(r_t))}{\partial \alpha_p} = \sum_{m=1}^{M}\sum_{n=1}^{N} \mathrm{Re}(\omega_{nm}) \times\left[\cos\left(n\frac{2\pi}{\lambda}d_x u(r_t)\right)\cos\left(m\frac{2\pi}{\lambda}d_y v(r_t)\right) - \sin\left(n\frac{2\pi}{\lambda}d_x u(r_t)\right)\sin\left(m\frac{2\pi}{\lambda}d_y v(r_t)\right)\right], \tag{15}$$

where $u(r_t), v(r_t)$ represent the u, v values determined by the r_t direction. Once the Jacobian matrix is calculated, the LM algorithm can be applied iteratively over F_{LM} as

$$\left[\mathbf{J}_i^T \cdot \mathbf{J}_i + \mu_i \cdot \mathrm{diag}\left(\mathbf{J}_i^T \cdot \mathbf{J}_i\right)\right] \cdot \boldsymbol{\delta}_i = \mathbf{J}_i^T \cdot \mathbf{F}_{t,i}, \tag{16}$$

where the subindex i represents each iteration, $\mathrm{diag}(\cdot)$ is the diagonal matrix, $\mathbf{J}_i$ is the Jacobian matrix of $\boldsymbol{\alpha}_i$ (in each iteration i), μ_i is a convergence parameter that depends on i, and $\mathbf{F}_{t,i}$ is a $T \times 1$ vector which represents the T samples of F_t in (9) for each i. Note that either $\mathbf{J}_i$ or $\mathbf{F}_{t,i}$ present null samples which do not contribute in the optimization,

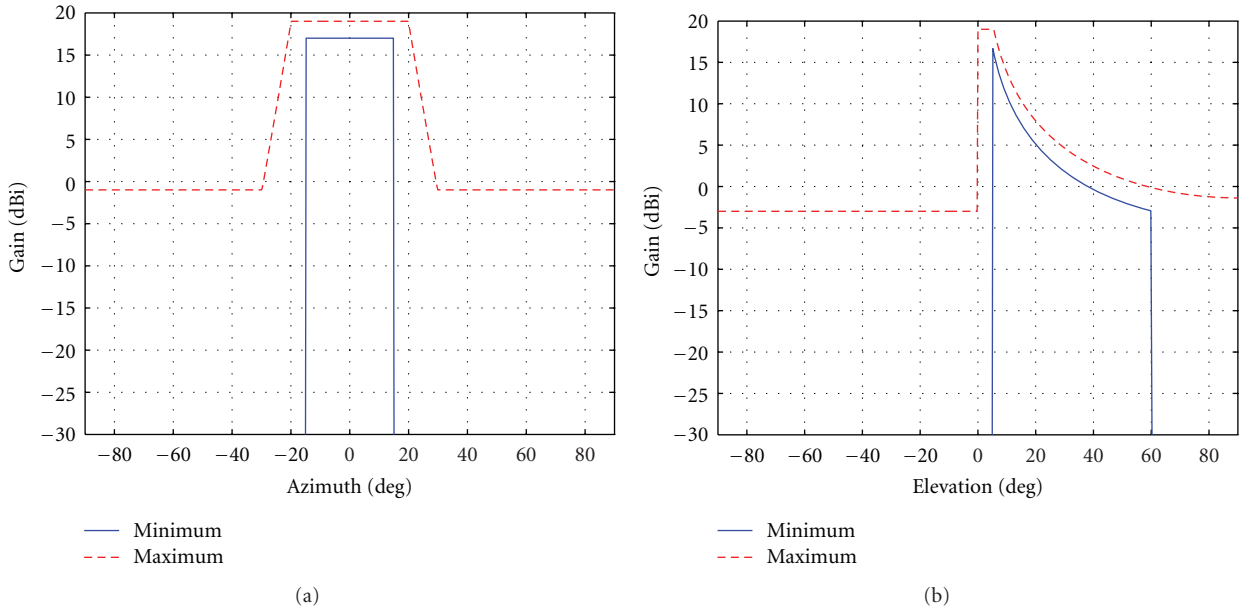

FIGURE 2: Pattern requirements in azimuth (a) and elevation (b). Maximum (dashed lines) and minimum (solid lines) templates.

because of the fact that there is no error in those directions; moreover, the directions r_t where the field is inbounds are different depending on the iteration, and should increase as the algorithm progresses. Finally, $\boldsymbol{\delta}_i$ is an update vector satisfying the equality, which is calculated as the solution of the normal equation associated to the previous least square problem as

$$\boldsymbol{\delta}_i = \left(\mathbf{B}_i^T \cdot \mathbf{B}_i\right)^{-1} \cdot \mathbf{B}_i^T \cdot \mathbf{b}_i, \tag{17}$$

where matrix $\mathbf{B}_i = [\mathbf{J}_i^T \cdot \mathbf{J}_i + \mu_i \cdot \text{diag}\,(\mathbf{J}_i^T \cdot \mathbf{J}_i)]$, vector $\mathbf{b}_i = \mathbf{J}_i^T \cdot \mathbf{F}_{t,i}$, and $(\cdot)^{-1}$ indicates the inverse matrix. Vector $\boldsymbol{\delta}_i$ is iteratively updating the solution as

$$\boldsymbol{\alpha}_{i+1} = \boldsymbol{\alpha}_i + \boldsymbol{\delta}_i. \tag{18}$$

Note that the solution for the phases in each iteration is given by $tg^{-1}(\boldsymbol{\alpha}_{i+1})$ according to (12).

LM requires certain operations over a high dimensional matrix $\mathbf{J}_i$. The Jacobian matrix inversion may have an important temporal cost, or an ill-conditioned matrix $\mathbf{J}_i$ might lead to instability in (17). As a result, a gradient descent technique, such as the *Conjugate Gradient Squared* (CGS) method [22], is implemented to calculate $\boldsymbol{\delta}_i$ (given $\mathbf{B}_i$ and $\mathbf{b}_i$) and prevent this issue.

In order to achieve convergence, the starting parameters should be chosen to provide a valid solution. As it will be shown in the next section, the priori knowledge of the LMDS bounds can provide initial values of $\boldsymbol{\alpha}$ which accelerates the optimization process. Moreover, the parameter μ controls the speed of convergence, so it must be selected carefully to avoid divergence. It defines the steps size to achieve the minimum, closer to the gradient descent direction. One of the most extended techniques to choose this parameter consists in starting with μ_0 proportional to the maximum value of diag $(\mathbf{J}_i^T \cdot \mathbf{J}_i)$ [18], and defining a real parameter $\beta > 1$, so that $\mu_{i+1} = \mu_i\beta$ or $\mu_{i+1} = \mu_i/\beta$ if the cost function increases or decreases, respectively, each iteration i [19]. The high number of variables in the current reflectarray problem requires an exhaustive control of μ_i, so its increase is only allowed when the cost function decreases in more than five iterations consecutively, forcing a decrease every time $F_{\text{LM},i}$ goes higher. Note that $\mu_i = 0$ converts LM into the Gauss-Newton's method [19], easy to diverge in a nonlinear problem with a high number of unknowns, so this value must be disregarded.

4. Simulations and Results

In this section, the proposed technique is demonstrated by the phase-only synthesis of a reflectarray designed for LMDS applications. This antenna must be synthesized to fulfill the coverage specifications of a central station of LMDS service in the 24.5–26.5 GHz band, where a shaped beam both in elevation (squared cosecant) and in azimuth (sectored) [11] is required. The templates of minimum and maximum requirements are shown in Figures 2 and 3. To achieve this beam shaping and gain, a reflector surface is defined. Since the bandwidth of the application is about 8% (24.5 to 26.5 GHz), a two-layer printed reflectarray working at central frequency of the band (25.5 GHz) is considered [9]. The grating lobes are avoided or negligible in the entire frequency band. This flat reflectarray is composed of 30×30 rectangular patches of variable size arranged in a regular mesh, with a periodic cell $d_x \times d_y$ defined as 5.88×5.88 mm (half a wavelength at the central frequency). The phase centre of the feed-horn is placed at $(-94, 0, 214)$ mm in the reflectarray reference system. The resulting f/D of the antenna is 1.2.

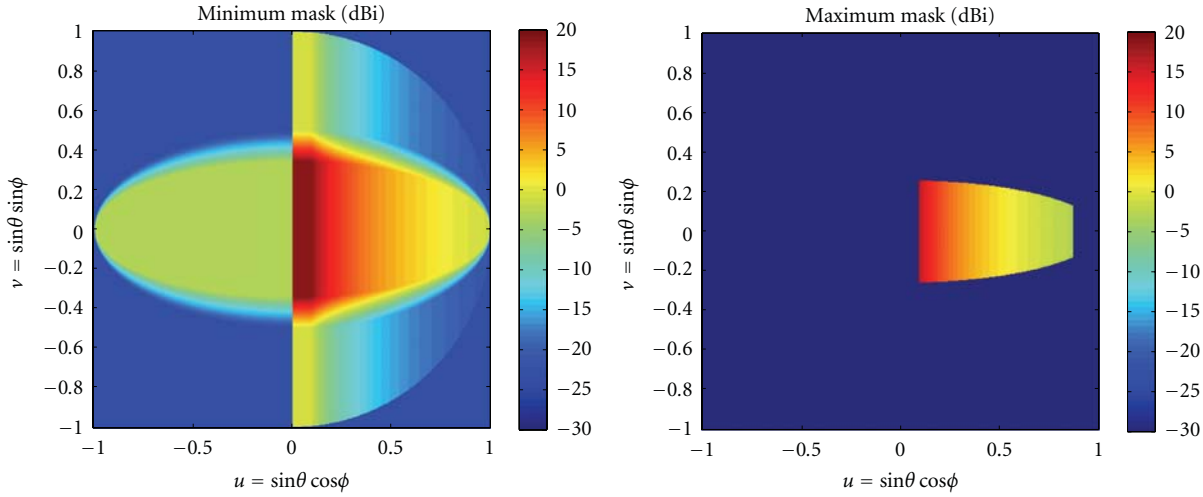

FIGURE 3: Pattern requirements $G_M(r_t)$ (a) and $G_m(r_t)$ (b), in all the considered directions $r_t = (u, v)_t$.

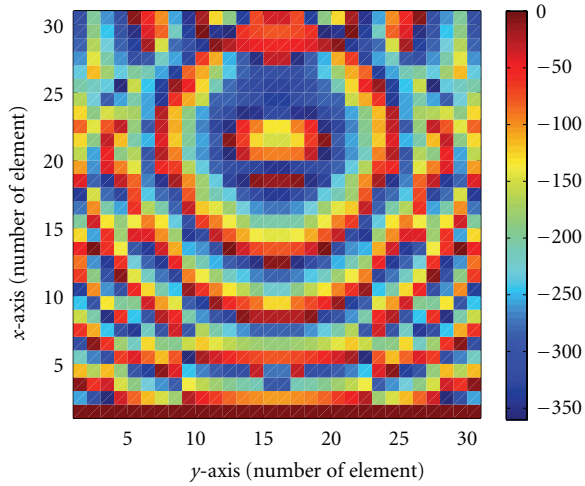

FIGURE 4: Synthesized phase distribution of the reflection coefficient for the X_R-polarization (degrees).

The phase distribution of the reflection coefficient is obtained using the method described in Section 3. The incident field that defines $|\omega_{nm}|$, $n = 1 \cdots N$, $m = 1 \cdots M$, is determined by the $\cos^q(\theta)$ (see Table 1), and the bounds $G_M(r_t)$, $G_m(r_t)$ are the required in LMDS [11], shown in Figure 3.

The resulting phase distribution for X_R-polarization after applying the technique that is discussed in the previous section is shown in Figure 4, being the corresponding to Y_R-polarization very similar. The small difference between both phase distributions is the result of slight differences in the incident field for both linear polarizations.

This solution has been obtained after 3900 iterations of the proposed algorithm, where $T = 16384$ considered directions (taking 128 samples uniformly in $u, v \in [-1, 1]$), and less than a minute per iteration on an Intel Core 2 Duo PC with 2.4 GHz processor. The parameter $C_t = 1/(G_M(r_t) - G_m(r_t))$, so the directions with demanding restrictions are more penalized. The convergence parameter has been empirically set at $\mu_0 = 5$, a value which allows a soft descent toward the solution. This value has been modified as it was explained in 3.1, with $\beta = 1.2$, so $\mu \in (0.13, 331.24)$ in the different iterations of the algorithm. On the other hand, the starting point of the synthesis process (initial phase distribution) is chosen to have a high value at the maximum of the azimuth and elevation masks, which allows a useful initial point to begin the optimization process. The algorithm stops at iteration 3900, when $F_{\mathrm{LM},i} < F_{\mathrm{LM},i-50}/2$ and $F_{\mathrm{LM},i} < 0.01$. The final error in the synthesis process is $F_{\mathrm{LM}} = 0.56 \cdot 10^{-2}$, and $\overline{F_{\mathrm{LM}}} = F_{\mathrm{LM}}/T = 3.42 \cdot 10^{-7}$ if all directions T are considered, even the ones with no error, which means that the field is inbounds in most of the directions. It is a low value, which represents the convergence of the iterative algorithm.

The obtained phase distribution is used to calculate the three-dimensional radiation pattern, which has been simulated at the central frequency of the band (25.5 GHz), for dual linear polarization (vertical and horizontal polarizations), see Figure 5. The final phases for each polarization X/Y are not equal, due to the difference in the illumination of the reflectarray produced by the feed for the two polarizations. Note that the projection of the incident field on the reflectarray cells is different for the two orthogonal linear polarizations.

Main cuts of the beams (elevation and azimuth) are also depicted in Figure 6. Although ideal phase-shift elements have been assumed as reflectarray elements, the radiation patterns have been computed considering the illumination and spillover efficiency of the antenna and they are given in gain (dBi). The results show good agreement with requirements in both polarizations, particularly in the coverage

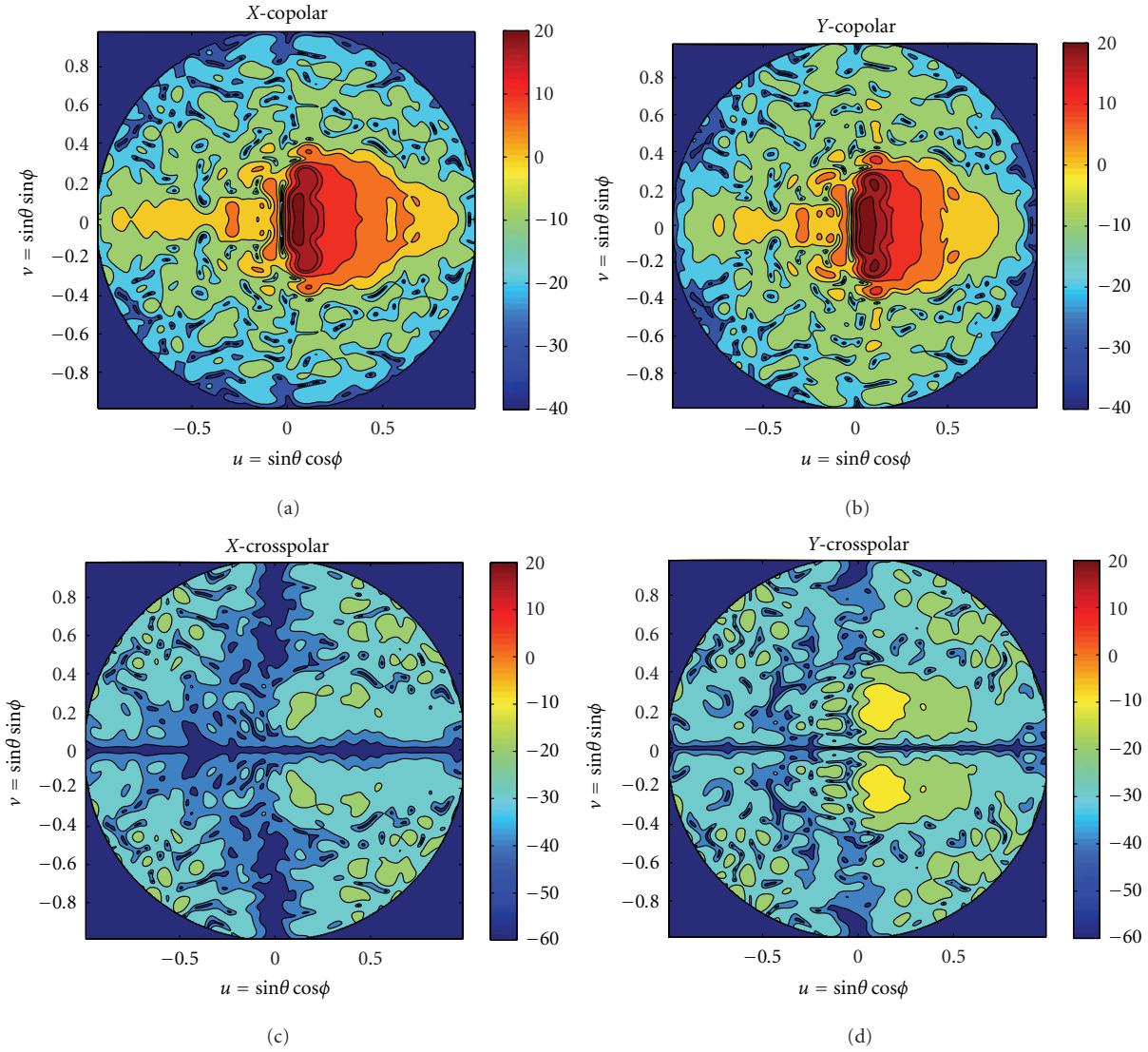

FIGURE 5: Simulated three-dimensional radiation patterns considering the synthesized phase distribution; vertical (a and c) and horizontal (b and d) polarizations for copular (a and b) and crosspolar (c and d) components.

regions. The beam shaping is achieved, and the gain requirements are fulfilled in a high percentage of the coverage. However, small disagreement is found in noncoverage zone but with low side-lobe level. In elevation (Figure 6(b)), the beam shaping requirement is more restrictive and shows a higher gain than required or some ripple is obtained in the region defined by negative elevation angles. Moreover, those negative elevation angles are outside the coverage region of the central station and some error can be acceptable. The pointing directions towards the Earth surface are defined by the positive elevation angles, which correspond to the squared cosecant pattern. Thus, this error is not critical for the station performances. The most critical direction is the zero angle in elevation, where an interference with other LMDS base stations may exist. However, the radiation pattern in this direction produces a deep null, avoiding the potential interference. In spite of those limitations, the squared cosecant in elevation is properly achieved and the radiated field is inbounds in almost all the pointing angles. Moreover, the obtained results are similar in quality to LMDS radiated patterns achieved with traditional methods [9], with the advantage of the use of a systematic framework for optimizing the required phases. These features demonstrate the success of the proposed method.

5. Conclusions

A phase-only synthesis technique for shaped beams has been discussed and proposed for the systematic synthesis of reflectarrays, providing a framework suitable for general reflectarrays synthesis problems. It has been shown to lead to excellent results when used in the presented examples with antennas in LMDS central stations or Direct Broadcast Satellite (DBS) antennas applications.

Using a cost function properly defined and the *Levenberg-Marquardt* optimization algorithm, the reflection

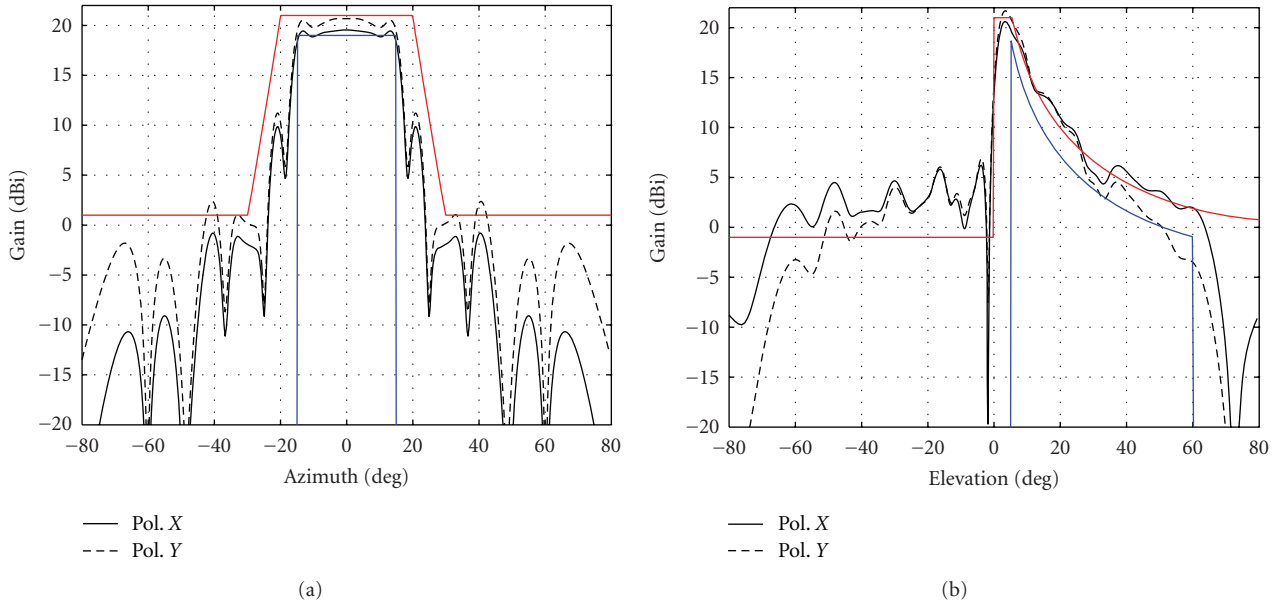

Figure 6: Simulations (vertical and horizontal polarizations) at the central frequency. Main cuts in azimuth (a) and elevation (b), compared with the maximum and minimum required gains (solid red and blue lines).

coefficients of each reflectarray element are obtained. The technique has been applied to the synthesis of a LMDS central station antenna covering 30-degree azimuth sector. The results match with the application requirements. Moreover, the required squared cosecant in the elevation plane is properly obtained, which demonstrates the capabilities of the proposed method to synthesize stringent-shaped beams with low time requirements. Thus, avoiding either the combination of other synthesis techniques or the control on the algorithm while the optimization progresses, the proposed framework provides proper results in LMDS applications.

Finally, this phase-only synthesis technique can be applied to other reflectarray configurations, with more feed horns or different number of reflectarray elements. Only defining the incident beam and specifying the needed bounds, this method provides the synthesized values which fulfill demanding requirements without the need of any adaptation of the method.

Acknowledgments

This work has been supported by the Ministerio de Ciencia e Innovación of Spain/FEDER under Projects CONSOLIDER-INGENIO CSD2008-00068 and TEC2011-24492; by the Gobierno del Principado de Asturias (PCTI)/FEDER-FSE under Projects EQUIP08-06, FC09-COF09-12, EQUIP10-31, and PC10-06 (Flexant); Grant BP10-165; by Cátedra Telefónica-Universidad de Oviedo.

References

[1] J. Huang and J. A. Encinar, *Reflectarray Antennas*, IEEE Press/Wiley, Piscataway Township, NJ, USA, 2007.

[2] A. Jacomb-Hood and E. Lier, "Multibeam active phased arrays for communicatons satellites," *IEEE Microwave Magazine*, vol. 1, no. 4, pp. 40–47, 2000.

[3] L. Schulwitz and A. Mortazawi, "A compact dual-polarized multibeam phased-array architecture for millimeter-wave radar," *IEEE Transactions on Microwave Theory and Techniques*, vol. 53, no. 11, pp. 3588–3594, 2005.

[4] P. Balling, K. Tjonneland, L. Yi, and A. Lindley, "Multiple contoured beam reflector antenna systems," in *Proceedings IEEE Antennas and Propagation Society International Symposium*, Ann Arbor, Mich, USA, June 1993.

[5] W. Menzel, M. Al-Tikriti, and R. Leberer, "A 76 GHz multiple-beam planar reflector antenna," in *Proceeding of the 32nd European Microwave Conference*, pp. 977–980, Milano, Italy, October 2002.

[6] J. A. Encinar, L. S. Datashvili, J. A. Zornoza et al., "Dual-polarization dual-coverage reflectarray for space applications," *IEEE Transactions on Antennas and Propagation*, vol. 54, no. 10, pp. 2827–2837, 2006.

[7] J. A. Encinar, M. Arrebola, L. F. de la Fuenta, and G. Toso, "A transmit-receive reflectarray antenna for direct broadcast satellite applications," *IEEE Transactions on Antennas and Propagation*, vol. 59, no. 9, pp. 3255–3264, 2011.

[8] A. Trastoy, J. A. Rodríguez, F. Ares, J. Vassal'lo, and E. Moreno, "University of santiago de compostela contribution to ARCO project: synthesis of footprint patterns for planar reflectarrays," in *Proceedings of the 18th International Conference on Applied Electromagnetics and Communications (ICECom '05)*, October 2005.

[9] M. Arrebola, J. A. Encinar, and M. Barba, "Multifed printed reflectarray with three simultaneous shaped beams for LMDS central station antenna," *IEEE Transactions on Antennas and Propagation*, vol. 56, no. 6, pp. 1518–1527, 2008.

[10] A. Chakraborty, B. N. Das, and G. S. Sanyal, "Beam shaping using nonlinear phase distribution in a uniformly spaced array," *IEEE Transactions on Antennas and Propagation*, vol. 30, no. 5, pp. 1031–1034, 1982.

[11] ETSI EN 301 215 v1.3.1, "'European standard (Telecommunications series), fixed radio systems, pointto-multipoint antennas, antennas for point-to-multipoint fixed radio systems in the 11 GHz to 60 GHz band, Part 2:24 GHz to 30 GHz', Standard," 2002.

[12] F. Las-Heras and T. K. Sarkar, "A direct optimization approach for source reconstruction and NF-FF transformation using amplitude-only data," *IEEE Transactions on Antennas and Propagation*, vol. 50, no. 4, pp. 500–510, 2002.

[13] F. Las-Heras, B. Galocha, and J. L. Besada, "Equivalent source modelling and reconstruction for antenna measurement and synthesis," in *Proceedings of the IEEE Antennas and Propagation Society International Symposium*, pp. 156–158, Montreal, Canada, July 1997.

[14] J. Nocedal and S. J. Wright, *Numerical Optimization*, Springer, 2nd edition, 2006.

[15] S. C. Chapra and R. P. Canale, *Numerical Methods for Engineers*, McGraw Hill, 1985.

[16] D. E. Goldberg, *Genetic Algorithms for Search, Optimization, and Machine Learning*, Addison-Wesley Longman Publishing, Reading, Mass, USA, 1989.

[17] K. V. Price, R. M. Storn, and J. A. Lampinen, *Differential Evolution: A Practical Approach to Global Optimization*, Springer, Berlin, Germany, 2006.

[18] K. Madsen, H. B. Nielsen, and J. Sondergaard, "Robust subroutines for non-linear optimization," Tech. Rep. IMM-REP-2002-02, Technical University of Denmark, 2002.

[19] T. H. Ismail, D. I. Abu-Al-Nadi, and M. J. Mismar, "Phase-only control for antenna pattern synthesis of linear arrays using the Levenberg-Marquardt algorithm," *Electromagnetics*, vol. 24, no. 7, pp. 555–564, 2004.

[20] Y. Wen, W. S. Gan, and J. Yang, "Nonlinear least-square solution to flat-top pattern synthesis using arbitrary linear array," *Signal Processing*, vol. 85, no. 9, pp. 1869–1874, 2005.

[21] M. Arrebola, Y. Álvarez, J. A. Encinar, and F. Las-Heras, "Accurate analysis of printed reflectarrays considering the near field of the primary feed," *IET Microwaves, Antennas and Propagation*, vol. 3, no. 2, pp. 187–194, 2009.

[22] A. V. Knyazev and I. Lashuk, "Steepest descent and conjugate gradient methods with variable preconditioning," *Journal on Matrix Analysis and Applications*, vol. 29, no. 4, pp. 1267–1280, 2007.

Hindawi Publishing Corporation
International Journal of Antennas and Propagation
Volume 2012, Article ID 912809, 7 pages
doi:10.1155/2012/912809

Research Article

Open Resonator System for Reflectarray Elements Characterization

G. Di Massa, S. Costanzo, and O. H. Moreno

Dipartimento di Elettronica, Informatica e Sistemistica, Universitá della Calabria, 87036 Rende, Italy

Correspondence should be addressed to S. Costanzo, costanzo@deis.unical.it

Received 29 February 2012; Accepted 5 June 2012

Academic Editor: Manuel Arrebola

An open resonator system is proposed in this work to study the phase behavior of reflectarrays cells. The characterization of the single reflectarray element is performed by assuming a Gaussian plane wave normally incident on an infinite periodic array of identical radiating elements. An equivalent circuit model is properly derived for the open cavity including the reflectarray test structure, in order to retrieve the phase design curve of the single reflectarray element. K-band experimental validations are presented and discussed to show the effectiveness of the approach.

1. Introduction

Printed reflectarray antennas are low profile reflectors consisting of a planar array of microstrip patches illuminated by a feed [1–6]. Each reflectarray element is designed to compensate for the phase delay due to the relative feed-element path and to properly reradiate the incident field for obtaining a prescribed beam shape and direction. Reflectarray antennas inherit all appealing features of microstrip technology, such as less weight, easy manufacturing, and low cost, so revealing useful in many application fields such as remote sensing and satellite communications, millimeter wave [7], and infrared frequencies [8].

Many different phase tuning methods have been introduced in the literature for microstrip reflectarray antennas. These include variable size microstrip patches [9], variable size dipoles, and identical patches elements having variable length phase delay lines with or without angular rotations [10, 11].

Recently, phase-tunable elements have been considered to give reflectarrays with a steerable main beam [12–14]. These configurations, combined with dedicated electronic control systems and ad-hoc synthesis algorithm [15], are able to provide extremely versatile reconfigurable antennas [16–18].

To successfully perform the design of a microstrip reflectarray, the characterization of the field reflected by the single radiating element embedded on the whole reflecting surface is of primary importance. As a matter of fact, the behavior of the reflected phase versus frequency and/or tuning element variation is used as design curve in the synthesis algorithm [15] to properly choose those elements that are able to give the prescribed reflectarray beam features.

The measurement of phased-array antennas in waveguide technology is a well-established technique [19]. In [20, 21], an equivalent waveguide approach is proposed for reflectarrays of variable size patches, with the unit cell enclosed in a rectangular waveguide having perfect electric and magnetics walls.

In [22, 23], an equivalent electrical circuit is adopted for the reflectarray, in order to derive the input reflection coefficient. In [22], the analysis is done in the terahertz frequencies band. The reflected phase is directly computed from the input reflection coefficient of a plane wave at the interface between the substrate and the air transmission layers. The input impedance of the reflecting cell is found in terms of the parallel between the patch impedance and the input impedance of the transmission line which is terminated into a short circuit. In [23], a resonant LC parallel circuit is adopted to model the reflectarray unit cell. Losses

Table 1: Expressions for the circuit elements of Figure 2.

L_o	$\mu_0 l$ (H)	C	$\epsilon l/(k_o l)^2$ (F)
L'	$\mu_0 \delta$ (H)	R'	$2/\sigma\delta$ (Ω)
L_e	$16.5\ 10^{-3}\,\mu_0 a$ (H)		

are taken into account by placing a resistor in series with the capacitor. The analysis is performed at 10 GHz. In [24], two resonant LC series circuits are considered instead of the simple resonant LC parallel circuit discussed in [23]. Four frequencies are considered, two resonant and two antiresonant.

In this paper, an open resonator [25] system is considered to characterize the phase response of variable size reflectarray patch elements. At this purpose, a full equivalent circuit is derived to include both the open resonator as well as the grounded reflecting surface, and the phase behavior of the field reirradiated by the reflectarray element is simply derived from the resonance behavior of the assumed equivalent circuit. K-band experimental validations are discussed to prove the validity of the proposed approach.

2. Equivalent Circuit Description

The standard configuration of an open cavity, composed by two spherical mirrors at distance $2l$ and coupled with a rectangular waveguide, is reported in Figure 1. This structure has been studied in details in literature [26], thus confirming that the coupling between the cavity modes is negligible, so that the single resonant mode approximation gives a good description of the cavity field as only this last mode is practically excited. At the same time, the analysis of the solutions has also demonstrated that the excitation of higher-order waveguide modes TE_{n0} is important for the accurate coupling description.

The equivalent circuit, adopted in [26] to accurately model an empty cavity coupled to a feeding waveguide, is illustrated in Figure 2.

The explicit expressions of the circuit elements as a function of the cavity and the waveguide parameters are reported in Table 1. In particular, the component R' models the losses due to the finite conductivity of the mirrors, while the term L' gives the effect of the skin depth δ. It sums to the inductive circuit part L_o modelling the cavity, thus producing a shift in the resonant frequency, which is equivalent to a cavity enlargement. The L_o, C series models the resonant cavity, while the component L_e takes into account the effect of cut-off modes in the feeding waveguide. The term β_{01} gives the waveguide-cavity factor as reported in [26], and Z_g is the characteristic impedance of feeding rectangular waveguide excited in its fundamental mode TE_{10}.

In Table 1, the term $2l$ gives the cavity length, a is the major waveguide dimension, σ represents the conductivity, while $k_o = 2\pi f_o/c$ is the free-space propagation constant, with c being the velocity of light and f_o the resonant frequency of the empty resonator.

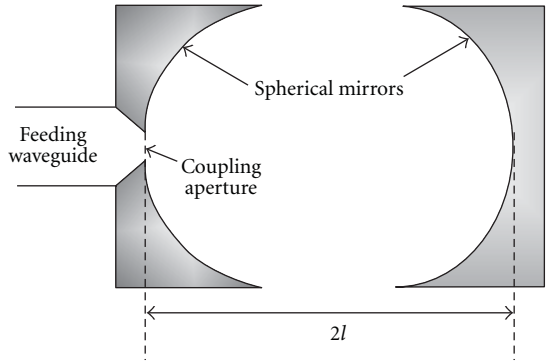

Figure 1: Open cavity fed by a rectangular waveguide.

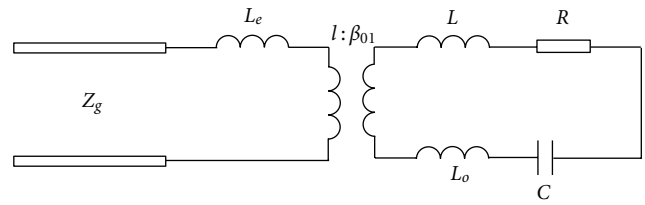

Figure 2: Equivalent circuit of open cavity fed by a rectangular waveguide.

From the circuit reported in Figure 2, it is straightforward to deduce the waveguide input impedance Z_i and the reflection coefficient Γ, respectively, given as

$$Z_i = j\omega L_e + \frac{Z_R}{\beta_{01}^2}, \qquad \Gamma = \frac{Z_i - Z_{10}}{Z_i + Z_{10}}, \tag{1}$$

where

$$Z_R = j\omega L_T + R' + \frac{1}{j\omega C}, \qquad L_T = L_o + L'. \tag{2}$$

In order to characterize the reflecting behavior of the single reflectarray element, a periodic array of identical elements is inserted at the center of the open cavity, as illustrated in Figure 3, where R_o gives the radius of the spherical mirror and w is the radius of the Gaussian beam. The open cavity configuration of Figure 1 results to be modified in Figure 3 by the insertion of a plane mirror at distance l, over which the microstrip array grid is fixed, thus half reducing the original open resonator system dimensions. As a consequence of this, the equivalent circuit of Figure 2 results to be modified as in Figure 4, with the addition of the impedance Z_a taking into account the presence of the reflecting surface. It must be observed that, due to the presence of the metallic plane at the center of the cavity, only odd modes are admissible.

The insertion of the grounded reflecting surface can be modelled by the equivalent circuit of Figure 5, where parameters L_1, C_1 depends on both the variable length L of the

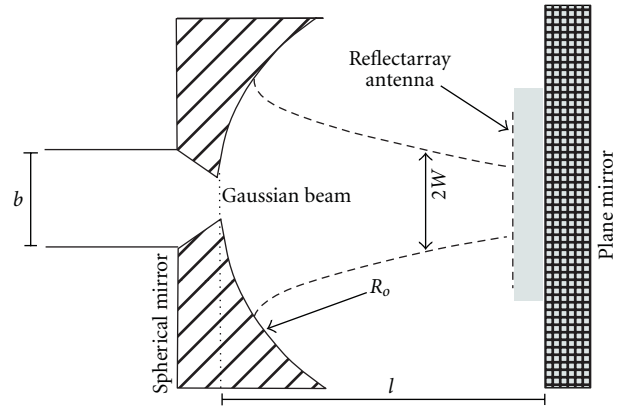

Figure 3: Open resonator system for reflectarray elements characterization.

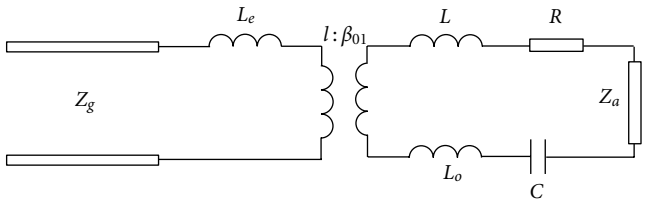

Figure 4: Equivalent circuit of open resonator system in Figure 3.

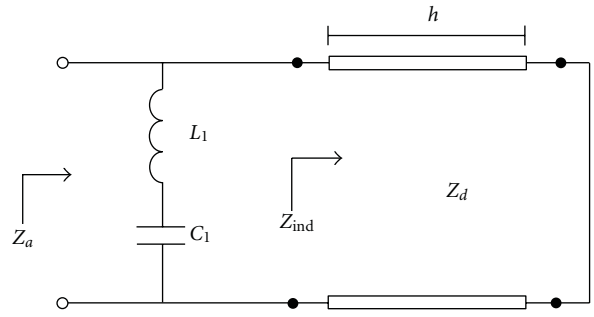

Figure 5: Equivalent circuit of grounded reflecting surface.

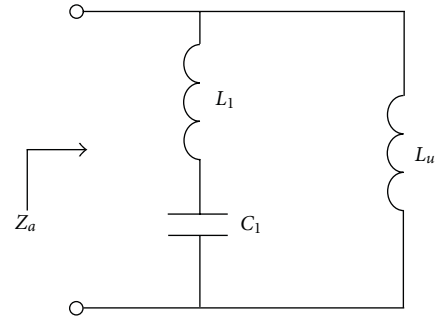

Figure 6: Simplification of equivalent circuit in Figure 5.

reflectarray patches and the grid spacing D between adjacent elements.

Due to the small thickness h, usually less than a quarter wavelength, the impedance Z_{ind} (Figure 5) can be simplified as follows:

$$Z_{\text{ind}} = jZ_d(k_d h - \phi_G), \tag{3}$$

where $Z_d = Z_o/\sqrt{\epsilon_r}$, $k_d = k_o\sqrt{\epsilon_r}$, Z_o and k_o being, respectively, the free-space impedance and propagation constant, while the phase shift ϕ_G takes into account the Gaussian nature of the beam [27, 28], and is given as

$$\phi_G = \arctan\frac{h}{z_R}. \tag{4}$$

The term $z_R = \sqrt{Rl - l^2}$ into (4) represents the Rayleigh distance.

To simplify the treatment, without loss of generality, the assumption of lossless dielectric with a relative permittivity ϵ_r is made for the reflectarray surface. However, few additional derivations can be performed to treat the real loss case.

It is straightforward to recognize into expression (3) an inductive effect, which can be modelled in terms of an equivalent inductance $L_u = Z_d(k_d h - \phi_G)$, as reported in Figure 6.

When inserting the equivalent circuit of Figure 6 into that of Figure 4, the resonator will show two resonant frequencies $f_{1,2}$, relevant to the circuit of Figure 7, which are given as

$$f_{1,2} = \frac{1}{2\pi}\sqrt{\frac{c \pm \sqrt{c^2 - 4d}}{2d}}, \tag{5}$$

where

$$\begin{aligned} c &= L_o C(L_1 + L_u)C_1 + CL_1L_uC_1, \\ d &= L_oC + (L_1 + L_u)C_1 + L_uC. \end{aligned} \tag{6}$$

From expressions (6), the unknown circuit parameters L_1, C_1 can be easily derived as

$$\begin{aligned} L_1 &= \frac{C_1A_1 + B_1}{C_1E_1}, \\ C_1 &= \frac{B_2E_1 - B_1E_2}{A_1E_2 - A_2E_1}, \end{aligned} \tag{7}$$

where

$$\begin{aligned} A_n &= (2\pi f_n)^2 L_u - (2\pi f_n)^4 L_u L_o C, \\ B_n &= (2\pi f_n)^2 (L_u + L_o)C - 1, \\ E_n &= (2\pi f_n)^4 (L_u + L_o)C - (2\pi f_n)^2 \end{aligned} \tag{8}$$

for $n = 1, 2$.

The resonant frequencies $f_{1,2}$ are directly obtained from the return loss measurement at the feeding waveguide input of the open resonator. This is loaded with a reflecting surface made of identical square patches having size L and spaced of a distance D. In order to best simulate the infinite array situation, a sufficient large array grid, typically greater than 7×7, must be considered.

As highlighted above, parameters L_1, C_1 are depending on the reflectarray geometry, so measurements need to be repeated for different patch dimensions in order to retrieve the phase response of the reflectarray element versus the tuning geometrical parameter.

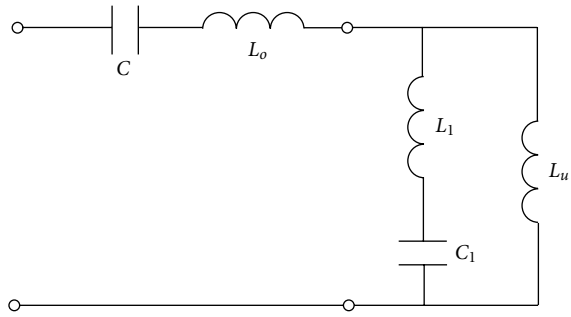

Figure 7: Resonant circuit for the computation of frequencies $f_{1,2}$.

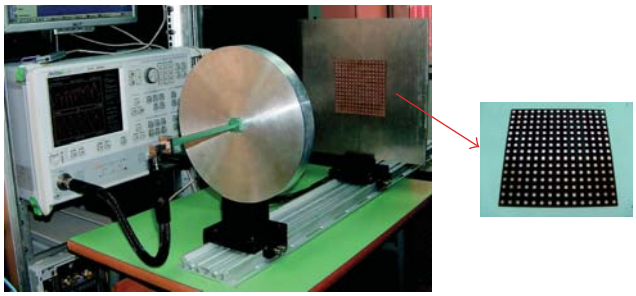

(a) (b)

Figure 8: Photograph of (a) open resonator system and (b) realized reflecting surface.

3. Experimental Validations

In order to experimentally validate the method outlined in the previous section, a K-band open resonator is designed with a mirror radius $R_o = 529$ mm and a distance $l = 421$ mm between the spherical and the flat mirrors. The resonator is tuned to work at a design frequency $f_o = 24$ GHz (the center operating frequency of the reflectarray to be tested), which corresponds to the excitation of $TEM_{0,0,131}$ mode inside the cavity.

The optimization of the waveguide-to-cavity transition is performed by following the approach outlined in [26], thus reducing the standard $WRG2$ waveguide height $b = 4.33$ mm to a value of 0.7 mm.

Reflectarray grids of 16×16 square patches with a spacing $D = 0.65\lambda_o$, for three different patch lengths L (3.2 mm, 3.5 mm, and 3.7 mm), are considered as test surfaces. A substrate dielectric with a nominal value $\epsilon_r = 2.33$ and thickness $h = 0.762$ mm is considered. In Figure 8(a), a photograph showing the open resonator system loaded with the testing array is reported, while in Figure 8(b) one of the realized reflecting surface is illustrated.

The test setup is mounted into the Microwave Laboratory at University of Calabria, equipped with complete facilities for both nearfield and far-field measurements [29, 30].

The magnitude of the measured reflection coefficient at the waveguide input for the three different dimensions is illustrated in Figures 9–11. For all cases, several resonances couples are visible, corresponding to the various modes excited into the cavity. However, the only couple to be considered is that modelled by the equivalent circuit of Figure 4, corresponding to the $TEM_{0,0,131}$ mode, which is associated to an empty cavity resonance $f_o = 24$ GHz. In the presence of each reflecting surface, two resonant frequencies $f_{1,2}$ are produced, as highlighted in the previous section. They can be easily identified in the return loss measurements (Figures 9–11) as follows.

Table 2: Resonant frequencies $f_{1,2}$ and relative values of parameters L_1, C_1.

Patch length L (mm)	f_1 (GHz)	f_2 (GHz)	L_1 (nH)	C_1 (fF)
3.2	23.95	25.88	4.06	7.55
3.5	23.78	24.22	4.24	8.44
3.7	22.95	24.02	4.54	8.70

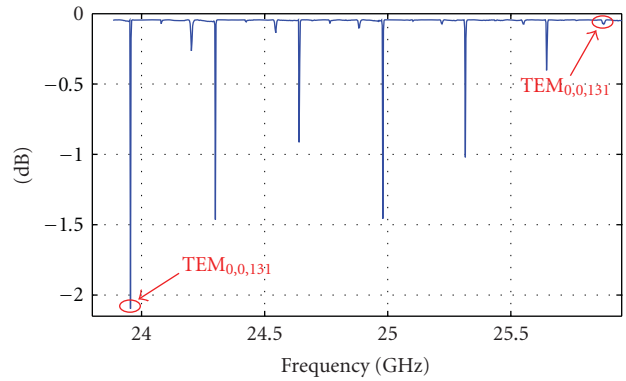

Figure 9: Measured return loss for the case $L = 3.2$ mm.

(i) For a patch side dimension L less than that providing the resonance condition, frequency f_1 is chosen as the nearest one (at the left side) to the resonance frequency f_o of the empty cavity, while the frequency f_2 corresponds to the resonance of the reflectarray grid, easily computed on the basis of the patch dimension L. This is the case corresponding to Figure 9.

(ii) For a patch side dimension L which is equal to that providing the resonance condition, frequencies $f_{1,2}$ are chosen as those which are equally far from the resonance frequency f_o of the empty cavity. This is the case corresponding to Figure 10.

(iii) For a patch side dimension L greater than that providing the resonance condition, frequency f_1 is chosen as the nearest one (at the right side) to the resonance frequency f_o of the empty cavity, while the frequency f_2 corresponds to the resonant frequency of the reflectarray grid, again computed on the basis of the patch dimension L. This is the case corresponding to Figure 11.

The relevant resonances $f_{1,2}$ are highlighted in Figures 9–11 and summarized in Table 2.

The measured resonance frequencies $f_{1,2}$ are used to retrieve the values of parameters L_1, C_1 (Table 2), which are applied into the equivalent circuit of Figure 5 to compute

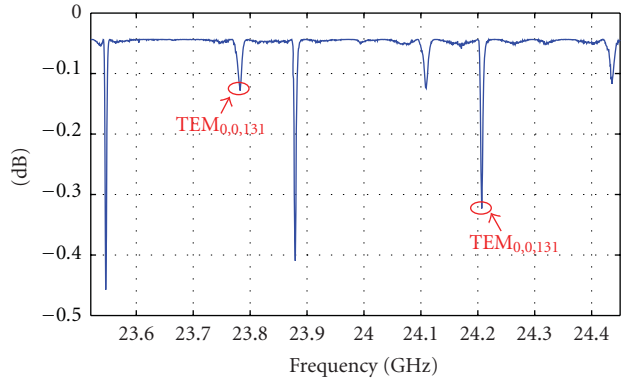

Figure 10: Measured return loss for the case $L = 3.5$ mm.

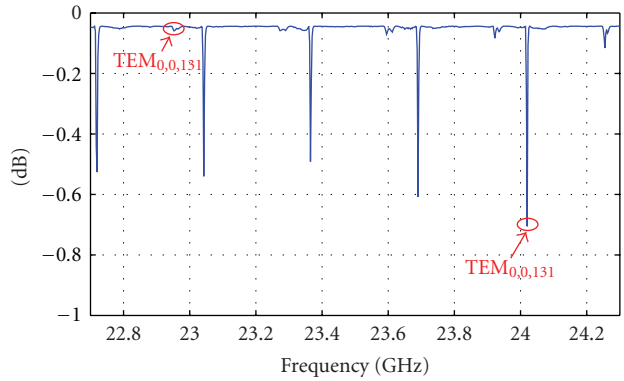

Figure 11: Measured return loss for the case $L = 3.7$ mm.

the impedance Z_a, subsequently adopted in the circuit of Figure 4 to obtain the phase of the reflection coefficient relative to the reflectarray grid. Results are reported in Figures 12–14 as a function of frequency for the three different dimensions of the patch side L. When performing the synthesis of microstrip reflectarrays [15], the reflection phase behavior of the single radiating element is of primary importance, as providing the proper dimensions of the tuning parameter (e.g., the patch side L) which are able to guarantee the phase distribution on the array grid assuring the prescribed-field pattern. To validate the results provided by the proposed approach, the reflection phase computed by Ansoft Designer software (infinite array approach) is also reported in Figures 12, 13, and 14, and a successful agreement can be observed.

Finally, the information retrieved from the three different measurements are combined to obtain the reflectarray phase design curve versus the patch length L. Again, the effectiveness of the approach is successfully demonstrated in Figure 15 by comparison with the results coming from Ansoft Designer simulations.

4. Conclusions

The use of an open cavity has been proposed in this work to characterize variable patches microstrip reflectarrays. An equivalent circuit including both the open resonator and the

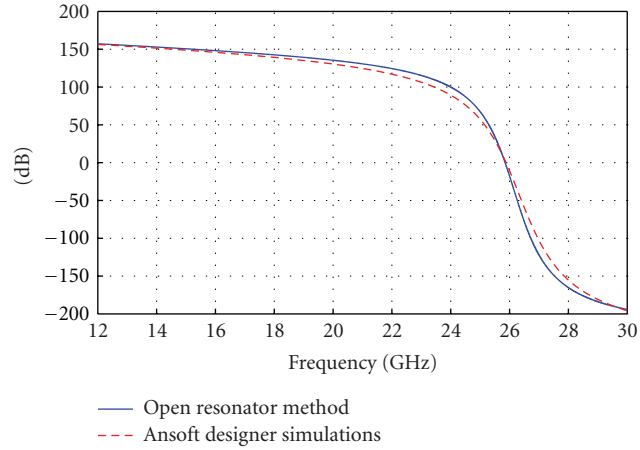

Figure 12: Reflection phase versus frequency for the case $L = 3.2$ mm.

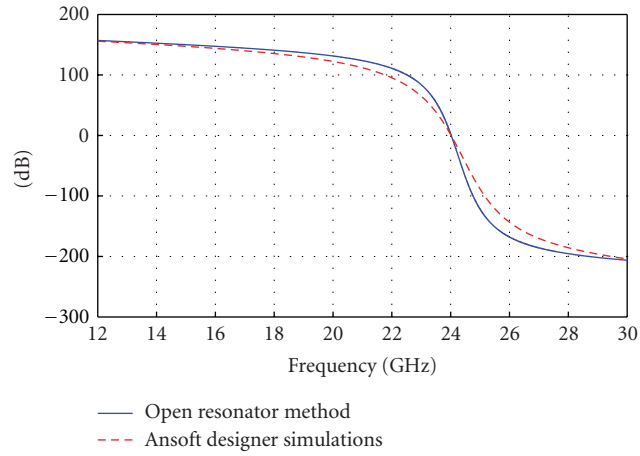

Figure 13: Reflection phase versus frequency for the case $L = 3.5$ mm.

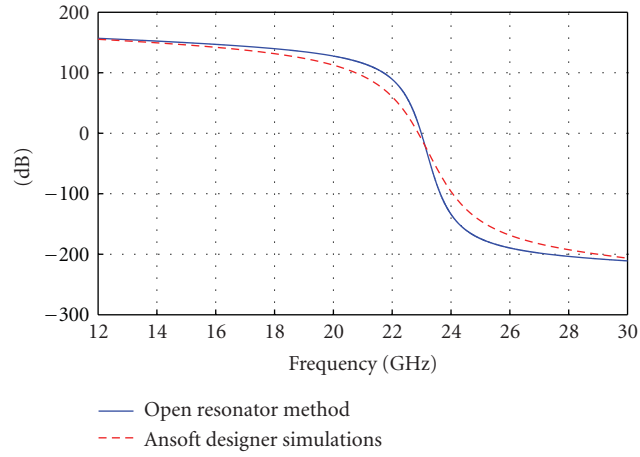

Figure 14: Reflection phase versus frequency for the case $L = 3.7$ mm.

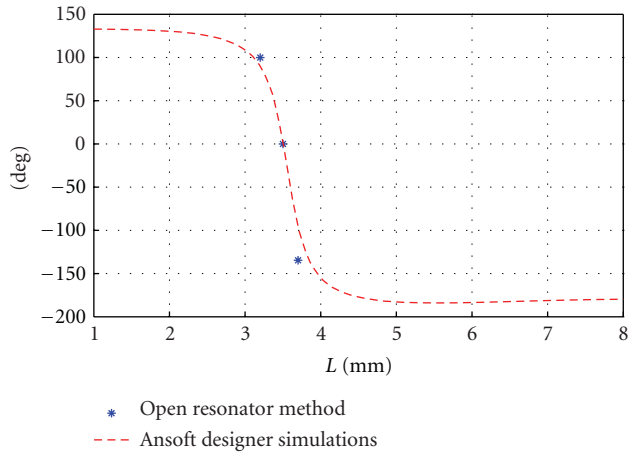

Figure 15: Reflection phase versus patch length L.

reflecting surface has been adopted to recover the reflection phase versus the patch length from return loss measurements at the feeding waveguide input. Experimental validations have been successfully discussed on K-band reflectarrays prototypes.

The proposed characterization method is particularly suitable for millimeter-wave applications [31, 32], where the reduced dimensions [33] make impractical the adoption of standard techniques.

Concerning further developments, an extended formulation of the method including also the dielectric losses will be considered in future studies to fully characterize the reflectarray element response in both amplitude and phase.

References

[1] J. Huang and Analysis of a microstrip reflectarray antenna for microspacecraft applications, TDA Progress Report 153173, 1995.

[2] J. Huang, "Capabilities of printed reflectarray antennas," in *Proceedings of the 1996 IEEE International Symposium on Phased Array Systems and Technology*, pp. 131–134, October 1996.

[3] D. Berry, R. Malech, and W. Kennedy, "The reflectarray antenna," *IEEE Transactions on Antennas and Propagation*, vol. 11, no. 6, pp. 645–651, 1963.

[4] H. Fang, M. Lou, J. Huang, L.M. Hsia, and G. Kerdanyan, "Design and development of an inflatable refectarray antenna," IPN Progress Report 42-149, 2002.

[5] R. D. Javor, X. D. Wu, and K. Chang, "Design and performance of a microstrip reflectarray antenna," *IEEE Transactions on Antennas and Propagation*, vol. 43, no. 9, pp. 932–939, 1995.

[6] J. Huang and A. Encinar, *Reflectarray Antennas*, IEEE Press, NY, USA.

[7] D. M. Pozar, S. D. Targonski, and H. D. Syrigos, "Design of millimeter wave microstrip reflectarrays," *IEEE Transactions on Antennas and Propagation*, vol. 45, no. 2, pp. 287–296, 1997.

[8] J. C. Ginn, B. A. Lail, and G. D. Boreman, "Phase characterization of reflectarray elements at infrared," *IEEE Transactions on Antennas and Propagation*, vol. 55, no. 11 I, pp. 2989–2993, 2007.

[9] D. M. Pozar, S. D. Targonski, and R. Pokuls, "A shaped-beam microstrip patch reflectarray," *IEEE Transactions on Antennas and Propagation*, vol. 47, no. 7, pp. 1167–1173, 1999.

[10] A. Kelkar, "FLAPS: conformal phased reflecting surfaces," in *Proceedings of the 1991 IEEE National Radar Conference*, pp. 58–62, March 1991.

[11] J. Huang and R. J. Pogorzelski, "A ka-band microstrip reflectarray with elements having variable rotation angles," *IEEE Transactions on Antennas and Propagation*, vol. 46, no. 5, pp. 650–656, 1998.

[12] L. Boccia, F. Venneri, and G. Di Massa, "A Varactor Loaded Reflectarray Antenna," in *Proceedings of the International Conference on Electromagnetics in Advanced Applications (ICEAA'01)*, September 2001.

[13] F. Venneri, S. Costanzo, G. Di Massa et al., "Beam-scanning reflectarray based on a single varactortuned element," *International Journal of Antennas and Propagation*, vol. 2012, Article ID 290285, 5 pages, 2012.

[14] F. Venneri, S. Costanzo, and G. Di Massa, "Reconfigurable aperturecoupled reflectarray element tuned by single varactor diode," *Electronics Letters*, vol. 48, pp. 68–69, 2012.

[15] F. Venneri, S. Costanzo, G. Di Massa, and G. Angiulli, "An improved synthesis algorithm for reflectarrays design," *IEEE Antennas and Wireless Propagation Letters*, vol. 4, no. 1, pp. 258–261, 2005.

[16] F. Venneri, S. Costanzo, G. Di Massa, P. Corsonello, and M. Salzano, "Design of a reconfigurable reflectarray based on a varactor tuned element," in *Proceedings of the European Conference on Antennas and Propagation (EuCAP'12)*, Prague, Czech Republic, March 2012.

[17] S. V. Hum, M. Okoniewski, and R. J. Davies, "Modeling and design of electronically tunable reflectarrays," *IEEE Transactions on Antennas and Propagation*, vol. 55, no. 8, pp. 2200–2210, 2007.

[18] M. R. Chaharmir, J. Shaker, M. Cuhaci, and A. R. Sebak, "Novel photonically-controlled reflectarray antenna," *IEEE Transactions on Antennas and Propagation*, vol. 54, no. 4, pp. 1134–1141, 2006.

[19] R. C. Hansen, *Phase Array Antennas*, Wiley & Sons, New York, NY, USA, 2009.

[20] F. C. E. Tsai and M. E. Bialkowski, "An equivalent waveguide approach to designing of reflect arrays with the use of variable-size microstrip patches," *Microwave and Optical Technology Letters*, vol. 34, no. 3, pp. 172–175, 2002.

[21] F. C. E. Tsai and M. E. Bialkowski, "Designing a 161-element Ku-band microstrip reflectarray of variable size patches using an equivalent unit cell waveguide approach," *IEEE Transactions on Antennas and Propagation*, vol. 51, no. 10, pp. 2953–2962, 2003.

[22] J. C. Ginn, B. A. Lail, and G. D. Boreman, "Phase characterization of reflectarray elements at infrared," *IEEE Transactions on Antennas and Propagation*, vol. 55, no. 11 I, pp. 2989–2993, 2007.

[23] M. Bozzi, S. Germani, and L. Perregrini, "A figure of merit for losses in printed reflectarray elements," *IEEE Antennas and Wireless Propagation Letters*, vol. 3, no. 1, pp. 257–260, 2004.

[24] F. A. Tahir, *Electromagnetic modeling of microstrip reflectarrays using scale changing technique [Ph.D. thesis]*, Universit di Toulouse, 2011.

[25] C. Fabry and A. Perot, "Theorie et applications d'une nouvlle method de spectroscopie interfrentielle," *Annales de Chimie et de Physique*, vol. 716, p. 115, 1899.

[26] O. M. Bucci and G. Di Massa, "Open resonators powered by a rectangular waveguide," *IEE Proceedings H: Microwaves, Antennas and Propagation*, vol. 139, no. 4, pp. 323–329, 1992.

[27] Yu. P. K. and A. L. Cullen, "Measurement of permittivity by means of an open resonator - 1. theoretical," *Proceedings of The Royal Society of London, Series A*, vol. 380, no. 1778, pp. 49–71, 1982.

[28] A. C. Linch, "Measurement of permittivity by means of an open resonator. II Experimental," *Proceedings of the Royal Society A*, vol. 380, pp. 73–76, 1982.

[29] S. Costanzo and G. Di Massa, "An integrated probe for phaseless near-field measurements," *Measurement*, vol. 31, pp. 123–129, 2002.

[30] S. Costanzo and G. Di Massa, "Direct far-field computation from bi-polar near-field samples," *Journal of Electromagnetic Waves and Applications*, vol. 20, pp. 1137–1148, 2006.

[31] S. Costanzo, I. Venneri, G. Di Massa, and G. Amendola, "Hybrid array antenna for broadband millimeter-wave applications," *Progress In Electromagnetics Research—PIER*, vol. 83, pp. 173–183, 2008.

[32] S. Costanzo, I. Venneri, G. Di Massa, and A. Borgia, "Benzocyclobutene as substrate material for planar millimeter-wave structures: dielectic characterization and application," *Journal of Infrared, Millimeter and Terahertz Waves*, vol. 31, pp. 66–77, 2010.

[33] S. Costanzo, "Synthesis of multi-step coplanar waveguide-to-microstrip transition," *Progress in Electromagnetics Research—PIER*, vol. 113, pp. 111–126, 2011.

Hindawi Publishing Corporation
International Journal of Antennas and Propagation
Volume 2012, Article ID 541354, 10 pages
doi:10.1155/2012/541354

Research Article

Neural Network Characterization of Reflectarray Antennas

Angelo Freni,[1] Marco Mussetta,[2] and Paola Pirinoli[3]

[1] *Dipartimento di Elettronica e Telecomunicazioni, Università degli Studi di Firenze, 50121 Florence, Italy*
[2] *Dipartimento di Energia, Politecnico di Milano, 20156 Milan, Italy*
[3] *Dipartimento di Elettronica e Telecomunicazioni, Politecnico di Torino, 10129 Turin, Italy*

Correspondence should be addressed to Marco Mussetta, marco.mussetta@polimi.it

Received 3 March 2012; Accepted 11 May 2012

Academic Editor: Sandra Costanzo

An efficient artificial neural network (ANN) approach for the modeling of reflectarray elementary components is introduced to improve the numerical efficiency of the different phases of the antenna design and optimization procedure, without loss in accuracy. The comparison between the results of the analysis of the entire reflectarray designed using the simplified ANN model or adopting a full-wave characterization of the unit cell finally proves the effectiveness of the proposed model.

1. Introduction

Printed reflectarrays (RAs) have become nowadays a well-established technology for the realization of high performance antennas to be used in different applications, ranging from earth stations or onboard antennas in satellite communication systems to radar antennas mounted on vehicles (see e.g., [1–10]).

The need of providing high performances and satisfying potentially conflicting requirements generally forces the use of complex configurations, with a large number of reradiating elements. At their turn, the latter could present a complex structure, with several degrees of freedom, which have to be adjusted in order to satisfy the antenna constraints. All these factors concur to increase the RA design complexity and, therefore, the use of an indirect synthesis procedure based on an optimization algorithm could be convenient, since it can handle a large number of degrees of freedom and provide a configuration satisfying at the best the different constraints on the antenna [11–13].

The RA design procedure can be seen as the cascade of two steps, organized as in the block diagram of Figure 1: the characterization of the single RA reradiating element with respect to several parameters, and the optimized design of the entire structure, managed by a global optimization tool. A further step could be added, before the antenna manufacturing, consisting in a full-wave analysis of the entire RA (virtual prototyping).

The starting point of the design procedure is to obtain a map of the phase and the amplitude of the reflection coefficient of the RA single element as a function of selected geometrical parameters. This is usually done adopting a full wave MoM approach and considering the single RA element embedded in a periodic lattice on which a plane wave impinges. The generation of these maps is computationally expensive, since it requires the full-wave analysis of the periodic array for several values of the free geometrical parameters, as well as for different frequencies and angles of incidence. Moreover, if the design of the entire reflectarray is carried out exploiting an optimization procedure, based on the use of a pseudo-stochastic algorithm, the reflection coefficient sampling rate has to be quite high. Finally, the storage of data produced by these simulations requires a large amount of dynamic memory. In view of reducing these computational and memory efforts, it would be useful to introduce an equivalent model of the reradiating element. If its geometry is simple, its behavior could be approximated with an equivalent transmission line model [11, 14]: in this case, no full-wave analysis has to be carried out, since the simplified model is directly managed by the optimization tool. Unfortunately, such an approximation is no longer applicable when the geometry complexity increases and a more general model is required.

Here, a modeling technique, independent from the RA reradiating element structure and able to reproduce its

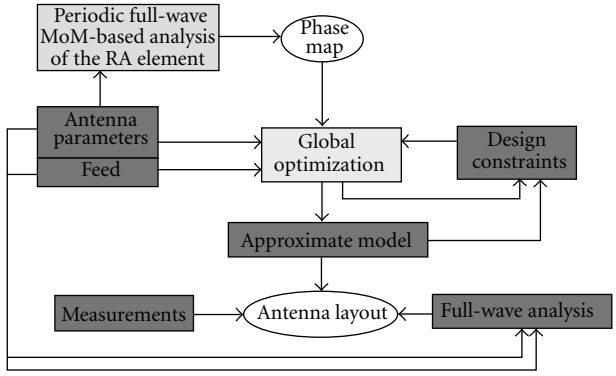

Figure 1: Block diagram of the proposed design procedure.

behavior at a reduced computational cost, is presented. It is based on the use of an artificial neural network (ANN) for simulating the relationship between the local re-radiated field and the geometrical parameters of the element, so that it becomes possible to compute the reflection coefficient of the reradiating element for any value of the RA parameters, starting from a reduced set of data obtained through the standard full-wave analysis.

Preliminary results of the modeling of a RA reradiating element behavior with an ANN have been presented in [15], where only some plots of the phase of the reflection coefficient computed with the ANN and a guess of the introduced error are shown, and in [16] where the reflection coefficient phase reconstructed by the ANN has been used to compute the field re-radiated by a reflectarray in which the reradiating elements are double square concentric rings and only one geometric parameter has been used to control the phase variation. The validity of the approach has been confirmed also in [17], where it is used for the reflection coefficient phase of a multilayer reradiating element; however, also in this paper only the results about the comparison between the full-wave and the ANN computed reflection coefficient are shown.

Here, the ANN model will be used for computing the variation of the *entire* reflection coefficient for both the vertical and horizontal polarizations with the reradiating element geometrical parameters, the frequency, and the angle of incidence. First, the computational time and the memory reduction due to the introduction of the ANN are investigated, considering reradiating elements of increasing complexity. Then, the attention has been focused on the RA introduced in [7] where the reradiating elements are modified Malta Cross, characterized by two geometrical degrees of freedom for controlling the re-radiated field: the effect of the use of the ANN model will be considered not only analyzing the error introduced on the reflection coefficient, but also that on the field radiated by the entire reflectarray.

2. Artificial Neural Networks

An artificial neural network (ANN) is a computational model that simulates the features and behaviors of the human brain neurons [18, 19], that is, it is a self-adaptive data modeling tool that changes its structure on the basis of external or internal information that flows through the network during the learning phase. In particular, an ANN consists of an interconnected group of artificial neurons that suitably processes information according to the strength of connections among them.

In more practical terms neural networks are nonlinear statistical data modeling tools. They can be used to model complex relationships between inputs and outputs or to find patterns in data. For this reason, ANNs are useful tools when it is necessary to understand the complex and nonlinear relationships among data, without any a priori assumption concerning the nature of these correlations.

In recent years, ANN have been extensively employed in many antenna applications and in particular in problems involving smart antennas: in [20] an ANN is employed to model the active-aperture antenna shape in real time, in [21, 22] direction-of-arrival and multiple-source tracking for wireless terrestrial, and satellite mobile communications are addressed employing neural-network-based smart antennas. Moreover, in [23] ANNs are applied to the scattering of a nonlinearly loaded antenna by modeling its RCS. ANN has been also used for antenna optimization in conjunction with evolutionary algorithms: in [24] the design of a wideband microstrip antenna is performed using a genetic-algorithm-coupled ANN in computing the radiation pattern and the resonant frequency; in [25] an ANN is proposed to predict the input impedance of a broadband antenna as a function of its geometric parameters. The antenna structure is then optimized for broadband operation via a genetic algorithm that uses input impedance estimates provided by the trained ANN. Patch antenna modeling is another application of ANN: in [26] an ANN is used to design the parameters of square and rectangular patch antenna; in [27] a neural network model of slotted patch antenna is developed to calculate the resonant frequency and minimum value of S_{11} parameter considering both antenna dimensions and dielectric characteristics. Moreover, in [28] a neural network-based solution is employed to relate a given radiated field distribution with the voltages that must be applied to each radiating element taking into account mutual coupling effects without increase of complexity.

The characteristics of an ANN depend on its topology, that is, on the pattern of connections between the neurons and the propagation of data. Here, for the modeling of the reradiating element behavior, the multilayered perceptron (MLP), has been used.

The MLP implements a feed-forward topology, in which the data flow from the input to the output layers is strictly forward, and consists of an input layer, one or more hidden layer, and an output layer. The resulting network structure is that depicted in Figure 2, where the dependencies between variables are represented by the connections among neurons. The input composition in each neuron is made by a nonlinear weighted sum,

$$f(x) = k(x)\left(\sum_i w_i g_i(x)\right), \tag{1}$$

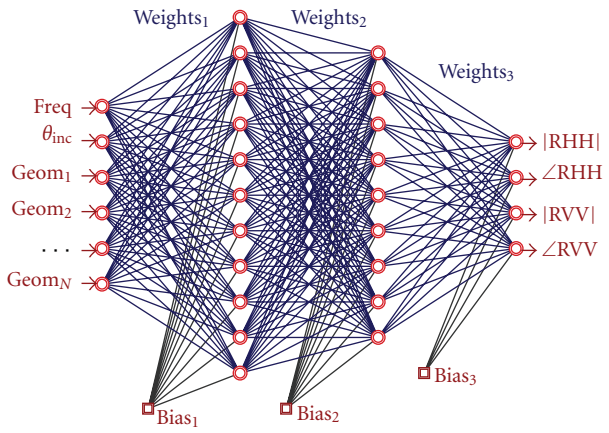

Figure 2: A typical multilayered perceptron structure, with 6 input and 4 output neurons and 2 hidden layers of 11 and 9 neurons, respectively.

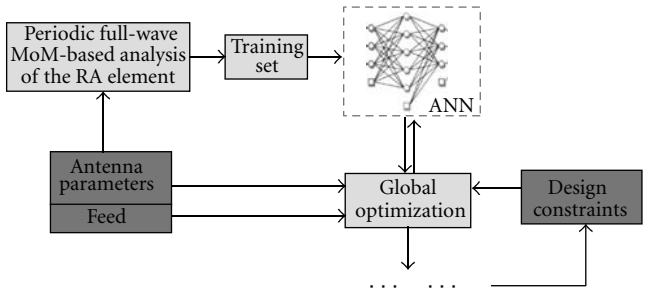

Figure 3: Part of the block diagram of Figure 1 modified by introduction of ANN.

where $k(x)$ is a nonlinear activation function which models the activity of biological neurons in the brain. This function must always be normalizable and differentiable and it is modeled in several ways; the most common is the hyperbolic tangent, which ranges from -1 to 1:

$$k(x) = \tanh(x). \tag{2}$$

2.1. Neural Network Training. A neural network works properly when, for any set of inputs, it produces the desired set of outputs. This means that the connections between the different nodes in the network are set properly, that is, the weights w_i have been correctly chosen.

The definition of these weights is generally done during a training phase: in the so-called *supervised learning* scheme the neural network is fed with a set of input-output pairs already known, called Training Set (TS): for a given number N of these pairs (x_i, y_i), where $x_i \in X$, $y_i \in Y$, it is necessary to find a function:

$$f : X \longrightarrow Y, \tag{3}$$

that matches the examples of the TS. Thus, weights are changed according to a suitable learning rule, until the error on the ANN outputs is minimized [29].

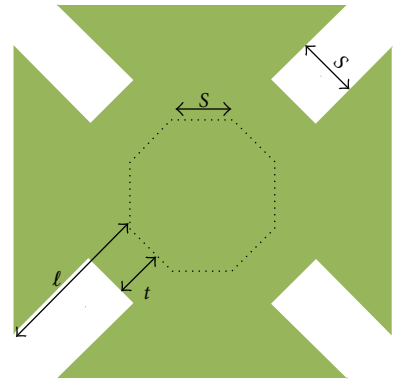

Figure 4: Single cell of the modified Malta Cross.

Among different learning rules, error backpropagation (EBP) is a well-known analytical algorithm used for neural networks training. In literature, there are several forms of backpropagation, all of them requiring different levels of computational efforts; the conventional back-propagation method is, however, the one based on the gradient descent algorithm. EBP propagates error backwards through the network to allow the error derivatives for all network weights to be efficiently computed. In other words, network weights are optimized in order to reach a good and accurate output and this objective is reached typically minimizing the mean-squared error between the network's output, $f(x_i)$, and the target value y_i over all the N example pairs.

Training is time and memory consuming and is the most critical phase in the ANN set up, since it must provide continuous feedback on the quality of solutions obtained thus far.

To test the ANN generalization capability, a validation set (VS) is defined too, containing known (x_i, y_i) pairs not used in the TS, in order to check the correct association between unknown input and output data.

2.2. Neural Network Use in RA Characterization. Once trained, the ANN can be considered as a black box: the desired output can be forecast for any arbitrary set of input data. For the case under analysis, the inputs are represented, as sketched in Figure 2, by the reradiating element geometrical degrees of freedom, the frequency, and the angle of incidence, while the expected output is the total reflection coefficient for both the horizontal and vertical polarization. Note that the angle of incidence of the impinging field could noticeably vary from one border to the other of the planar reflector, especially when it has a large electrical size and the feed is offset. Note also that generally the amplitude of the reflection coefficient is neglected during the design of a RA, since it is assumed to be equal to unity; however, for some particular values of the geometrical parameters, this amplitude decreases (at the structure resonances), and therefore it becomes necessary to take into account also of this phenomenon.

It has been found that the relation between the above inputs and outputs could properly model with an ANN

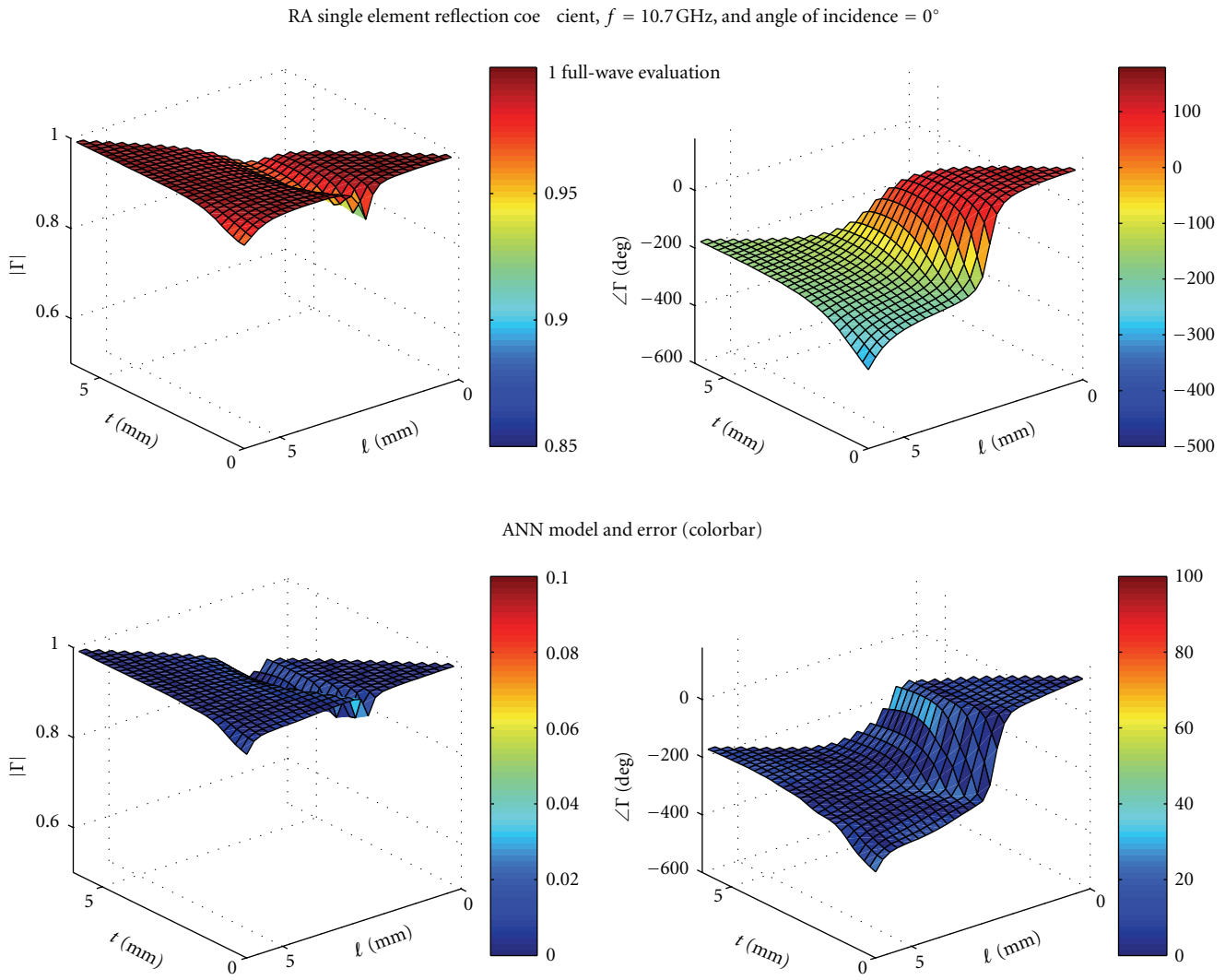

FIGURE 5: Reflection coefficient amplitude (left) and phase (bottom) versus the two RA geometrical parameters ℓ and t of the modified Malta Cross, computed with direct full-wave (top) and reconstructed with the ANN (bottom). $f = 10.7$ GHz, $\theta_{inc} = 0°$.

consisting in two hidden layers with 11 neurons in the first layer and 9 in the second one.

Introducing the ANN model of the reradiating element, the RA design procedure is modified as sketched in Figure 3, with the advantage that only the TS data are computed with the full wave approach and stored only for the training phase, since after that they are useless. In fact, during the RA design procedure, guided by the optimization tool, this latter will directly introduce in the ANN the geometrical free parameters relative to each RA element and the ANN will produce the corresponding reflection coefficient, with a clear reduction of the computational time and of the memory requirements, as proved by the results relative to different types of reradiating elements reported in the next section.

3. Numerical Results

The effectiveness of the use of a proper ANN for modeling the behavior of a single RA element has been investigated, considering both its numerical efficiency and the error introduced not only on the single element reflection coefficient, but also on the radiation patterns of an entire RA.

For what concerns the ANN model numerical efficiency, we have considered different types of reradiating elements, with different degrees of complexity, and for all of them we have computed the time and the memory reduction introduced by the ANN model. For doing that, first we have computed the reflection coefficient maps with the periodic full-wave approach; since they depend also on both the frequency and the angle of incidence, which, at their turn, vary from one application to another, we have decided to refer, as a reference example, to a particular reflectarray, the one that is described in [7]: it consists of 36×36 elements, corresponding to an electrical size of almost $16\lambda \times 16\lambda$ at the central frequency of 11.7 GHz, it is offset fed, and the direction of maximum radiation forms a slant angle of 15° with respect to the broadside. Moreover, the design has been carried out so that the antenna works on the frequency band

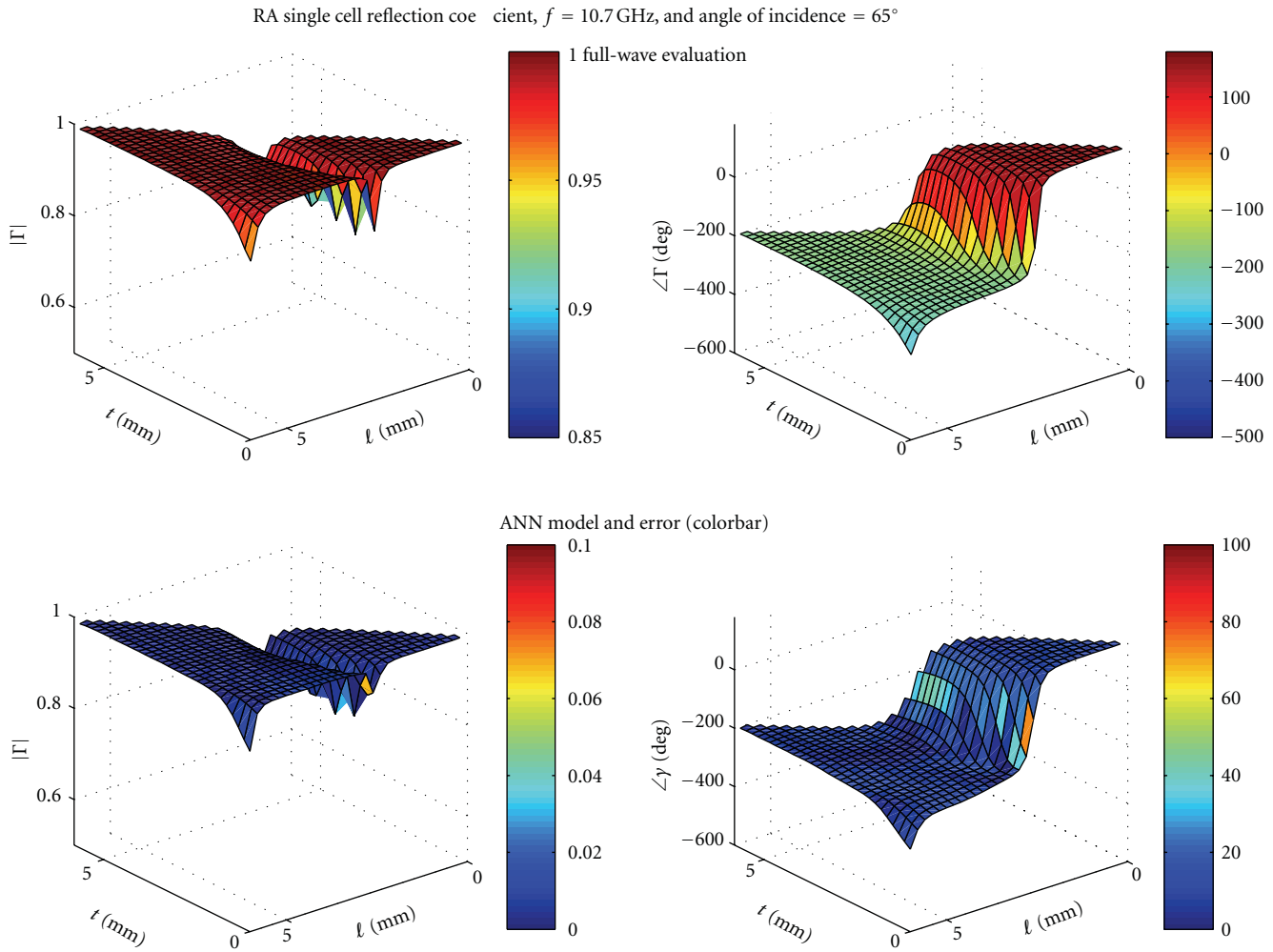

FIGURE 6: Reflection coefficient amplitude (left) and phase (bottom) versus the two RA geometrical parameters ℓ and t of the modified Malta Cross, computed with direct full-wave (top) and reconstructed with the ANN (bottom). f = 10.7 GHz, $\theta_{inc} = 65°$.

[10.7–12.7] GHz. For such a structure, it has been seen that a total number of 50 samples is required to well represent the reflection coefficient variation with frequency and angle of incidence. Note that the maximum angle of incidence considered is equal to 65° and that the variation of the reflection coefficient increases for greater angle of incidence. This behaviour makes it necessary to consider a not uniform sampling of this quantity. This number of frequency and angle of incidence samples will be assumed to be the same for all the different types of reradiating element that will be considered in the following.

The simplest type of reradiating element we have considered has been a square, single-layer patch, for which the reflection coefficient variation is obtained varying the side ℓ of the patch itself. It has been seen that a reasonable discretization of the interval of variation for ℓ is obtained with 35 samples. As a second example of reradiating element, we have considered the modified Malta Cross introduced in [7] and shown also in Figure 4 for the sake of clarity, in which, to better control the frequency dependence of the re-radiated field and to enhance the bandwidth, two geometrical parameters, that is, ℓ and t in Figure 4, are used. Their good discretization is reached with 31 samples for each of the two geometrical quantities. The other two configurations considered consist in two and three-layer stacked square patches. In both cases the geometrical free parameters are the side of the square patches, whose interval of variation has been discretized with 34 samples each.

In the second and third columns of Table 1, it is reported the total time needed to compute the reflection coefficient maps and the dynamic memory necessary for their storage using the periodic full-wave approach relatively to the four types of reradiating elements. These full-wave simulations have been performed using Ansoft Designer, on an Intel Core2 Duo E4700, 2.6 GHz, 2 Gb RAM system. Note that both the computational cost and the memory requirements increase drastically with the reradiating element complexity.

In view of reducing both the computational time and the memory occupation, the dependence of the reflection coefficient from the free geometrical parameters of each reradiating element, from the frequency, and from the angle

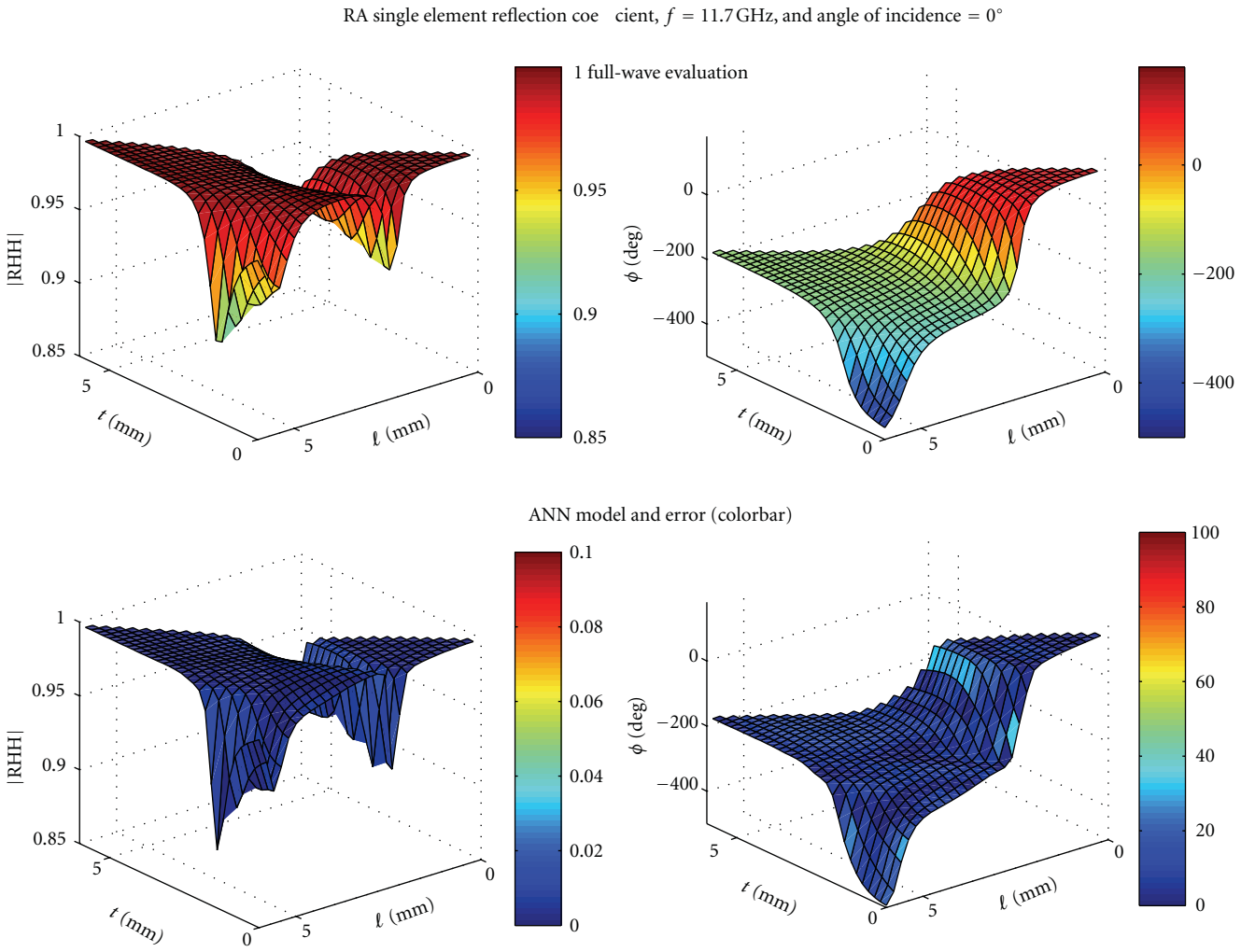

Figure 7: Reflection coefficient amplitude (left) and phase (bottom) versus the two RA geometrical parameters ℓ and t of the modified Malta Cross, computed with direct full-wave (top) and reconstructed with the ANN (bottom). $f = 11.7$ GHz, $\theta_{\text{inc}} = 0°$.

Table 1: Computational time and memory requirement for the evaluation and the storage of the reflection coefficient maps for different types of re-radiating elements, with the periodic full-wave approach and the ANN training.

Element type	Full wave		ANN training	
	Computational time	Memory requirement	Computational time	Memory requirement
1-layer square patch	4 h 45 min	0.9 Mb	55 min	9.5 Kb
1-layer modified Malta Cross	65 h	2.5 Mb	4 h	134 Kb
2-layer stacked patches	241 h	3.2 Mb	13 h 30 min	160 Kb
3-layer square patches	1.2×10^4 h	67 Mb	341 h 50 min	2.87 Mb

of incidence has been modeled with the ANN described in Section 2.

Since the most critical end expensive phase in the use of an ANN is its training, we consider here as the ANN computational cost and memory occupation those required in that phase. The computational time required for the neural network training is given by the sum of the time necessary to compute the data for the training and that required by the actual training. In the fourth column of Table 1 the training total computational time for the four reradiating element is reported. The data for the training are still obtained with the full-wave simulations: it has been seen that a good reconstruction of the reflection coefficient has been guaranteed by 10 samples for the total of frequency and angle of incidence, while the number of samples for the geometrical parameters varies from one element to another. Comparing the second and the fourth columns of Table 1, it is possible to see that the ANN training requires globally a computational cost varying from 0.19 to 0.028 times that needed for collecting the data when the traditional approach

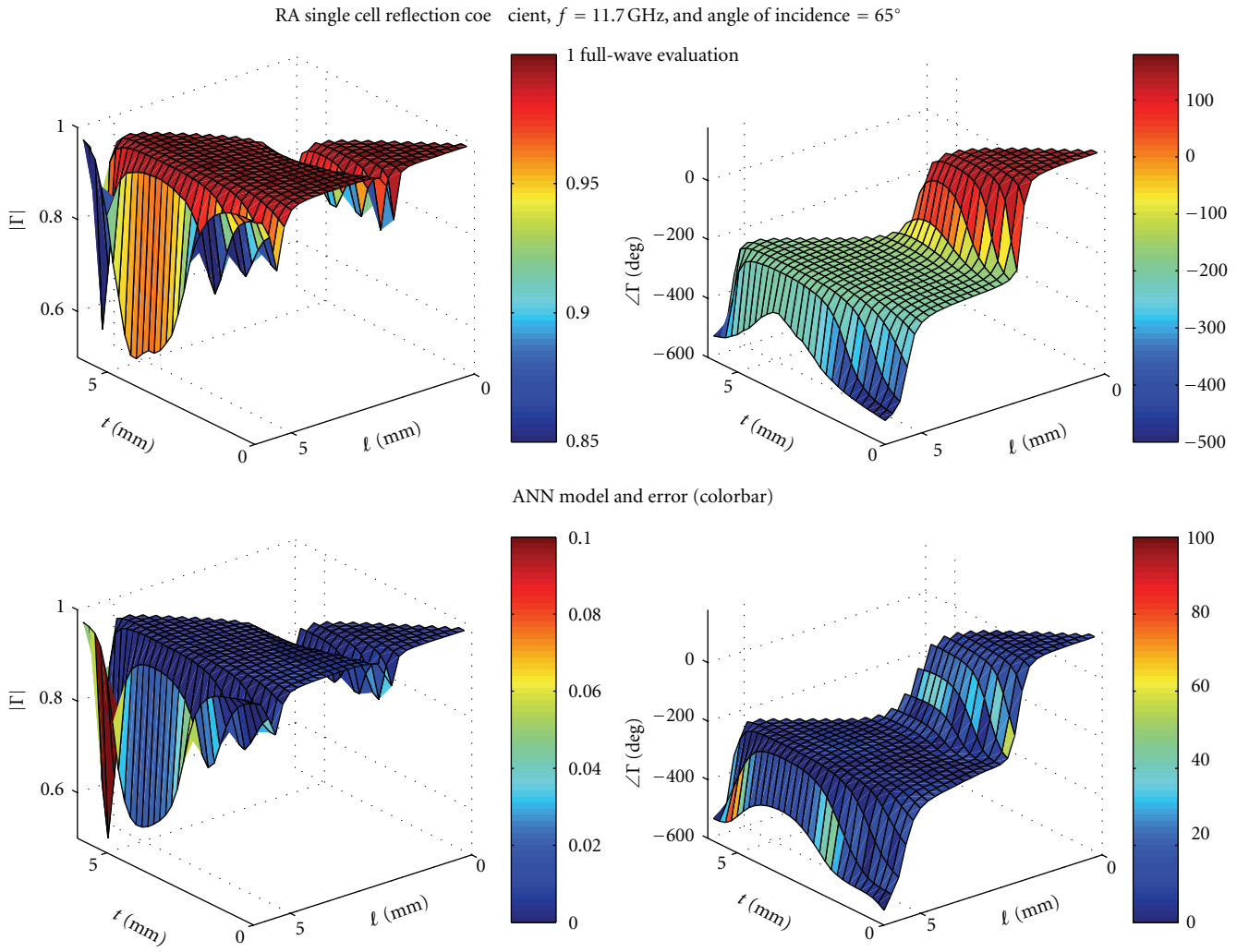

Figure 8: Reflection coefficient amplitude (left) and phase (bottom) versus the two RA geometrical parameters ℓ and t of the modified Malta Cross, computed with direct full-wave (top) and reconstructed with the ANN (bottom). $f = 11.7$ GHz, $\theta_{\text{inc}} = 65°$.

is used. Note that, when used in the RA design and/or analysis procedure, the computational time required by the ANN to compute the reflection coefficient in correspondence of a value for the geometrical degrees of freedom, for the frequency and for the angle of incidence is of the order of 40 μsec.

The use of the neural network drastically reduces also the memory occupation: in the fifth column of Table 1, it is reported the dynamic memory needed to store the data during the training section, obviously lower than the case in which the full-wave approach is used. However, it has to be remarked that the memory reduction factor, that comes out from comparing the third and the fifth column of Table 1, is valid only for the training section, since at the end of the training these data could be removed, and the memory occupation of the neural network is around 5 KB, equal to 0.002 times that required by collecting all the data used in the traditional approach.

In order to verify if the use of the ANN for the modeling of the RA single cell does not only guarantees a strong reduction of both the computational cost and of the memory requirement but also gives its accurate representation, we have also investigated the error that ANN model introduces on the reflection coefficient and on the radiating characteristics of the RA. With this aim, we have considered the 16×16 offset reflectarray already introduced in [7] and described at the beginning of this section, in which the reradiating elements are the modified Malta Cross.

Figures 5, 6, 7, and 8 show the variation of the reflection coefficient phase and amplitude with the two geometrical parameters ℓ and t reconstructed using the ANN (bottom) or obtained by the direct full-wave analysis of the periodic structure (top), for one of the extremes and the central frequency of the RA band and for two different angles of incidence ($\theta_{\text{inc}} = 0°$ and $\theta_{\text{inc}} = 65°$). The colorbars on the top give the values of the reflection coefficient amplitude (left) and phase (right), while those on the bottom show the error introduced by the use of the ANN model.

From the plots in Figures 5, 6, 7, and 8, it is possible to draw the following conclusions:

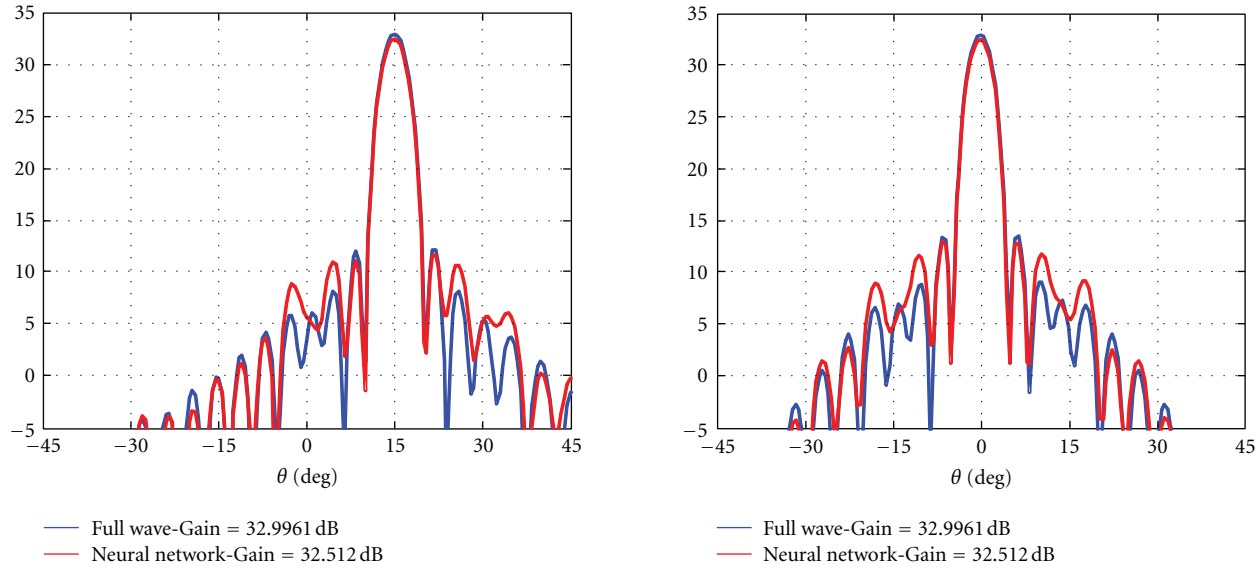

Figure 9: Radiation pattern of the RA antenna with modified Malta Cross reradiating elements at 7.8 GHz: comparison between the results obtained using full-wave computed reflection coefficient values or ANN.

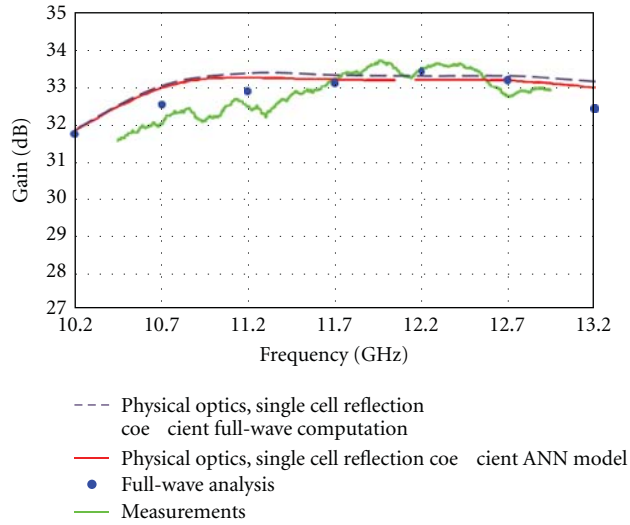

Figure 10: Variation of the maximum gain on the band 10.7–12.7 GHz for the RA with modified Malta Cross reradiating elements.

(i) the amplitude of the reflection coefficient does not vary substantially for low values of frequency and angles of incidence;

(ii) the error introduced by the ANN on the amplitude of the reflection coefficient is really small;

(iii) the phase varies in the range [0–600°];

(iv) the error introduced by the use of the ANN on the phase is well controlled, even if there are some single spots, where the slope of the phase curve is higher than could become remarkable. It is worth noting that these spots take place in correspondence of the RA element resonances where the full-wave analysis is critical. However, this error is really localized and it will not affect the computation of the RA radiation parameters.

The ANN model of the single reradiating element has then be used in computing the gain pattern of the entire RA by using the physical optics approximation. Figure 9 shows the antenna gain patterns at the central frequency of 11.7 GHz for both the principal planes. The gain patterns have been computed by using both the exact value and the ANN approximation of the reflection coefficient. The relevant plots show a good agreement: the main beams are almost coincident and also the relative error introduced by the ANN on the sidelobes is always below few percent.

A similar observation applies also to the plot in Figure 10, in which the variation of the maximum gain versus frequency, computed with different techniques or obtained from the measurement of a prototype of the designed antenna, is shown. In particular, when we compare the results obtained by using the physical optics approximation together with the data for the reflection coefficient computed through the full-wave simulation of the unit cell (dash line) or by adopting the ANN approximated model (continuous line), it is evident that the latter underestimates the antenna gain. However, if we look at the values obtained by applying the MoM to the entire antenna [30] (dots) and the measurement results, it is evident that the error introduced by the ANN approximated model is negligible with respect to the one introduced by the physical optics approximation itself. Thus, the ANN approximated model can be conveniently used to obtain a reflectarray layout and to make a first optimization of the RA with the same uncertainty of the time-consuming accurate interpolation of the reflection coefficients.

4. Conclusions

The results of the previous section confirm the validity of the proposed characterization technique for the modeling of the behaviour of the RA reradiating element. The use of the artificial neural network for the characterization of the relationship between the RA single element reflection coefficient and the geometrical parameters that affect it allows a drastic reduction of both the computational time and the memory storage, without altering the accuracy of the solution.

References

[1] J. Huang and J. A. Encinar, *Reflectarray Antennas*, Wiley-IEEE Press, 2007.

[2] J. A. Encinar and J. A. Zornoza, "Broadband design of three-layer printed reflectarrays," *IEEE Transactions on Antennas and Propagation*, vol. 51, no. 7, pp. 1662–1664, 2003.

[3] D. Cadoret, A. Laisné, R. Gillard, L. Le Coq, and H. Legay, "Design and measurement of new reflectarray antenna using microstrip patches loaded with slot," *Electronics Letters*, vol. 41, no. 11, pp. 623–624, 2005.

[4] J. A. Encinar, L. Datashvili, J. A. Zornoza et al., "Dual-polarization dual-coverage reflectarray for space applications," *IEEE Transactions on Antennas and Propagation*, vol. 54, no. 10, pp. 2827–2837, 2006.

[5] S. Costanzo, F. Venneri, and G. Di Massa, "Bandwidth enhancement of aperture-coupled reflectarrays," *Electronics Letters*, vol. 42, no. 23, pp. 1320–1322, 2006.

[6] Z. H. Wu, W. X. Zhang, Z. G. Liu, and W. Shen, "A dual-layered wideband microstrip reflectarray antenna with variable polarization," *Microwave & Optical Technology Letters*, vol. 48, no. 7, pp. 1429–1432, 2006.

[7] P. De Vita, A. Freni, G. L. Dassano, P. Pirinoli, and R. E. Zich, "Broadband element for high-gain single-layer printed reflectarray antenna," *Electronics Letters*, vol. 43, no. 23, pp. 1247–1249, 2007.

[8] P. Pirinoli, P. T. Cong, M. Mussetta, and M. Orefice, "Concentric square ring elements for dual band reflectarray antenna," in *Proceedings of the 3rd European Conference on Antennas and Propagation (EUCAP '09)*, pp. 1342–1344, Berlin, Germany, March 2009.

[9] L. Moustafa, R. Gillard, F. Peris, R. Loison, H. Legay, and E. Girard, "The phoenix cell: a new reflectarray cell with large bandwidth and rebirth capabilities," *IEEE Antennas and Wireless Propagation Letters*, vol. 10, pp. 71–74, 2011.

[10] K. K. Kishor and S. V. Hum, "An amplifying reconfigurable reflectarray antenna," *IEEE Transactions on Antennas and Propagation*, vol. 60, no. 1, pp. 197–205, 2012.

[11] M. Mussetta, G. L. Dassano, P. Pirinoli, R. E. Zich, and M. Orefice, "18 GHz microstrip reflectarray: GA optimization and experimental measurements," in *Proceedings of the Journes Internationales de Nice sur les Antennes*, pp. 240–241, Nice, France, 2004.

[12] I. Barriuso, A. L. Gutiérrez, M. Lanza et al., "Comparison of heuristic methods when applied to the design of reflectarrays," in *Proceedings of the 5th European Conference on Antennas and Propagation (EUCAP '11)*, pp. 970–974, Rome, Italy, April 2011.

[13] Y. Aoki, H. Deguchi, and M. Tsuji, "Reflectarray with arbitrarily-shaped conductive elements optimized by genetic algorithm," in *Proceedings of the IEEE International Symposium on Antennas and Propagation and USNC/URSI National Radio Science Meeting*, pp. 960–963, 2012.

[14] M. Bozzi, S. Germani, and L. Perregrini, "A figure of merit for losses in printed reflectarray elements," *IEEE Antennas and Wireless Propagation Letters*, vol. 3, no. 1, pp. 257–260, 2004.

[15] D. Caputo, A. Pirisi, M. Mussetta, A. Freni, P. Pirinoli, and R. E. Zich, "Neural network characterization of microstrip patches for reflectarray optimization," in *Proceedings of the 3rd European Conference on Antennas and Propagation (EUCAP '09)*, pp. 2520–2522, Berlin, Germany, March 2009.

[16] M. Mussetta, P. Pirinoli, P. T. Cong, M. Orefice, and R. E. Zich, "Optimization of a dual-layer reflectarray antenna by means of soft-computing techniques," in *Proceedings of the 12th International Conference on Electromagnetics in Advanced Applications (ICEAA '10)*, pp. 716–719, September 2010.

[17] P. Robustillo, J. A. Encinar, and J. Zapata, "ANN element characterization for reflectarray antenna optimization," in *Proceedings of the 5th European Conference on Antennas and Propagation (EUCAP '11)*, pp. 957–960, Rome, Italy, April 2011.

[18] Haykin, *Neural Networks: A Comprehensive Foundation*, Prentice-Hall, Upper Saddle River, NJ, USA, 1999.

[19] Q. J. Zhang and K. C. Gupta, *Neural Networks for RF and Microwave Design*, Artech House, Norwood, Mass, USA, 2000.

[20] G. Washington, "Aperture antenna shape prediction by feed-forward neural networks," *IEEE Transactions on Antennas and Propagation*, vol. 45, no. 4, pp. 683–688, 1997.

[21] E. Charpentier and J.-J. Laurin, "An implementation of a direction-finding antenna for mobile communications using a neural network," *IEEE Transactions on Antennas and Propagation*, vol. 47, no. 7, pp. 1152–1159, 1999.

[22] A. H. El Zooghby, C. G. Christodoulou, and M. Georgiopoulos, "A neural network-based smart antenna for multiple source tracking," *IEEE Transactions on Antennas and Propagation*, vol. 48, no. 5, pp. 768–776, 2000.

[23] K. C. Lee, "Application of neural network and its extension of derivative to scattering from a nonlinearly loaded antenna," *IEEE Transactions on Antennas and Propagation*, vol. 55, no. 3, part 2, pp. 990–993, 2007.

[24] D. K. Neog, S. S. Pattnaik, D. C. Panda, S. Devi, B. Khuntia, and M. Dutta, "Design of a wideband microstrip antenna and

the use of artificial neural networks in parameter calculation," *IEEE Antennas and Propagation Magazine*, vol. 47, no. 3, pp. 60–65, 2005.

[25] K. Youngwook, S. Keely, J. Ghosh, and H. Ling, "Application of artificial neural networks to broadband antenna design based on a parametric frequency model," *IEEE Transactions on Antennas and Propagation*, vol. 55, no. 3, part 1, pp. 669–674, 2007.

[26] A. Mishra, A. B. Nandgaonkar, V. D. Bhagile, S. C. Mehrotra, and P. M. Patil, "Design of square and rectangular microstrip antenna with the use of FFBP algorithm of artificial neural network," in *Proceedings of the Applied Electromagnetics Conference (AEMC '09)*, December 2009.

[27] M. Milijić, Z. Stanković, and B. Milovanović, "Efficient model of slotted patch antenna based on neural networks," in *Proceedings of the 9th International Conference on Telecommunications in Modern Satellite, Cable, and Broadcasting Services (TELSIKS '09)*, pp. 384–387, 2009.

[28] R. G. Ayestarán, F. Las-Heras, and L. F. Herrán, "Neural modeling of mutual coupling for antenna array synthesis," *IEEE Transactions on Antennas and Propagation*, vol. 55, no. 3, part 2, pp. 832–840, 2007.

[29] L. Hamm, B. W. Brorsen, and M. T. Hagan, "Global optimization of neural network weights," in *Proceedings of the International Joint Conference on Neural Networks (IJCNN '02)*, pp. 1228–1233, May 2002.

[30] P. De Vita, F. De Vita, A. Di Maria, and A. Freni, "An efficient technique for the analysis of large multilayered printed arrays," *IEEE Antennas and Wireless Propagation Letters*, vol. 8, pp. 104–107, 2009.

Hindawi Publishing Corporation
International Journal of Antennas and Propagation
Volume 2012, Article ID 914868, 6 pages
doi:10.1155/2012/914868

Research Article

Resonant Elements for Tunable Reflectarray Antenna Design

M. Y. Ismail and M. Inam

Wireless and Radio Science Centre (WARAS), Faculty of Electrical and Electronic Engineering, Universiti Tun Hussein Onn Malaysia (UTHM), 86400 Batu Pahat, Johor, Malaysia

Correspondence should be addressed to M. Y. Ismail, yusofi@uthm.edu.my

Received 8 February 2012; Revised 5 April 2012; Accepted 5 June 2012

Academic Editor: Sandra Costanzo

This paper presents an accurate analysis of different configurations of reflectarray resonant elements that can be used for the design of passive and tunable reflectarrays. Reflection loss and bandwidth performances of these reflectarray elements have been analyzed in the X-band frequency range with the Finite Integral Method technique, and the results have been verified by the waveguide scattering parameter measurements. The results demonstrate a reduction in the phase errors offering an increased static linear phase range of 225° which allows to improve the bandwidth performance of single layer reflectarray antenna. Moreover a maximum dynamic phase range of 320° and a volume reduction of 22.15% have been demonstrated for a 10 GHz reflectarray element based on the use of rectangular patch with an embedded circular slot.

1. Introduction

Due to the modern day need for long distance communications, higher data rate and finer radar imaging resolution, high gain or large aperture antennas are usually required. Deep space exploration and earth remote sensing are few missions of NASA where the antenna performance requirements are increasing in order to extract more information. On the other hand, lower mass and smaller stowage volume for the space craft antennas are demanded in order to reduce payload weight and required shroud space to minimize overall launch cost. Traditionally high gain applications have relied upon parabolic reflectors and phased arrays [1]. However, due to the curvature of their surface, parabolic reflectors are difficult to be manufactured in many cases at higher microwave frequencies [2]. The shape of the parabolic reflector also causes an increased weight and size of the antenna. Moreover, it has also been demonstrated in [3] that wide-angle electronic beam scanning cannot be achieved using a parabolic reflector. On the other hand, high gain phased array antennas offer the possibility to electronically scan the main beam along wide angle positions provided they are equipped with controllable phase shifters. However in order to reduce the problem of power inefficiency due to the problem of high loss beamformers and phase shifters, suitable amplifier modules have to be integrated with the array antennas. These amplifier modules are usually of high cost so making phased array antennas a very expensive solution for high gain applications. Therefore in order to eliminate these problems, a flat and low cost microstrip array antenna, known as reflectarray, has been acknowledged as a potential alternative to these traditionally used high gain antennas. Reflectarray in its basic form is a combination of a flat reflector and an array of microstrip patches illuminated by a primary feed horn. Reflectarray can achieve a wide-angle electronic beam scanning. Direct Broadcast Satellites (DBS) and Multibeam Antennas (MBAs) are also considered as potential applications of reflectarrays. Moreover they can also act as amplifying arrays by including an amplifier in each reflectarray element [4].

Despite of the large number of reflectarrays advantages, the factors that limit its use in some applications are the limited bandwidth and high loss performance. Many different techniques have been proposed in order to increase the bandwidth performance of reflectarrays and up to 15% bandwidth has been reported [3]. Recently the authors have demonstrated the feasibility of designing a reflectarray with different types of slots embedded in a rectangular

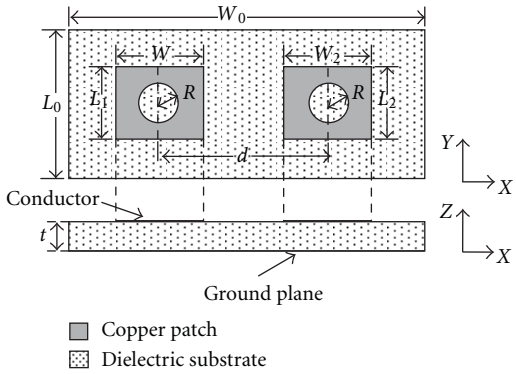

Figure 1: Geometry of a two patch element unit cell reflectarray ($L_1 = L_2$ is length of patch, $W_1 = W_2$ is width of patch, R is radius of circular slot, L_0 and W_0 are the length and width of substrate, resp., t is thickness of substrate, and d is the interelement spacing).

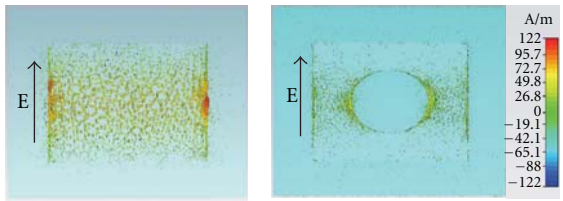

(a) (b)

Figure 2: Surface current distribution on (a) rectangular patch of reflectarray and (b) reflectarray rectangular patch element with circular slot in the centre.

patch [5]. In this work, a reflectarray element based on the use of a rectangular patch with an embedded circular slot is proposed. The reflection losses and bandwidth performances of X-band elements are obtained through simulations and measurements. The proposed reflectarray design is also integrated with PIN diodes in order to obtain a tunable configuration.

2. Proposed Reflectarray Configuration

In order to improve the performance of reflectarray and to provide resonant elements for tunable reflectarray antenna design, a circular slot has been introduced in the centre of the reflectarray patch element. Figure 1 shows the top and the side view of the reflectarray unit cell composed by two patch elements. The circular slot elements have the same dimensions and are designed on a dielectric substrate with a thickness (t). The interelement spacing (d) between the two patch elements is kept to be half wavelength in order to minimize the mutual coupling effects.

Figure 2 shows the current distribution on the single reflectarray element obtained by using CST Microwave Studio (MWS). In this work a Rogers RT/duroid 5880 substrate with a thickness of 0.508 mm has been used to design an infinite reflectarray at 10 GHz. Figure 2(a) shows that the current amplitude is maximum at the centre of the top surface of conducting rectangular patch element while

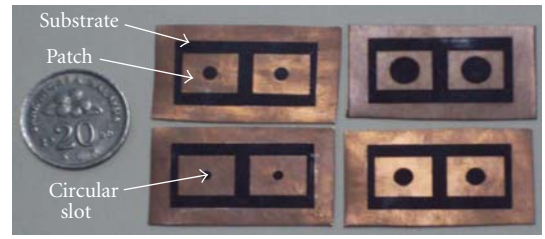

Figure 3: Fabricated unit cells rectangular patch elements embedded with different circular slots.

Figure 2(b) shows a clear modification of surface current distribution when a circular slot is embedded in the centre of patch element. This phenomenon of surface current modification is exploited in this work to tune the reflection phase of the proposed reflectarray element.

Measurements of the scattering parameters for infinite reflectarrays fabricated using Rogers RT/duroid 5880 have recently been demonstrated in [6] for operation in X-band frequency range. Waveguide simulator technique has been used to represent a two-patch element unit cell with an infinite reflectarray. For this work unit cells reflectarrays have been fabricated by integrating the circular slots of different radius with rectangular patch elements as shown in Figure 3. The dimensions of each radiating element, depicted in Figure 2, are fixed to the following values: $W_1 = W_2 = 10$ mm, $L_1 = L_2 = 9.4$ mm. In order to tune the phase of the field reflected by the elements, the radius of each circular slot is varied from 1 mm to 3 mm. Reflection losses and phase range performances of the designed unitary cell are discussed in the following sections. Furthermore, in the last part of this work, the designed elements are integrated with a PIN diode in order to demonstrate the effectiveness of the proposed configuration to design tunable reflectarray antennas.

2.1. Reflection Loss Performance. Figure 4 depicts the measured and simulated reflection loss for different radius of circular slots and reflection loss for a patch without slot. A significant change in the resonant frequency from 10 GHz to 8.5 GHz has been observed as the element was varied from the case without slot to the one having a slot radius equal to 3.0 mm. It has been shown that an increase in the slot radius from 1.0 mm to 3.0 mm also caused an increase in the measured reflection loss from 1.7 dB to 2.65 dB.

Moreover the trend of the loss performance of both measured and simulated reflectarrays is in good agreement. The change in resonant frequency and reflection loss with variable radius of slots is due to the change in electrical dimensions which in turn modifies the surface current distribution on the patch element of a reflectarray. It can also be observed that the measured reflection loss is higher than the simulated reflection loss because of the losses introduced by the interconnections and material properties.

2.2. Phase Range Performance. In order to compare the phase range performance of different reflection phase curves, a

Table 1: Performance comparison for different resonant elements of reflectarray.

Resonant element	Reflection loss (dB)	f_o (GHz)	Dynamic phase range		Volume reduction at 10 GHz (%)
			Measured (degrees)	Simulated (degrees)	
Rectangular patch	1.50	—	—	—	—
Circular slot (R = 1.5 mm)	1.75	9.75	104	110	5.24
Circular slot (R = 2.0 mm)	2.20	9.45	290	298	9.19
Circular slot (R = 2.5 mm)	2.50	9.25	310	314	15.76
Circular slot (R = 3.0 mm)	2.65	9.10	320	323	22.15

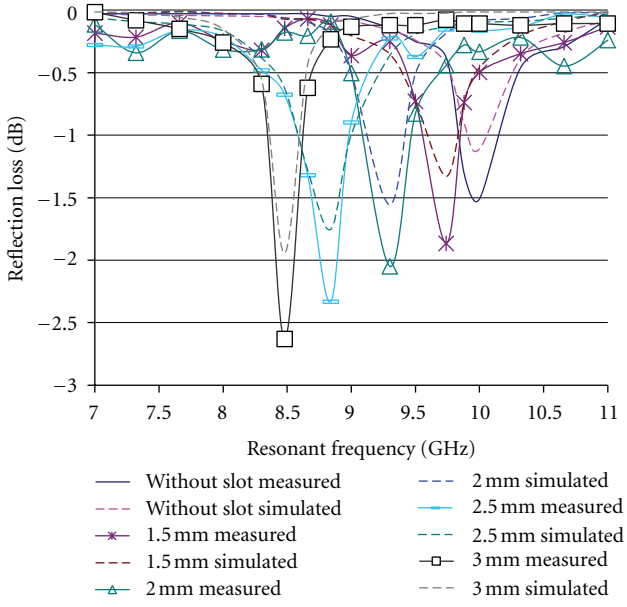

Figure 4: Measured and simulated reflection loss for patch without slot and patch with different radius of circular slots in the centre of patch.

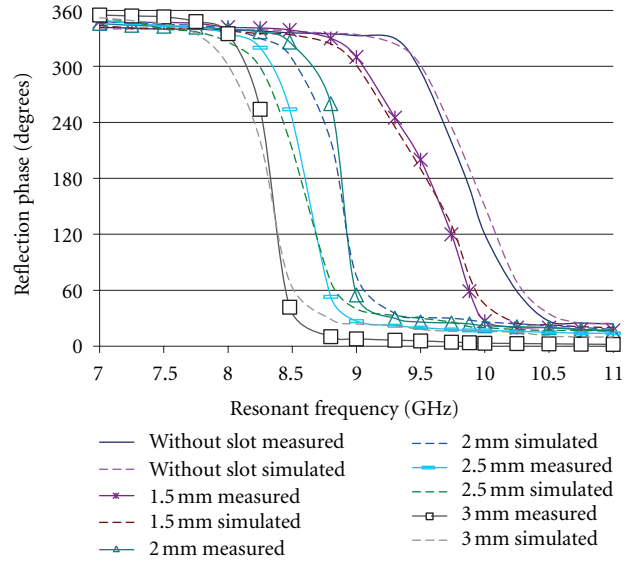

Figure 5: Measured and simulated reflection phase for patch without slot and patch with different radius of circular slots in the centre of patch.

figure of merit (FoM) has been defined which is related to the slope of the phase curves. The FoM is given by

$$\text{FoM} = \frac{\Delta\phi}{\Delta f}, \tag{1}$$

where $\Delta\phi$ is the change in the reflection phase in degrees and Δf is the change in the reflectarray antenna resonant frequency in MHz, thus FoM is calculated here in °/MHz. For a reflectarray antenna the FoM or the slope of the phase curve around the resonance is required to be minimum in order to have better bandwidth performance. Measured and simulated reflection phases for different radius of circular slots (R) embedded in the centre of patch and for a patch without slot are shown in Figure 5. It can be observed from Figure 5 that as the unit cell was varied from patch element without slot to a circular slot of 3.0 mm radius, the slope of the reflection phase curve increases from 0.24°/MHz to 1.04°/MHz. This is due to the fact that the surface current distribution is modified by the introduction of the slot in the patch. In fact, the surface current density and the electric field intensity decrease by increasing the circular slot radius.

A further parameter adopted to evaluate the phase curves behavior is the dynamic phase range. This parameter can be defined as the difference between two different phase curves, respectively, computed for the patch without slot and the patch with a variable radius slot. The phase difference is evaluated at the mean resonant frequency (Figure 6(a)). Table 1 shows measured and simulated dynamic phase range for different radius of circular slots. It can be observed from Table 1 that a maximum measured dynamic phase range of 320° is shown by an element with a circular slot of 3.0 mm radius. Another parameter considered for the comparison of patch with slot and patch without slot is the volume reduction which provides the feasibility of miniaturizing the reflectarray antenna. It is measured as the percentage difference between the volume of the proposed

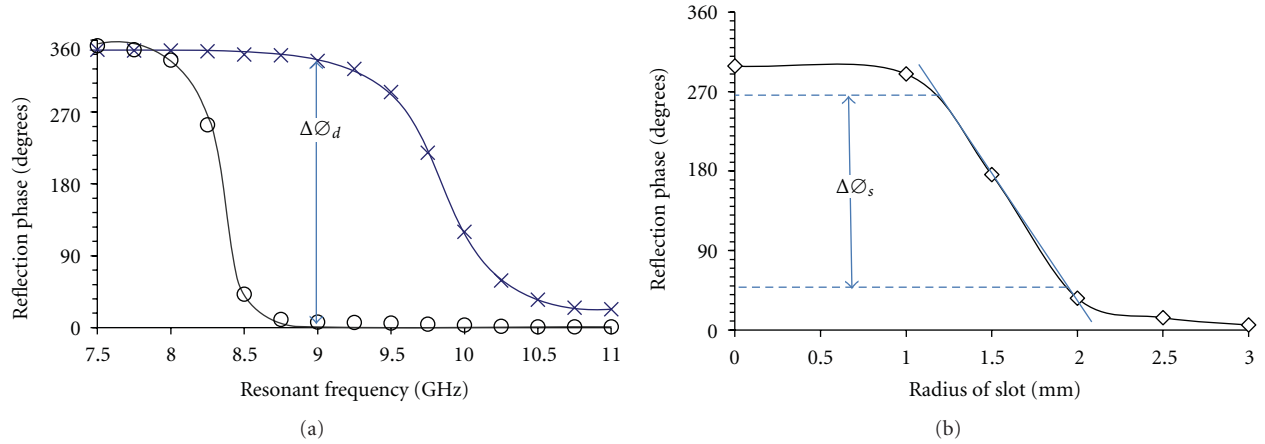

Figure 6: (a) Dynamic phase range, (b) measured static linear phase range of phase shift versus slot size curve for circular slot configurations at 9.75 GHz.

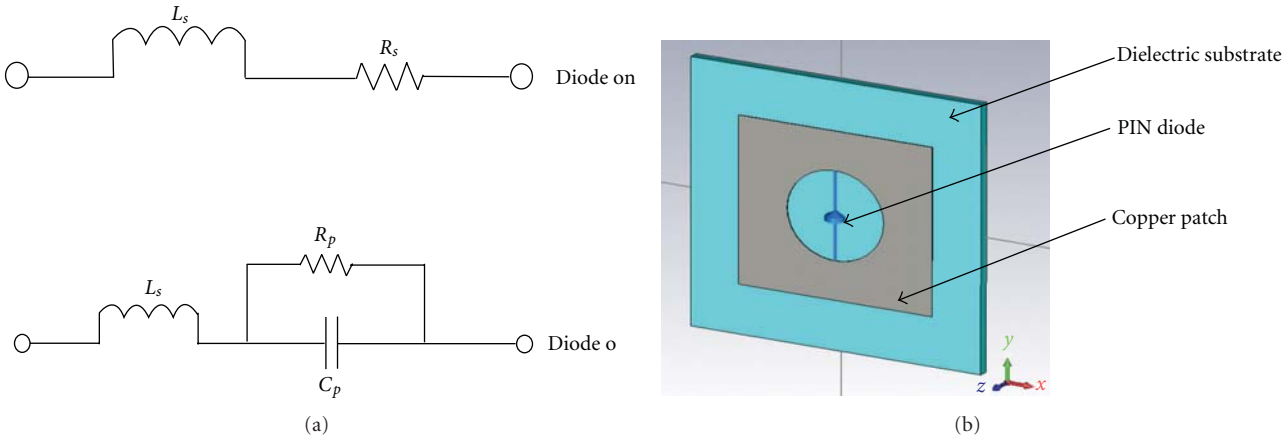

Figure 7: (a) On and off states of a PIN diode, (b) proposed design with integrated PIN diode.

slot embedded patch element and the rectangular patch element designed at 10 GHz. A maximum volume reduction of 22.15% is shown to be achieved by an element with a circular slot of 3.0 mm.

In order to compare the results of the reflection phase plots produced in this work, the static linear phase range ($\Delta\varnothing_s$) defined in Figure 6(b) has been used. The previous studies [6, 7] which proposed the slots in the ground plane demonstrated a simulated static linear phase range of 180° and 210°, respectively, for single layer structures. The results depicted in Figure 6(b) demonstrate that an increased measured static linear phase range of 225° is achieved using slots of variable radius in the patch element. Therefore due to the increased attainable static linear phase range, the phase error contribution in the reduction of reflectarray bandwidth can be minimized by using the proposed slotted configurations.

3. Design of a Tunable Reflectarray Antenna Using PIN Diodes

The reflectarray configuration proposed in Section 2 can be loaded with diodes in order to design tunable planar reflectarrays for beam steering applications. A potential type of diode that can be used for frequency tunability is PIN diode. The on and off states of a PIN diode, result in different equivalent lumped circuits as shown in Figure 7(a). In the case of the on state the pin diode provides a series resistance which affects the reflection loss of the reflectarray and therefore needs to be kept low. On the other hand, in the off state the PIN diode provides a low capacitance which affects the tunability performance of the reflectarray element. In order to verify the functionality of the electronically switchable reflectarray design, PIN diodes have been integrated with circular slots as shown in Figure 7(b).

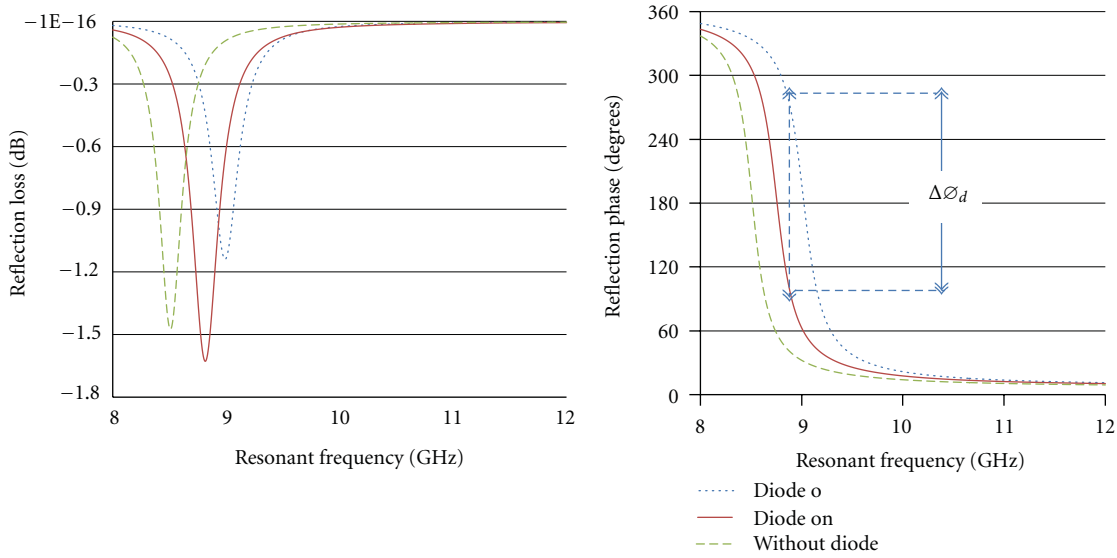

Figure 8: Reflection loss and reflection phase curves for tunable reflectarray design with PIN diodes.

In this work, a circular slot with $R = 2.5$ mm has been integrated with an APD 0805-000 PIN diode. The APD 0805-000 PIN diode can operate at high frequencies and has low capacitance and low series resistance which provides lower losses and a higher degree of tunability. Figure 8 shows reflection loss and refection phase curves for the design without diode and with two different states of a PIN diode. It can be observed from Figure 8 that the on state of PIN diode provides a higher reflection loss equal to 1.64 dB with respect to the other states. A frequency tunability of 270 MHz and a dynamic phase range of 171° at 8.88 GHz can be observed by the results shown in Figure 8. The results demonstrate the feasibility of effectively utilizing the proposed slot configurations with PIN diodes for the design of tunable reflectarray antennas.

4. Conclusion

A reflectarray element based on the use of a rectangular patch with an embedded circular slot has been proposed. It has been demonstrated that the configuration can be effectively utilized for the design of passive and tunable reflectarrays with low loss and high bandwidth performance. From the measurements of the slot embedded patch element, it can be concluded that proposed configuration can be employed for the miniaturization of the reflectarrays as a wide range of resonant frequencies can be achieved without varying the size of the patch element. Moreover the reduction in the phase errors produced by the limited phase range and the possibility of designing a miniaturized reflectarray has also been demonstrated using the proposed configurations. Preliminary investigations for the integration of slots and PIN diodes have shown that the dynamic phase range can be utilized to design electronically controllable reflectarrays with progressive phase distribution.

Acknowledgments

This research work is fully funded by Prototype Research Grant Scheme (PRGS VOT 0904) and Best Awarded Fundamental Research Grant Scheme (FRGS VOT 0983), Ministry of Higher Education, Malaysia. The authors would like to thank the staff of Wireless and Radio Science Centre (WARAS), Universiti Tun Hussein Onn Malaysia (UTHM) for the technical support.

References

[1] G. D. G. Berry, R. G. Malech, and W. A. Kennedy, "The reflect array antenna," *IEEE Transactions on Antennas and Propagation*, vol. 11, pp. 645–651, 1963.

[2] J. Huang and J. A. Encinar, *Reflectarray Antennas*, Wiley Interscience, 2007.

[3] J. A. Encinar, M. Arrebola, M. Dejus, and C. Jouve, "Design of A 1-metre reflectarray for DBS application with 15% bandwidth," in *Proceedings of the European Conference on Antennas and Propagation (EuCAP '06)*, pp. 1–5, Nice, France, November 2006.

[4] M. E. Bialkowski, A. W. Robinson, and H. J. Song, "Design, development, and testing of X-band amplifying reflectarrays," *IEEE Transactions on Antennas and Propagation*, vol. 50, no. 8, pp. 1065–1076, 2002.

[5] M. Y. Ismail, M. Inam, and J. Abdullah, "Design optimization of reconfigurable reflectarray antenna based on phase agility technique," in *Proceedings of the 3rd Conference on Antenna & RCS Measurement (ATMS '10)*, vol. 33, pp. 01–05, Delhi, India, 2010.

[6] M. I. Abbasi and M. Y. Ismail, "Reflection loss and bandwidth performance of X-band infinite reflectarrays: simulations and measurements," *Microwave and Optical Technology Letters*, vol. 53, no. 1, pp. 77–80, 2011.

[7] H. Rajagopalan, Y. Rahmat-Samii, and W. A. Imbriale, "RF MEMS actuated reconfigurable reflectarray patch-slot element," *IEEE Transactions on Antennas and Propagation*, vol. 56, no. 12, pp. 3689–3699, 2008.

Hindawi Publishing Corporation
International Journal of Antennas and Propagation
Volume 2012, Article ID 784045, 6 pages
doi:10.1155/2012/784045

Research Article

Radiation Analysis and Characteristics of Conformal Reflectarray Antennas

Payam Nayeri,[1] Fan Yang,[1,2] and Atef Z. Elsherbeni[1]

[1] *Electrical Engineering Department, The University of Mississippi, Oxford, MS 38677, USA*
[2] *Electronic Engineering Department, Tsinghua University, Beijing 100084, China*

Correspondence should be addressed to Payam Nayeri, pnayeri@olemiss.edu

Received 3 February 2012; Accepted 11 May 2012

Academic Editor: Sandra Costanzo

This paper investigates the feasibility of designing reflectarray antennas on conformal surfaces. A generalized analysis approach is presented that can be applied to compute the radiation performance of conformal reflectarray antennas. Using this approach, radiation characteristics of conformal reflectarray antennas on singly curved platforms are studied and the performances of these designs are compared with planar designs. It is demonstrated that a conformal reflectarray antenna can be a suitable choice for applications requiring high-gain antennas on curved platforms.

1. Introduction

Printed reflectarray antennas combine the favorable features of both printed arrays and parabolic reflectors and create a low-profile, low-mass, and low-cost antenna [1]. A reflectarray antenna imitates the conventional parabolic reflectors, with the added advantage of having a flat surface instead of the curved reflecting surface. Owing to their high-gain and low-loss characteristics, the reflectarray antenna has received considerable attention over the years. The surface of the reflectarray antenna consists of phase changing elements, which create the collimated beam and are usually distributed on a planar aperture.

Several applications require the use of conformal antenna technology. While the need for a conformal antenna system generally depends on the specific application, the advantages can usually be attributed to either mechanical (aerodynamic, hydrodynamic) or electrical benefits [2]. In terms of the mechanical advantages, a conformal antenna is designed according to a prescribed shape, which can be some part of an airplane, high-speed train, or other vehicle. The main purpose is to build an antenna that becomes integrated with the structure and causes less disturbance such as extra drag. The electrical advantages of conformal antennas are typically wide angle scanning capabilities. Conformal beam-scanning array antennas can achieve full azimuth and wide elevation coverage [3], which in most cases is not possible with planar designs.

In this paper, we investigate the feasibility of designing reflectarray antennas on conformal surfaces. In section II, a generalized analysis approach to compute the radiation pattern of conformal reflectarray antennas is presented. In section III, reflectarray antennas on singly curved conformal cylindrical platforms are studied and radiation performances of these designs are compared with planar designs. It is demonstrated in these studies that a conformal reflectarray antenna can be a suitable choice for a high-gain antenna where curved platforms are required.

2. Radiation Analysis of Conformal Reflectarrays

2.1. Radiation Pattern Calculation. The radiation pattern of a planar reflectarray antenna with thousands of elements can be computed quite efficiently using the classical array theory formulation with proper element excitation [4]. In a recent study, it was shown that the calculated radiation pattern using this approach shows a good agreement with full-wave simulations [5]. In particular, the main beam direction, beam width, and side lobe level match closely with those obtained using full-wave simulations. Therefore, the array

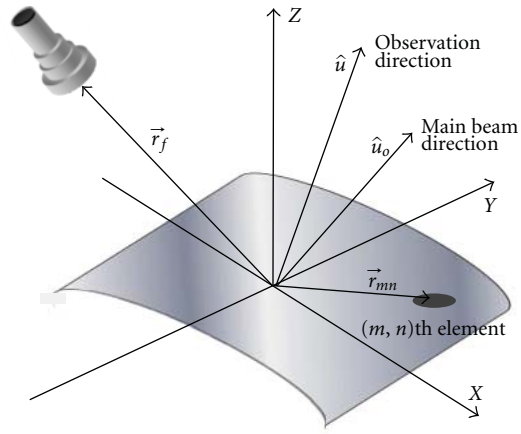

Figure 1: Coordinate system of the reflectarray antenna.

theory approach is used in this paper to study the radiation characteristics of conformal reflectarrays.

The formulation developed for planar reflectarray antennas can be generalized to analyze the performance of conformal reflectarrays. With the array theory formulation, as long as the elements on the conformal surface are correctly modeled with mutual coupling included, array summation can provide accurate results. Therefore, an important consideration in radiation analysis of conformal designs is the accurate modeling of element radiation characteristics. One should realize that the peak of the element pattern is normal to the local surface, so the peaks will not all point in the same direction for a conformal array [6]. Furthermore, a reflectarray antenna is functioning in the reflection mode, which is different from conventional antenna arrays [2]. Scattering properties of curved surfaces are more complicated than planar surfaces, and in general high order diffraction effects such as generation of creeping waves, and depolarization should be taken into account [7]. Nonetheless, if the conformal surface is not highly curved, edge diffraction is minimized, and hence microwave optic approaches are suitable for the analysis.

The radiation pattern of a conformal array with $M \times N$ elements can be calculated using the following general formula:

$$\vec{E}\,(\hat{u}) = \sum_{m=1}^{M}\sum_{n=1}^{N} \vec{A}_{mn}(\hat{u}) \cdot \vec{I}\,\left(\vec{r}_{mn}\right), \qquad (1)$$

$$\hat{u} = \hat{x}\sin\theta\cos\varphi + \hat{y}\sin\theta\sin\varphi + \hat{z}\cos\theta,$$

where A is the element pattern vector function, I is the element excitation vector function, and $\vec{r}_{mn}$ is the position vector of the mnth element. The geometry of the conformal reflectarray system is given in Figure 1.

A cosine q_e model is usually used for the element pattern function A, which in general is not symmetric due to the surface curvature. Some highly curved conformal arrays may have a $\cos^{1.5}$ behavior in the strong coupling plane and a $\cos^1$ behavior in the weak coupling plane [7]. As discussed earlier, in our studies the conformal reflectarray surface is not highly curved, therefore each unit cell can be approximated with a planar surface that is tangential to the conformal surface. The element pattern can then be approximated with a symmetric $\cos^1$ model with its peak normal to the unit cell surface. Therefore, the important considerations for element pattern modeling are to (1) determine the exact angle of incidence for each element that controls the receive mode element pattern and (2) determine the orientation of the local cell coordinates with respect to the global coordinates which controls the transmit mode element pattern.

The transmit element pattern function can be written as

$$A_{mn}(\theta,\varphi) \approx \cos^{q_e}\theta_{\text{local}} \cdot e^{jk(\vec{r}_{mn}\cdot\hat{u})}. \qquad (2)$$

In comparison with planar designs [5], this function takes into account the effect of surface curvature on the transmit element pattern by using local element coordinates for each radiating element.

The element excitation function I is determined by both the incident field and element property [4]. By approximating the feed horn pattern function using a cosine q_f model and taking into account the Euclidian distance between the feed horn and the element, the illumination of the aperture can be obtained. The element receive pattern is essentially part of the element excitation function, which determines the reflected power from the element based on the angle of excitation and element pattern shape, that is,

$$|\Gamma_{mn}| = \cos^{q_e}\theta_e(m,n). \qquad (3)$$

While the function here is similar to the planar case, the difference is that for conformal reflectarrays the element angle θ_e depends on both the element location and the local surface orientation.

With these approximations, the radiation pattern of a conformal reflectarray antenna can be simplified to the scalar form

$$E(\theta,\varphi) = \sum_{m=1}^{M}\sum_{n=1}^{N} \cos^{q_e}\theta_{\text{local}}\,\cos^{q_e}\theta_e(m,n)\; e^{j\phi_{mn}} \times \frac{\cos^{q_f}\theta_f(m,n)}{\left|\vec{r}_{mn}-\vec{r}_f\right|}\; e^{-jk(|\vec{r}_{mn}-\vec{r}_f|-\vec{r}_{mn}\cdot\hat{u})}. \qquad (4)$$

In this equation θ_f is the spherical angle in the feed coordinates and $\vec{r}_f$ is the position vector of the feed. The required phase delay of the mnth element ϕ_{mn} is adjusted to set the main beam in the $\hat{u}_o$ direction.

The radiation pattern calculation method described here uses a conventional array summation technique with scalar function approximations. If the cross-polarization of the reflectarray is concerned, the polarization of the feed horn and elements need to be accounted for in a comprehensive model instead of the simplified cosine q model presented above.

2.2. Gain Calculations. For an accurate calculation of the reflectarray antenna gain, it is imperative to determine the

overall aperture efficiency of the antenna. Different kinds of efficiency factors are considered in conventional reflector antennas [8]. Amongst these efficiency factors however, the major terms that influence the reflectarray antenna gain are the spillover and taper efficiency [9].

The formulation presented in the previous section for calculating the radiation pattern, accurately takes into account the illumination of the aperture. In other words, the effect of taper efficiency is already taken into account when one calculates the radiation pattern directivity using (4). The spillover efficiency on the other hand requires some attention. By definition, spillover efficiency (η_s) is the percentage of radiated power from the feed that is intercepted by the reflecting aperture. Mathematically this can be written as

$$\eta_s = \frac{\iint_\sigma \vec{P}\left(\vec{r}\right) \cdot d\,\vec{s}}{\iint_\Sigma \vec{P}\left(\vec{r}\right) \cdot d\,\vec{s}}, \tag{5}$$

where both integrals are fluxes of the Poynting vector $P(r)$ through certain surface areas. The denominator is the total power radiated by the feed; therefore the integral is performed over the entire surface area of a sphere centered at the feed, denoted by Σ. The numerator is the power incident on the array aperture, thus it is evaluated over a portion σ of the sphere, where σ and the array aperture share the same solid angle with respect to the feed. With this model, the denominator in (5) will have a simple closed-form expression [9]. The numerator can be computed numerically for any conformal surface. This is generally the same approach one follows for spillover efficiency calculations of a planar reflectarray, however the difference here is that the integration has to be performed over a curved surface. The gain of the reflectarray antenna is then computed using

$$G = \eta_s D. \tag{6}$$

Here D is the maximum directivity of the reflectarray antenna which is defined as the maximum radiation intensity of the antenna over the average, and is calculated using (4). It should be noted that the gain calculations discussed here don't include the factors associated with the feed loss, reflectarray element loss, and polarization loss. However in most cases for reflectarrays with low-loss substrates, these factors don't contribute much to the overall loss of the system [10].

3. Radiation Characteristics of Singly Curved Conformal Reflectarrays

Low-profile printed antennas flush mounted on singly curved surfaces such as cylinders represent an important class of conformal arrays used in many radar and communication systems [11]. Cylindrical array antennas are mainly utilized for either full azimuth scanning or sector arrays covering a specific subtended angle. In this section, the radiation characteristics of reflectarrays on conformal sector cylindrical surfaces are investigated. The analysis of this singly curved canonical problem can provide an insight into many radiation characteristics of conformal reflectarrays. The cross-section of the conformal reflectarray system is shown in Figure 2, where concave and convex surfaces are compared with their planar counterpart with the same surface area. In this figure, R_c is the radius of the cylinder for the conformal systems, and D represents the physical aperture size.

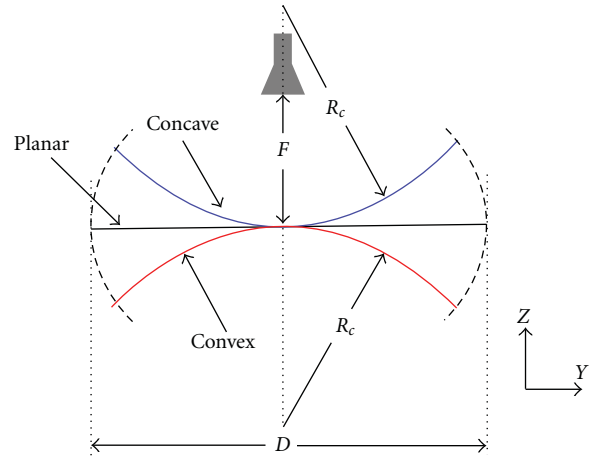

Figure 2: Cross-section of the conformal cylindrical reflectarrays systems.

It is important to point out that for conformal arrays with a broadside beam, using large element spacing (relative to wavelength) will result in generation of grating lobes in the visible range [7]. For element spacing in the order of half-wavelength, however, this error is substantially minimized, and this value is used for all numerical studies reported here. In addition, it should be noted that while, in general, there is a direct relation between the unit cell size (or element spacing) and the aperture curvature, for the half-wavelength unit cells used in this study, the maximum surface curvature of a single element is in the order of 1/20th of a radian, which ensures that a planar multifaceted approximation for the element performance is a suitable assumption.

3.1. Radiation Patterns of Cylindrical Reflectarrays. The numerical approach presented here is applied to the radiation analysis of sector reflectarray antennas mounted on cylindrical surfaces. For a meaningful comparison of the surface curvature effect, the feed properties and the physical aperture size are kept constant, and the only parameter that is changed is the cylinder radius. The reflectarray antennas have a $20\lambda \times 20\lambda$ aperture and are designed to generate a beam in the broadside direction. Ideal phasing elements are used and the element pattern is modeled as a $\cos^1$ function with no azimuth dependence. The feed is prime focus, positioned with an $F/D = 0.75$ and the power q of radiation pattern model is 6.5.

The radiation pattern of the reflectarray systems in the curvature plane (yz-plane) is shown in Figure 3 for various

cases. It should be noted that the radiation pattern in the *xz*-plane was similar to the planar case and is not shown here for brevity.

It can be seen that due to the effects of the conformal surface, the radiation patterns show a noticeable difference with planar designs ($R_c \to \infty$). In particular, for the concave design, the side lobes are higher than the planar case. On the other hand, the convex designs show a lower side lobe level (SLL), but a much wider beamwidth. For both designs however, as the cylinder radius increases, the radiation patterns of the conformal designs approach that of a planar case. While this limit generally depends on the aperture size, for the cases studied here, the limit is almost $R_c = 40\,\lambda$.

3.2. Beamwidth and Side Lobe Level. The conformal cylindrical systems studied in the previous section were defined based on the size of the cylinder radius (R_c). The aperture size (D) however also plays an important role. For a fixed cylinder radius, a larger aperture means a wider subtended angle ($\alpha = D/R_c$) and a higher level of surface curvature. To study this, effect we consider three different aperture sizes and compare the beamwidth and SLL of these designs. Similarly in all the designs, the feed ($q = 6.5$) is prime focus, and positioned with an F/D of 0.75. This would ensure that the aperture taper is identical for the different aperture sizes studied here. The normalized half-power beamwidth (HPBW) in the curvature plane as a function of cylinder radius is given in Figure 4 for different aperture sizes.

It can be seen that in comparison between the two conformal designs, a convex reflectarray shows a much wider beamwidth. In general, however, both conformal designs show defocusing effects, that is, a wider beamwidth in comparison with a planar design. This is mainly attributed to the fact that the elements on the conformal surface radiate in the outward (convex) or inward (concave) radial directions of the cylinder which defocus the main beam. It should be noted that for a concave design, an optimum position exists for the feed that can achieve maximum focusing. More discussion on this topic will be given in a subsequent section.

The change in SLL as a function of cylinder radius is given in Figure 5 for different aperture sizes. Comparisons of these results also show that in all cases as the aperture size increases, the SLL increases for the concave design and decreases for the convex design. In other words, the effect of the conformal surface on the radiation performance becomes more noticeable as the aperture size increases.

The results in Figures 4 and 5 indicate that the radiation performance of conformal cylindrical reflectarrays is a function of both cylinder radius and aperture size. However, it will be quite advantageous if one can determine the overall performance of the system based on a single conformal parameter. The subtended angle α, takes into account the aperture size, D, which controls the gain, in addition to the cylinder radius, R_c, which controls the curvature of the conformal surface. As such, it can be a suitable measure to evaluate the performance of the system. Table 1 summarizes the change in radiation characteristics of some conformal designs with a fixed subtended angle of 1 radian.

Table 1: Change in Radiation Performance of Conformal Cylindrical Reflectarrays with $D/R_c = 1$.

Aperture size	Design	$10\lambda \times 10\lambda$	$20\lambda \times 20\lambda$	$30\lambda \times 30\lambda$
HPBW ratio	Concave	0.036	0.033	0.037
	Convex	0.077	0.080	0.083
SLL ratio (dB)	Concave	2.81	2.73	2.73
	Convex	−0.40	−0.25	−0.38

From these results, it can be seen that the ratio of the change in HPBW and SLL is almost identical for all three cases. Similar results were observed for other values of subtended angle. In other words, it is possible to correctly specify the radiation performance of a conformal reflectarray system based on the value of α. This is quite advantageous from a system design view point, since for any available curved platform the radiation characteristics of the conformal reflectarray can be determined with only one conformal parameter. As an example for a 10% acceptable increase in HPBW in comparison with a planar design, α is equal to 1.62 and 1.13 radians for concave and convex designs, respectively, for any aperture size.

It is important to point out that the subtended angle (α) decreases as the cylinder radius increases. For the smallest cylinder radius, the aperture size increase corresponds to an increase in α from almost $\pi/3$ to π. Larger apertures will not be practical here, since: (1) the elements cannot be properly excited (shadow region of feed), and (2) the pattern of the elements at the sector edges point far away from the broadside direction.

3.3. Gain and Bandwidth. The reflectarray antenna gain is directly proportional to its projected aperture. As such for a fixed aperture size, the projected aperture, and corresponding antenna gain of conformal designs will be slightly smaller than a planar design. For a $20\,\lambda \times 20\,\lambda$ aperture with a fixed value of $\alpha = 1$, this will result in a gain reduction of 0.1 and 0.6 dB for concave and convex designs, respectively. While it is possible to mitigate this slight difference in antenna gain by increasing the aperture size, for the bandwidth comparisons here we will compare the normalized antenna gain as a function of frequency.

The bandwidth of the reflectarray antenna is affected by the phase error associated with the spatial delay as well as the bandwidth of elements [12]. While the element bandwidth generally depends on the design methodology [1], for this comparative study, we consider a frequency-independent reflection phase for the elements, that is, only the bandwidth limitation associated with spatial phase delay is taken into account. Figure 6 shows the normalized gain bandwidth of a $20\,\lambda \times 20\,\lambda$ reflectarray antenna with planar and conformal apertures ($\alpha = 1$ radian).

It can be seen that a concave design shows a notable improvement in gain bandwidth in comparison with the planar case. On the other hand, as expected, a convex design shows a reduction in bandwidth. It is also interesting to observe the bandwidth performance of these designs as

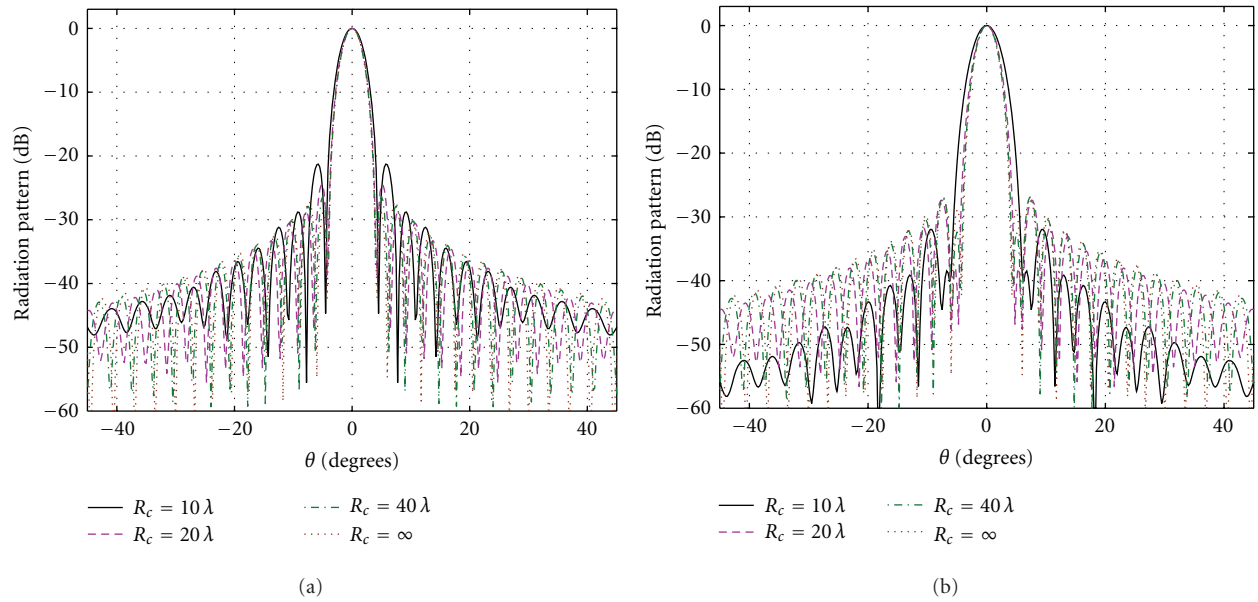

Figure 3: Radiation patterns of cylindrical reflectarrays: (a) concave, (b) convex.

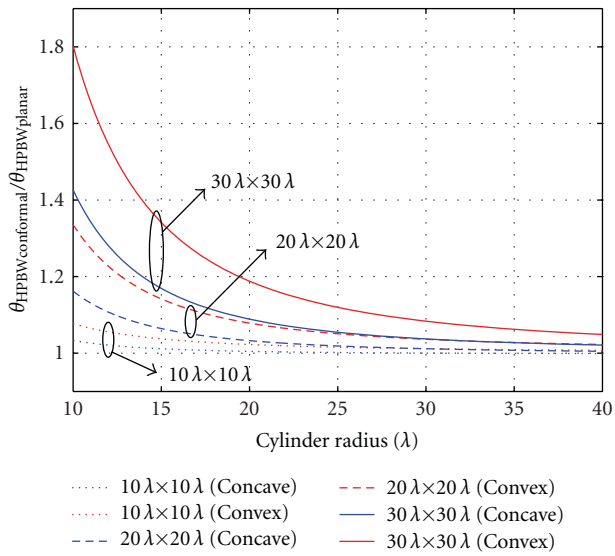

Figure 4: Normalized HPBW in the curvature plane as a function of cylinder radius.

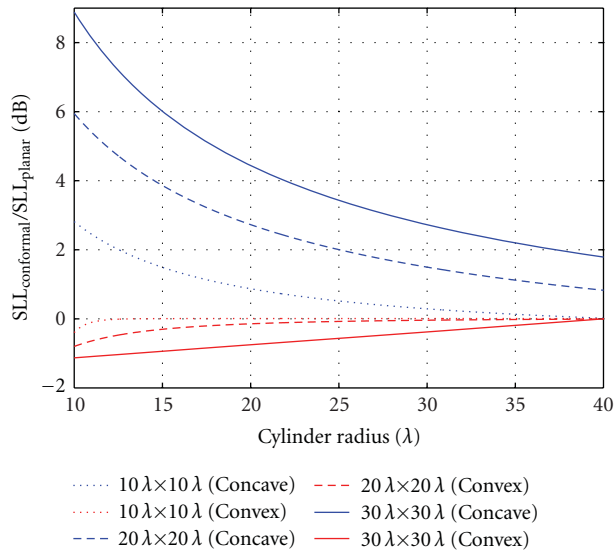

Figure 5: Normalized SLL in the curvature plane as a function of cylinder radius.

a function of cylinder radius. It should be noted here that in all designs the reflectarray aperture size is held constant ($20\lambda \times 20\lambda$), and the change in cylinder radius corresponds to changing the subtended angle α from 2 to 0.5 radian. These results are shown in Figure 7.

For a convex design, the bandwidth of the reflectarray increases monotonously with R_c. For a concave design however, an optimum subtended angle exists where the antenna achieves the maximum bandwidth. For the design here, this optimum subtended angle is 0.67 radians.

4. Conclusion

The feasibility of designing reflectarray antennas on conformal surfaces is investigated numerically. A generalized array theory formulation is presented to compute the radiation pattern of conformal reflectarray antennas. The radiation characteristics of concave and convex conformal reflectarrays on cylindrical surfaces are compared with planar designs. It is shown that in general, conformal reflectarrays will have a wider beamwidth than planar reflectarrays. The SLL depends on the platform, where concave designs show a higher SLL, while convex designs can achieve a lower SLL. In addition,

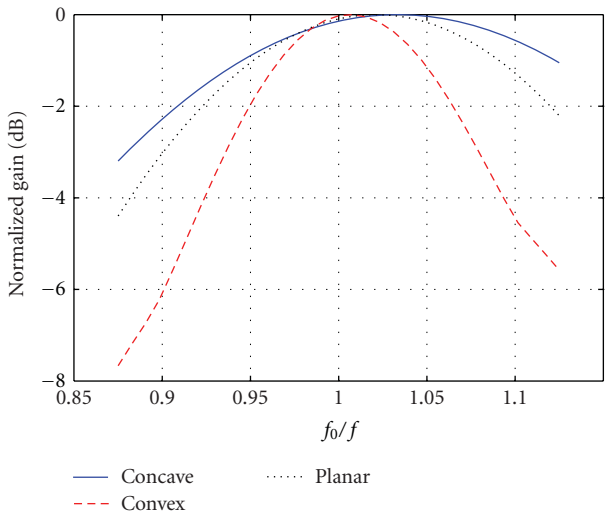

Figure 6: Normalized gain versus frequency for the reflectarray antennas.

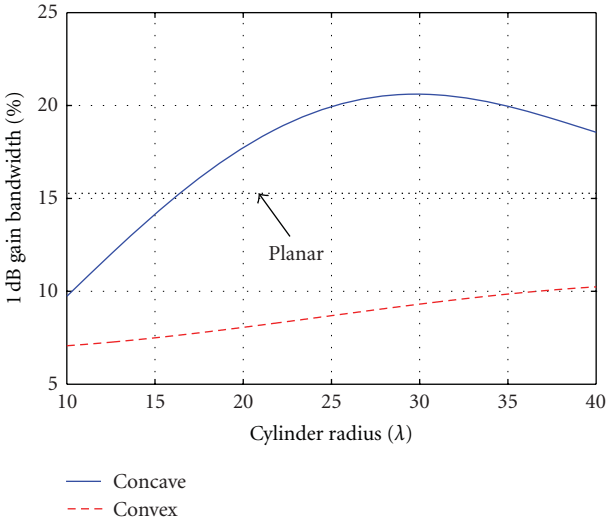

Figure 7: Gain bandwidth of the reflectarray antennas as a function of cylinder radius.

the gain bandwidth of a reflectarray antenna can be increased by using a concave cylindrical platform. These studies show that for applications where a slightly curved platform is available, a reflectarray antenna can be a suitable choice for the design.

Acknowledgment

This work was supported in part by NASA EPSCoR program under the contract number NNX09AP18A.

References

[1] J. Huang and J. A. Encinar, *Reflectarray Antennas*, Institute of Electrical and Electronics Engineers, John Wiley & Sons, 2008.

[2] L. Josefsson and P. Persson, *Conformal Array Antenna Theory and Design*, IEEE Press Series on Electromagnetic Wave Theory, John Wiley & Sons, 2006.

[3] A. M. Polegre, G. Caille, L. Boyer, and A. Roederer, "Semi-active conformal array for ESA's GAIA mission," in *Proceedings of the IEEE Antennas and Propagation Society Symposium*, pp. 4108–4111, Monterey, Calif, USA, June 2004.

[4] J. Huang and R. J. Pogorzelski, "A ka-band microstrip reflectarray with elements having variable rotation angles," *IEEE Transactions on Antennas and Propagation*, vol. 46, no. 5, pp. 650–656, 1998.

[5] P. Nayeri, F. Yang, and A. Z. Elsherbeni, "Radiation analysis of reflectarray antennas: numerical approaches versus full-Wave simulations," in *Proceedings of the National Radio Science Meeting*, Boulder, Colo, USA, 2012.

[6] R. L. Haupt, *Antenna Arrays: A Computational Approach*, John Wiley & Sons, 2010.

[7] R. C. Hansen, *Phased Array Antennas*, John Wiley & Sons, 2nd edition, 2009.

[8] Y. Rahmat-Samii, "Reflector antennas," in *Antenna Handbook: Theory, Applications, and Design*, Y. T. Lo and S. W. Lee, Eds., Van Nostrand Reinhold, 1988.

[9] A. Yu, F. Yang, A. Z. Elsherbeni, J. Huang, and Y. Rahmat-Samii, "Aperture efficiency analysis of reflectarray antennas," *Microwave and Optical Technology Letters*, vol. 52, no. 2, pp. 364–372, 2010.

[10] D. M. Pozar, S. D. Targonski, and H. D. Syrigos, "Design of millimeter wave microstrip reflectarrays," *IEEE Transactions on Antennas and Propagation, Colorado, U.S.*, vol. 45, no. 2, pp. 287–296, 1997.

[11] R. J. Mailloux, *Phased Array Antenna Handbook*, Artech House, 2nd edition, 2005.

[12] D. M. Pozar, "Bandwidth of reflectarrays," *Electronics Letters*, vol. 39, no. 21, pp. 1490–1491, 2003.

Hindawi Publishing Corporation
International Journal of Antennas and Propagation
Volume 2012, Article ID 708429, 10 pages
doi:10.1155/2012/708429

Research Article

Comparison of Synthesis Strategies for a Dual-Polarized Reflectarray

Loic Marnat,[1] Renaud Loison,[1] Raphaël Gillard,[1] Daniele Bresciani,[2] and Hervé Legay[2]

[1] *Antennes et Hyperfréquences, Institut d'Electronique et de Télécommunications de Rennes, UMR CNRS 6164, INSA, 20 Avenue des Buttes de Coësmes, CS 70839, 35 708 Rennes, France*
[2] *Thales Alenia Space Toulouse, 26 Avenue JF Champollion, BP 1187, 31037 Toulouse Cedex, France*

Correspondence should be addressed to Loic Marnat, loic.marnat@kaust.edu.sa

Received 30 January 2012; Accepted 14 May 2012

Academic Editor: Manuel Arrebola

This paper presents and compares four optimization strategies for printed reflectarrays. They are applied to synthesize a dual-polarized reflectarray using two kinds of slot-loaded patches. They provide objective criteria to deal with the numerous geometrical parameters available to tune the phase. The study relies on the comparative measurements of four different prototypes for the same $22\lambda_0 \times 22\lambda_0$ reflectarray (with λ_0 the wavelength at $f_0 = 14.25$ GHz).

1. Introduction

A reflectarray antenna combines advantages of reflectors and phased array antennas. Indeed, neither lossy feeding network nor heavy and cumbersome profile are involved. A reflectarray antenna is composed of a primary feed lighting elementary cells that delay the impinging wave and permit to shape the radiated field. In most cases, the reflected phase is controlled by the geometry or orientation of the radiating elements [1, 2], stubs or delay lines [3], or the use of reconfigurable material [4]. To achieve the phase law all over the reflectarray surface, the unit cell must be able to cover the whole 360° phase range. In [3], a reflectarray has been synthesized with a multiple layer structure allowing a true time delay compensation. A large bandwidth has then been achieved 20 (%). Single-layer reflectarrays are usually more limited in term of bandwidth. The required 360° phase range is more difficult to obtain without a strong resonance which introduces more losses. On the other hand, single substrate layer is cost effective and easy to manufacture.

In this paper, the used radiating element is a patch loaded with slots (Figure 1), having dual polarization capabilities [5]. It is an extension of the single-polarized patch structure introduced in [6, 7]. Furthermore, a reconfigurable cell can be obtained by controlling slots with PIN diodes or MEMS [8, 9]. The considered cell design is defined with six parameters for each polarization. As a consequence, a large number of cell designs are available to produce a given phase shift. This amount of solutions is advantageous for an accurate reflectarray synthesis and it also increases its complexity.

The aim of this paper is to present and validate an original reflectarray layout synthesis. This synthesis technique is based on specific cell selection strategies. Three strategies are proposed and compared. In the first part of the paper, the used elementary cell is described and its RF characteristics are studied. The proposed synthesis process is presented in the second part. In the third one, it is applied to a specific space telecommunication antenna configuration. Finally, the measurement of the resulting reflectarray are presented.

2. Elementary Cell

2.1. Description. Figure 1 presents the proposed dual-polarized cells. Two cell configurations are considered. Figures 1(a) and 1(b) depicts the centered slots configuration (defined by a microstrip square patch loaded with a Jerusalem cross slot) and the emerging slots configuration (defined by two pairs of orthogonal slots located at the edges of the microstrip square patch), respectively. For each

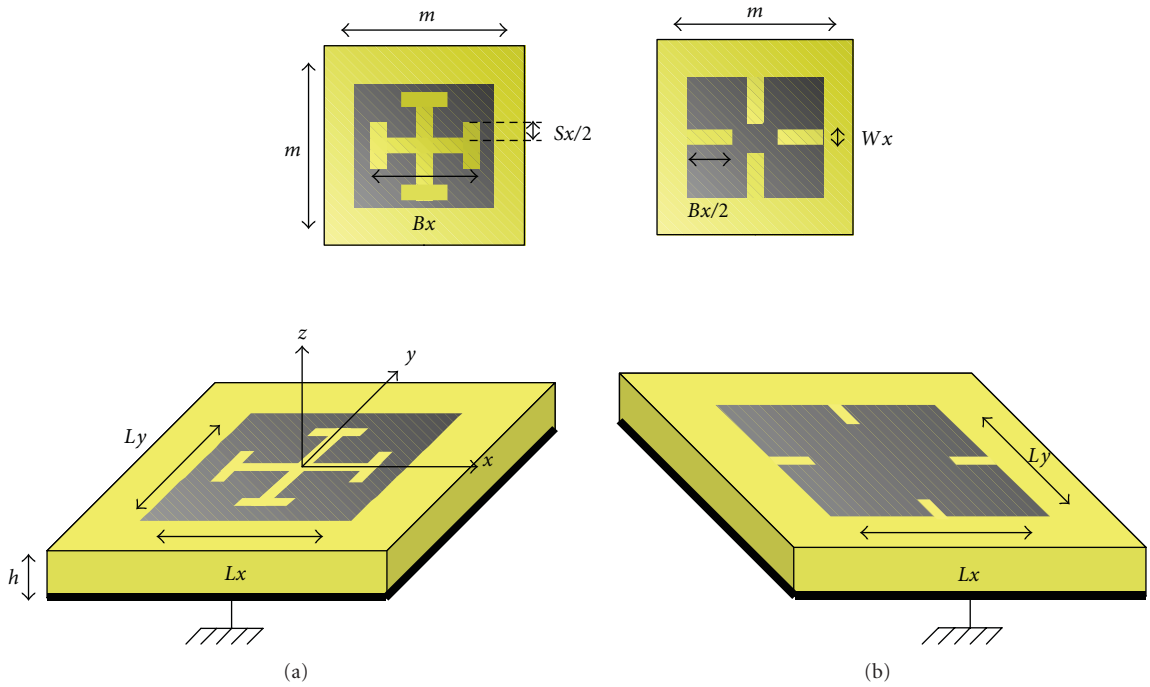

FIGURE 1: Patch loaded by (a) centered crossed slots or (b) emerging slots ($h = 4\,\text{mm}$, $\varepsilon_r \simeq 1$).

polarization, the phase reflected by the cell is tuned by varying six geometrical parameters characterizing the cell design in each direction: the patch size (Lx and Ly), the slot length (Bx and By) and width (Wx and Wy), the stub length (Sx and Sy) and width (WSx and WSy), and the slot configuration (centered crossed and emerging).

2.2. Analysis of the Reflected Phase. The phase response of the cell is simulated for a linearly polarized incident plane wave under normal incidence with a self-developed 2.5D electromagnetic simulator. It has been specifically developed for planar self-similar structures and validated through different simulation comparisons and measurements [10]. Floquet hypotheses are used in order to take mutual coupling effects into account while keeping a reasonable simulation time. In these conditions, the cell is assumed to be extracted from an infinite periodic array. A y polarized incident field is applied and the phase computed is the one of the direct reflection coefficient: $\angle\Gamma_{yy}$. In the following, this achieved phase is noted ϕ^{ach}.

Figure 2 presents the phase shift for the centered slots configuration (Figure 1(a)) versus the slots lengths for different patch dimensions. In this section, a symmetrical cell is considered which means the x and y cell parameters are equal. The size of the array lattice is set to $0.5\,\lambda_0$ at $f_0 = 14.25\,\text{GHz}$ ($m = 10.526\,\text{mm}$). The substrate is a 4 mm thick composite panel whose equivalent dielectric constant is approximated by 1.

Two areas can be identified in Figure 2. The first one corresponds to short slots (Bx smaller than 4 mm) with a phase shift which is mainly controlled by the size of the patch. In the second one, where Bx is greater than 4 mm, the slot

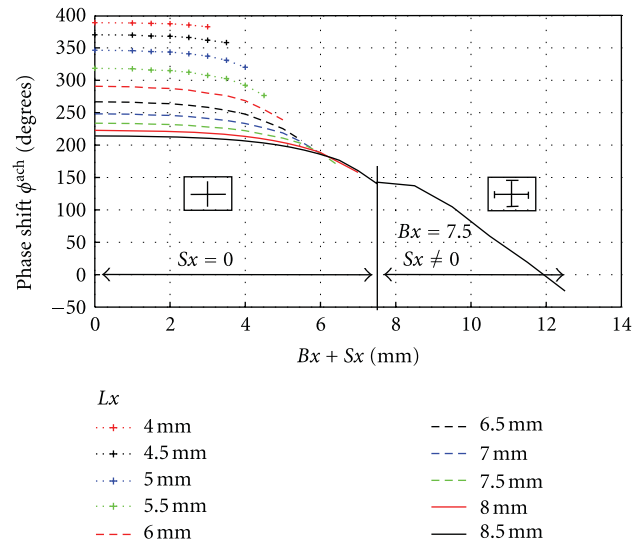

FIGURE 2: Phase shift versus slots lengths for different patch sizes (Lx) at $f_0 = 14.25\,\text{GHz}$ in normal incidence, and $Wx = 0.9\,\text{mm}$.

length becomes the most effective tuning parameter. The addition of stubs (here, only for $Lx = 8.5\,\text{mm}$ and $Bx = 7.5\,\text{mm}$) permits to extend the phase range up to 414.1°. Note that the phase range could be increased further by using thinner slots (up to 548.5° for 0.1 mm slot widths).

The same results are presented in Figure 3 for the emerging slots configuration (Figure 1(b)). It appears that the slot lengths are more influent for this cell configuration. Indeed, they directly affect the currents which are mainly

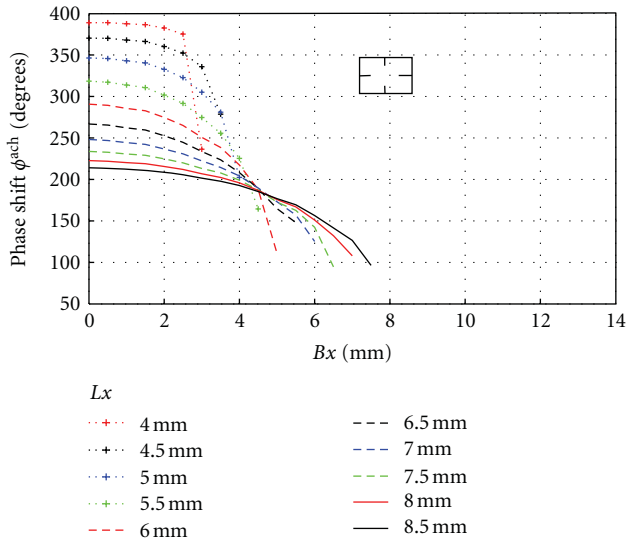

FIGURE 3: Phase shift versus slot lengths for different patch sizes (Lx) at $f_0 = 14.25$ GHz under normal incidence, and $Wx = 0.9$ mm.

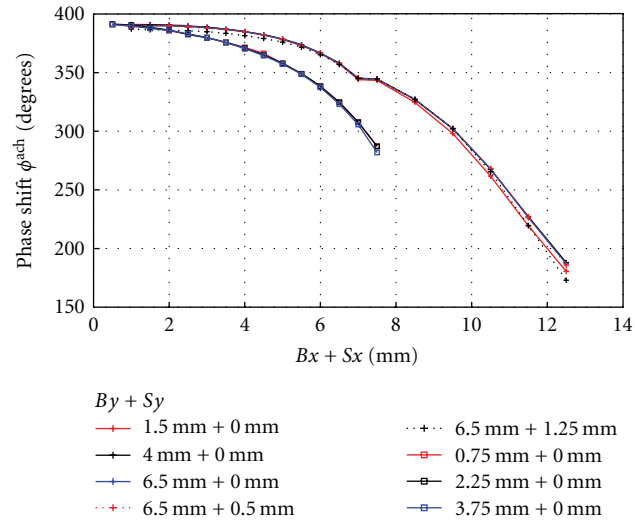

FIGURE 4: Effect of the parasitic slots ($By + Sy$) on the phase of the direct reflection coefficient for the centered (+) and the emerging (□) slots configurations at $f_0 = 14.25$ GHz under normal incidence, and $Wx = 0.9$ mm.

concentrated on patch edges. These different behaviors motivate the use of the two complementary configurations. As will be seen later on, this provides an additional flexibility to the optimization process.

It can be highlighted that the considered cells are patches on air substrate which gives low loss elements. Nevertheless, the losses of the centered crossed slots configuration are higher when stubs are used due to the resonance of the cell which is shifted close to the operating frequency.

2.3. Dual-Polarization Capabilities. In this section, the dual polarization capabilities of the cell are investigated. As previously, the cell is excited by a y polarized electric field. The phase of the reflected wave is thus controlled by the x oriented main slot (Bx) and y oriented stubs (Sx) referred to as the *excited* slots. The orthogonal slots defined by By and Sy should not affect the reflected wave and are referred to as the *parasitic* slots. The evolution of the phase of the direct reflection coefficient is plotted in Figure 4 as a function of the lengths of the excited slots at the central frequency. Different lengths of parasitic slots are considered for the two cell configurations.

This figure shows that the reflected phase can be tuned by varying the excited slots while the effect of the parasitic slots is negligible. As a consequence, both orthogonal linear polarizations can be controlled independently.

2.4. Cell Diversity. One key issue in the reflectarray layout synthesis is to select the appropriate design for each cell in order to comply with the desired antenna performance. One cell design is defined by six geometrical parameters for each polarization. Consequently, a large number of cell designs can be obtained, with several ones that produce the same phase shift. This diversity gives flexibility to the synthesis process but increases its complexity.

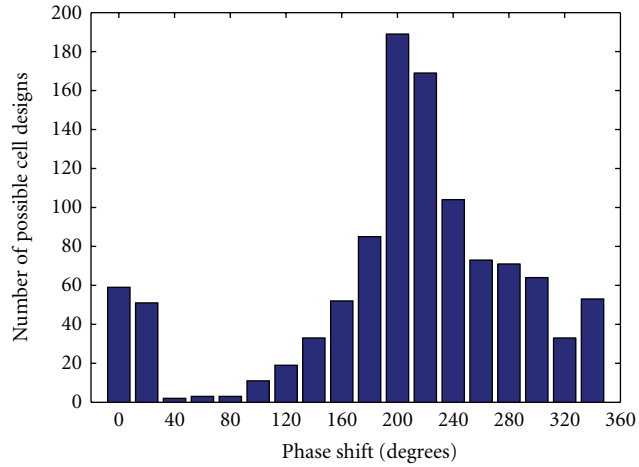

FIGURE 5: Number of cell designs producing a given range of phase shift (20° by 20°) under normal incidence at 14.25 GHz for a uniform sampling of the geometrical parameter.

As an illustration, we consider the situation where each geometrical parameter has been sampled so that 1074 different cell designs are obtained. The resulting phase distribution, corresponding to the number of cell designs producing a given phase shift under normal incidence, is plotted in Figure 5.

This figure shows the multiplicity of cell designs available to reach a given phase shift. However, it can be noted that this distribution is not uniform. For instance, a "pinched zone" can be observed from 40 to 100° where only few cell designs are available. This restricts the possible choices in this phase range for the optimization process. Nevertheless, the phase distribution is different for each incident angle. At the end, for a given reflectarray, many layouts can be generated satisfying the phase law at the central frequency. For instance,

in [5], up to 6.45×10^{3187} distinctive layouts could theoretically be generated for the studied antenna.

In these conditions, cell selection strategies must be implemented in order to optimize the reflectarray layout.

3. Synthesis Process

3.1. Cell Selection Strategies. A cell selection strategy aims at choosing the best design for each element in the array. The minimum requirement is that the achieved phase at the central frequency, f_0, matches the desired one:

$$\phi_i^{\text{ach}}(f_0) = \phi_i^{\text{des}}(f_0) \tag{1}$$

for $i = 1$ to N, where N is the number of elements in the array.

The *reference cell*, defined as the starting point when filling up the layout, is arbitrarily located at the center of the array. The cells are then successively designed from the reference one and moving to the edges of the array. In this section, four cell selection strategies are proposed and described.

(i) The *Random* strategy only operates a random selection among available cell designs achieving the desired phase shift at f_0 without any consideration on the geometry or other electrical characteristics. In this paper, these layouts are called "*R* layout" for "Random" strategy.

(ii) The *Dispersion* optimization consists in selecting cell designs that not only produce the required phase shifts at central frequency (f_0) but also the best achievable ones at the bandwidth extremities ($f_{\min}$ and $f_{\max}$). It is the most conventional strategy when designing large-bandwidth reflectarrays [11].

The best cell design, for the ith array element, is the one that minimizes the phase error between the desired and the achieved ones:

$$\varepsilon_i(f) = \left| \phi_i^{\text{des}}(f) - \phi_i^{\text{ach}}(f) \right| \tag{2}$$

at $f = f_{\min}$ and $f_{\max}$.

In this paper, such layouts are called "*D* layout" for "Dispersion" strategy.

(iii) The third strategy is called *Geometrical* optimization and has been introduced in [12]. The aim of this original strategy is to maximize the geometrical similarity between contiguous cells in the reflectarray layout. The goal is to comply with the used Floquet simulation hypotheses and thus improve the prediction accuracy of the antenna performance.

As it has been shown in Section 2, each geometrical parameter does not equally affect the phase shift. Thus, to quantify the similarity between two cells i and j, a *similarity factor* is defined in which a different weight is attributed to each geometrical parameter:

$$\text{SF}_{(i,j)} = \sqrt{\alpha_{Lx} \cdot \left(Lx_i - Lx_j\right)^2 + \alpha_{Ly} \cdot \left(Ly_i - Ly_j\right)^2 + \cdots}. \tag{3}$$

In this paper, $\alpha_{Lx} = 7$ (patch size), $\alpha_{Bx} = 4$ (slot length), $\alpha_{Sx} = 1$ (stub length), $\alpha_{Wx} = 10$ (slot width), and $\alpha_{WSx} = 10$ (stub width). In other words, a variation of slot width (Wx) leads to a larger $\text{SF}_{(i,j)}$ value than the same variation of stub length (Sx). The similarity between cell i and its neighbors is noted $\overline{\text{SF}_i}$. It is defined by averaging the similarity factor between this cell and each of its nearest neighbors (eight for a rectangular lattice). An iterative process is used that results in a layout which minimizes the $\overline{\text{SF}_i}$ factor for each array element and thus ensures smooth geometrical variations. The first iteration initializes the geometry of each cell by minimizing the $\overline{\text{SF}_i}$ factor only considering those of its 8 nearest neighbors that have already been defined. As a consequence, the geometry of the first cell is chosen arbitrarily (only complying with the desired phase). In the next steps, the cell's geometry is progressively updated until the average value of $\overline{\text{SF}_i}$ converges to its lowest value.

In this paper, these layouts are called "*G* layout" for "Geometrical" strategy.

(iv) The last proposed strategy is called *MRC* optimization for "Maximization of Reflection Coefficients" strategy. It has been developed to improve both the reflectarray losses and the cross-polarization level. To do so, the direct reflection coefficient magnitude, $|\Gamma_{yy}(f_0)|$, is maximized for each array element at the central frequency (f_0).

The simple *Random* cell selection will be used to assess the relevance of these strategies for reflectarray synthesis.

3.2. Layout Selection. In addition to the proposed cell selection strategies, it is possible to synthesize layouts with different initial conditions associated to the reference cell. Indeed, any phase offset can theoretically be applied to the phase law in the radiating aperture without changing the associated radiation pattern. The phase of the reference cell at the central frequency, $\phi_0 = \phi_0^{\text{des}}(f_0)$, determines the absolute phase values for all the array elements at this frequency. Thus, the phase of the reference cell can be chosen arbitrarily. In practice, however, its choice is not neutral [13]. As seen in Figure 5, the phase distribution is not uniform. Thus, a judicious ϕ_0 value is one that maximizes the number of possible cell designs for most of the array elements.

Although this general principle is quite simple, its direct application is not straightforward as the phase distribution depends on the incident angle (in Figure 5, it is only given for the normal incidence). As a consequence, in the following, the optimization process is repeated for different ϕ_0 values. Then, the solution with the best simulated performance is selected.

To do so, some indicators are defined as follows.

(i) The phase errors between the simulated and the desired phase shifts over the array at a given frequency f are quantified by the following mean and standard deviation:

$\bar{\varepsilon}(f) = (1/N) \sum_{i=1}^{N} \varepsilon_i(f)$ quantifies the mean phase errors over the array. Note that $\bar{\varepsilon}(f_0) = 0$ as all proposed strategies match the specification at f_0 (1).

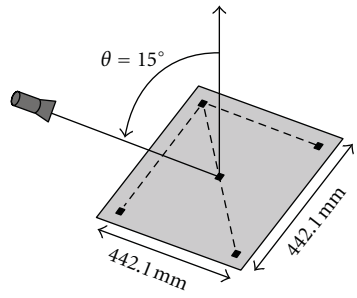

(a) Offset configuration

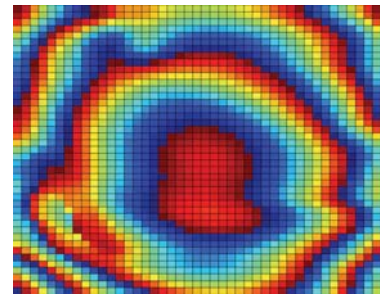

(b) Desired aperture phase shift at $f_0 = 14.25$ GHz

FIGURE 6: Antenna configuration ($F/D = 1.3$, maximum cell incidence angle =38°, radiating aperture =$22\lambda_0 \times 22\lambda_0$, and interelement spacing =$0.5\lambda_0$).

(ii) The magnitude of the reflection coefficients is averaged over the array to quantify the ohmic losses and/or the polarization conversions of the generated layout but does not account for the tapering of the illumination on the array. It is noted $\overline{\Gamma_{yy}}(f)$.

(iii) To quantify the similarity over the layout, a global similarity criterion, noted $\overline{\text{SF}}$, is defined by averaging the $\overline{\text{SF}}_i$ values all over the array.

Layouts can objectively be compared using these indicators and the best candidate can then be chosen.

4. Application to a Specific Antenna Configuration

4.1. RF Requirements. The synthesis process is applied to the design of a dual-polarized reflectarray antenna for spatial communications in the Ku band (from 14 to 14.5 GHz). The considered antenna configuration is depicted in Figure 6(a). The size of the antenna aperture is $22\lambda_0 \times 22\lambda_0$. The F/D ratio is set to 1.3 as a trade-off between frequency dispersion and spillover effects. Moreover, an offset configuration is chosen to limit feed blockage.

The same radiation pattern is required for both polarizations with a CONUS type coverage (for CONtinental United States). To get the phase shift required in the reflectarray aperture, a complex ratio between the field coming from the primary feed and the field reconstructed from the desired shaped radiation pattern in the aperture is performed. The desired aperture phase shift at $f_0 = 14.25$ GHz is shown in Figure 6(b).

4.2. Layout Synthesis and Optimization

4.2.1. Layouts Generation and Selection. Different layouts are generated using the four cell selection strategies. For each strategy, eight layouts are synthesized by considering eight initial conditions (ϕ_0) regularly distributed over the 360° range. Among the eight layouts, the best one is then selected using the indicators defined in Section 3.2.

TABLE 1: Indicators of layouts synthesized with the *MRC* strategy for eight ϕ_0 values.

		$f_{\min}$		f_0	$f_{\max}$	
ϕ_0	$\overline{\text{SF}}$	$\overline{\Gamma_{yy}}$	$\bar{\varepsilon}$	$\overline{\Gamma_{yy}}$	$\overline{\Gamma_{yy}}$	$\bar{\varepsilon}$
0	1.17	0.917	5.2	0.951	0.948	7.9
50	1.12	0.915	5.0	0.950	0.949	8.2
100	1.12	0.912	3.8	0.950	0.948	8.6
150	1.10	0.908	4.3	0.948	0.949	8.8
200	1.07	0.907	3.6	0.948	0.949	8.6
250	1.10	0.907	4.3	0.947	0.945	8.1
300	1.16	0.913	4.7	0.948	0.947	7.5
350	1.19	0.917	5.4	0.950	0.947	8.0

For illustrative purpose, the procedure is detailed only for the *MRC* strategy. The results obtained with the four cell selection approaches are summarized in the next section.

Table 1 reports the indicators associated to each synthesized *MRC* layout. Note that $\bar{\varepsilon}(f_0)$ is not reported in Table 1 as it is null.

The relatively low values of $\overline{\Gamma_{yy}}$ shown in Table 1 might be related to cross-polarization generated by cells distant from the center of the array, with high incidence angle (38°). To mitigate this phenomenon, nonsymmetrical cells could be used. $\overline{\Gamma_{yy}}$ is an arbitrary indicator used for layout selection and is not directly related to the losses and cross-polarization levels radiated by the reflectarray (does not account for the tapering on the array). It can be noticed that the $\overline{\Gamma_{yy}}$ parameter is not really affected by the ϕ_0 value. This is consistent with the used *MRC* strategy that aims at maximizing $|\Gamma_{yy}|$ for each array element. However, larger variations can be observed for the nonoptimized indicators ($\overline{\text{SF}}$ and $\bar{\varepsilon}$).

As a consequence, the selection consists in choosing the ϕ_0 value that results in the best trade-off among these indicators. For the *MRC* strategy, the layout obtained with $\phi_0 = 50°$ is selected.

4.2.2. Selected Layouts. The same layout selection is applied for each strategy. The RF performance of the four resulting layouts are summarized in Table 2. It can be observed that

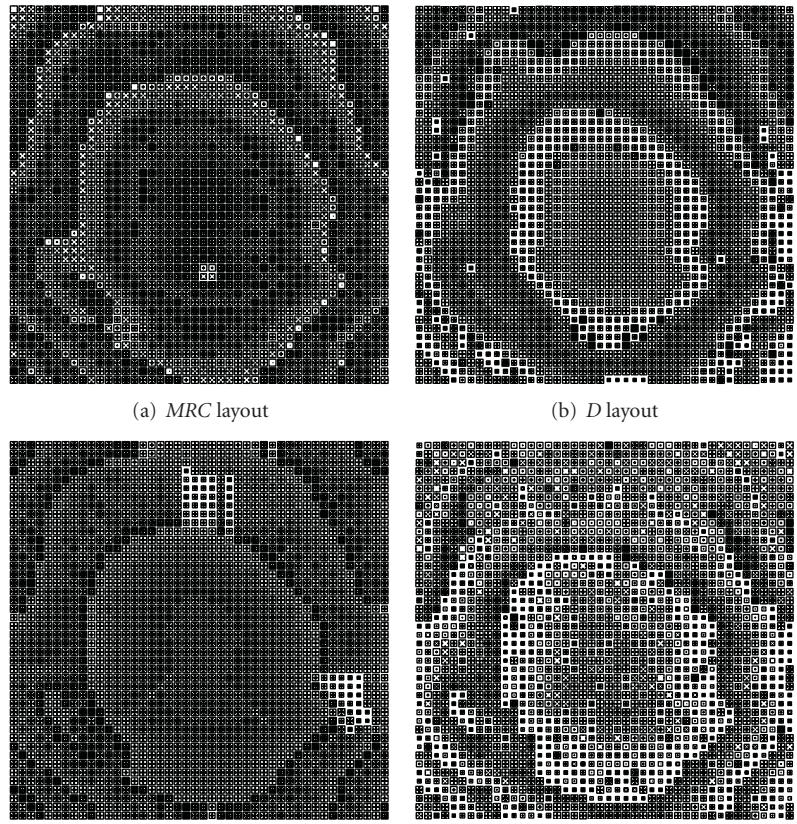

(a) *MRC* layout (b) *D* layout

(c) *G* layout (d) *R* layout

Figure 7: Visualization of the four selected layouts.

Table 2: Indicators of the four layouts synthesized with the four cell selection strategies.

			$f_{\min}$		f_0	$f_{\max}$	
Name	ϕ_0	$\overline{\text{SF}}$	$\overline{\Gamma_{yy}}$	$\overline{\varepsilon}$	$\overline{\Gamma_{yy}}$	$\overline{\Gamma_{yy}}$	$\overline{\varepsilon}$
MRC	50	1.12	**0.92**	13.6	**0.90**	**0.95**	9.5
D	100	0.97	0.86	**10.4**	0.89	0.89	**7.5**
G	100	**0.17**	0.82	38.1	0.77	0.87	29.6
R	150	1.41	0.85	32.7	0.79	0.83	31.8

each strategy leads to a layout that optimizes its own indicator. This characteristic is highlighted by bold numbers in Table 2. The bad RF performance of the *R* layout confirms the interest to use a specific cell selection strategy.

The four layouts are depicted in Figure 7(a). As expected, the *G* layout has the smoothest geometrical variations to provide the best accuracy between simulation and measurement. Nevertheless, the accuracy of the prediction also relies on the number of resonant cells in the array: mutual coupling is larger for cells close to resonance [7] which makes these cells more sensitive to their actual environment. The *R* layout has large geometrical variations distributed all over the panel while for *MRC* and *D* layouts, variations are localized only at transition areas. This regularity results from the restricted cell choice imposed by the *MRC* and *D* approaches. Indeed, the *R* layout is synthesized with only one criterion whereas the *MRC* and the *D* layouts are optimized with two criteria. A zoom of a 12 by 12 array elements area on the layouts is presented in Figure 8 to show more clearly the evolution of the geometry of the chosen cells in the four layouts (Figure 7).

5. Measurement Results

The chosen layouts have been manufactured and measured. This section compares the results in order to assess the proposed strategies.

5.1. Radiation Patterns at the Central Frequency. The required radiation pattern is presented in Figure 9. We can observe one main beam for the continental USA, Canada, and Puerto-Rico and another one for Hawaii. Figures 10(a)–10(d) show the superimposition of the required and measured radiation patterns of the four manufactured layouts for a conical view of the earth ($\pm 8^\circ$ angles).

The measured radiation patterns of the *MRC*, *D*, and the *G* layouts match the required coverage quite well regarding the small size of the considered antenna while for the *R* layout, large differences occur. For this layout which presents the largest geometrical irregularities, the local periodicity assumed in the simulation process is strongly violated. This

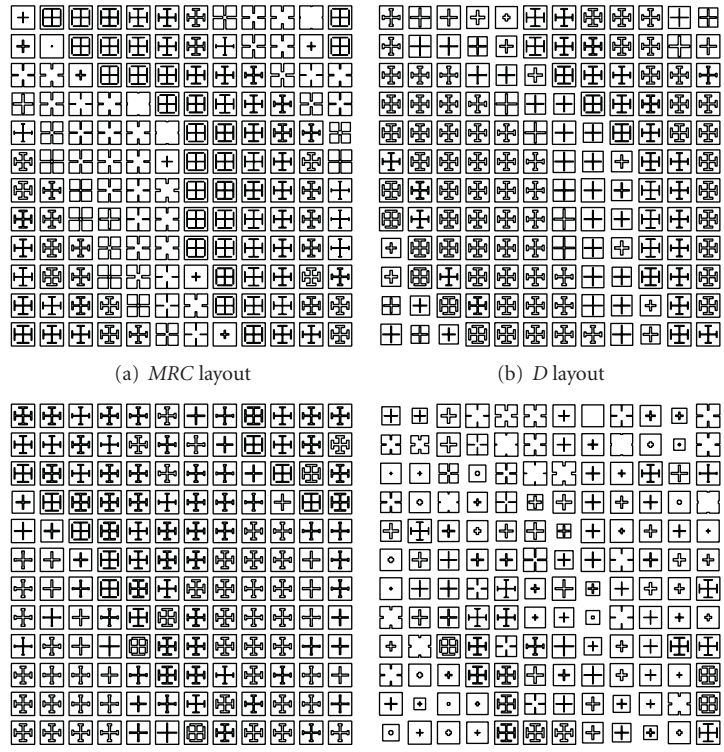

(a) *MRC* layout (b) *D* layout

(c) *G* layout (d) *R* layout

Figure 8: Zoom in on the top right area of the four layouts (12 by 12 elements area).

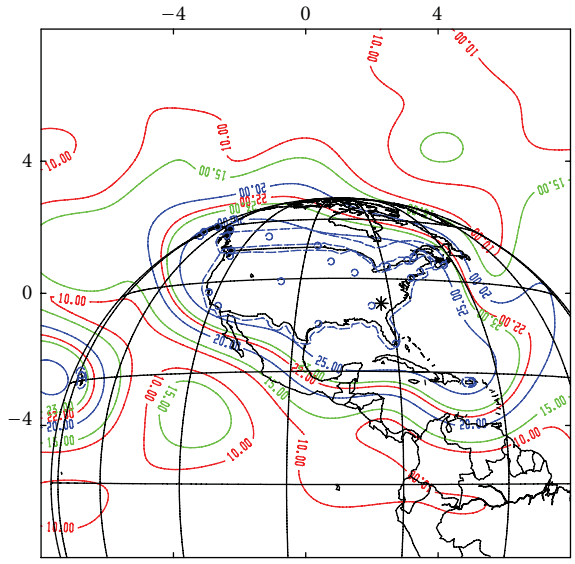

Figure 9: Required radiation patterns in the direct polarization at 14.25 GHz.

results in poor RF performance which confirms the necessity to use a specific cell selection process. As a consequence, this layout is no longer studied in the following.

5.2. Losses and Cross-Polarization. Table 3 summarizes the measured ohmic losses for the three layouts at the central frequency and the extremities of the band. The *MRC* layout does not only provide a good spatial coverage, it also exhibits the lowest losses. This is consistent with the optimization of $|\Gamma_{yy}(f_0)|$ performed for this layout. The losses exhibited by the *D* layout are high compared to the other measured layouts. This phenomenon is explained by the use of a larger number of dispersive cells in order to match the phase law requirements over the frequency band.

Table 3: Measured losses of three manufactured layouts.

	Measured losses (dB)		
Name	14 GHz	14.25 GHz	14.5 GHz
MRC	0.5	0.2	0.1
D	1.4	1.2	1.27
G	0.63	0.5	0.53

Table 4 summarizes the maximum measured cross-polarization level for the three layouts. The cross-polarization levels remain under −25 dB for the *G* and *MRC* layouts whereas for the *D* layout, it goes up to −22.4 dB at the lower frequency. However, these levels are suitable with the specifications for all cases.

5.3. Radiation Patterns over the Frequency Band. Figures 11(a)–11(f) show the superimposition of the required and measured radiation patterns at 14 and 14.5 GHz for the conical view of the earth.

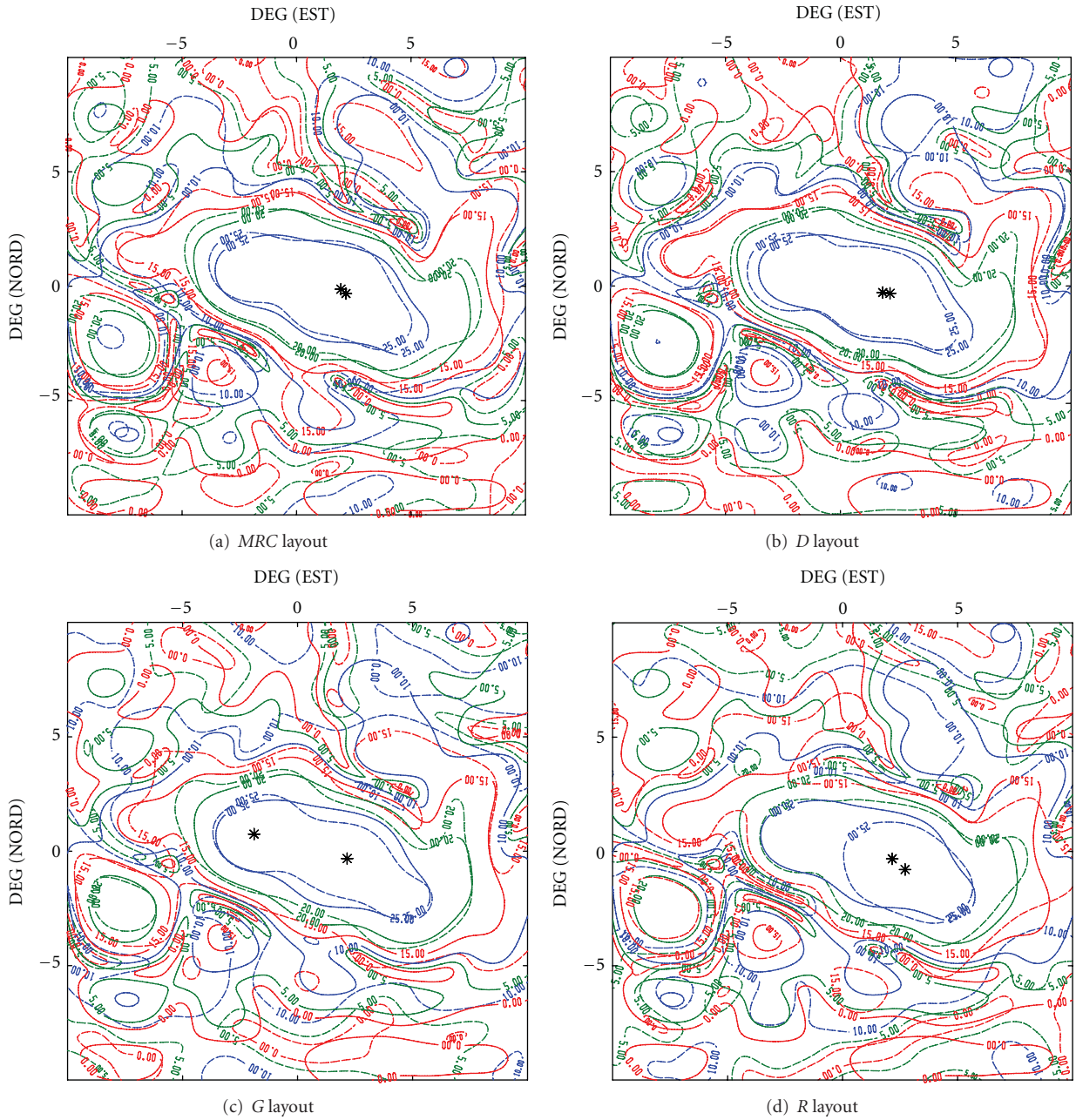

(a) *MRC* layout (b) *D* layout

(c) *G* layout (d) *R* layout

Figure 10: Superimposition of the required (solid) and measured (dashed) radiation patterns at 14.25 GHz in the direct polarization.

Table 4: Measured cross-polarization of three manufactured layouts.

	Measured cross-polarization (dB)		
Name	14 GHz	14.25 GHz	14.5 GHz
MRC	−25.7	−26.3	−26.8
D	−22.4	−25.4	−27.1
G	−27.3	−26.9	−26.6

These layouts exhibit quite stable radiation patterns over the frequency band. As expected, the *D* layout has a very good matching with the required coverage at the extremities of the frequency band. However, in the present case, the best performance over the frequency band are exhibited by the *MRC* layout. It can be explained because, unlike the other strategies, it is not a "phase only synthesis" as the module of the direct reflection coefficients are also optimized. It should be noticed that the small size of the breadboard is certainly favorable to the *MRC* layout. In a larger array, the frequency dispersion would be higher and the improvement brought by the *D* strategy would be more obvious.

5.4. Radiation Pattern of the MRC Layout. The two main cut views corresponding to the *MRC* layout are presented in

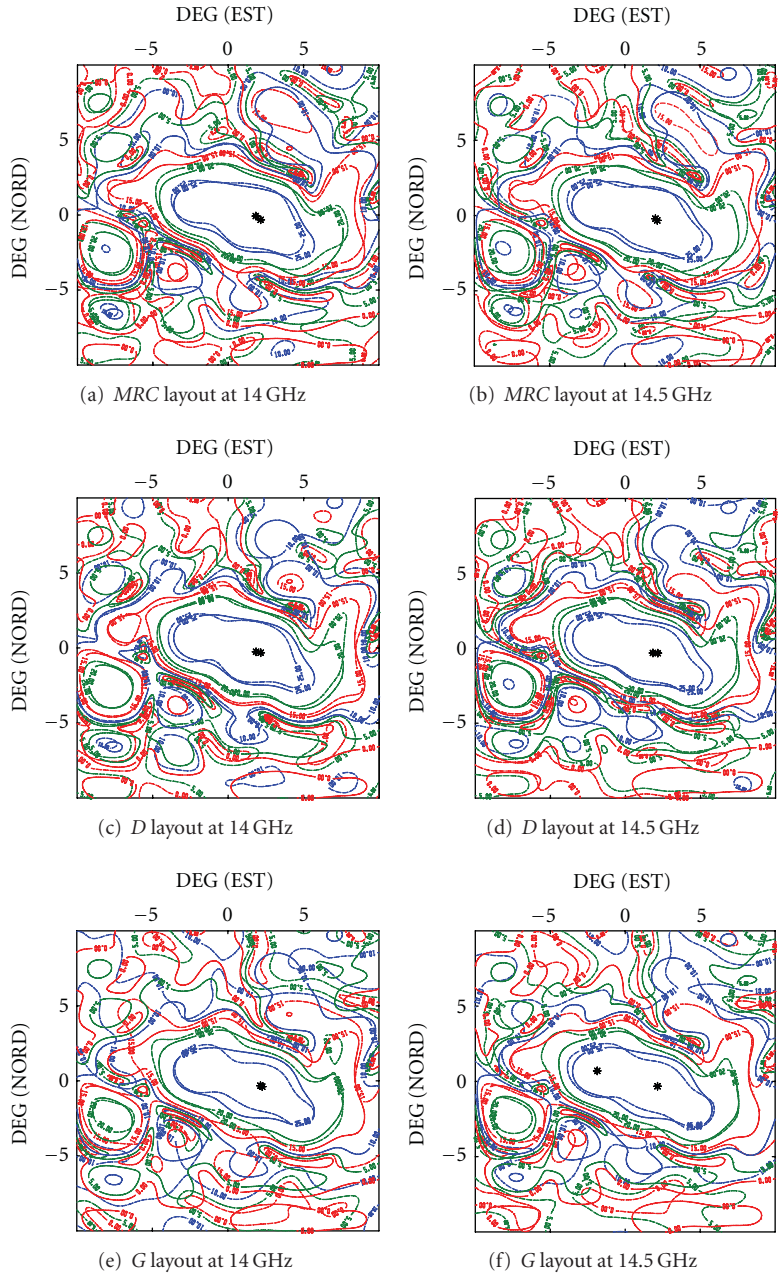

(a) *MRC* layout at 14 GHz (b) *MRC* layout at 14.5 GHz

(c) *D* layout at 14 GHz (d) *D* layout at 14.5 GHz

(e) *G* layout at 14 GHz (f) *G* layout at 14.5 GHz

Figure 11: Superimposition of the required (solid) and measured (dashed) radiation patterns in the direct polarization of synthesized layouts.

Figures 12(a) and 12(b) at 14.25 GHz for the direct and the cross-polarizations.

The good coverage matching is confirmed by a maximum gain difference in the direct polarization of 1.5 dB between the required and the measured ones within the −10 dB bandwidth.

6. Conclusion

In this paper, optimization strategies have been proposed to select the geometry of the radiating cells when designing a reflectarray. They have been applied to improve the performance of a dual-polarized reflectarray with slot-loaded patches. It has been shown that such advanced synthesis procedures are required to take full benefit of the numerous geometrical degrees of freedom provided by this radiating cell. Comparisons of measured performance have confirmed the superiority of the optimization strategies combining phase and magnitude goals. The corresponding *MRC* layout reveals low losses and a satisfactory cross-polarization level. Moreover, its radiation pattern is quite stable over the considered frequency band (0.5 GHz centered on 14.25 GHz).

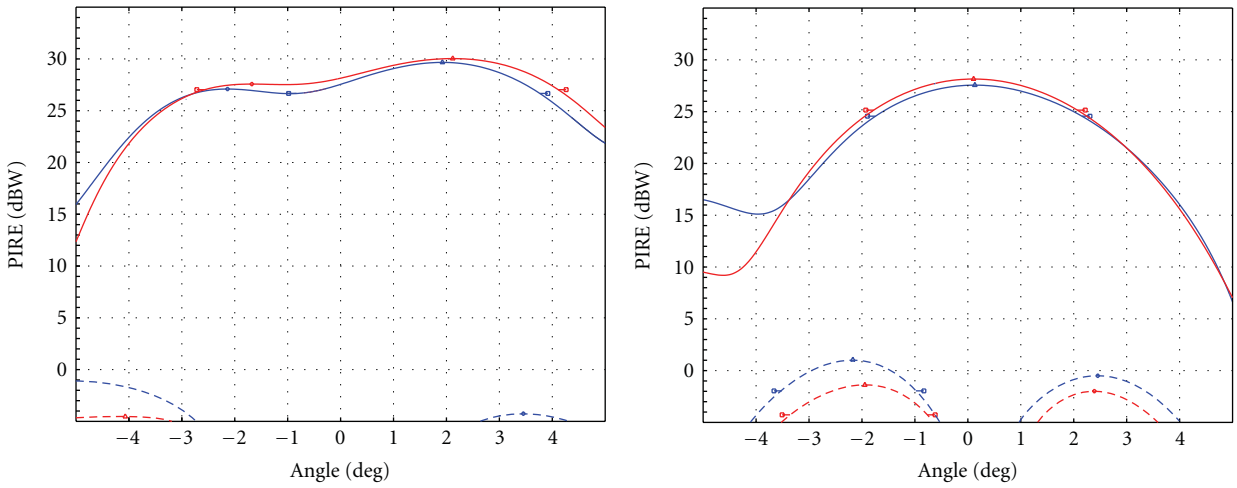

(a) *MRC* layout at 0° longitude

(b) *MRC* layout at 0° latitude

FIGURE 12: Superimposition of the required (red) and measured (blue) radiation patterns at 14.25 GHz in direct (solid) and crossed (dashed) polarizations.

Acknowledgment

The authors would like to thank Dr. R. Chiniard for the support on analysis and measurements.

References

[1] D. M. Pozar and T. A. Metzler, "Analysis of a reflectarray antenna using microstrip patches of variable size," *Electronics Letters*, vol. 29, no. 8, pp. 657–658, 1993.

[2] J. Huang, "Bandwidth study of microstrip reflectarray and a novel phased reflectarray concept," in *Proceedings of the IEEE Antennas and Propagation Society International Symposium (AP-S '08)*, vol. 1, pp. 582–585, June 1995.

[3] E. Carrasco, J. A. Encinar, and M. Barba, "Bandwidth improvement in large reflectarrays by using true-time delay," *IEEE Transactions on Antennas and Propagation*, vol. 56, no. 8, pp. 2496–2503, 2008.

[4] W. Hu, M. Y. Ismail, R. Cahill et al., "Liquid-crystal-based reflectarray antenna with electronically switchable monopulse patterns," *Electronics Letters*, vol. 43, no. 14, pp. 744–745, 2007.

[5] D. Cadoret, L. Marnat, R. Loison, R. Gillard, H. Legay, and B. Salome, "A dual linear polarized printed reflectarray using slot loaded patch elements," in *Proceedings of the 2nd European Conference on Antennas and Propagation (EuCAP '07)*, pp. 1–5, November 2007.

[6] D. Cadoret, A. Laisne, R. Gillard, L. Le Coq, and H. Legay, "Design and measurement of new reflectarray antenna using microstrip patches loaded with slot," *Electronics Letters*, vol. 41, no. 11, pp. 623–624, 2005.

[7] M. A. Milon, R. Gillard, D. Cadoret, and H. Legay, "Analysis of mutual coupling for the simulation of reflectarrays radiating cells," in *Proceedings of the 1st European Conference on Antennas and Propagation (EuCAP '06)*, pp. 1–6, November 2006.

[8] J. McSpadden, L. Fan, K. Chang, and J. Huang, "Ka-band beam steering reflectarray study," in *Proceedings of the IEEE Antennas and Propagation Society International Symposium*, vol. 3, pp. 1662–1665, August 1999.

[9] H. Legay, B. Pinte, M. Charrier, A. Ziaei, E. Girard, and R. Gillard, "A steerable reflectarray antenna with mems controls," in *Proceedings of the IEEE International Symposium on Phased Array Systems and Technology*, pp. 494–499, October 2003.

[10] D. Bresciani, "Unified approach to the characterization of frequency and polarization selective surfaces," in *Proceedings of the IEEE International Symposium Digest of Antennas and Propagation (AP-S '93)*, vol. 3, pp. 1960–1963, July 1993.

[11] J. A. Encinar and J. A. Zornoza, "Three-layer printed reflectarrays for contoured beam space applications," *IEEE Transactions on Antennas and Propagation*, vol. 52, no. 5, pp. 1138–1148, 2004.

[12] L. Marnat, R. Loison, R. Gillard, D. Bresciani, and H. Legay, "Accurate synthesis of a dual linearly polarized reflectarray," in *Proceedings of the 3rd European Conference on Antennas and Propagation (EuCAP '09)*, pp. 2523–2526, March 2009.

[13] L. Marnat, R. Loison, R. Gillard, and D. Bresciani, "Optimization strategies for dual linear polarized reflectarrays," in *Proceedings of the 30th ESA Antenna Workshop on Antennas for Earth Observation, Science, Telecommunication and Navigation Space Missions*, pp. 1–4, May 2008.

Hindawi Publishing Corporation
International Journal of Antennas and Propagation
Volume 2012, Article ID 125287, 10 pages
doi:10.1155/2012/125287

Review Article

Recent Developments of Reflectarray Antennas in Dual-Reflector Configurations

Carolina Tienda,[1] Manuel Arrebola,[2] and José A. Encinar[1]

[1] *Department of Electromagnetism and Circuit Theory, Technical University of Madrid, 30 Complutense Avenue, 28040 Madrid, Spain*
[2] *Department of Electrical Engineering, Group of Signal Theory and Communications, University of Oviedo, Academic Campus, 33203 Gijón (Asturias), Spain*

Correspondence should be addressed to Carolina Tienda, carotienda@gmail.com

Received 2 March 2012; Accepted 23 May 2012

Academic Editor: Raphaël Gillard

Recent work on dual-reflector antennas involving reflectarrays is reviewed in this paper. Both dual-reflector antenna with a reflectarray subreflector and dual-reflectarrays antennas with flat or parabolic main reflectarray are considered. First, a general analysis technique for these two configurations is described. Second, results for beam scanning and contoured-beam applications in different frequency bands are shown and discussed. The performance and capabilities of these antennas are shown by describing some practical design cases for radar, satellite communications, and direct broadcast satellite (DBS) applications.

1. Introduction

Dual-reflector antennas are used to reduce the cross-polarization and the overall antenna volume in many applications, particularly in space applications. The use of a reflectarray as sub- or main reflector in a dual-reflector configuration [1] can provide some advantages in the antenna performance and in the manufacturing process. For example, a parabolic reflector with a reflectarray as subreflector has been proposed for compensating the errors on the surface of very large deployable reflectors [2, 3], for beam scanning in a limited angular range [4] and contoured beam applications [5]. This antenna configuration, based on parabolic main reflector and a reflectarray subreflector, offers several advantages compared to a single reflectarray antenna. First of all, it can provide a broad-band performance for large apertures, by using a reflectarray subreflector of small electrical dimensions and a large parabolic reflector. In addition, this dual-reflector configuration can be used to scan or reconfigure the beam by electronically controlling the phase-shift at the elements of a limited-size subreflectarray [4]. These configurations can be used for active or reconfigurable antennas by inserting amplifier modules or phase shifters on the elements of the reflectarray subreflector, in order to achieve high-power transmission or fine beam-pointing adjustment [6].

If the main reflector is replaced by a flat reflectarray, a dual-reflectarray antenna is obtained [7, 8]. This configuration provides phase control on both surfaces, which can be used for different proposals as amplitude and phase synthesis [9], or to reduce the crosspolar radiation and shape the beam. The two-surface control permits to improve the performance of the antenna and extend the applicability of reflectarrays. Moreover this configuration provides advantages for transportable antenna application since the two flat arrays can be easily folded and deployed [10]. In a dual-reflectarray antenna, active control devices can be included in both reflectarrays, being the subreflectarray preferred because of their smaller size. Finally, a dual-reflectarray antenna comprising a parabolic main reflectarray can be used to provide beam shaping in a broad band [11].

These antenna configurations including a controllable reflectarray subreflector can present a great potential in several space applications, such as Synthetic Aperture Radar (SAR), remote sensing, and reconfigurable antennas for direct broadcast satellites (DBSs). Although an SAR antenna

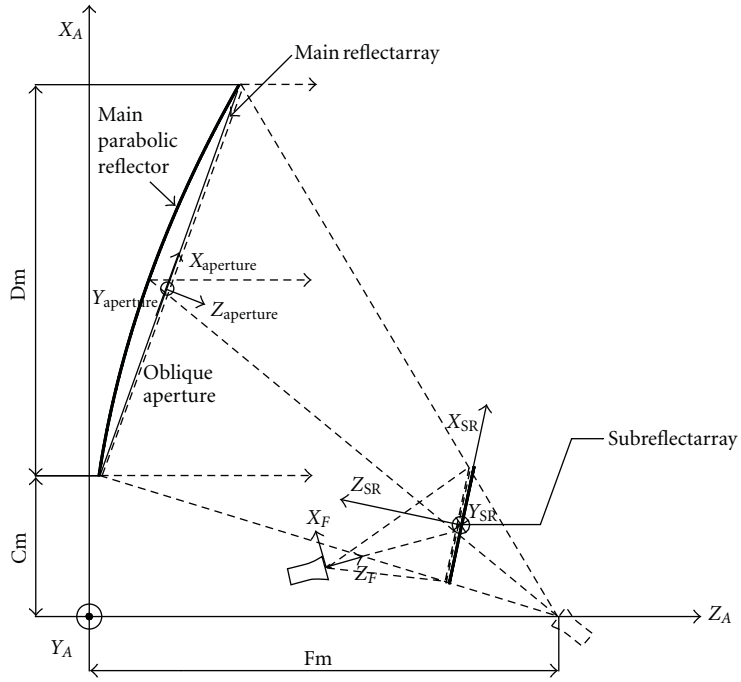

Figure 1: Scheme of dual-reflector antenna with a reflectarray subreflector and with a parabolic main reflector or a flat reflectarray as main reflector.

is usually implemented by active arrays, a reconfigurable reflectarray subreflector can provide beam scanning at a moderate cost and complexity. A second application is in radiometric remote sensing in millimeter and sub-millimeter frequency bands, which requires a beam scanning in a limited range actually implemented by motors [12]. An alternative for electronic beam scanning in this frequency bands can be reflectarrays based on liquid crystals [13–15]. Finally, the reflectarray subreflector can be used to shape the beam in contoured-beam DBS antennas. In this configuration, the beam can be shaped by adjusting the phase-shift distribution on the subreflectarray, while the main parabolic reflector focuses the beam without any bandwidth limitation. If the phase is electronically controlled on the subreflectarray by using MEMS [16, 17] or varactor diodes [18], the beam can be reconfigured to change the coverage during the life-time of the satellite. This aspect is a real need in telecommunications and DBS missions, since the demand in data traffic (TV broadcast, phone, video or data transmission, multimedia direct-to-home, etc. ...) can change during the 15–20 year lifetime of the satellites.

2. Analysis of Dual-Reflector Antennas Involving Reflectarrays

As shown in Figure 1, the proposed antenna configuration is made up of three components: a primary feed, a flat subreflectarray, and a main reflector that can be either a parabolic classic reflector or a flat or curved reflectarray. Figure 1 shows a dual-offset optics using a horn antenna as primary feed, however a centered configuration can also be analysed. In the analysis of the dual-reflector antenna involving one or two reflectarrays, four coordinate systems are considered. Two of these systems are associated to two components of the antenna: the feed reference system (X_F, Y_F, Z_F), which is centered at the phase centre of the primary feed; and the subreflectarray reference system, defined by $(X_{\text{SR}}, Y_{\text{SR}}, Z_{\text{SR}})$, whose origin is placed at the centre of the subreflectarray surface. The third coordinate system is used to define the aperture for the computation of the radiated field: the aperture reference system $(X_{\text{aperture}}, Y_{\text{aperture}}, Z_{\text{aperture}})$, which is placed at the centre of the antenna aperture. All these coordinate systems are referred to as a common one, the antenna coordinate system (X_A, Y_A, Z_A), with the Z_A axis on the direction of the beam, as usual in reflector antennas.

This antenna can be analyzed through a modular procedure in four steps. First, the field radiated by the primary feed horn should be evaluated and the incident field must be computed at the centre of each subreflectarray cell. Although, in some cases, a conventional $\cos^q(\theta)$ function can be used to model the field radiated by the feed within a good accuracy [19]. In general, the subreflectarray elements are placed in the Fresnel zone of the primary feed, and therefore the near field of the feed must be considered, which can be obtained through full-wave simulations, measurements of the feed or spherical mode expansion of the field radiated by the feed horn, [20, 21]. Dual linear polarization is considered, vertical and horizontal, which corresponds to X_F and Y_F directions, respectively, according to Figure 1.

In the second step, the subreflectarray is analysed to compute the field reflected by each reflectarray cell. This analysis is carried out element by element through the general technique implemented for multilayer reflectarrays

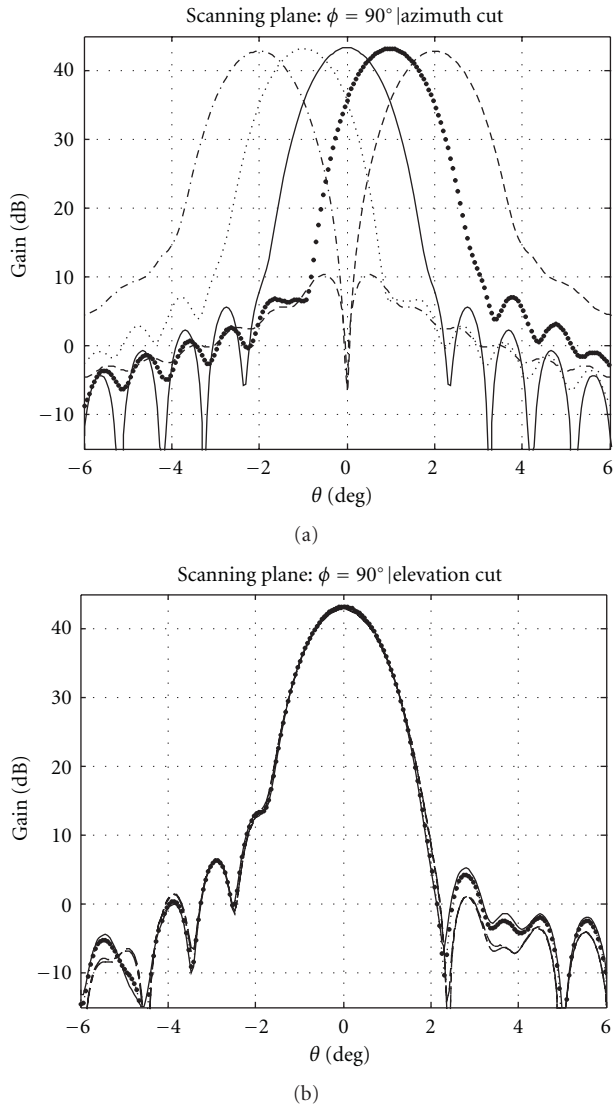

FIGURE 2: Simulated patterns of the dual-reflector antenna at 11.95 GHz for beam scanning in azimuth in the principal planes. (a) Azimuth plane, (b) elevation plane.

[21–23]. The technique is based on Method of Moments in Spectral Domain, considering local periodicity and the real angle of incidence on each periodic cell of the wave coming from the feed, which has been demonstrated to be accurate for reflectarrays in single-reflector configurations. All the field components are taken into account, and the incident and reflected fields on each reflectarray cell, defined by the subindexes (p, q), are related through a reflection matrix $\mathbf{P}^{p,q}$ as follows:

$$E_{\text{ref}}(p,q) = \mathbf{P}^{p,q} \cdot E_{\text{in}}(p,q). \tag{1}$$

The matrix $\mathbf{P}^{p,q}$ depends on the incidence angle and its complex elements relate the Cartesian components of the incident and the reflected fields, considering the cross-polarization produced by printed elements:

$$\mathbf{P}^{p,q} = \begin{pmatrix} \rho_{xx}^{p,q} & \rho_{yx}^{p,q} \\ \rho_{xy}^{p,q} & \rho_{yy}^{p,q} \end{pmatrix}. \tag{2}$$

Third, the analysis of the main reflector is carried out. In case of considering a classic parabolic reflector as main, the analysis will be based on physical optics. Thus, the electric printed currents on the reflector surface are computed, adding the contributions of the field radiated by all the subreflectarray elements. Once the currents are computed, the field is projected on the aperture plane through the Jacobian transformation.

In the case of having a flat reflectarray main reflector, it is analyzed using the same technique as for the subreflectarray, but we have to compute first the incident field on the elements of the main reflectarray. Now, the cells of the main reflectarray are placed in the Fresnel zone of the subreflectarray, but in the far-field region of the subreflectarray cells which are small apertures. Thus, the computation of the incident electric field on the main reflectarray surface can be computed as the superposition of all the contributions from the subreflector elements. In this case, the reflectarray surface is considered as the aperture plane. In the case that the main reflectarray is printed on a curved surface, the same procedure is applied but using a local coordinate system on each element of the main curved reflectarray and analyzing each element, assuming a locally flat periodic environment.

In the fourth step the radiation pattern of the entire antenna is computed starting from the electric field on the antenna aperture (aperture of the main reflector), using an algorithm based in FFT. Because of the analysis method, the radiation patterns are computed taking into account the ohmic losses in the reflectarray, the illumination, and spillover efficiencies.

3. Applications

Dual-reflector antennas involving reflectarrays have been identified as possible solutions for different applications. First, they can be used in beam-scanning applications since the beam pointing can be achieved with a small electronically-reconfigurable subreflectarray. In this applications, the use of a reflectarray as main reflector can be used to improve the folding and deploying performance of the antenna, which is very convenient for transportable antennas. Second, a reflectarray subreflector can be used to synthesize a contoured beam for DBS applications. These beams can also be achieved with a dual-reflectarray antenna using a main parabolic reflectarray to appropriately shape the beam in a broad frequency band and a passive subreflectarray, which can be used to improve the cross-polarization of the antenna. Finally, a reflectarray subreflector has been proposed to compensate the phase error introduced by main parabolic reflector surface because of the manufacturing tolerances [2].

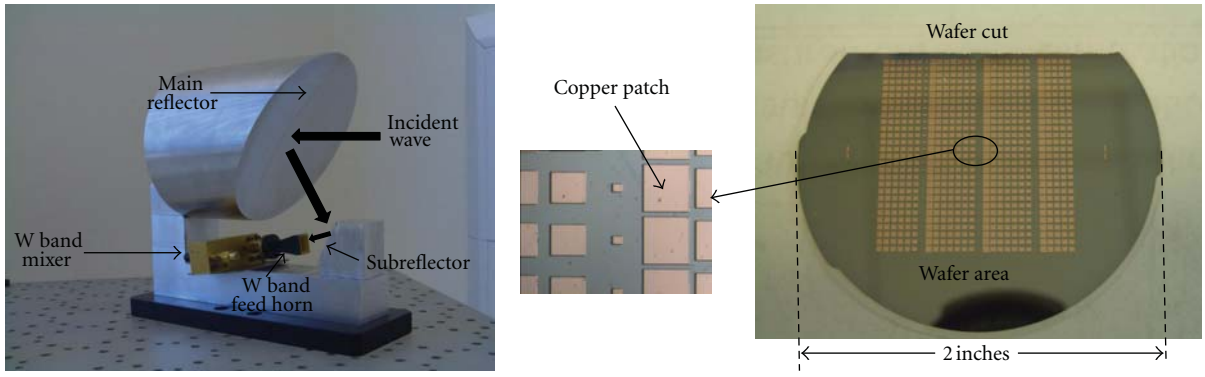

Figure 3: Dual reflector antenna at 94 GHz. (a) Photograph and (b) reflectarray subreflector. (From [21] © 2009 IEEE).

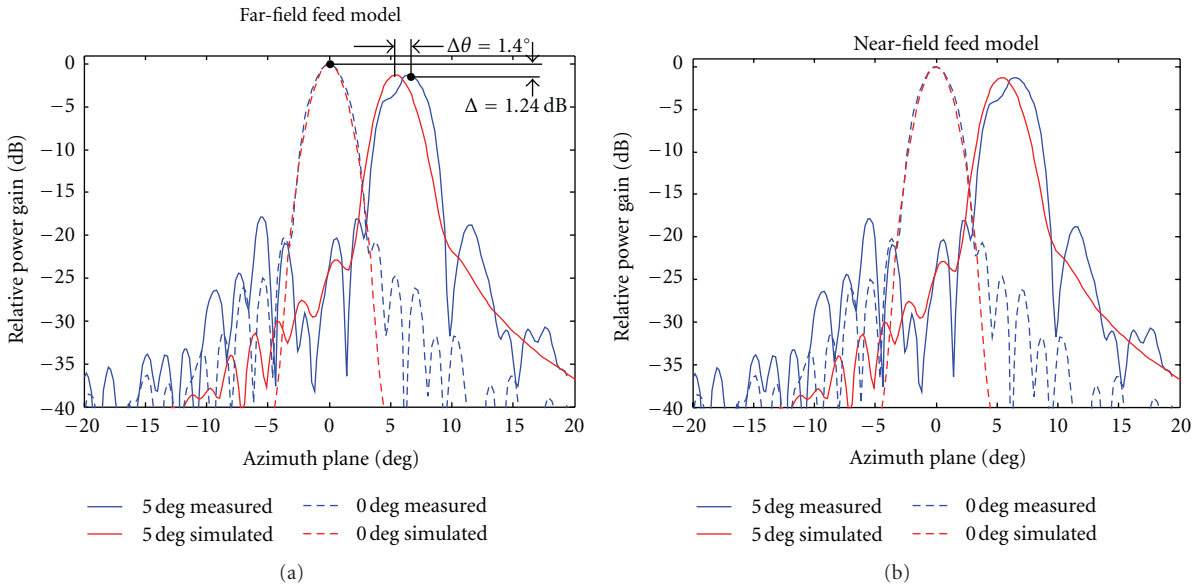

Figure 4: Measured and simulated radiation patterns of the dual reflector antenna with reflectarray subreflector in the azimuth plane at 94 GHz, using (a) far-field and (b) near-field models of the feed horn. (From [21] © 2009 IEEE).

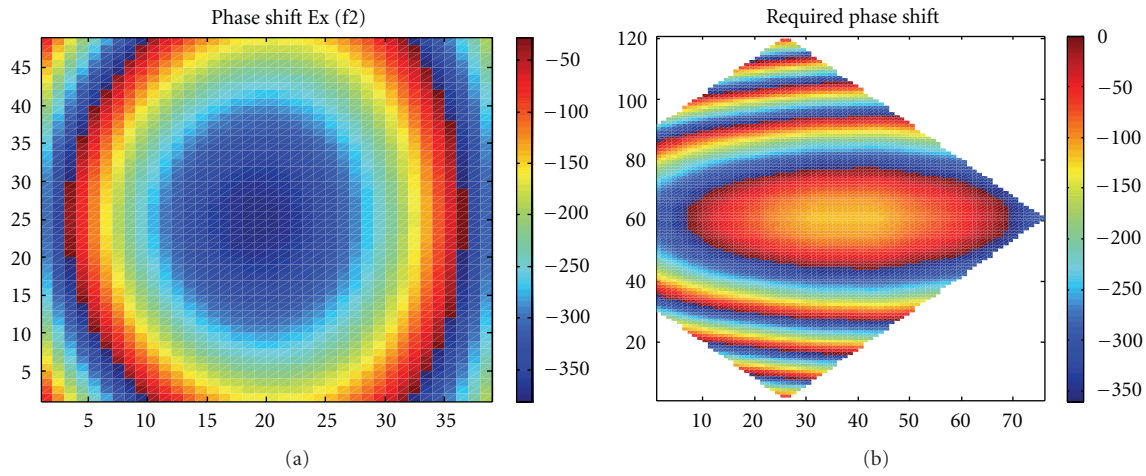

Figure 5: Phase distribution to be implemented on the subreflectarray (a) and on the main reflectarray at 12.75 GHz (b).

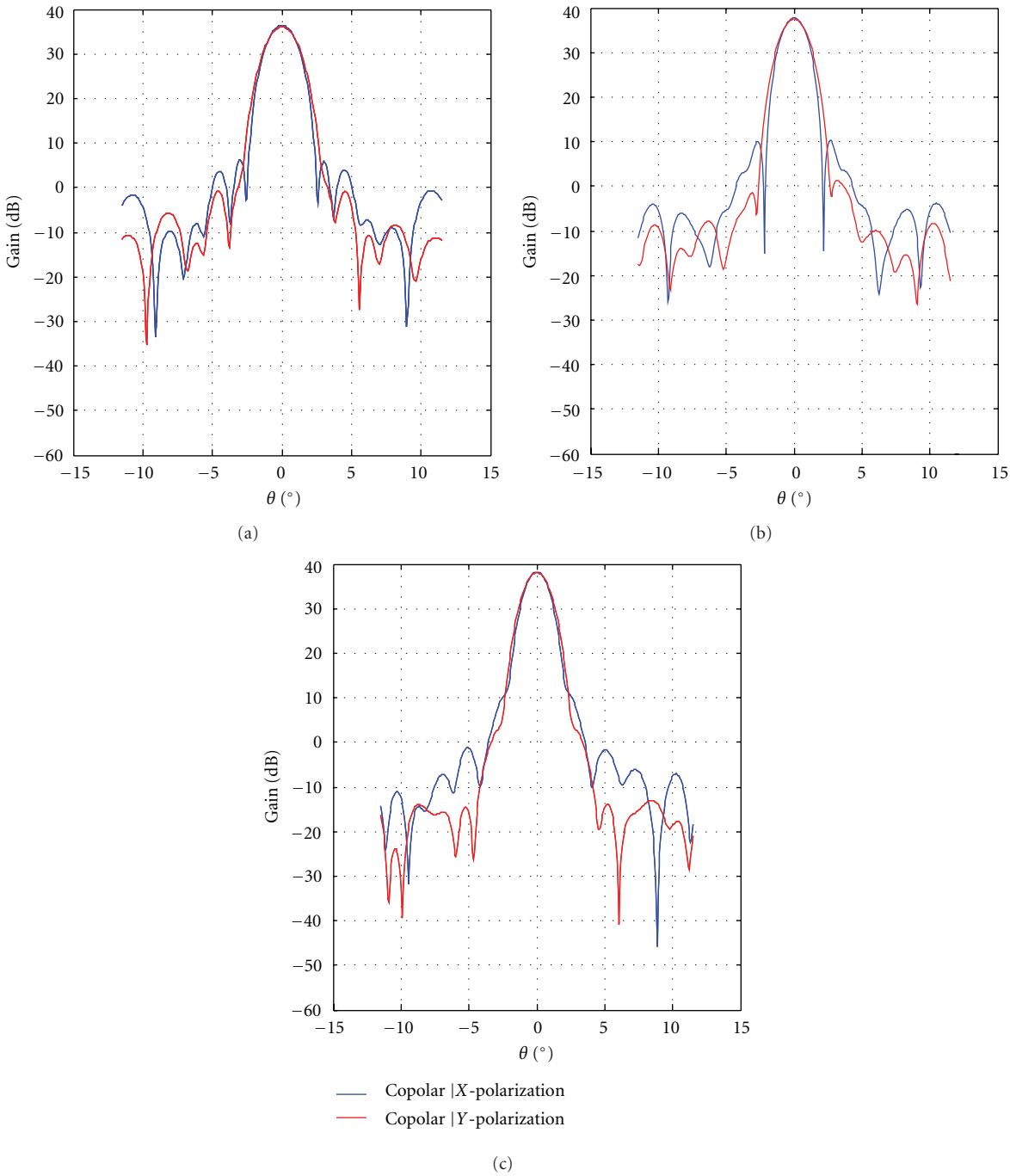

FIGURE 6: Azimuth cut of radiation pattern for X-polarisation at 10.7 GHz (a), 12.75 GHz (b), and 14.25 GHz (c) when using the required phase distribution on the main reflectarray.

3.1. Beam-Scanning Applications

3.1.1. Dual-Reflector Antenna with Reflectarray Subreflector. The dual-reflector antenna with a reflectarray subreflector has been proposed as a high-gain beam-scanning antenna by adding controllable phase shifter on the subreflectarray. Thus, the beam pointing can be controlled through a reduced number of controls. In [4], the beam scanning performance of an antenna made of a 1.5 m aperture parabolic reflector and a rectangular subreflectarray (520 mm × 494 mm) at 11.95 GHz was studied in an angular range of ±2° from the antenna boresight. In this example, the feed horn is modeled as a $\cos^q(\theta)$ function, with the q-factor chosen to provide an illumination taper on the subreflectarray around −18 dB, from the centre to the edges. The phase center of the horn is placed at coordinates $(-194, 0, 326)$ mm referring to the subreflectarray coordinate system (X_R, Y_R, Z_R), and the center of the subreflectarray is placed at coordinates $(294, 0, 1174)$ mm

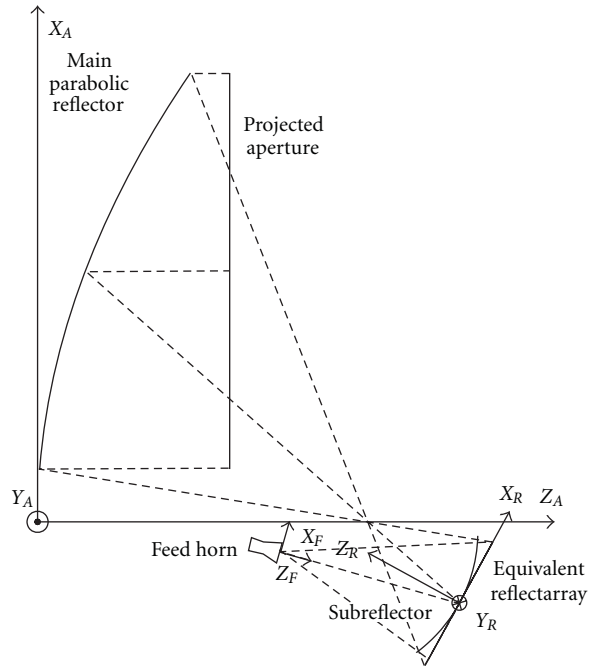

Figure 7: Scheme of the subreflectarray-parabolic reflector antenna.

in the antenna reference system (X_A, Y_A, Z_A). In this work, the scanning is achieved by introducing a progressive phase shift along the reflectarray subreflector. This approach permits to deflect the beam in one plane. For example, if a progressive phase is introduced along the Y_R-axis of the subreflectarray, the beam is scanned the azimuth plane $(Y_A Z_A)$. As a result, the control circuits are simplified, since the phase control should be the same for all the elements in a column or a row. The radiation patterns of this antenna for the X_A polarization (electric field in X_A direction) in the principal planes are shown in Figure 2, assuming an ideal progressive phase on the subreflectarray for beam scanning in azimuth. The gain has been computed for a beam scanning from -2° to $+2^\circ$, showing a reduction in gain less than 1 dB in all the cases. In the case of ideal phase shifters considered here, the cross-polarization for the overall antenna is slightly increased when the beam is defocused, being in the order of -30 dB below the copolar gain. If a larger beam-scanning angular range is required, the phase control at row or column level is not accurate enough and a synthesis technique must be applied to obtain the phase distribution required on the subreflectarray surface for each beam pointing. A simple synthesis technique for this application is discussed in [24] showing that the angular scanning range can be extended up to $\pm 7^\circ$, with the beam distorted for broader angles because of the spillover.

3.1.2. 94 GHz Dual-Reflector Antenna. The beam deflecting performance of this antenna configuration has been demonstrated in the 94 GHz band, as discussed in [21]. In this work, the dual-reflector antenna is designed, manufactured, and tested to show that it is possible to steer the beam up to $\pm 5^\circ$ from boresight by replacing a flat metal subreflector with a small reflectarray. The antenna demonstrator is made up of an offset parabolic reflector of diameter 120 mm (38λ) and a flat subreflector printed on a 50 mm diameter quartz wafer, see Figure 3. The beam scanning capability of the antenna is demonstrated by replacing a solid metal flat subreflector, which produces a focused beam in the boresight direction, by a passive 28×28 elements reflectarray printed on a 115 μm thick metal-backed quartz wafer. The reflectarray is made of a single layer of varying-size patches, see Figure 3(b), designed to produce a progressive phase distribution in the Y_R direction to deflect the beam 5° in the azimuth plane. The copolar far field radiation patterns of the antenna were measured between -20° and $+20^\circ$ in the azimuth plane at 94 GHz at Queen's University Belfast (QUB). Figure 4 shows the measured radiation pattern using the reflectarray subreflector to tilt the beam 5° and also the results using a flat metallic subreflector to produce a boresight-directed beam. The measured radiation patterns are compared in Figure 4 with the simulated patterns obtained through the technique described in the previous section, in two cases: (a) considering the ideal far-field model and (b) considering the near field of the primary feed horn, see [21]. These results show very good agreement with the measurements when the near-field model is used, which demonstrates the need to use the near field radiated by the feed for an accurate analysis of the antenna. The gain for the boresight beam computed by the analysis tool is 38.7 dBi, with the gain reduced in 1.26 dB for the deflected beam. The predicted reduction in gain is 0.86 dB due to the 5° beam deflection and 0.40 dB because of phase errors and losses in the reflectarray. Some distortion of the tilted beam and a deviation of 1.4° in the beam direction are found because the antenna design was carried by implementing a progressive phase distribution on the reflectarray assuming the far-field model of the feed. However the far-field model of the horn does not provide a realistic estimation of the incident field, neither in amplitude nor in phase, as shown in [21]. In order to reduce the distortion of the deflected beam, the reflectarray subreflector should be designed considering the near field of the feed horn [20].

3.1.3. Dual-Reflectarray Antenna for Bidirectional Satellite Link. A dual-reflectarray antenna can be used for beam-scanning application, [10]. This configuration is very convenient for transportable antennas since the two flat reflectarrays are ease to fold and deploy. In this case, the dual-reflectarray antenna is made up of a passive sub- and main reflectarrays. The main reflectarray can be also implemented with 1-bit electronic control for beam pointing. The antenna is defined to provide a directive beam in receive (10.70–12.75 GHz) and transmit (14.0–14.5 GHz) frequency bands with electronic scanning capabilities within a limited angular range when using 1-bit electronic control elements on the main reflectarray. As discussed in [10], the main reflectarray has pentagonal shape with dimensions of 1500 mm $\times$ 750 mm. This reflectarray comprises 5250 elements distributed in 75 rows and 120 columns. The elements

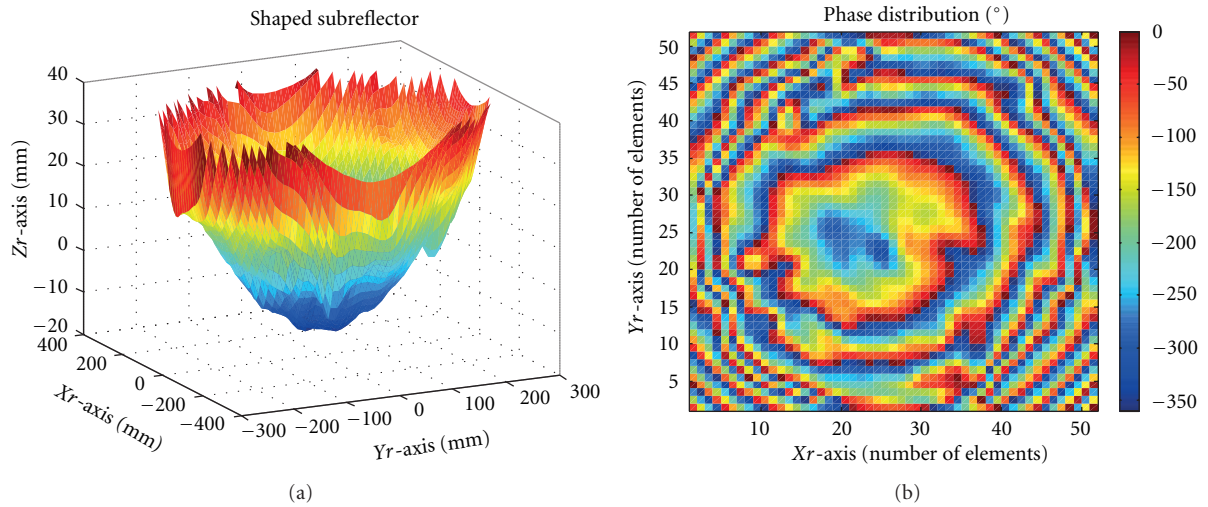

FIGURE 8: Shaped ellipsoid as subreflector (a) and phase distribution of the reflection coefficient for the equivalent reflectarray at 11.95 GHz (b).

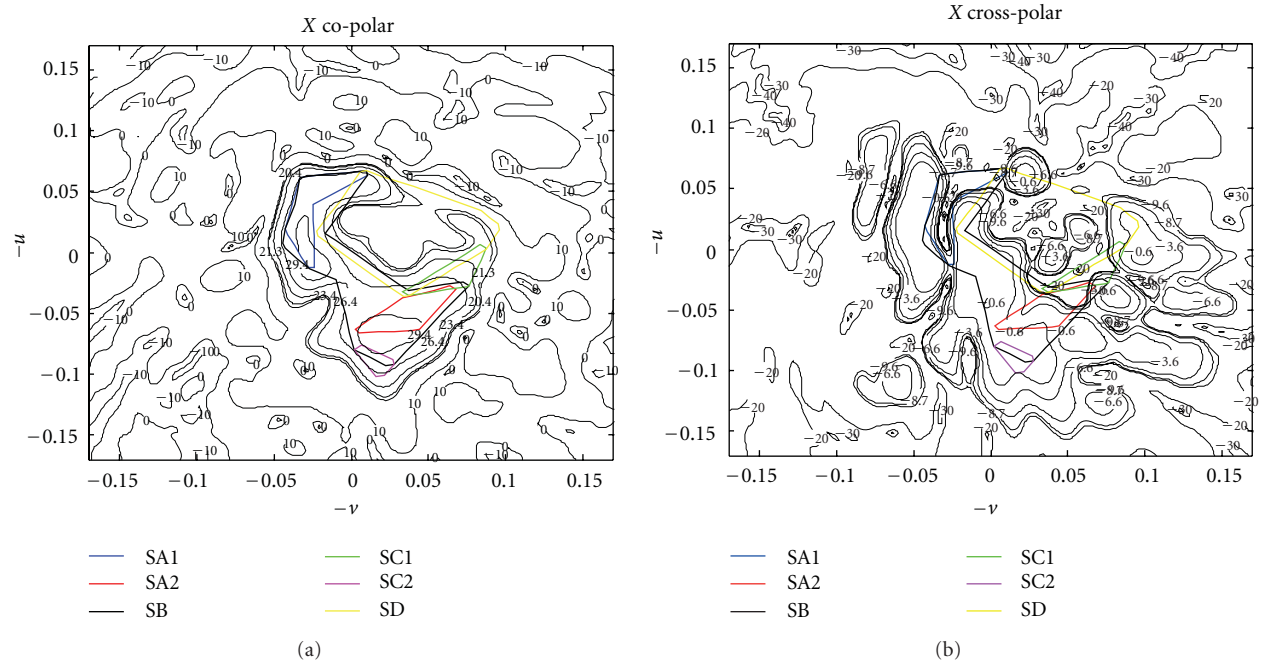

FIGURE 9: Copolar (a) and cross-polar (b) radiation patterns at 11.95 GHz (X_m-pol.) with the coverage template superimposed.

are arranged in a periodic lattice of 10 mm × 10 mm. The subreflectarray is tilted 27.69° with respect to the main reflectarray, with dimensions of 475 mm × 600 mm and placed with its centre at coordinates $(-473, 0.0, 690)$ mm referring to the main coordinate system. The subreflectarray is rectangular, with 38 × 48 elements in a periodic mesh of 12.5 mm × 12.5 mm periodicity. The phase centre of the feed horn is located at coordinates $(300, 0, 30)$ mm in the main reflectarray coordinate system. The subreflectarray has been designed to provide a very large equivalent focal distance in order to illuminate efficiently the main reflector. A simple model of the horn antenna based on $\cos^q(\theta)$ function is used. The q factor is defined at each frequency to provide an illumination level at the edge of the main reflector between −10 dB and −15 dB.

Figure 5(a) shows the phase distribution on the subreflectarray. Figure 5(b) shows the required phase shift for the main reflectarray to obtain a pencil beam pointing at 40° from the z-axis. The radiation patterns at 10.7 GHz, 12.75 GHz (Rx), and 14.25 GHz (Tx) are shown in Figure 6.

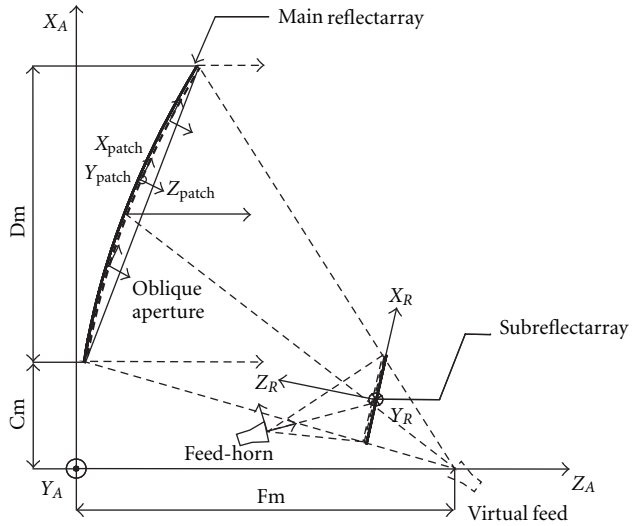

Figure 10: Scheme of a dual-reflectarray structure analysis.

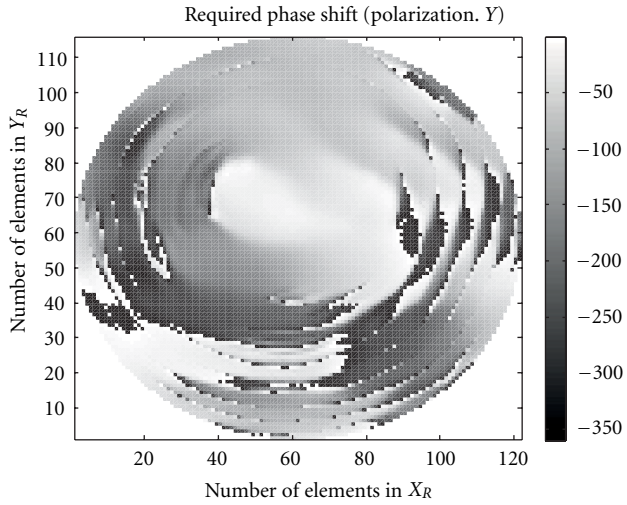

Figure 11: Required phase-shift for a 1.5 m parabolic reflectarray at 11.95 GHz, $F/D = 1.2$ [25].

3.2. Contoured-Beam Antenna for DBS Applications

3.2.1. Contoured-Beam Antenna with a Shaped Subreflectarray. A dual-reflector antenna based on a reflectarray subreflector and a main parabolic reflector has been proposed to obtain contoured beams for DBS applications [5]. The classic solution in this application consists on single or dual reflector antenna based on shaped reflectors. This solution is expensive and time consuming since the reflector surface shaping depends on the coverage footprint, and the manufacture requires specific moulds which are different for each mission. In the case of a dual-reflector antenna with a reflectarray sub-reflector, the beam shaping can be achieved by the phase-shift introduced on the reflectarray surface. In this work, the coverage specified for a South American mission on Amazonas satellite in Ku-band transmit band (11.95 GHz) is selected. The geometry of the antenna is derived from a dual-offset Gregorian optics with a main aperture of 1.5 m diameter, see Figure 7. In this antenna, the ellipsoidal subreflector (0.5 m diameter) is replaced by a reflectarray with the appropriate phasing. As shown in Figure 7, the equivalent subreflectarray is placed on the $X_R Y_R$ plane, being its centre placed at $(-308, 0, 1596)$ mm in the antenna coordinate system. The subreflectarray is made up of 51×51 elements arranged in regular mesh with period 11 mm $\times$ 11 mm. As in previous sections, the feed horn is modeled as a $\cos^q(\theta)$ function which provides an illumination taper at edges of -22 dB in order to reduce the spillover.

In order to synthesize the subreflectarray phases, the shape of a subreflector that fulfils the coverage requirements is achieved and used as the starting point in the process to obtain the phase distribution of the reflection coefficient of the equivalent reflectarray, see Figure 8(a). The phase distribution shown in Figure 8(b) is the same for the two linear polarizations of the antenna, since it has been derived from the distances from the shaped ellipsoid to the equivalent reflectarray plane. The radiation pattern for X_A polarization of the antenna is plotted in Figure 9, being the results similar for the orthogonal polarization. Co- and cross-polar components have been calculated considering the elements of the reflectarray as ideal phase shifters and no losses (ideal reflectarray elements), see Figures 9(a) and 9(b). The shape of the footprint obtained shows some distortion. However, the performance is near to the coverage required mask; see Figure 9(a). This phase distribution can be a suitable starting point for a further optimization process.

3.2.2. Parabolic Reflectarray in Dual-Reflector Configuration. The South American coverage antenna shown in the previous section can also be implemented with a dual-reflectarray antenna using a main parabolic reflectarray and a flat subreflectarray. The contoured beam was previously synthesized in a single offset parabolic reflectarray as discussed in [25]. The general scheme of this antenna is shown in Figure 10.

The antenna projected aperture has a diameter of 1.5 m, resulting an elliptic parabolic reflectarray of axes 1551 mm $\times$ 1500 mm. The clearance of the antenna is 200 mm and the focal distance is 1800 mm. The subreflector is a flat reflectarray with axes 598 mm $\times$ 559 mm. In principle, the antenna optics is defined to compact the overall volume. In this case, the subreflectarray behaves as a metal plane introducing a constant phase distribution, equivalent to a flat metal plate, in order to be able to compare the results with those previously reported for a single offset parabolic reflectarray [25]. Although the degree of freedom in the phase distribution on the subreflectarray can be used to reduce the cross-polarization of the antenna. The phase distribution on the main reflectarray surface required to obtain the South American coverage is shown in Figure 11. To implement this phase distribution, a unit cell with two stacked rectangular patches has been used as a reflectarray element. The patches are arranged in a periodic lattice of 13 mm$\times$13 mm and they are assumed to be printed on a 125-micron Kapton film bonded to a quartz-fabric composite

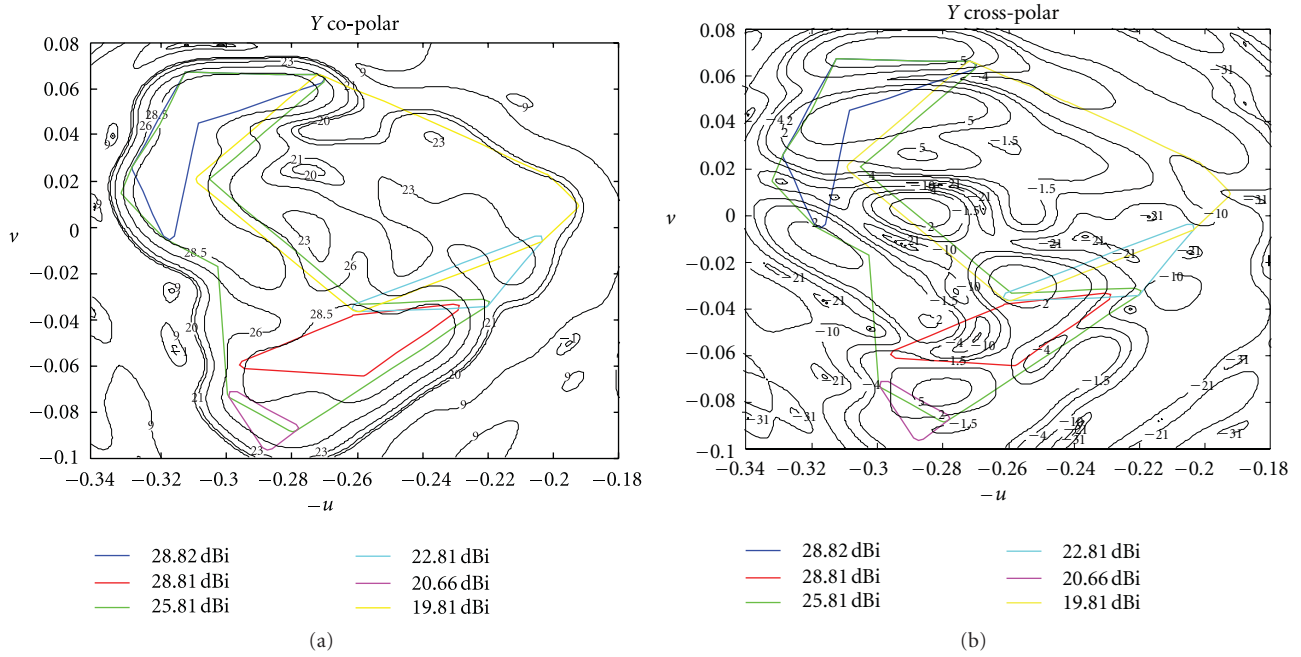

Figure 12: Radiation patterns obtained by MoM for a two-layer reflectarray in Tx band, 11.95 GHz. (a) Copolar component. (b) Crosspolar component.

layer and separated by quartz-honeycomb separators with 3.5 mm thickness.

The radiation pattern was computed at three frequencies: 11.7, 11.95, and 12.2 GHz, corresponding to the central and extreme frequencies of the transmit band (TX). Accurate predictions of both copolar and cross-polar radiation patterns at central frequency are provided in Figure 12, showing that the contoured patterns are close to the requirements, which are also shown in the figures as coloured polygons. Similar results were obtained for the extreme frequencies of the band. Two small holes at the border of the 28.81 dBi contour are found as a result of ohmic losses and phase errors produced by the approximate design technique, in which the pattern synthesis is applied on the planar aperture and the required phase distribution is obtained by geometrical optics. The contoured patterns can be improved by a suitable pattern synthesis taking into account the curved surface.

The analysis technique provides an accurate prediction of the cross-polarization pattern performance, since it takes into account the cross-polarization produced by the printed patches and by the offset reflector. The cross-polarization shown in Figure 8(b) can be reduced by synthesizing a proper phase distribution on the subreflectarray surface.

4. Conclusions

A review of recent work on dual-reflector antennas involving reflectarrays has been presented, considering a flat reflectarray subreflector and parabolic reflector, flat reflectarray, or parabolic reflectarray as main reflectors. A modular technique for the analysis of dual-offset antennas involving one or two reflectarrays has been described. The technique has been applied to analyze several antenna configurations for beam scanning and contoured beam for DBS applications.

Three examples of beam scanning dual-reflector antennas involving reflectarrays have been presented. First, a high-gain beam-scanning antenna based on a flat subreflectarray and a main parabolic reflector has been studied. The beam scanning can be realized by adding controllable phase shifters on the subreflectarray. The beam scanning performance of an antenna in a reduced angular range of $\pm 2^\circ$ has been presented. Second, a dual-offset antenna with a reflectarray sub-reflector working at 94 GHz has been designed to provide electronic beam scanning in a limited angular range ($\pm 5^\circ$). This antenna has been manufactured and tested, demonstrating the capability of this configuration for beam scanning in submillimeter-wave frequencies. The results show that a near-field model of the feed horn is necessary for an accurate analysis and design of the antenna. Third, a dual-reflectarray antenna with electronic beam steering has been presented for portable systems to provide Ku-band satellite links with automatic pointing capabilities. The antenna configuration comprises a passive subreflectarray and a main reflectarray with 1-bit electronic control to provide a pencil beam steerable in a $\pm 5^\circ$ angular range.

Dual-reflector antennas with one or two reflectarrays have also been proposed for contoured-beam applications. Two antennas providing South American coverage have been presented. A first solution consists of a dual-reflector dual-offset antenna with a 56 cm subreflectarray and a 1.5 m main parabolic reflector. In this case the coverage is achieved by synthesizing the phase distribution on the subreflectarray surface. The same coverage is also obtained by a dual-reflectarray antenna with 1.5 m parabolic reflectarray. In

this antenna the beam shaping is achieved by the main reflectarray, while sub reflectarray can be used to reduce the cross-polar radiation of the entire antenna.

All the configurations and applications presented in the paper show the versatility that a dual-offset antenna involving reflectarrays may offer, as beam scanning, beam shaping, or reduction of cross-polarization.

Acknowledgments

This work has been supported in part by the "Ministerio de Ciencia e Innovación" (Spanish Government) under projects CONSOLIDER-INGENIO CSD2008-00068 (TERASENSE) and TEC2010-17567 and also by the European Space Agency (ESA).

References

[1] B. Khayatian, Y. Rahmat-Samii, and J. Huang, "Radiation characteristics of reflectarray antennas: methodology and applicatios to dual configurations," in *Proceedings of the European Conference on Antennas and Propagation (EuCAP '06)*, Nice, France, November 2006.

[2] S. Xu, H. Rajagopalan, Y. Rahmat-Samii, and W. A. Imbriale, "A novel reflector surface distortion compensating technique using a sub-reflectarray," in *Proceedings of the IEEE Antennas and Propagation Society International Symposium (AP-S '07)*, pp. 5315–5318, Honolulu, Hawaii, USA, June 2007.

[3] S. Xu, Y. Rahmat-Samii, and W. A. Imbriale, "Subreflectarrays for reflector surface distortion compensation," *IEEE Transactions on Antennas and Propagation*, vol. 57, no. 2, pp. 364–372, 2009.

[4] M. Arrebola, L. de Haro, and J. A. Encinar, "Analysis of dual-reflector antennas with a reflectarray as subreflector," *IEEE Antennas and Propagation Magazine*, vol. 50, no. 6, pp. 39–51, 2008.

[5] M. Arrebola, L. De Haro, J. A. Encinar, and L. F. De La Fuente, "Contoured-beam Gregorian antenna with a reflectarray as subreflector," in *Proceedings of the 2nd European Conference on Antennas and Propagation (EuCAP '07)*, Edinburgh, UK, November 2007.

[6] W. Huang and J. R. Lesh, "Reflectarray elements on subreflector for fine beam pointing," JPL New Technology Report 41562, 2004.

[7] W. Menzel and D. Kessler, "A folded reflectarray antenna for 2D scanning," in *German Microwave Conference*, pp. 1–14, March 2009.

[8] C. Tienda, M. Arrebola, J. A. Encinar, and G. Toso, "Analysis of a dual-reflect array antenna," in *Proceedings of the IET on Microwaves, Antennas & Propagation*, vol. 5, no. 13, pp. 1636–1645, October 2011.

[9] R. Leberer and W. Menzel, "A dual planar reflectarray with synthesized phase and amplitude distribution," *IEEE Transactions on Antennas and Propagation*, vol. 53, no. 11, pp. 3534–3539, 2005.

[10] C. Tienda, J. A. Encinar, S. Montori, R. Vincenti Gatti, M. Arrebola, and R. Sorrentino, "Dual-reflectarray antenna for bidirectional satellite links in Ku-band," in *Proceedings of the 5th European Conference on Antennas and Propagation (EUCAP '11)*, pp. 1404–1407, Rome, Italy, April 2011.

[11] Y. Álvarez, F. Las-Heras, and M. R. Pino, "Reconstruction of equivalent currents distribution over arbitrary three-dimensional surfaces based on integral equation algorithms," *IEEE Transactions on Antennas and Propagation*, vol. 55, no. 12, pp. 3460–3468, 2007.

[12] R. J. Martin and D. H. Martin, "Quasi-optical antennas for radiometric remote-sensing," *Electronics and Communication Engineering Journal*, vol. 8, no. 1, pp. 37–48, 1996.

[13] A. Möessinger, R. Marin, S. Mueller, J. Freese, and R. Jakoby, "Electronically reconfigurable reflectarrays with nematic liquid crystals," *Electronics Letters*, vol. 42, no. 16, pp. 899–900, 2006.

[14] W. Hu, M. Y. Ismail, R. Cahill et al., "Liquid-crystal-based reflectarray antenna with electronically switchable monopulse patterns," *Electronics Letters*, vol. 43, no. 14, pp. 899–900, 2007.

[15] A. Moessinger, R. Marin, D. Eicher, R. Jakoby, and H. Schlaak, "Liquid crystal reflectarray with electronic 2D-reconfiguration capability," in *Proceedings of the 29th ESA Antenna Workshop on Multiple Beams and Reconfigurable Antennas*, pp. 67–70, April 2007.

[16] L. Marcaccioli, B. Mencagli, R. Vincenti Gatti et al., "Beam steering MEMS mm-wave reflectarrays," in *MEMSWAVE International Symposium*, Orvieto, Italy, June 2006.

[17] H. Rajagopalan, Y. Rahmat-Samii, and W. A. Imbriale, "RF MEMS actuated reconfigurable reflectarray patch-slot element," *IEEE Transactions on Antennas and Propagation*, vol. 56, no. 12, pp. 3689–3699, 2008.

[18] S. V. Hum, M. Okoniewski, and R. J. Davies, "Realizing an electronically tunable reflectarray using varactor diode-tuned elements," *IEEE Microwave and Wireless Components Letters*, vol. 15, no. 6, pp. 422–424, 2005.

[19] M. Arrebola, J. A. Encinar, and M. Barba, "Multifed printed reflectarray with three simultaneous shaped beams for LMDS central station antenna," *IEEE Transactions on Antennas and Propagation*, vol. 56, no. 6, pp. 1518–1527, 2008.

[20] M. Arrebola, Y. Álvarez, J. A. Encinar, and F. Las-Heras, "Accurate analysis of printed reflectarrays considering the near field of the primary feed," *IET Microwaves, Antennas and Propagation*, vol. 3, no. 2, pp. 187–194, 2009.

[21] W. Hu, M. Arrebola, R. Cahill et al., "94 GHz dual-reflector antenna with reflectarray subreflector," *IEEE Transactions on Antennas and Propagation*, vol. 57, no. 10, part 2, pp. 3043–3050, 2009.

[22] C. Wan and J. A. Encinar, "Efficient computation of generalized scattering matrix for analyzing multilayered periodic structures," *IEEE Transactions on Antennas and Propagation*, vol. 43, no. 11, pp. 1233–1242, 1995.

[23] J. A. Encinar, "Design of two-layer printed reflectarrays using patches of variable size," *IEEE Transactions on Antennas and Propagation*, vol. 49, no. 10, pp. 1403–1410, 2001.

[24] M. Arrebola, E. Carrasco, and J. A. Encinar, "Beam scanning antenna using a reflectarray as sub-reflector," *ACES Journal*, vol. 26, no. 6, 2011.

[25] J. A. Encinar, M. Arrebola, and G. Toso, "A parabolic reflectarray for a bandwidth improved contoured beam coverage," in *Proceedings of the 2nd European Conference on Antennas and Propagation (EuCAP '07)*, EICC, November 2007.

Hindawi Publishing Corporation
International Journal of Antennas and Propagation
Volume 2012, Article ID 124348, 5 pages
doi:10.1155/2012/124348

Research Article

Implementation of an Innovative Method to Design Reflectarray Antennas

Abdelhamid Tayebi, Josefa Gómez, Iván González, and Felipe Cátedra

Electromagnetic Computing Group, Computer Science Department, University of Alcalá, Escuela Politécnica, Alcalá de Henares, 28871 Madrid, Spain

Correspondence should be addressed to Abdelhamid Tayebi, hamid.tayebi@uah.es

Received 2 March 2012; Revised 16 May 2012; Accepted 5 June 2012

Academic Editor: Sandra Costanzo

A novel computed aided technique for designing reflectarray antennas is presented. The developed approach automatically generates the geometrical model of reflectarray antennas taking into account some input parameters, such as, the unit cell type and dimensions, frequency, focal length, periodicity, dielectric materials, and desired main beam radiating direction. The characteristics of the reflecting elements are selected considering the spatial phase delay at each unit cell to achieve a progressive phase shift. The implemented procedure also provides the phase characteristic of the unit element, which is rapidly computed by using a parallelized Moment Method (MoM) approach. The MoM is also used to obtain the radiation pattern of the full reflectarray antenna. In order to evaluate the new technique, a dual-interface prototype has been designed and simulated showing high-performance capability.

1. Introduction

Reflectarray antennas [1] have become an attractive alternative to the traditional parabolic reflector antennas due to some advantages, such as, light weight, mechanical robustness, compatibility with active devices, simple manufacturing, low profile, and low cost. Moreover, reflectarray antennas offer the possibility of beam steering, like conventional phased arrays, but eliminate the complexity and losses of the feeding network, showing a higher efficiency. Their main limitation is the narrow-band behavior, which is inherent to the printed antenna structures. To overcome this shortcoming, some proposals based on multilayer configurations [2, 3] and concentric rings [4, 5] have been reported lately. For instance, the design reported in [2] is composed of microstrip stacked patches and shows good performance in dual frequency operation. The reflectarray presented in [3] consists of three stacked layers with rectangular patches and provides dual-polarization operation for space applications. Although the bandwidth is notably increased when using multilayer printed patches, other issues may arise, such as, the manufacturing complexity and higher weight and losses. On the other hand, reflectarrays based on concentric rings are also becoming very popular due to they provide excellent results using one-layer configurations. The schemes proposed in [4] achieve a significant improvement in gain-bandwidth using double square and double cross loop elements. A comparable elementary cell that contains double square and double circular rings is studied in [5], where the phasing characteristic of the single-layer cell is computed showing good results.

Reflectarray antennas are composed of one or more layers of metallic elements and dielectric substrates over a ground plane. They are typically fed by a horn antenna and their operation consists of converting a spherical wavefront into a desired scattered wavefront using a phase shift mechanism. Although it has been demonstrated that reflectarray antennas can be used to generate contoured beams [6], most of them are still designed to radiate a collimate wave front at a certain frequency. To achieve this, according to Figure 1, each

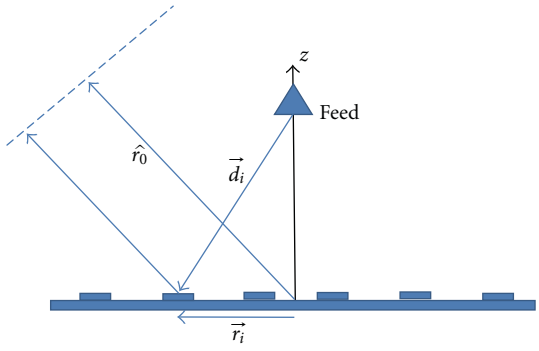

Figure 1: Diagram of the reflectarray antenna.

periodic cell must introduce a phase shift that is obtained as follows:

$$\phi_i = k_0\left(d_i - \vec{r}_i \cdot \hat{r}_0\right) + 2\pi N; \quad N = 0, 1, 2, \ldots, \qquad (1)$$

where k_0 is the propagation constant in vacuum, $\hat{r}_0$ is the unit vector in the desired direction of the main beam, $\vec{r}_i$ is the position vector from the center of the reflectarray plane to the ith radiating element, and d_i is the distance from the feed to the ith element.

Hence, the resonant size, periodicity, orientation, and substrate's properties of every cell must be properly selected to provide the phase shift given by (1).

Due to the radiating elements must reflect the incident electromagnetic field with a progressive phase distribution, the most challenging aspect when designing reflectarray antennas is to find the adequate phase shift to compensate the phase delay caused by the distance from the feed to each unit cell. Thus, the requirement of having a wide database that associates the properties of the cells and their correspondent phase shifts is crucial. In fact, many works proposing different techniques to achieve a wide phase range of the reflection coefficient have been recently published. In the literature, mainly four mechanisms can be found. The first one is the easiest to manufacture and more used [7, 8]. It achieves the phase variation by changing the size of the internal geometry of the unit cells. The second type tries to find the proper phase shift by adjusting the rotation angle of the elements [9]. The third method to provide the progressive phase shift of the reflected wave consists of using variable stub length attached to the radiating elements [10]. Finally, the fourth mechanism consists in using multilayer configurations [2, 3]. The proposed method applies these four techniques, since it is able to find the suitable characteristics of each elementary cell.

Other important aspect is the adequate choice of the radiating element's shape, since the scatter of the incident field strongly depends on its geometry. Hence, an essential goal is to obtain the type of cell that provides a wide reflection coefficient phase range when varying its properties. In fact, it is well-known that a reduced phase range lower than 360° implies a decreasing in directivity. On the other hand, it has been demonstrated [11, 12] that the phase variation depending on any geometrical parameter should be as lineal as possible, providing a smooth slope. This implies that good results are provided only if the 360° range is achieved by varying the considered parameter extremely slowly. In practical situations, the consequences of abrupt variations in the phase are narrower bandwidths and a more complicated manufacturing of the radiation elements due to the minimum tolerances.

Normally, the reflection coefficient phase as a function of the patch size is calculated to determine whether the phase range is wide enough and the curve slope is smooth enough. Thus, a lot of effort is usually required to find a unit cell able to provide the mentioned phase characteristic. The traditional shapes of microstrip patches have been crosses, squares, rectangles, rings, and circles. In this paper, the double square ring has been chosen to prove the efficiency of the developed computer tool.

A new method to automatically design reflectarray antennas is proposed. The properties of the radiating elements, including their resonant dimensions and substrate's characteristics, are computed by means of an efficient process that compensates the phase shift introduced by each elementary cell. Although several works have been recently carried out to investigate the phase characteristics of the cell elements, most of them do not report the reflectarray design once the phase curve has been properly achieved. The contribution of this paper also relies on the final design of the reflectarray, besides implementing the new approach and obtaining the widely used phase curve of the elementary cell. The proposed approach has been included in the computer tool NEWFASANT [13] to validate its performance.

The paper is organized as follows. The procedure to obtain the geometrical model of the reflectarray is described in Section 2, the design of a reduced-scale prototype is stated in Section 3, and finally some conclusions are remarked in Section 4.

2. Design Process

The basic idea of the new technique is the automatic design of reflectarray antennas by varying the parameters of the unit cells. The variation may include the resonant size of the cells, their position, orientation, stub's length, periodicity, number of layers, dielectric materials, and so forth, so that the phase shift given by every element is compensated according to the phase of the reflection coefficient.

First, a database which stores the values of the modified parameters and its correspondent reflection coefficient phase is created at a given frequency and for a determined periodicity. It is important to highlight that the analysis can be conducted by varying one or more parameters. Each entry in the database that associates pairs of parameter values and reflection phases is obtained by analyzing the behavior of a quasi-infinite array of identical elements by applying a full wave method based on the MoM [14], so truncation effects due to the finite size of real reflectarrays are also considered. Despite the big computational effort required to obtain the whole database, it is affordable in time because the MoM code is parallelized. A normal incident plane wave

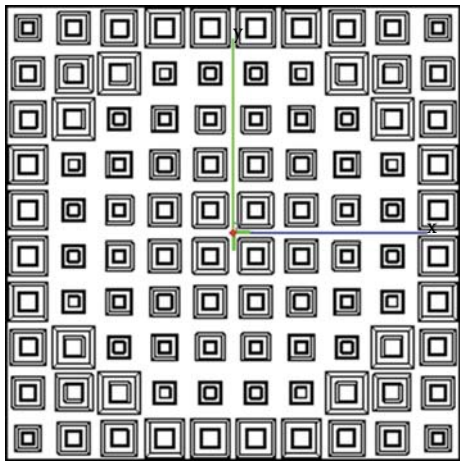

Figure 2: Top view of the reflectarray antenna.

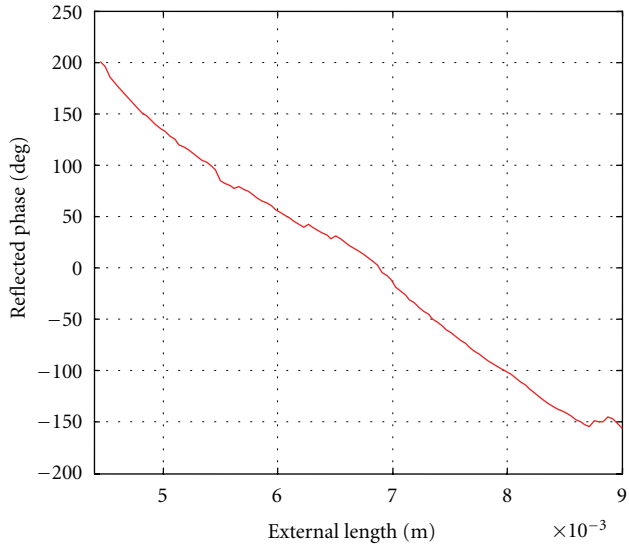

Figure 3: Phase characteristic of the unit cell varying the length of the external square ring.

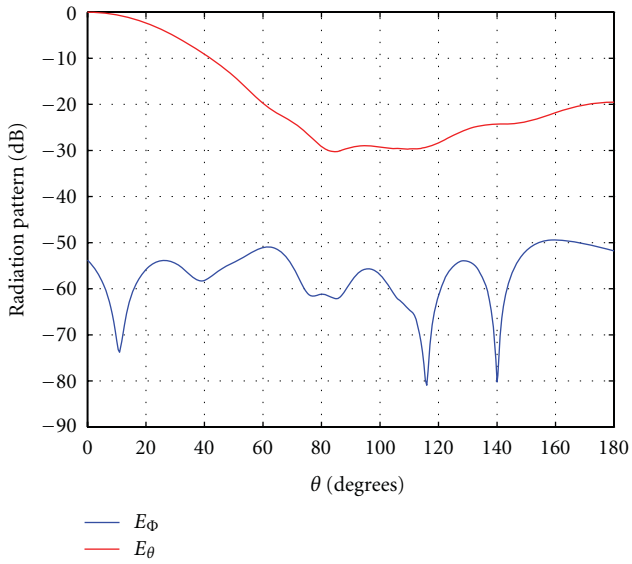

Figure 4: Radiation pattern of the feed antenna at 20 GHz.

is considered to compute the reflection coefficient phases. However, due to the fact that the radiation of the real feed antenna has an incidence direction with a certain angle, a further refinement can be done considering some incidence angles of the planar wave. In that case, the tool is able to provide as many databases as incidence angles are indicated.

Then, the phase delay caused by the path difference from the feed point is calculated taking into account the position of each unit cell. Once all phase delays are obtained, the system searches in the database the proper dimensions to compensate the required phase at every element. Hence, each cell can properly adjust their phase delay, introducing no errors and obtaining the maximum directivity. The phase shift needed in each cell when using several incident angles is obtained from one of those databases depending on its position and the feed location. The results provided considering several incident angles are slightly more accurate than only considering normal incidence. The next step consists in creating the geometrical model of the reflectarray, according to the values provided by the database. Finally, the ground plane is correctly located under the cells conforming to the dielectric thicknesses. By default, the reflectarray is created in the XY plane, but it is possible to fit it to curved surfaces. The user is also able to define the shape of the reflectarray, which can be rectangular, square, circular, or elliptical. When the reflectarray has been designed and we have the antenna geometry, the MoM is applied again to obtain a rigorous solution considering the full reflectarray antenna.

The flexibility when designing reflectarray antennas by using the presented tool is enormous, since many combinations of different shapes, dimensions, diverse substrates, incidences, and so forth can be used to design the radiating elements. In addition, the configuration of the unit cell is not constrained to a single layer. In fact, the tool provides a great versatility and allows defining various layers of metallic patches and interfaces of different substrates. Moreover, in order to facilitate the use of the implemented tool, several databases that contain correspondences between dimensions and reflection coefficient phases of many elementary cells (rectangular, circular and square patches, square and circular rings, metallic crosses, patches with holes, etc.) are available.

The module includes three techniques to model the feed antenna. The first one allows importing the radiation pattern of a real horn antenna. The second one allows importing the geometrical model of the feed antenna in several CAD formats, and the third one allows creating the physical model of the feed antenna.

3. Validation of the Implemented Tool

In order to validate the performance of the presented method, the specifications of an existing design recently published [15] have been considered. The reflectarray has

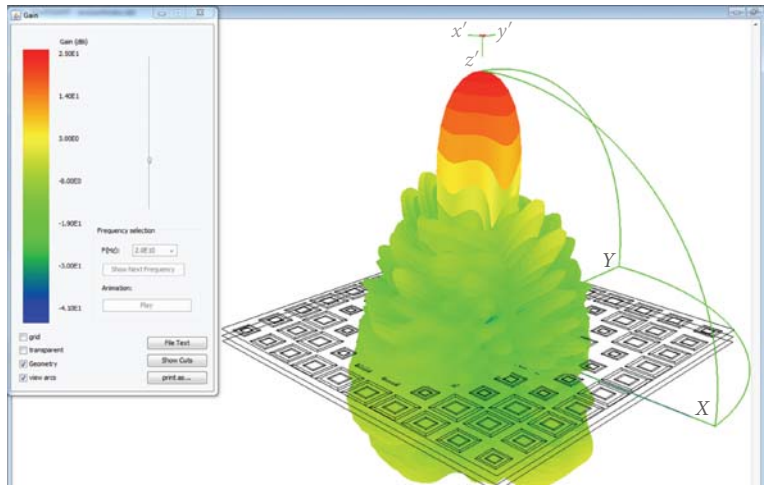

Figure 5: Radiation pattern in 3D at 20 GHz.

been redesigned using the propose procedure that adjusts the dimensions of the patches to focus or the main beam in the normal direction at 20 GHz. In our case, it is assumed that the antenna is composed of 100 identical unit cells symmetrically located in a square grid with periodicity of 9 mm. The top view is depicted in Figure 2.

Figure 3 shows the phase variation versus the length of the external square ring that has been automatically provided by our tool, [13]. The complete range of 360° is achieved by varying the length of the external square ring from 4.5 mm to 9 mm. It can be observed that the slope is practically lineal. These results have been achieved using a 2.95 mm substrate of foam under the metallic rings and a 0.85 mm layer of a material whose relative dielectric constant is 2.5 (same multilayer structure than in [15]). This thin layer is located on the cells, acting as a protective surface. On the other hand, the width of both rings and the gap between them have been fixed to 0.3 mm independently of the length variation.

As in [15], the reflectarray antenna is fed by means of a linearly polarized pyramidal horn located at $x = 0$, $y = 0$, $z = 0.0712$ m. The normalized radiation pattern of the fed antenna is depicted in Figure 4 at the central frequency of 20 GHz.

On the other hand, Figure 5 shows the 3D radiation pattern of the reflectarray antenna we have redesigned, where the main beam radiating in the normal direction is clearly depicted. Regarding the polarization purity, Figure 6 shows the cut $\varphi = 0°$ of the normalized radiation pattern at 20 GHz, where it can be observed that the cross-polar component is lower than −30 dB for every θ value. The second side lobes are also quite low, under −20 dB.

Finally, Figure 7 depicts the gain provided by the redesigned reflectarray. Note that the maximum value is 23.5 dBi, which is higher than the value of 20 dBi achieved in [15]. It is important to point out that the analysis of the final reflectarray has been conducted by using the MoM module of NEWFASANT, although it could have been used a different electromagnetic solver. Since reflectarray antennas are electrically very large structures, the multilevel fast multipole algorithm is used in the full wave analysis to reduce the required memory and time resources.

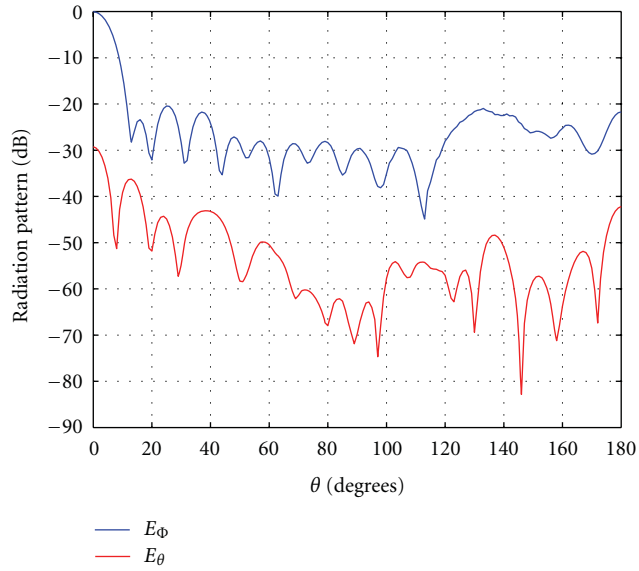

Figure 6: Normalized radiation pattern. Cut $\varphi = 0°$, frequency = 20 GHz.

4. Conclusion

A powerful tool to automatically design reflectarray antennas has been presented. The reported technique is able to generate the geometrical model of the antenna considering some input parameters, such as, the unit cell type, the operating frequency, the focal length, the periodicity, and the desired main beam radiating direction. The tool also computes and provides the phase curve of the unit cell. To evaluate the performance of the new method, a recently published reflectarray has been redesigned. Excellent results

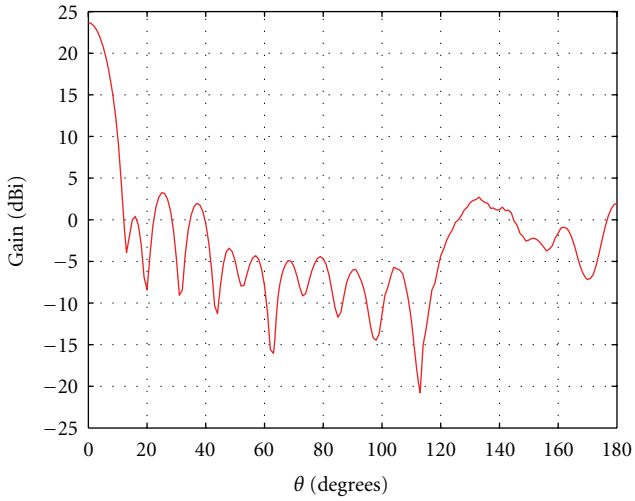

FIGURE 7: Gain. Cut $\varphi = 0°$, frequency = 20 GHz.

in terms of gain and polarization purity have been achieved. The developed tool can be very helpful for researchers.

Acknowledgments

This work has been supported, in part by the Comunidad de Madrid Project S-2009/TIC1485 and by the Castilla-La Mancha Project PPII10-0192-0083, by the Spanish Department of Science, Technology Projects TEC 2010-15706 and CONSOLIDER-INGENIO No CSD-2008-0068.

References

[1] D. Berry, R. Malech, and W. Kennedy, "The reflectarray antenna," *IEEE Transactions on Antennas and Propagation*, vol. 11, no. 6, pp. 645–651, 1963.

[2] J. A. Encinar, "Design of a dual frequency reflectarray using microstrip stacked patches of variable size," *Electronics Letters*, vol. 32, no. 12, pp. 1049–1050, 1996.

[3] G. Zhao and Y.-C. Jiao, "Broadband dual-polarization dual-coverage reflectarray antenna," in *Proceedings of the IEEE 4th International Symposium on Microwave, Antenna, Propagation, and EMC Technologies for Wireless Communications (MAPE '11)*, pp. 102–105, November 2011.

[4] M. R. Chaharmir, J. Shaker, M. Cuhaci, and A. Ittipiboon, "A broadband reflectarray antenna with double square rings as the cell elements," in *Proceedings of the European Conference on Antennas and Propagation (EuCAP '06)*, pp. 1–4, November 2006.

[5] M. E. Bialkowski and K. H. Sayidmarie, "Phasing characteristics of variable size double rings of square or circular shape for design of a single layer microstrip reflectarray," in *Proceedings of the 17th International Conference on Microwaves, Radar and Wireless Communications (MIKON '08)*, pp. 1–4, May 2008.

[6] J. A. Encinar, L. S. Datashvili, J. A. Zornoza et al., "Dual-polarization dual-coverage reflectarray for space applications," *IEEE Transactions on Antennas and Propagation*, vol. 54, no. 10, pp. 2828–2837, 2006.

[7] J. A. Encinar, "Analysis and design of dual frequency reflectarrays using microstrip stacked patches of variable size," in *Proceedings of the 26th European Microwave Conference*, vol. 1, pp. 221–224, September 1996.

[8] J. A. Encinar, "Design of two-layer printed reflectarrays using patches of variable size," *IEEE Transactions on Antennas and Propagation*, vol. 49, no. 10, pp. 1403–1410, 2001.

[9] M. E. Cooley, J. F. Walker, D. G. Gonzalez, Pollon, and G. E, "Novel reflectarray element with variable phase characteristics," *IEE Proceedings*, vol. 144, no. 2, pp. 149–151, 1997.

[10] R. D. Javor, X. D. Wu, and K. Chang, "Design and performance of a microstrip reflectarray antenna," *IEEE Transactions on Antennas and Propagation*, vol. 43, no. 9, pp. 932–939, 1995.

[11] M. E. Bialkowski and K. H. Sayidmarie, "Investigations into phase characteristics of a single-layer reflectarray employing patch or ring elements of variable size," *IEEE Transactions on Antennas and Propagation*, vol. 56, no. 11, pp. 3366–3372, 2008.

[12] P. Krachodnok and R. Wongsan, "Phase-bandwidth enhancement of microstrip patch reflectarray with cross slot loads," in *Proceedings of the Asia-Pacific Microwave Conference (APMC '07)*, pp. 1–4, December 2007.

[13] http://www.fasant.com/.

[14] F. Cátedra, C. Delgado, E. García, and I. González, "Combination of MLFMA and an iterative method to compute large scattering or radiation problems," in *Proceedings of the 4th European Conference on Antennas and Propagation (EuCAP '10)*, Barcelona, Spain, April 2010.

[15] B. Ma, L. Yan, M. Xia, C. Wang, and L. Cui, "Design of reflectarray antenna using double square ring elements," in *Proceedings of the 2nd IEEE International Conference on Microwave Technology and Computational Electromagnetics (ICMTCE '11)*, pp. 213–216, May 2011.

Hindawi Publishing Corporation
International Journal of Antennas and Propagation
Volume 2012, Article ID 139146, 8 pages
doi:10.1155/2012/139146

Research Article

Analysis of a Reflectarray by Using an Iterative Domain Decomposition Technique

Carlos Delgado, Josefa Gómez, Abdelhamid Tayebi, Iván González, and Felipe Cátedra

Computer Science Department, University of Alcalá, 28871 Madrid, Spain

Correspondence should be addressed to Carlos Delgado, carlos.delgado@uah.es

Received 3 March 2012; Revised 17 May 2012; Accepted 23 May 2012

Academic Editor: Manuel Arrebola

We present an efficient method for the analysis of different objects that may contain a complex feeding system and a reflector structure. The approach is based on a domain decomposition technique that divides the geometry into several parts to minimize the vast computational resources required when applying a full wave method. This technique is also parallelized by using the Message Passing Interface to minimize the memory and time requirements of the simulation. A reflectarray analysis serves as an example of the proposed approach.

1. Introduction

In the last years we have seen a rising interest in computer simulation tools in several engineering and science fields, due to technological breakthroughs and the development of novel efficient numerical algorithms. Many researchers are involved in the development of new methods focused on the acceleration and improvement of conventional electromagnetic field solvers. The logical consequence of this fact is a great increase in the demand for computer simulation tools.

Addressing Method-of-Moments- (MoM-) based electromagnetic solvers, we have seen a good number of efficient approaches in the last years. Many of these are related to the reduction of the computational requirements of the legacy MoM by only storing the coupling between basis and testing functions that are located in the near field region. There are very well-known methods, like the Multilevel Fast Multipole Algorithm (MLFMA) [1], that compute the matrix-vector products efficiently by aggregating a number of active currents to some specific points, translating them and disaggregating those multipoles in order to take into account the effect of the active basis functions over the testing functions. Other efficient techniques reduce the total number of unknowns by defining extended sets of macrobasis functions [2–6]. Fast matrix compression and low-rank approximation approaches can also be mentioned as efficient methods in terms of memory and CPU time requirements [7, 8]. In addition to the MLFMA there are a number of techniques that also take advantage of the fast evaluation of matrix-vector products in the iterative solution of large problems, among which we can mention the Complex Multipole Beam Approach (CMBA) [9], the Impedance Matrix Localization (IML) technique [10], the Adaptive Integral Method (AIM) [11], or the Multilevel Matrix Decomposition Algorithm (MLMDA) [12]. However, there are some cases for which the use of a full-wave method still poses a bottleneck, even considering these fast approaches, due to the size of the problem, slow convergence, or other issues. In these cases it is sometimes possible to resort to high-frequency methods [13] or hybrid combinations [14] if the nature of the geometrical properties of the problem and the excitation lie within the scope of such techniques. Unfortunately this is not usually the case when analyzing reflectarray antennas. Domain decomposition techniques (DD) allow to limit the maximum size of the system matrix to be solved [15] regardless of the size of the objects involved. It is necessary to include interactions between the domains in order to reach the final solution, which is usually done in an iterative or

recursive way [16–18]. There are some works worthwhile to be mentioned that study the convergence problems that may prevent reaching a stop situation [19, 20]. Some typical strategies to avoid this undesirable divergence rely on the definition of a relaxation factor [19, 21], make use of an extension of the original domains [17, 18, 21] and/or use preconditioners [17].

Due to the interest raised by the analysis of reflectarray antennas and similar geometries, a number of works reported in the last years deal specifically with this kind of problems. For instance, [22] presents an efficient technique based on the extension of an adaptive integral method that allows the full-wave analysis of electrically large multilayered printed arrays that have one or more planar metallizations and vertical conductors. The technique proposed in [23] computes the generalized scattering matrix of a dielectric interface with periodic metallizations, which is based on a spectral domain Moment Method, but assuming multiple incident Floquet-harmonics. A full-wave analysis using the finite integration technique is applied in [24], where the mutual coupling between the feeding horn and the elements of the reflectarray is considered. The analysis reported in [25] is based on an application of the Moment Method. In [26] the authors make use of a fast simulation tool based on MoM-MLFMA to analyze a three-layered reflectarray. The work reported in [27] combines MoM-MLFMA with the use of macrobasis functions to address large problems, including reflectarray antennas.

In this work we propose a combination of the MLFMA with a new domain decomposition technique that provides fast analysis of arbitrary structures in complex environments and contains a novel procedure for selecting the interactions between domains that will have a noticeable contribution to the final results. This new domain decomposition method has been validated and compared with the MoM-MLFMA approach. The simulation results of both approaches are compared with measurements of a reflectarray antenna that has been previously designed, fabricated, and measured [28] in the Research Advanced Antenna Technology Communications Research Centre, Canada.

The geometry of the bodies considered in this work is defined using parametric surfaces [29, 30], as well as the mesh required in order to apply the MoM-based approach. We obtain a continuous quadrangular mesh by using the mesher described in [31]. The use of parametric subpatches enables us to conform them to curved surfaces and maintain a high accuracy degree reducing at the same time the sampling rate (which in traditional approaches is considered to be around 10 samples per wavelength). It represents an advantage when compared with other approaches that use a faceted meshing, which loses the real shape of the original bodies. Once the geometry has been discretized, high-order modified rooftop and razor blade functions are used as basis and testing functions, respectively. In addition, the proposed approach also allows the analysis of structures embedded in dielectric slabs. In this case, volumetric rooftops and razor blade functions are defined over curved volumetric elements. For very thin dielectric slabs a surface representation is considered instead of the previously mentioned volumetric approach, and the MoM impedance matrix elements are corrected by a term that depends on the size of the subdomain, the frequency, the electric permittivity, and the thickness of the slab.

Regarding the convergence issues that can be derived from the application of domain decomposition methods, the approach proposed in this work relies on the definition of extensions for each domain. After computing the updated currents over the extended version we only retain those which are included in the original, nonextended domain. We reach a double goal with this strategy: the improvement of the convergence properties in the iterative process, and the correction of the artificial edge behavior of the current. Extension values of about 0.4 to 0.7 wavelengths typically yield good results. The negative side of this strategy is the extra CPU time required to solve the extended problem. However we have found that it only represents a small fraction of the total simulation time for the typical domain sizes considered.

The MPI is used for the parallelization of the approach. This paradigm provides communication functionalities between a set of processes. Therefore, it is possible to address this kind of problems using a multiprocessor computer or cluster, increasing the computational efficiency [32, 33].

The paper is organized as follows. The main features of the proposed approach are addressed in Section 2. Some remarks about the selection of active and passive domains are given in Section 3. Section 4 presents the results obtained when analyzing a specific reflectarray antenna, and Section 5 contains the conclusions derived from this work.

2. Background of the Technique

The domain decomposition approach combines the MoM and MLFMA together with an iterative process used to calculate the interactions between different domains, which will be described in the next section. The first step will be, therefore, a partitioning process of the geometry into several domains. Thus, the total current over the original geometry can be expressed as

$$\vec{J} = \sum_{d=1}^{N_d} \vec{J}_d, \tag{1}$$

where N_d denotes the number of domains. Subsequently, a full wave analysis is individually applied over each domain using the MoM and MLFMA, obtaining the *primary currents*, which are those obtained by considering each block isolated from the rest and the excitation vector given by the external field. Several small problems are solved instead of a very large one, which is the main advantage when compared to the analysis of the whole structure.

The artificial edges derived from the partitioning of the objects in terms of domains may affect noticeably the final results. The solution to this potential burden is to extend the area of each domain and compute the induced currents while considering the extended domain. Figure 1 illustrates this decomposition procedure and one example of an extended domain.

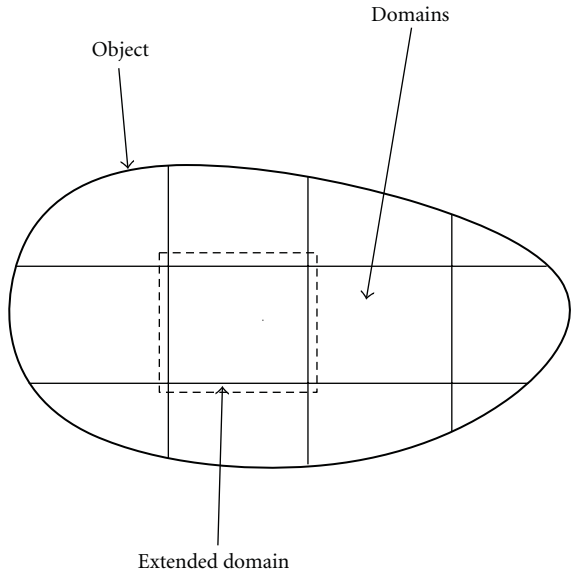

Figure 1: Scheme of the decomposition approach.

Once the currents have been calculated, those that are located inside the extension are discarded. By doing this we avoid the negative effect of the singular behavior of the currents near the artificially introduced edges. According to our experience an extension with a side length between 0.7 to 1.0 wavelengths is enough to obtain good accuracy.

After computing the primary currents an iterative process is performed to calculate the influence of the currents obtained inside one domain over the others. This stage of the process is required in order to update the primary currents calculated with the MoM. In order to compute the interactions between different parts of the geometry, a selective process is necessary to avoid unnecessary calculations. Let us denote as *active domains* the ones that contain previously computed currents which will radiate over other domains of the geometry (these ones called *passive domains*). It can be inferred that a given domain D can serve as active and passive domain at the same time, since the current distribution calculated over D in the kth iteration may produce interactions with other parts of the geometry in the $(k+1)$th iteration, while other active domains may contribute to update the current distribution on D as well. A ray-tracing approach determines which active domains contribute to the updating current process of a certain passive domain, and therefore only a few computations are required to obtain the final currents. Multiscale problems can take advantage of this methodology because only the resulting fields radiated by an active domain are required to feed the passive domain.

3. The Iterative Selection of Active and Passive Domains

In order to increase the efficiency of the approach, it is very important to discard interactions between active and passive domains when these interactions are negligible. This strategy reduces significantly the CPU time required. Moreover, realistic structures with complex small details can be efficiently analyzed because no geometrical approximation is considered. The immediate benefit of this method is a significant decrease in the required CPU time and memory storage resources.

The total current over a given domain (let us consider domain-i) can be seen as the superposition of the currents computed by a number of interactions between that domain and the rest of the domains contained in the geometry:

$$\vec{J}_i = \vec{J}_i^{\,0} + \sum_{j=1}^{M_i} \vec{J}_i^{\,j}, \tag{2}$$

where the term $\vec{J}_i^{\,0}$ represents the primary current computed over domain-i. The other terms of the expression indicate the currents due to the interaction between domain-i and the rest of the domains, where M_i stands for the highest order of the interactions with domain-i considered as the passive domain.

In order to compute the interactions between different domains, it is necessary to calculate the fields radiated by the previously computed currents on the rest of the domains over each passive domain, which can be iteratively performed. Thus, the impress field over domain-i due to the kth order effect can be written as

$$\vec{V}_i^{\,k} = \beth_i \left\{ \sum_{n=1, n\neq i}^{N_d} \vec{J}_n^{\,k-1} \right\}, \tag{3}$$

where the operator $\beth_i$ computes the field over domain-i due to the previously calculated currents over the rest of the geometry, which serve as active domains. The MLFMA approach is very well suited to obtain $\vec{V}_i^{\,k}$. Now it is possible to obtain the current over domain-i due to the kth order effect, $\vec{J}_i^{\,k}$, by solving the conventional MoM equation for the isolated domain. This current can be efficiently obtained by utilizing MLFMA with an iterative solver such as the Biconjugate Stabilized Gradient method (BiCGStab).

Expression (3) needs to be modified in order to select those pairs of active and passive domains that will entail a noticeable contribution to the final current, and discard the negligible interactions. In practical applications this procedure allows us to reduce the amount of primary memory and CPU time maintaining the same degree of accuracy. In order to take into account this consideration, the modified expression can be seen as follows:

$$\vec{V}_i^{\,k} = \beth_i \left\{ \sum_{n=1, n\neq i}^{N_d} \aleph_i\left(\vec{J}_n^{\,k-1}\right) \right\}, \tag{4}$$

where we have introduced the function $\aleph_i(\vec{J}_n^{\,k-1})$ that takes a zero value if the interaction between domain-i and domain-n is negligible and takes the value of $\vec{J}_n^{\,k-1}$ if such interaction entails a noticeable contribution to the current distribution over the passive domain. For the selection of the passive domains which interact with an active one it is important to consider the possibility of total or partial eclipse situations,

as well as the shape of the pattern radiated by the active currents. We utilize the following mechanisms to accomplish this task.

First, using the multipole aggregation of the current over the active domain we determine the main directions in which such domain radiates, discarding the passive domain if it is not located in the path of the main set of output directions. This set of directions is determined by setting a threshold over the strongest field value.

In addition to the previous procedure we also consider a ray-tracing algorithm, very successfully used in high-frequency methods, known as the Angular Z-Buffer (AZB) [34, 35]. With the AZB the space is divided into angular regions (anxels), and the surfaces of the geometry are classified depending on which anxels contain them. This information is stored in the AZB matrices in a preprocessing step. As an example, let us consider a domain of the problem called D_1. The AZB matrix associated to D_1 contains a number of cells which are assigned to different angular ranges, since one of the dimensions of such matrix makes reference to the theta position of the angular range and the other dimension indicates its phi position. For the generation of the AZB matrix, different ray tubes are shot over D_1 (depending on the nature of the external excitation) and the output directions are obtained. The output ray tubes are then checked for intersections with other domains. If some rays belonging to the same tube intersect with different domains, these are processed in order to analyze the possibility of eclipse effects. Only the nonhidden domains are included in the AZB matrix of D_1. Further information can be found in great detail in [36]. This technique is very well suited to be used in combination with the previous approach based on the multipole expansion of the currents over the active domain, because the former gives the initial tube rays to be considered for the search of passive domain candidates to interact with the active domain.

Thus, for a given direction (from the main output radiation directions of the active domain) the AZB yields the passive domains where there can be a strong coupling, discarding the negligible interactions. This can be extended to consider multiple effects between domains, as shown in Figure 2 where D_1, D_2, and D_3 are domains contained in the geometry.

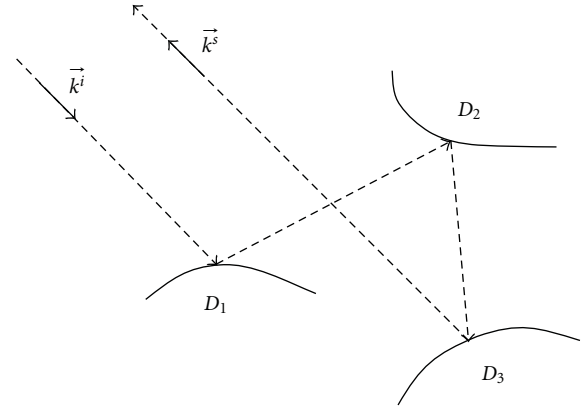

Figure 2: Example of ray tracing for multiple effects.

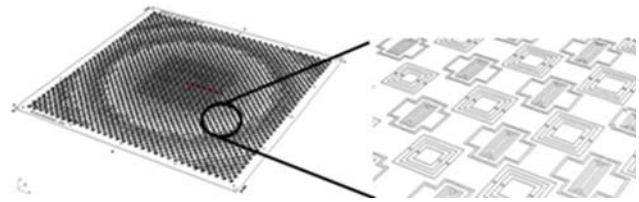

Figure 3: Schematic view of the original reflectarray.

4. Analysis of a Reflectarray

In this work we have modified and analyzed a reflectarray antenna for applications such as radar or long-distance communication. Some preliminary results of the numerical approach presented here can be seen in [37]. The design of the broadband reflectarray is presented in [28] and provides high radiation efficiency, approximately 60%. Regarding its construction, flat reflectors are often defined by several layers of periodical metallic patches and dielectric slabs over a ground plane [38]. Although microstrip reflectarray antennas are narrow in bandwidth, they are well suited for dual-frequency operation [39]. In addition to the original reflectarray considered here, there are other works in the literature presenting dual-band reflectarrays [40–43]. Currently, reflectarray antennas are widely used as an alternative to conventional reflector antennas due to several advantages such as reduced weight and volume, mechanical robustness, compatibility with active devices, low cost, and short manufacturing time.

Figure 3 shows the original reflectarray and the shape of the unit cells. The individual elements are designed to scatter the incident field while impressing the appropriate phase shifts in such a way as to form a plane wave front that propagates in a prescribed direction or, more generally, to create the required radiation pattern. The dimensions of the whole square structure are 40 cm $\times$ 40 cm, and the reflective surface is located over the XY plane.

The modifications we have introduced consist of a new compact feed system comprising an offset cassegrain structure where the horn is located under the plane of the reflectarray, for which it is necessary to open a hole on the reflectarray to feed the subreflector. This configuration can be seen in Figure 4. The feeding antenna is a pyramidal horn polarized along the X-axis. Figure 4 shows the location of the feed antenna over the reflectarray, and Figure 5 displays its far-field radiation pattern.

The aim of the modification provided in this work is the generation of a more compact layout for this antenna, while maintaining its original features up to a certain degree. The Cassegrain structure allows this goal, with good radiation properties as the final result.

The reflectarray is composed of a dielectric layer over a metallic ground plane, and the metallic strips are located over the dielectric. The period of the reflective elements is defined as 12 $\times$ 12 mm. The substrate has a thickness of 3.175 mm and a permittivity of 2.17. The simulation

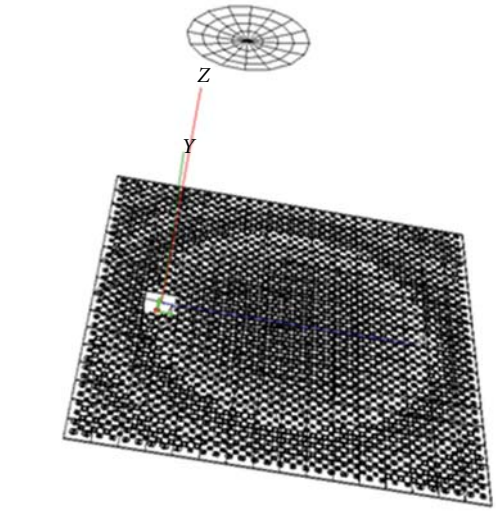

(a)

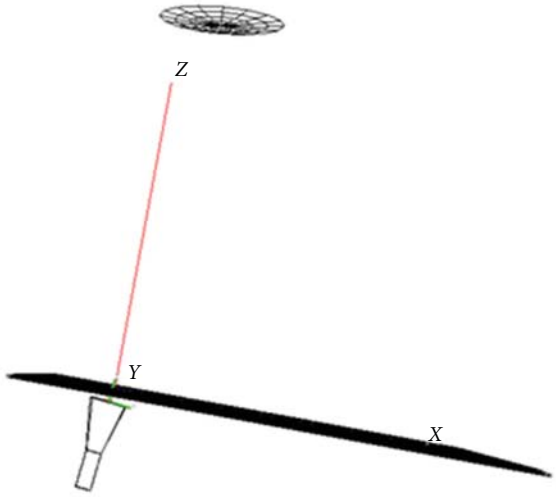

(b)

Figure 4: Geometrical views of the modified reflectarray.

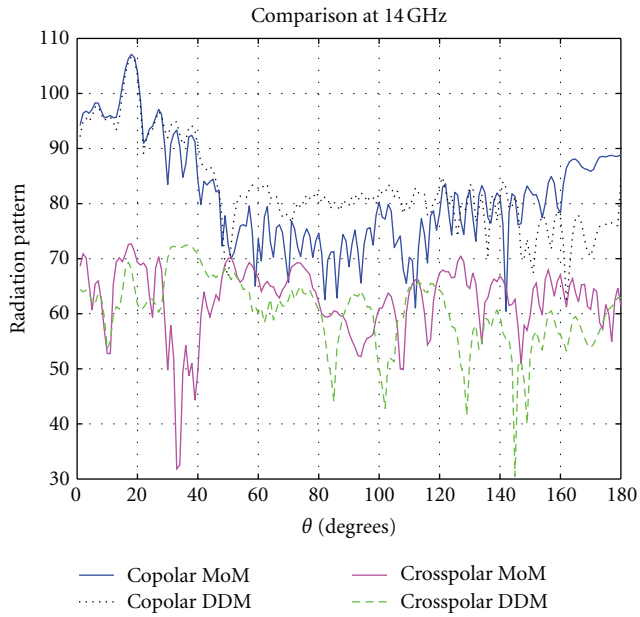

Figure 5: Comparison of radiation patterns applying the Moment Method and the domain decomposition approach at 14 GHz.

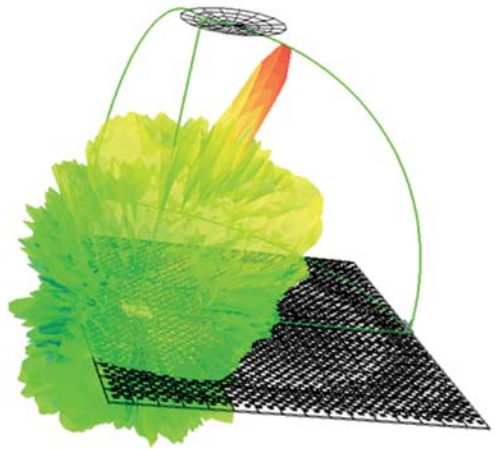

Figure 6: 3D pattern view.

has been performed considering a superficial thin layer approximation for the dielectric region.

The reflectarray was originally designed to radiate in the direction defined by $\theta = 16^\circ$ and $\varphi = 0^\circ$ at 14 GHz. The horn is located at $x = y = z = 0$ and feeds a subreflector whose center is $x = y = 0$, $z = 0.21$ and radius is 0.106 m. The focal length of the subreflector is 0.215 m, and the offset is -0.02 m. We have computed the radiation patter of the geometry using two different approaches, namely, the full wave technique given by the MoM-MLFMA and the domain decomposition approach described in this work. With the latter method we have considered 6 domains in the geometry: the first one comprises the horn, the second domain contains the subreflector, and the reflectarray is partitioned into 4 domains. The CPU-time required by the MoM is 4806 seconds, while the Domain decomposition approach took 987 seconds to obtain the results. The total number of unknowns when analyzing the reflectarray antenna at 14 GHz is 271636 unknowns. Around 27% of that amount (73720 unknowns) belongs to the dielectric part. However, the efficiency of the developed technique compared to the conventional full-wave analysis increases when the electrical size of the structure is even higher.

Figure 5 depicts the comparison between the radiation patterns obtained by these two approaches at 14 GHz. The direction of the main beam is now given by $\theta = 18^\circ$ and $\varphi = 0^\circ$ at both frequencies. A good agreement can be appreciated, with some discrepancies for the lower levels, due to the fact that, even considering the offset, there is still some blockage owing to the location of the horn and subreflector. A 3D view of the pattern obtained by the proposed approach can be seen in Figure 6, and the current distribution obtained

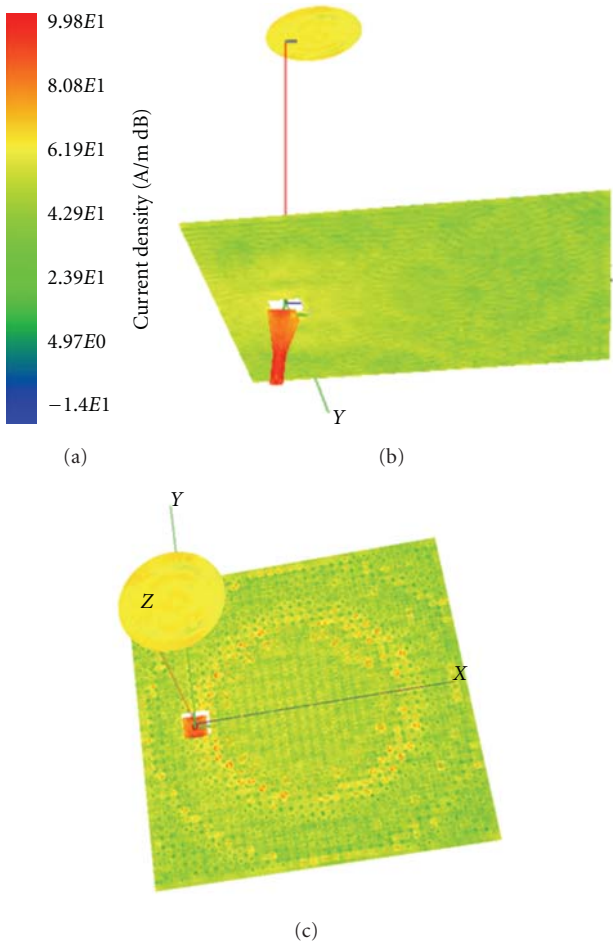

Figure 7: Current distribution.

is shown in Figure 7. In Figures 8 and 9 we compare the radiation pattern obtained with the modified configuration with the original configuration. It is possible to appreciate the differences due to the effect of the subreflector blockage and the hole required for the new horn placement, but the overall behaviour of this more compact configuration can be of interest for a number of practical applications.

5. Conclusion

An efficient approach based on the MoM-MLFMA combined with a domain decomposition scheme has been presented and validated comparing to the full-wave solution. This approach considerably reduces the memory and time requirements by solving several small problems instead of a single large one. The predictions given by both methods show a good agreement. The MPI paradigm was incorporated to increase the performance in the simulations.

Acknowledgments

This work has been supported in part by the Comunidad de Madrid Project S-2009/TIC1485, by the Castilla-La Mancha Project PPII10-0192-0083, by the Spanish Department of Science, Technology Projects TEC 2010-15706 and CONSOLIDER-INGENIO no. CSD-2008-0068, and by University of Alcalá Project UAH2011/EXP-014. The authors thank Dr. Reza Chaharmir for the original model and measurements of the reflectarray antenna reported in this paper.

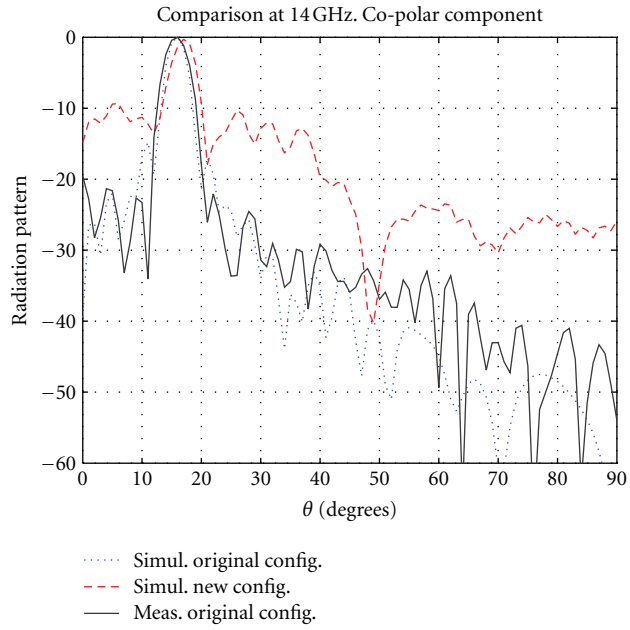

Figure 8: Radiation pattern of the original and modified configurations. Copolar component.

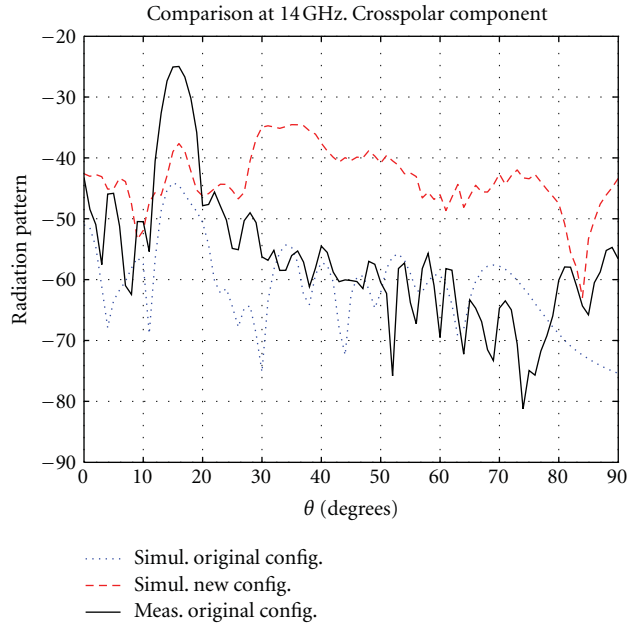

Figure 9: Radiation pattern of the original and modified configurations. Crosspolar component.

References

[1] W. C. Chew, J. Jin, E. Michielssen, and J. Song, *Fast and Efficient Algorithms in Computational Electromagnetics*, Arctech House, 2001.

[2] E. García, C. Delgado, I. G. Diego, and M. F. Cátedra, "An iterative solution for electrically large problems combining the characteristic basis function method and the multilevel fast multipole algorithm," *IEEE Transactions on Antennas and Propagation*, vol. 56, no. 8, pp. 2363–2371, 2008.

[3] C. Delgado, M. F. Cátedra, and R. Mittra, "Efficient multilevel approach for the generation of characteristic basis functions for large scatters," *IEEE Transactions on Antennas and Propagation*, vol. 56, no. 7, pp. 2134–2137, 2008.

[4] C. Delgado, M. F. Cátedra, and R. Mittra, "Application of the characteristic basis function method utilizing a class of basis and testing functions defined on NURBS patches," *IEEE Transactions on Antennas and Propagation*, vol. 56, no. 3, pp. 784–791, 2008.

[5] C. Craeye, "A fast impedance and pattern computation scheme for finite antenna arrays," *IEEE Transactions on Antennas and Propagation*, vol. 54, no. 10, pp. 3030–3034, 2006.

[6] L. Matekovits, V. A. Laza, and G. Vecchi, "Analysis of large complex structures with the synthetic-functions approach," *IEEE Transactions on Antennas and Propagation*, vol. 55, no. 9, pp. 2509–2521, 2007.

[7] K. Zhao, M. Vouvakis, and J.-F. Lee, "The adaptive cross approximation algorithm for accelerated method of moments computations of EMC problems," *IEEE Transactions on Electromagnetic Compatibility*, vol. 47, no. 4, pp. 763–773, 2005.

[8] A. Heldring, J. M. Rius, J. M. Tamayo, J. Parrón, and E. Ubeda, "Multiscale compressed block decomposition for fast direct solution of method of moments linear system," *IEEE Transactions on Antennas and Propagation*, vol. 59, no. 2, pp. 526–536, 2011.

[9] A. Boag and R. Mittra, "Complex multipole beam approach to electromagnetic scattering problems," *IEEE Transactions on Antennas and Propagation*, vol. 42, no. 3, pp. 366–372, 1994.

[10] F. X. Canning, "The impedance matrix localization (IML) method for moment-method calculations," *IEEE Antennas and Propagation Magazine*, vol. 32, no. 5, pp. 18–30, 1990.

[11] E. Bleszynski, M. Bleszynski, and T. Jaroszewicz, "AIM: adaptive integral method for solving large-scale electromagnetic scattering and radiation problems," *Radio Science*, vol. 31, no. 5, pp. 1225–1251, 1996.

[12] E. Michielssen and A. Boag, "Multilevel evaluation of electromagnetic fields for the rapid solution of scattering problems," *Microwave and Optical Technology Letters*, vol. 7, no. 17, pp. 790–795, 1994.

[13] E. F. Knott, "A progression of high-frequency RCS prediction techniques," *Proceedings of the IEEE*, vol. 73, no. 2, pp. 252–264, 1985.

[14] U. Jakobus and F. M. Landstorfer, "Improved PO-MM hybrid formulation for scattering from three-dimensional perfectly conducting bodies of arbitrary shape," *IEEE Transactions on Antennas and Propagation*, vol. 43, no. 2, pp. 162–169, 1995.

[15] K. R. Umashankar, S. Nimmagadda, and A. Taflove, "Numerical analysis of electromagnetic scattering by electrically large objects using spatial decomposition technique," *IEEE Transactions on Antennas and Propagation*, vol. 40, no. 8, pp. 867–877, 1992.

[16] D. Torrungrueng and E. H. Newman, "The multiple sweep method of moments (MSMM) analysis of electrically large bodies," *IEEE Transactions on Antennas and Propagation*, vol. 45, no. 8, pp. 1252–1258, 1997.

[17] W. D. Li, W. Hong, and H. X. Zhou, "An IE-ODDM-MLFMA scheme with DILU preconditioner for analysis of electromagnetic scattering from large complex objects," *IEEE Transactions on Antennas and Propagation*, vol. 56, no. 5, pp. 1368–1380, 2008.

[18] W. D. Li, W. Hong, and H. X. Zhou, "Integral equation-based overlapped domain decomposition method for the analysis of electromagnetic scattering of 3D conducting objects," *Microwave and Optical Technology Letters*, vol. 49, no. 2, pp. 265–274, 2007.

[19] D. Çolak, R. J. Burkholder, and E. H. Newman, "On the convergence properties of the multiple sweep method of moments," *Applied Computational Electromagnetics Society Journal*, vol. 22, no. 2, pp. 207–218, 2007.

[20] J. Laviada, M. R. Pino, and F. Las-Heras, "Convergence of certain class of enhanced spatial domain decompositions," *Microwave and Optical Technology Letters*, vol. 53, no. 10, pp. 2388–2393, 2011.

[21] J. Laviada, M. R. Pino, and F. Las-Heras, "On the influence of domain extensions and the relaxation parameter on spatial domain decomposition methods," in *Proceedings of the 6th European Conference on Antennas and Propagation (EUCAP '12)*, Prague, Czech Republic, March 2012.

[22] P. De Vita, F. De Vita, A. Di Maria, and A. Freni, "An efficient technique for the analysis of large multilayered printed arrays," *IEEE Antennas and Wireless Propagation Letters*, vol. 8, pp. 104–107, 2009.

[23] C. Wan and J. A. Encinar, "Efficient computation of generalized scattering matrix for analyzing multilayered periodic structures," *IEEE Transactions on Antennas and Propagation*, vol. 43, no. 11, pp. 1233–1242, 1995.

[24] S. H. Zainud-Deen, A. M. Abd-Elhady, A. A. Mitkees, and A. A. Kishk, "Design of dielectric resonator reflectarray using full-wave analysis," in *Proceedings of the 26th National Radio Science Conference (NRSC '09)*, pp. 1–9, New Cairo, Egypt, March 2009.

[25] C. Tienda, M. Arrebola, J. A. Encinar, and G. Toso, "Analysis of parabolic reflectarray in dual-reflector configuration," in *Proceedings of the 4th European Conference on Antennas and Propagation (EuCAP '10)*, Barcelona, Spain, April 2010.

[26] I. González, E. García, F. S. De Adana, and M. F. Cátedra, "Monurbs: a parallelized fast multipole multilevel code for analyzing complex bodies modeled by NURBS surfaces," *Applied Computational Electromagnetics Society Journal*, vol. 23, no. 2, pp. 134–142, 2008.

[27] E. García, C. Delgado, L. Lozano, I. González, and F. Cátedra, "An efficient hybrid scheme combining the characteristic basis function method and the multilevel fast multipole algorithm for solving bistatic RCS and radiation problems," *Progress in Electromagnetic Research B*, vol. 34, pp. 327–343, 2011.

[28] M. R. Chaharmir, J. Shaker, and N. Gagnon, "Broadband dual-band linear orthogonal polarisation reflectarray," *Electronics Letters*, vol. 45, no. 1, pp. 13–14, 2009.

[29] G. Farin, *Curves and Surfaces for Computer Aided Geometric Design*, Academic Press, 1988.

[30] L. Valle, F. Rivas, and M. F. Cátedra, "Combining the moment method with geometrical modelling by NURBS surfaces and Bezier patches," *IEEE Transactions on Antennas and Propagation*, vol. 42, no. 3, pp. 373–381, 1994.

[31] J. Moreno, L. Lozano, M. J. Algar, I. González, and F. Cátedra, "Pre-processing and meshing optimization for electromagnetic tools," in *Proceedings of IEEE International Symposium*

on Antennas and Propagation (APSURSI '11), pp. 317–320, Spokane, Wash, USA, July 2011.

[32] W. Gropp, E. Lusk, and A. Skjellum, *Using MPI Portable Parallel programming with the Message-Passing Interface*, The MIT Press, 1999.

[33] D. J. Ludick and D. B. Davidson, "Investigating efficient parallelization techniques for the Characteristic Basis Function Method (CBFM)," in *Proceedings of the International Conference on Electromagnetics in Advanced Applications (ICEAA '09)*, pp. 400–403, Torino, Italy, September 2009.

[34] M. F. Cátedra and J. Pérez, *Cell Planning for Wireless Communications*, Artech House, Boston, Mass, USA, 1999.

[35] F. S. De Adana, O. Gutiérrez, I. González, L. Lozano, and M. F. Cátedra, *Practical Applications of Asymptotic Techniques in Electromagnetics*, Artech House, 2010.

[36] F. Cátedra, L. Lozano, I. González, E. García, and M. J. Algar, "Efficient techniques for accelerating the ray-tracing for computing the multiple bounce scattering of complex bodies modeled by flat facets," *Applied Computational Electromagnetics Society Journal*, vol. 25, no. 5, pp. 395–409, 2010.

[37] C. Delgado, E. García, and F. Cátedra, "Application of a hybrid domain decomposition approach for the analysis of large reflector antennas," in *Proceedings of the 5th European Conference on Antennas and Propagation (EUCAP '11)*, pp. 846–848, Rome, Italy, April 2011.

[38] M. H. Jamaluddin, R. Gillard, R. Sauleau, P. Dumon, and L. Le Coq, "Reflectarray element based on strip-loaded dielectric resonator antenna," *Electronics Letters*, vol. 44, no. 11, pp. 664–665, 2008.

[39] M. Mussetta, P. Pirinoli, P. T. Cong, M. Orefice, and R. E. Zich, "Optimization of a dual-band reflectarray antenna," in *Proceedings of IEEE International Symposium on Antennas and Propagation (APSURSI '10)*, pp. 1–4, Toronto, Canada, July 2010.

[40] S. H. Hsu, C. Han, J. Huang, and K. Chang, "An offset linear-array-fed Ku/Ka dual-band reflectarray for planet cloud/precipitation radar," *IEEE Transactions on Antennas and Propagation*, vol. 55, no. 11, pp. 3114–3122, 2007.

[41] J. Huang, C. Han, and K. Chang, "A cassegrain offset-fed dual-band reflectarray," in *Proceedings of IEEE International Symposium on Antennas and Propagation (APSURSI '06)*, pp. 2439–2442, Albuquerque, NM, USA, July 2006.

[42] P. Pirinoli, P. T. Cong, M. Mussetta, and M. Orefice, "Dual-band reflectarray antenna: design and experimental validation," in *Proceedings of the International Conference on Electromagnetics in Advanced Applications (ICEAA '09)*, pp. 1024–1027, Torino, Italy, September 2009.

[43] M. R. Chaharmir, J. Shaker, and N. Gagnon, "Broadband dual-band linear orthogonal polarisation reflectarray," *Electronics Letters*, vol. 45, no. 1, pp. 13–14, 2009.

Hindawi Publishing Corporation
International Journal of Antennas and Propagation
Volume 2012, Article ID 290285, 5 pages
doi:10.1155/2012/290285

Research Article

Beam-Scanning Reflectarray Based on a Single Varactor-Tuned Element

F. Venneri, S. Costanzo, G. Di Massa, E. Marozzo, A. Borgia, P. Corsonello, and M. Salzano

Dipartimento di Elettronica, Informatica e Sistemistica, Università della Calabria, 87036 Rende, Italy

Correspondence should be addressed to S. Costanzo, costanzo@deis.unical.it

Received 3 February 2012; Accepted 16 April 2012

Academic Editor: Raphaël Gillard

A single varactor-tuned element is investigated as effective solution for the realization of reconfigurable reflectarray antennas. The proposed configuration is successfully implemented for the design of an *X*-band reflectarray prototype of 3×15 radiators. A dedicated electronic control board is designed as an integral part of the antenna. Good performances in terms of beam-scanning capabilities are obtained from measurements.

1. Introduction

Microstrip reflectarray antennas have received considerable interests in the last two decades, due to their appealing features in terms of low cost, high efficiency, and reduced mass and volume. Many different implementations of the reflectarray concept have been proposed, ranging from the first simple configurations, based on the use of variable size patches [1] or identical elements with variable length stubs [2], up to more sophisticated structures, such three layers stacked [3] or aperture coupled patches [4]. The success obtained in the realization of passive reflectarray structures has recently attracted the attention towards the application of this technology to the design of reconfigurable reflector antennas. The main advantage deriving from the development of active reflectarrays over traditional-phased arrays is the elimination of complicated beam-forming networks, which typically introduce very high losses. Many different configurations have been proposed as phase-tunable reflectarray elements such as mechanically reconfigurable patches [5, 6], varactor-loaded microstrip radiators [7–9], reflectarrays printed on tunable liquid crystal substrates [10], and MEMS-based structures [11–14].

In this paper, a tunable radiating element based on the use of a single varactor diode [9] is implemented for the realization of a reconfigurable reflectarray antenna. The adopted element consists of a patch aperture-coupled to a varactor loaded line. The phase tuning capabilities of this configuration have been already demonstrated by the authors in [9]. When compared with the existing solutions, the adopted configuration offers a uniform reflecting surface, due to the fact that the tunable element and the biasing circuitries are located on the opposite side below the ground plane. Furthermore, as demonstrated in [9], an optimum phase tuning range of about 320 degrees is obtained by integrating a single diode to each radiating element.

The proposed configuration is properly synthesized for the design of an *X*-band reflectarray with beam-scanning capabilities. A printed electronic circuit is integrated to the antenna in order to actively control the bias voltages across the diodes. The radiation pattern measurements of the reflectarray prototype show the ability to electronically scan the main beam along some prescribed directions.

2. Reflectarray Element Design

The single radiator adopted for the realization of the proposed reconfigurable reflectarray is based on the use of a patch printed on a grounded dielectric substrate and slot coupled to a varactor loaded microstrip line (Figure 1). By changing the bias voltage across the diode, a variable capacitive load is obtained, which in turns introduces a tunable phase shift in the reradiated field. A biasing line is printed on the tuning line substrate, thus the reflectarray surface is

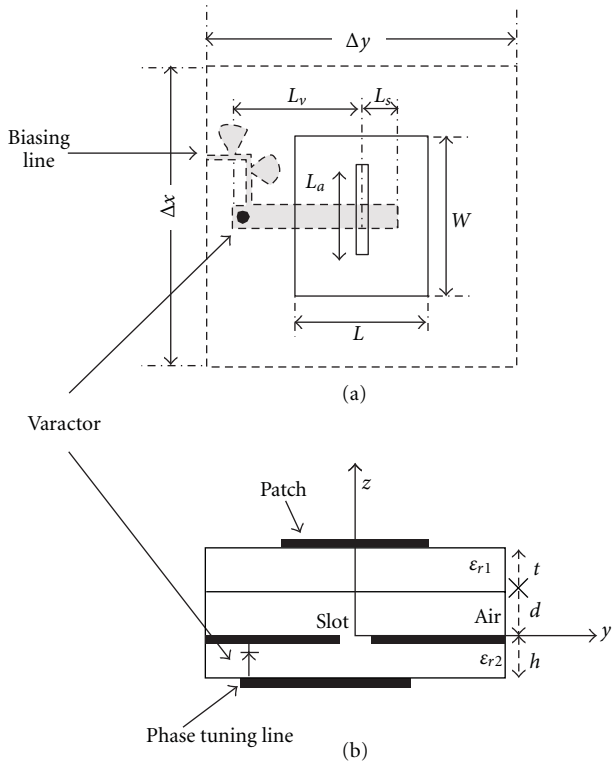

Figure 1: Reflectarray element configuration: (a) top view; (b) side view.

simply composed by identical rectangular patches separated by uniform spacings. This last feature makes the proposed reflectarray configuration free from unwanted reflections.

The adopted reflectarray element is designed in order to obtain a full phase tuning range at the operating frequency $f_0 = 11.5$ GHz. A MoM-based infinite array approach is adopted for the simulation and the optimization of the radiating structure. A cell size of $\Delta x \times \Delta y = 0.7\lambda_0 \times 0.7\lambda_0$ is fixed at the operating frequency f_0. Two identical dielectric slabs are chosen as patch and line substrates, having the following features: $\varepsilon_{r1} = \varepsilon_{r2} = 2.33$, $t = h = 0.762$ mm. A layer of air with a thickness $d = 0.762$ mm is placed between the antenna substrate and the ground plane. The following dimensions are obtained for the different parts composing the antenna: $W = 9.3$ mm, $L = 8.2$ mm, $W_a = 0.6$ mm, $L_a = 5.8$ mm, $W_s = 3.07$ mm (Figure 2(a)). The assumed line width W_s corresponds to a characteristic impedance of value equal to 40 Ω. The input impedance Z_t, (Figure 2(a)), evaluated at the center of the slot, results to be perfectly matched to the 40 Ω—line when the stub L_s is fixed at a value of 2 mm (Figure 2(b)).

A Microsemi MV31011-89 varactor diode, with a tunable capacitance ranging from 0.2 pF ($V_{\text{bias}} = 20$ Volt) to 2 pF ($V_{\text{bias}} = 0$ Volt), is integrated to the above element in order to obtain the required reconfiguration capabilities. In this case, the two line sections L_v and L_s (see Figure 1) are optimized in order to maximize the phase agility of the element in the assigned varactor capacitance range. At this purpose, the stub L_s is fixed to a value of 7.8 mm, while the length L_v is set to the value of 6.5 mm, in order to move the maximum phase variation within the diode capacitance range.

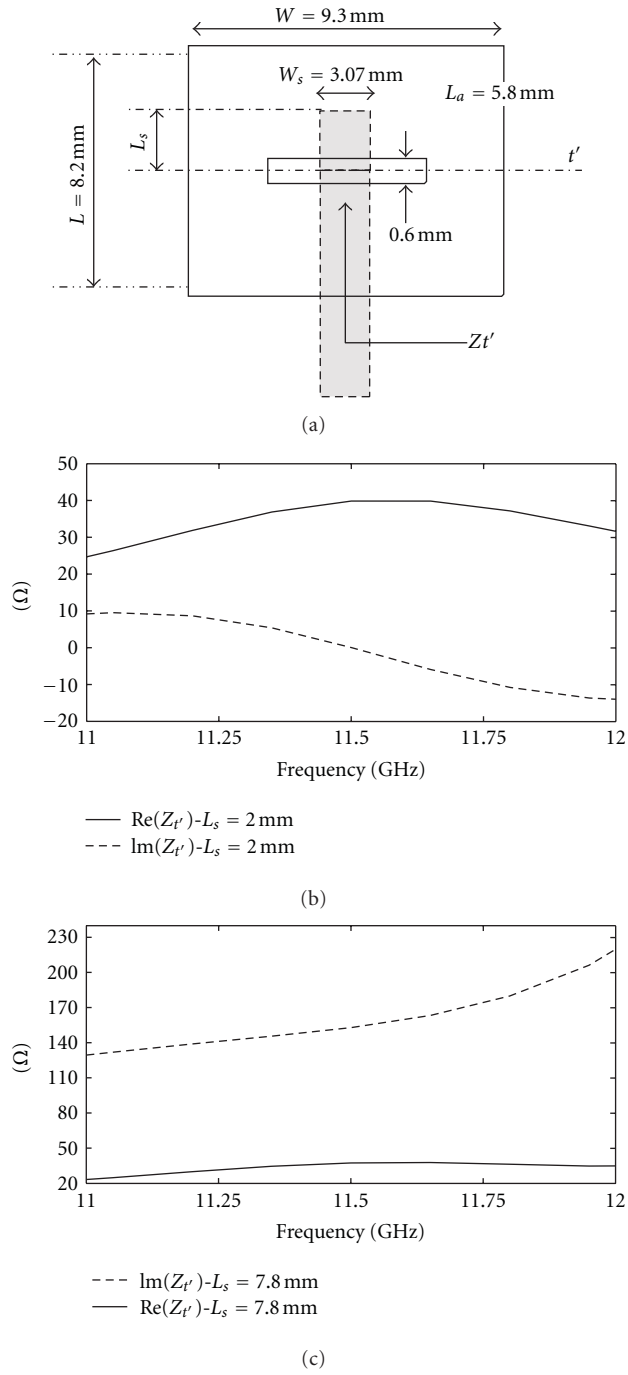

Figure 2: Synthesized aperture-coupled patch: (a) element layout; (b) simulated input impedance for $L_s = 2$ mm; (c) simulated input impedance for $L_s = 7.8$ mm.

The reflectarray element is analyzed in order to evaluate the behavior of the reflection phase versus diode capacitance, for different values of the stub length. A normally incident plane wave is assumed.

The reflection phase curves, computed in the case of length L_s equal to 2 mm and 7.8 mm, are reported in

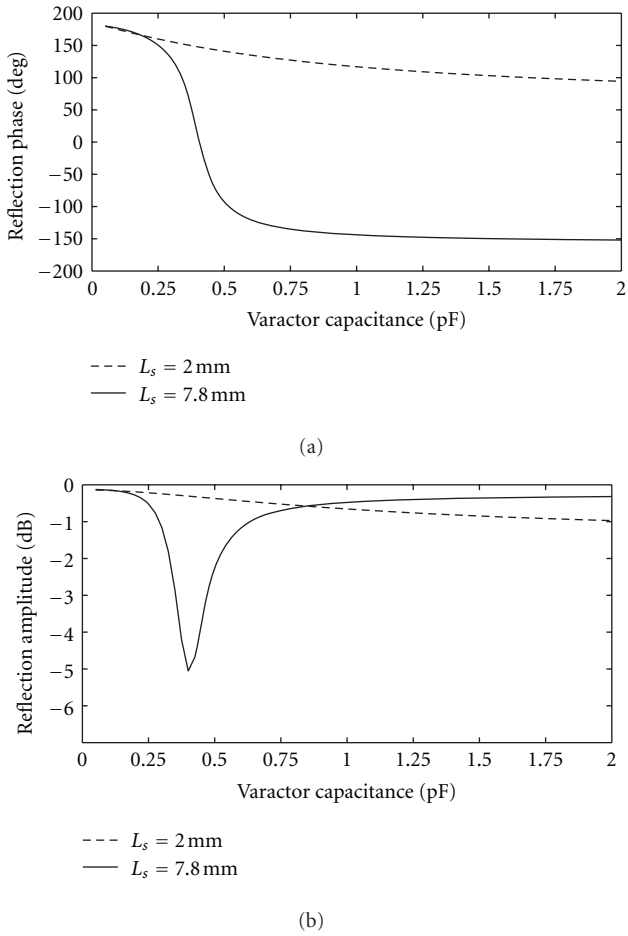

FIGURE 3: Simulated reflection coefficient for a normally incident plane wave: phase (a) and amplitude (b) versus varactor capacitance for different stub lengths.

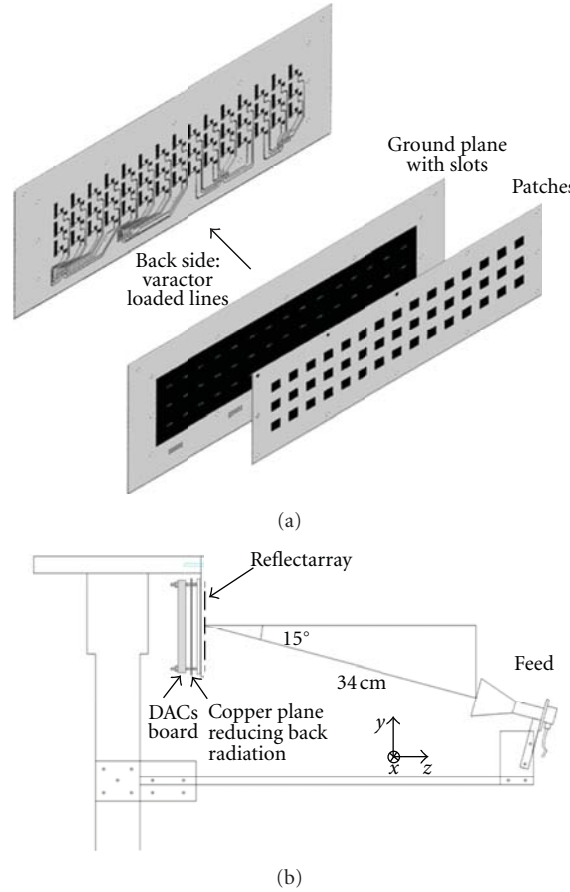

FIGURE 4: Reflectarray structure scheme—(a) aperture-coupled array; (b) array illuminated by the feed.

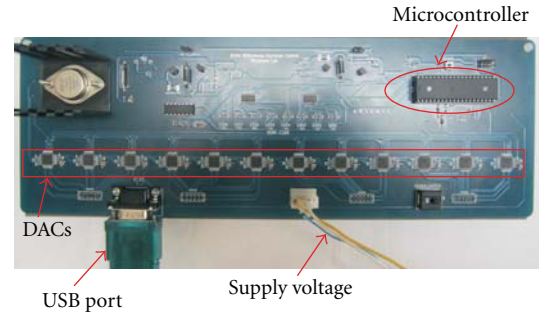

FIGURE 5: Photograph of the designed DACs board.

Figure 3(a). The curves are computed by varying the diode capacitance C_v in the range between 0.2 pF and 2 pF. From a comparison of the two considered curves, it can be stated that an higher phase tuning range can be obtained by introducing a proper inductive effect in the input impedance Z_t, (Figure 2(c)). In this case, more pronounced reflection losses are obtained (Figure 3(b)), which can be reduced by adopting a varactor with a lower series resistance. In the above simulations, a value of 1.36 Ω is assigned for this diode parameter, resulting into a value of 3.7 dB for the losses due to the varactor insertion.

The correctness of the simulated design curves has been experimentally verified in [9], where a good agreement between measurements and simulations can be appreciated.

3. Reflectarray Prototype Description and Experimental Results

The synthesized element is adopted as elementary cell of a 3× 15 reflectarray (Figure 4(a)). The array is illuminated by an X-band horn, located at a distance of 34 cm from the reflecting surface, with an offset angle of 15 degrees in the y-z plane (Figure 4(b)). The antenna is integrated with an electronic board composed by an array of digital to analog converters (AD5764R DACs) driven by a microcontroller (ATMEL ATmega1284P). Each AD5764R integrated circuit is composed by four 16-bit DACs. A photograph of the designed electronic board is illustrated in Figure 5.

A metallic plane is placed between the antenna and the DACs-board (Figure 4(b)) in order to reduce the back-radiation as well as the occurrence of any undesired interference effect.

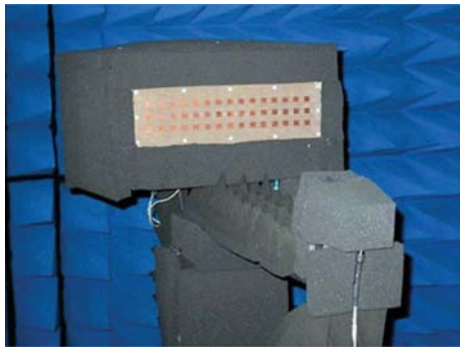

Figure 6: Photograph of the reflectarray prototype into the anechoic chamber.

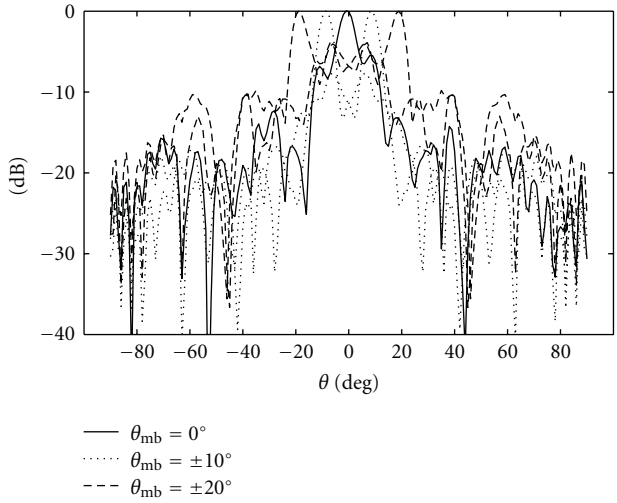

Figure 7: Normalized radiation patterns (copolar components on the *x*-*z* plane) measured for different biasing voltage distributions.

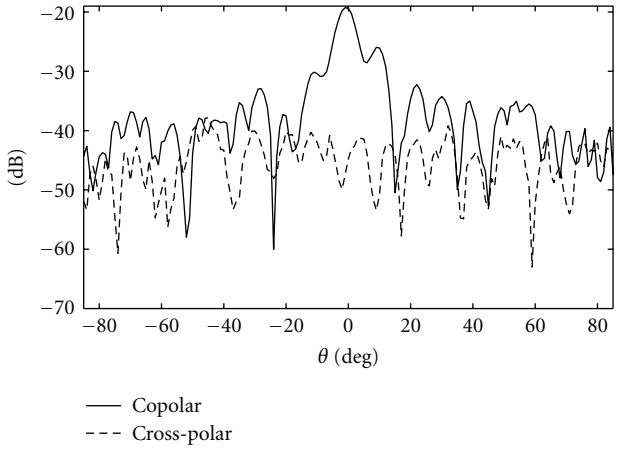

Figure 8: Measured radiation pattern (copolar and cross-polar components on *x*-*z* plane) for a main beam $\theta_{mb} = 0^\circ$.

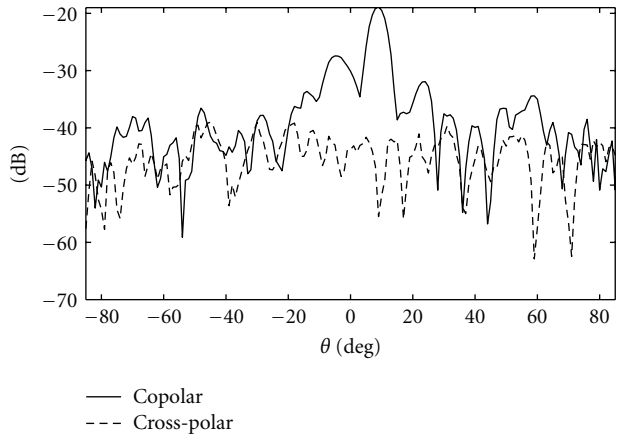

Figure 9: Measured radiation pattern (copolar and cross-polar components on *x*-*z* plane) for a main beam $\theta_{mb} = 10^\circ$.

The reflectarray antenna can be easily reconfigured by a PC, which communicates with the ATmega1284P microcontroller through an USART interface. The microcontroller sends the desired voltage levels to the DACs array, which is properly connected to the varactor diodes.

The fabricated structure, illustrated in Figure 6, is validated by performing the measurement of the radiation pattern for different configurations of the bias voltages across the diodes. The considered voltage distributions are determined in order to scan the radiation pattern main beam θ_{mb} from −20 to 20 degrees in the *x*-*z* plane (Figure 4). The required bias voltages levels are computed by a synthesis algorithm based on the iterative projection method [15].

A far-field measurement facility is adopted, which is placed into the anechoic chamber of the University of Calabria.

A double-ridged broadband horn, operating within the frequency range equal to $(1 \div 18)$ GHz, is adopted as probe at a far-field distance of 5.6 m from the reflectarray.

The measured copolar patterns on the *x*-*z* plane, reported under Figure 7, show the main beam θ_{mb} effectively scanned along the assigned directions. A measurement frequency equal to 11.25 GHz is assumed. As the aim of the realized prototype is to simply demonstrate the validity of the proposed scanning technique, a small number of elements is assumed on the *y*-*z* plane, with no specific tuning, so the characterization of the radiation patterns on this plane has no significant validity and it is not reported.

As a further characterization, the cross-polar patterns on the *x*-*z* plane are measured for three different main beam conditions, namely, $\theta_{mb} = 0^\circ, 10^\circ, 20^\circ$, and the comparison with the relative copolar components is reported in Figures 8, 9, and 10. In all cases, a cross-polarization approximately below −40 dB can be observed.

A loss analysis on the reflectarray is performed for a main beam in the broadside direction. The measured gain versus frequency is reported in Table 1. In particular, at the central design frequency of 11.25 GHz, a gain value of 9.3 dBi is obtained. At the same frequency, the maximum

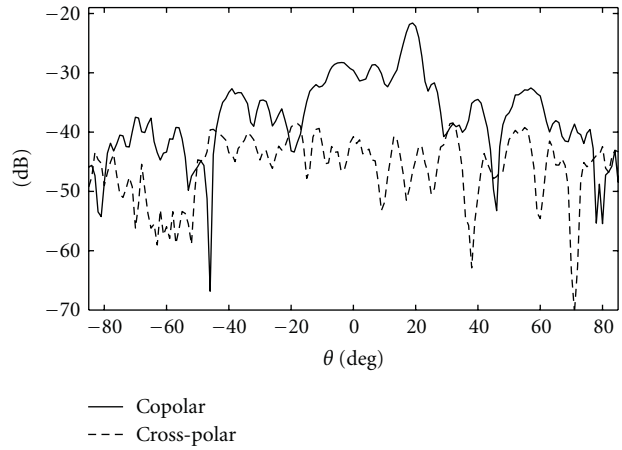

Figure 10: Measured radiation pattern (copolar and cross-polar components on x-z plane) for a main beam $\theta_{mb} = 20^\circ$.

Table 1: Measured Gain versus Frequency (Broadside Configuration).

Frequency (GHz)	Gain (dB)
10.9	6.6
11	8.1
11.1	7
11.15	7.8
11.2	8.6
11.25	9.3
11.35	5.8
11.5	6.6

directivity for a reflectarray with an aperture area of $21.21\lambda^2$ is calculated as 24.24 dBi. Using the measured gain, the antenna efficiency is estimated as 3.3%. This small value is mainly due to the high spillover in the y-z plane.

4. Conclusion

An aperture-coupled patch loaded by a single tunable varactor diode has been adopted for the implementation of a reconfigurable reflectarray prototype. The good phase agility associated to the designed reflectarray element has allowed the realization of a 3×15 reflectarray antenna with beam-scanning capabilities within an angular range of about 40 degrees. The experimental tests on the fabricated antenna have demonstrated the validity of the implemented reflectarray configuration.

References

[1] D. M. Pozar and T. A. Metzler, "Analysis of a reflectarray antenna using microstrip patches of variable size," *Electronics Letters*, vol. 29, no. 8, pp. 657–658, 1993.

[2] J. Huang, "Microstrip reflectarray," in *Proceedings of the IEEE International Symposium on Antennas and Propagation*, pp. 612–615, Ontario, Canada, June 1991.

[3] J. A. Encinar and J. Agustín Zornoza, "Broadband design of three-layer printed reflectarrays," *IEEE Transactions on Antennas and Propagation*, vol. 51, no. 7, pp. 1662–1664, 2003.

[4] E. Carrasco, M. Barba, and J. A. Encinar, "Reflectarray element based on aperture-coupled patches with slots and lines of variable length," *IEEE Transactions on Antennas and Propagation*, vol. 55, no. 3, pp. 820–825, 2007.

[5] J. Huang and R. J. Pogorzelski, "A ka-band microstrip reflectarray with elements having variable rotation angles," *IEEE Transactions on Antennas and Propagation*, vol. 46, no. 5, pp. 650–656, 1998.

[6] M. E. Cooley, J. F. Walker, D. G. Gonzalez, and G. E. Pollon, "Novel reflectarray element with variable phase characteristics," *IEE Proceedings*, vol. 144, no. 2, pp. 149–151, 1997.

[7] S. V. Hum, M. Okoniewski, and R. J. Davies, "Realizing an electronically tunable reflectarray using varactor diode-tuned elements," *IEEE Microwave and Wireless Components Letters*, vol. 15, no. 6, pp. 422–424, 2005.

[8] M. Riel and J. J. Laurin, "Design of an electronically beam scanning reflectarray using aperture-coupled elements," *IEEE Transactions on Antennas and Propagation*, vol. 55, no. 5, pp. 1260–1266, 2007.

[9] F. Venneri, S. Costanzo, and G. Di Massa, "Reconfigurable aperture-coupled reflectarray element tuned by single varactor diode," *Electronics Letters*, vol. 48, no. 2, pp. 68–69, 2012.

[10] A. Moessinger, S. Dieter, W. Menzel, S. Mueller, and R. Jakoby, "Realization and characterization of a 77 GHz reconfigurable liquid crystal reflectarray," in *Proceedings of the 13th International Symposium on Antenna Technology and Applied Electromagnetics and the Canadian Radio Sciences Meeting (ANTEM/URSI '09)*, February 2009.

[11] J. P. Gianvittorio and Y. Rahmat-Samii, "Reconfigurable patch antennas for steerable reflectarray applications," *IEEE Transactions on Antennas and Propagation*, vol. 54, no. 5, pp. 1388–1392, 2006.

[12] R. Sorrentino, R. V. Gatti, L. Marcaccioli, and B. Mencagli, "Electronic steerable mems antennas," in *Proceedings of the European Conference on Antennas and Propagation (EuCAP '06)*, November 2006.

[13] J. Perruisseau-Carrier and A. K. Skrivervik, "Monolithic MEMS-based reflectarray cell digitally reconfigurable over a 360° phase range," *IEEE Antennas and Wireless Propagation Letters*, vol. 7, pp. 138–141, 2008.

[14] O. Bayraktar, O. A. Civi, and T. Akin, "Beam switching reflectarray monolithically integrated with RF MEMS switches," *IEEE Transactions on Antennas and Propagation*, vol. 60, no. 2, part 2, Article ID 6056550, pp. 854–862, 2012.

[15] F. Venneri, S. Costanzo, G. Di Massa, and G. Angiulli, "An improved synthesis algorithm for reflectarrays design," *IEEE Antennas and Wireless Propagation Letters*, vol. 4, no. 1, pp. 258–261, 2005.